INVESTIGATIONS ON FIBER BRAGG GRATINGS FOR FIBER OPTIC COMMUNICATION SYSTEMS

A THESIS

SUBMITTED IN FULFILLMENT OF THE REQUIREMENT

FOR THE AWARD OF DEGREE OF

DOCTOR OF PHILOSOPHY

IN

ELECTRONICS & COMMUNICATION ENGINEERING

BY

NAVNEET SINGH AULAKH

DEPARTMENT OF ELECTRONICS & COMMUNICATION ENGINEERING

THAPAR UNIVERSITY

2010

CERTIFICATE

I, Navneet Singh Aulakh hereby certify that the work which is being presented in this thesis entitled "Investigations on Fiber Bragg Gratings for Fiber Optic Communication Systems" in fulfillment of requirements for the award of degree of Doctor of Philosophy in Electronics and Communication Engineering from Thapar University, Patiala, is an authentic record of my own work carried under the supervision of Dr. R. S. Kaler. The matter presented in this thesis has not been submitted in any other University/Institute for the award of any degree.

Navneet Singh Aulakh

Navneet Singh Aulakh

(Signature of the Student) Date: 20/9/2010

This is certified that the above statement made by the candidate is correct to the best of my knowledge.

(Dr. R. S. Kaler)

Guide & Professor of ECED

Thapar University, Patiala

Date 20/9/2010

Abstract

This thesis presents the Investigations on Fiber Bragg Gratings for Fiber Optic Communication Systems. A Fiber Bragg Grating (FBG) is a periodic or aperiodic perturbation of the effective absorption coefficient or the effective refractive index of an optical waveguide. A Bragg Grating can reflect a predetermined narrow or broad range of wavelengths of light incident on the grating, while passing all other wavelengths of the light. FBG can be fabricated by exposing a photosensitized fiber with an intensive pattern of excimer laser radiation.

Fiber Bragg Gratings have emerged as important components in a variety of applications. Their unique filtering properties and versatility as in-fiber devices is illustrated by their use in Wavelength-Stabilized Lasers, Fiber Lasers, Remotely Pump Amplifiers, Raman Amplifiers, Phase Conjugators, Wavelength Converters, Passive Optical Networks, Wavelength Division Multiplexers (WDM's), Demultiplexers, Add/drop Multiplexers, Dispersion Compensators, and Gain Equalizers. They are also stimulating growth in fiber optic applications outside of telecommunications, such as nonlinear frequency conversion, spectroscopy, and remote sensing.

Since the output of a Bragg grating sensor is present in the wavelength domain it requires sophisticated circuits to measure wavelength shift. One way of interrogating a Bragg grating sensor is to use a tunable filter. One option is the Fabry–Perot interferometer with a cavity length controlled by a piezoelectric actuator. Although this approach has a good resolution and is independent of light intensity variations, it is relatively slow and expensive. Chirped Fiber Bragg Grating (CFBG) can also be used as the wavelength-sensitive component. A chirped Bragg grating can be used as a device that converts wavelength into delay. By measuring this delay, the wavelength of light corresponding to the delay can be found. Very fast electronic circuitry is required for resolving this delay and it proves to be very expensive. An interferometer may be used to convert wavelength shifts into phase shifts, which can be detected by measuring variations in the light intensity as the path difference in the interferometer is varied. This technique potentially allows for very high sensitivity, but the equipment to do it is expensive and prone to environmental interference. A sloped optical filter, which may be another Bragg grating, can be used to convert wavelength shifts directly into intensity changes. If the filter is designed to have a known pass/reject ratio which varies with wavelength, then the

wavelength of a narrowband reflection from a single grating can be determined simply by measuring and comparing the passed and rejected intensities. This technique referred to as edge filtering technique is the simplest and most economical way of demodulating FBG. The accuracy in this technique is impaired by microbend losses that occur in the fiber connecting the Fiber Bragg Grating Interrogator to the Fiber Bragg Grating. If a portion of fiber is deformed, the fiber would exhibit excess light loss. Such perturbation of fiber axis results in redistribution of guided power between modes of the fiber and also coupling of the fiber from one mode/mode group to another. This thesis presents the technique to circumvent this problem.

Thus this thesis presents the Investigations on Fiber Bragg Gratings for Fiber Optic Communication Systems. The simulation of Fiber Bragg Gratings has been carried out and the results presented have been validated using theoretical and experimental work. A marginal change in the model of FBG has been proposed to account for the loss in accuracy due to non-identical refractive index modulation in the FBG. The wavelength shift in Fiber Bragg Gratings on simulated external perturbation using a wideband source has also been observed and finally a Fiber Bragg Grating Interrogator for Sensor/Communication systems has been designed. A new technique for mitigating the errors due to effect of microbending in the fiber lead from FBG to the interrogator has also been incorporated in the design of FBG interrogator. Most of the research findings of this thesis have been published in various international referred journals (Chapters 4, 5, 6, 7 and 8) as per the list at page (201).

Acknowledgement

I am highly indebted to my thesis supervisor Prof. R. S. Kaler, Department of Electronics and Communication Engineering, Thapar Engineering Campus, Thapar University, Patiala, India for giving me the opportunity to work under his supervision. He had encouraged me and guided me to accomplish this research work. I express my deep sense of gratitude to him for his keen interest, continuous assistance and superb guidance in the materialization of this dissertation.

I dedicate this work to my father, Late Mr. Kundan Singh Aulakh who always encouraged me to achieve my aspirations. A very special note of thanks to my mother, Mrs. Parminder Kaur Aulakh whose blessings have been a valuable asset to me in my life.

Last but not the least I thank from the core of my heart my wife Er. Inderdeep Kaur Aulakh for her enthusiastic help and constructive suggestions and my children Rehmat and Sidak for their patience and understanding.

Navneet Singh Aulakh

(Navneet Singh Aulakh)

TABLE OF CONTENTS

LIST OF FIGURES

LIST OF SYMBOLS

α_{int}	Total internal loss
α_c	Cladding loss
β	Propagation constant
δ	Deviation from real part of propagation constant (β-β_o)
δn	Amplitude of refractive index perturbation
Δn	Carrier induced refractive index change
E	Electric field
Λ	Grating period
$\sigma(z)$	Variations in the average refractive index
F	Forward propagating field
λ	Wavelength of Light
K	Grating wave vector,
ΔT	change in temperature
ε	Applied Strain
$\Delta\lambda_B$	Bragg wavelength
α_n	Thermo-optic coefficient
α_Λ	Expansion coefficient of the optical fiber,
D	Electric displacement vector
E	Applied electric field
ε_0	Dielectric constant
μ_0	Magnetic permeability
P	Induced polarization P
χ_{ij}	Linear susceptibility
$\delta_{\mu\vartheta}$	Kronecker's delta

$\emptyset(z)$	Spatially varying phase change
β_v	Electric field mode propagation
Δn_{eff}	Effective index difference between the modes
δ	Detuning wave vector
L	Length of the Bragg grating
P	Optical strain coefficient
F	Co-efficient of finesse

LIST OF ACRONYMS

FBG	Fiber Bragg Grating
WDM	Wavelength Division Multiplexing
NDE	Non-Destructive Evaluation
UV	Ultra violet
Nm	nanometer
Ge	Germanium
AWG	Arrayed Waveguide Grating
AOTF	Acousto-Optic Tunable Filter
FSK	Frequency Shift Keying
RF	Radio Frequency
GFPC	Grating Fabry-Perot cavity
TDM	Time-Division-Multiplexed
FMCW	Frequency-Modulated Continuous Wave
ADC	Analog to Digital Converter
uC	Microcontroller
LPG	Long-Period Grating
EDF	Erbium-Doped Fiber
MZI	Mach-Zehnder interferometer
SOA	Semiconductor Optical Amplifier
PC	Polarization Controller
PBS	Polarizing Beam Splitter
CFG	Chirped Fiber Grating
SNR	Signal to Noise Ratio
TFBG	Tilted Fiber Bragg Grating

PVA	Polyvinyl Alcohol
CTCB	Cylinder Taper Cantilever Beam
MCFBG	Microchannelled Chirped Fiber Bragg Grating
OADM	Optical Add-Drop Multiplexer
TE	Transverse Electric
TM	Transverse Magnetic
CCD	Charge-Coupled Device
EDFA	Erbium-Doped Fiber Amplifier
FPF	Fabry–Perot Filter
FWHM	Full Width Half Maxima
MSE	Mean Square Error
OFS	Optical Fiber Sensor
PIN	Positive-Intrinsic-Negative

Chapter 1
Introduction

1.1 Motivation and Overview

The demand for more bandwidth in telecommunication networks has rapidly increased the development of new optical components and devices [1]. Current efforts of research and development are aiming at increasing the total capacity of optical fibers as a medium and improving long haul optical transmission systems using new innovative technologies such as ultra-dense wavelength division multiplexing (WDM) [2]. The advances in the optical communications have been synergised by development of efficient and powerful optical components which eliminate the need of costly conversions from optical to electrical signal and back [3].

Fiber Bragg Gratings have been vital in the phenomenal growth of some of these products and are recognized as one of the most significant enabling technologies for fiber optic communications in the last decade [4]. Since their market introduction in 1995, the use of optical Fiber Bragg Gratings in commercial products has grown exponentially, largely in the fields of telecommunications [5] and stress sensors [6].

Fiber-optic sensors are generally used for several types of applications. In smart manufacturing they are attached or embedded in components, typically composites, during the manufacturing process and used to monitor such things as temperature, pressure, viscosity, degree of cure or residual strain [7]. During service, Fiber Bragg Grating sensors may be used for non-destructive evaluation (NDE) to measure strain profiles, monitor de-lamination or other changes in structural characteristics [8]. They may also be used in health monitoring and damage assessment of structures, or to support control systems by responding to changes in the environment [9]. Being EMI/RFI immune, flexible and compact fiber-optic sensors based on Bragg gratings have found applications in a wide variety of industries [10].

In civil engineering, FBG sensors have been used in mining and to monitor tunnels, bridges and dams [11]. In the nuclear industry they have been used for containment shells, cooling towers, steam pipes and storage sites and in marine engineering for masts, lock

gates and undersea acoustic monitors [12]. They have found particular application in aerospace, especially for composite materials where they are used for structural health monitoring, impact detection, cure processing, and shape control and vibration damping [13]. Their use is also being considered in biomedical engineering where, for example, monitoring of mechanical performance and damage in artificial limbs is extremely important for orthopaedic applications [14].

Another application for these gratings is wavelength stabilization of lasers, which means control of a laser's wavelength and possibly enforcement of single-axial-mode lasing [15]. Fiber Bragg Gratings are attractive devices for this application because they are easy to make and offer precise control of the center wavelength, excellent temperature stability and tenability [16]. These benefits can significantly improve the performance and capabilities of diode lasers and fiber lasers [17].

The benefits of Fiber Bragg Gratings make them attractive to other applications as well [18]. In telecommunications systems, they are used for dispersion compensation in fiber optic transmission systems, demultiplexing filters for wavelength division multiplexing systems, and long-period gratings for gain flattening of erbium-doped fiber amplifiers [19]. They are also stimulating growth in fiber optic applications outside of telecommunications, such as nonlinear frequency conversion, spectroscopy, and remote sensing [20].

The primary application of Fiber Bragg Gratings is in optical communications systems. They are specifically used as notch filters. They are also used in optical multiplexers and demultiplexers with an optical circulator, or Optical Add-Drop Multiplexer (OADM) [17].

A demultiplexer can be achieved by cascading multiple drop sections of the OADM, where each drop element uses a FBG set to the wavelength to be demultiplexed. Conversely, a multiplexer can be achieved by cascading multiple add sections of the OADM. FBG demultiplexers and OADMs can also be tunable. In a tunable demultiplexer or OADM, the Bragg wavelength of the FBG can be tuned by strain applied by a piezoelectric transducer. The main advantage is that in these applications since Fiber Bragg Grating can be incorporated in the optical fiber itself there is no need to insert lossy couplings in the form of connectors or to make costly conversions from optical to

electrical domain and back. Similarily in the field of Fiber Optic Sensors FBGs find many applications since here also the Optical sensor is integrated in Optical Fiber itself [21-30].

1.2 Bragg Grating

A "Bragg Grating" is a periodic or aperiodic perturbation of the effective absorption coefficient and/or the effective refractive index of an optical waveguide [31]. In the periodic structure of the FBG the coupling of energy between different co-propagating and counter-propagating modes of the fiber takes place. The mode coupling phenomenon is a strong function of wavelength. A Bragg Grating can reflect a predetermined narrow or broad range of wavelengths of light incident on the grating, while passing all other wavelengths of the light. The capability to photo-imprint gratings in optical fibers requires that the glass be photosensitive [32]. By irradiating the fiber with an intensive pattern that has a periodic or aperiodic distribution, a corresponding index perturbation is permanently induced in the core of the waveguide. The result is an index grating that is photo-imprinted in the optical waveguide. As a result, the Bragg Grating becomes a very selective spatial reflector in the core of the fiber [31].

There are several distinct types of Fiber Bragg Grating structures such as the common Bragg reflector, the blazed Bragg grating, and the chirped Bragg grating [33]. These Fiber Bragg Gratings are distinguished either by their grating pitch spacing between grating planes or tilt angle between grating planes and fiber axis. The most common Fiber Bragg Grating is the Bragg reflector, which has a constant pitch. The blazed grating has phase fronts tilted with respect to the fiber axis, that is, the angle between the grating planes and the fiber axis is less than 90°. The chirped grating has an aperiodic pitch, that is, a monotonic increase in the spacing between grating planes [34].

1.3 Externally written Bragg gratings in optical fibers

Inscribing Bragg gratings in optical fibers is a formidable task. The requirement of a submicron periodic pattern makes the stability a severe constraint on the techniques able to write Bragg gratings in optical fibers. To date, there are only a few externally written fabrication techniques, namely, the interferometric technique, the phase mask technique, and the point-by-point technique [31].

1.3.1 Interferometric fabrication technique

The interferometric fabrication technique, the first external writing technique of forming Bragg gratings in photosensitive fibers, utilized an interferometer that split the incoming UV light into two beams and then recombined them to form an interference pattern. The fringe pattern was used to expose a photosensitive fiber, inducing a refractive index modulation in the core. Bragg gratings in optical fibers have been fabricated using both amplitude splitting and wave-front-splitting interferometers [32].

1.3.1.1 Amplitude-splitting interferometer.

In an amplitude splitting interferometer, the UV writing laser light is split into two equal intensity beams and are later recombined after traversing through two different optical paths. This forms an interference pattern at the core of a photosensitive fiber. Cylindrical lenses are normally placed in the interferometer to focus the interfering beams to a fine line matching the fiber core. The Bragg grating period, L, which is identical to the period of the interference fringe pattern, depends on both the irradiation wavelength λ_w , and the half-angle between the intersecting UV beams [32].

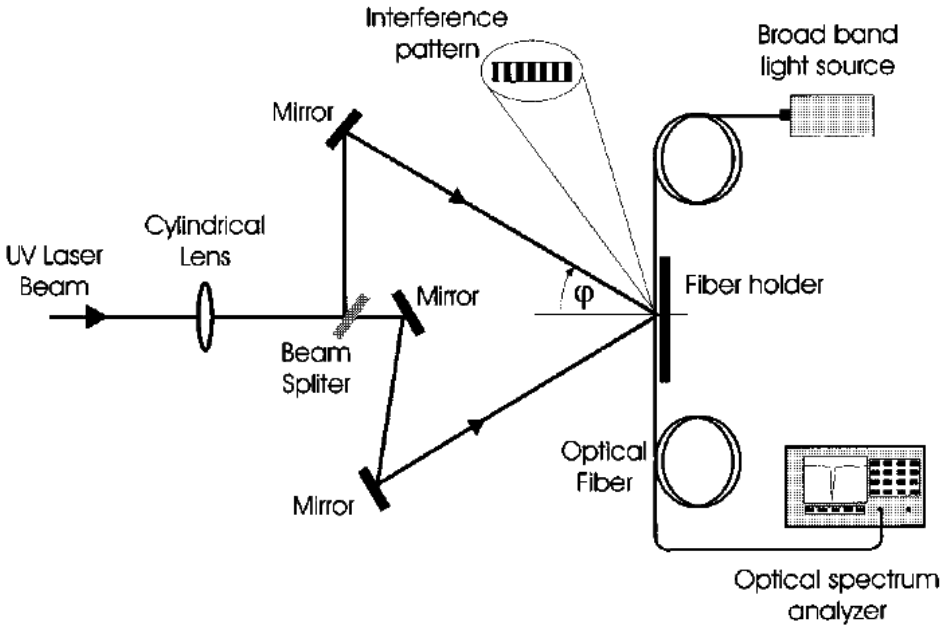

Figure 1.1 Amplitude-splitting interferometer

The period of the grating is given by

$$\Lambda = \frac{\lambda_w}{2 \sin \varphi}, \tag{1.1}$$

where λw , is the UV wavelength and φ is the half-angle between the intersection UV beams [31]. Although the interference pattern is formed in glass within the core of the optical fiber, its period is the same as it would be if the beams were interfering in air. This is a result of the refraction of the beams coupled with the shortening of the wavelength as they enter the glass. The Bragg condition $\lambda_B = 2n\Lambda$ states that the Bragg resonance wavelength, λ_B , in the core of the fiber is twice the product of the effective core index, *n*, and the period of the grating [32]. Hence, a Bragg grating resonance wavelength can be represented in terms of the UV writing wavelength and the half-angle between intersecting UV beams as

$$\lambda_B = \frac{n\lambda_w}{\sin \varphi}. \tag{1.2}$$

thus the Bragg grating wavelength can be varied either by changing λw and/or φ. The choice of λw is limited to the UV photosensitivity region of the fiber, however, there is no restriction set on the choice of the angle φ [31].

The most important advantage offered by the amplitude splitting interferometric fabrication technique is the ability to inscribe Bragg gratings at any wavelength. This is accomplished by simply changing the intersecting angle between the UV beams. This method also offers complete flexibility for producing gratings of various lengths, which allows the fabrication of wavelength narrowed or broadened gratings. Furthermore, unique grating geometries, such as linearly chirped gratings, can be produced by using curved reflecting surfaces in the beam delivery path [32].

The main disadvantage of the amplitude-splitting interferometric technique is its susceptibility to mechanical vibrations. Displacements as small as submicrons in the position of mirrors, beam splitter, or mounts in the interferometer can cause the fringe pattern to drift, washing out the grating [33].

Furthermore, due to long separate optical path lengths involved in the interferometers, air currents, which affect the refractive index locally, may cause a problem in the formation of a stable fringe pattern. In addition to the above shortcomings, quality gratings can only be produced with a laser source that has good spatial and temporal coherence with excellent output power stability [34].

1.3.1.2 Wave-front-splitting interferometers

Wave-front splitting interferometers are not as popular as the amplitude splitting interferometers for grating fabrication. However, they have some useful advantages over the amplitude splitting interferometers. Two such wave-front-splitting interferometers that have been used to fabricate Bragg gratings in optical fibers are the prism interferometer and the Lloyd's interferometer [31].

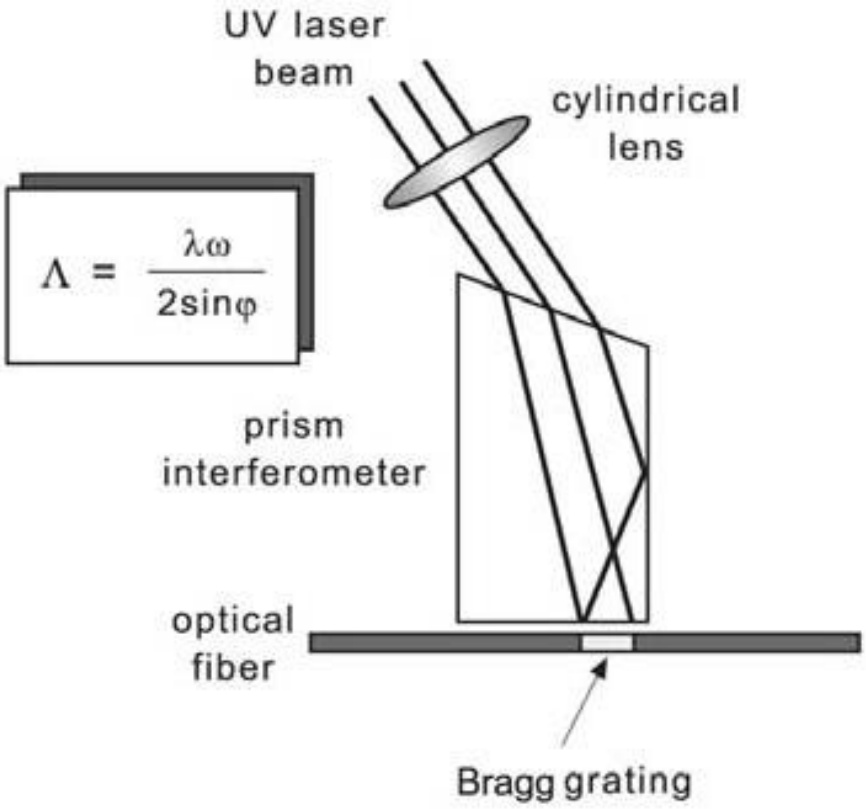

Figure 1.2 Wave-front-splitting interferometer

A schematic of the prism interferometer used in fabricating Bragg grating is shown in Figure 1.2 [31]. The prism is made from high homogeneity ultraviolet-grade fused silica allowing for good transmission characteristics. In this setup, the UV beam is expanded laterally by refraction at the input face of the prism. The expanded beam is spatially

bisected by the prism edge, and half of the beam is spatially reversed by total internal reflection from the prism face. The two half beams are then recombined at the output face of the prism, giving a fringe pattern parallel to the photosensitive fiber core. A cylindrical lens placed just before the setup helps in forming the interference pattern on a line along the fiber core [31]. The experimental setup for fabricating gratings with the Lloyd interferometer is shown in Figure 1.3 [31].

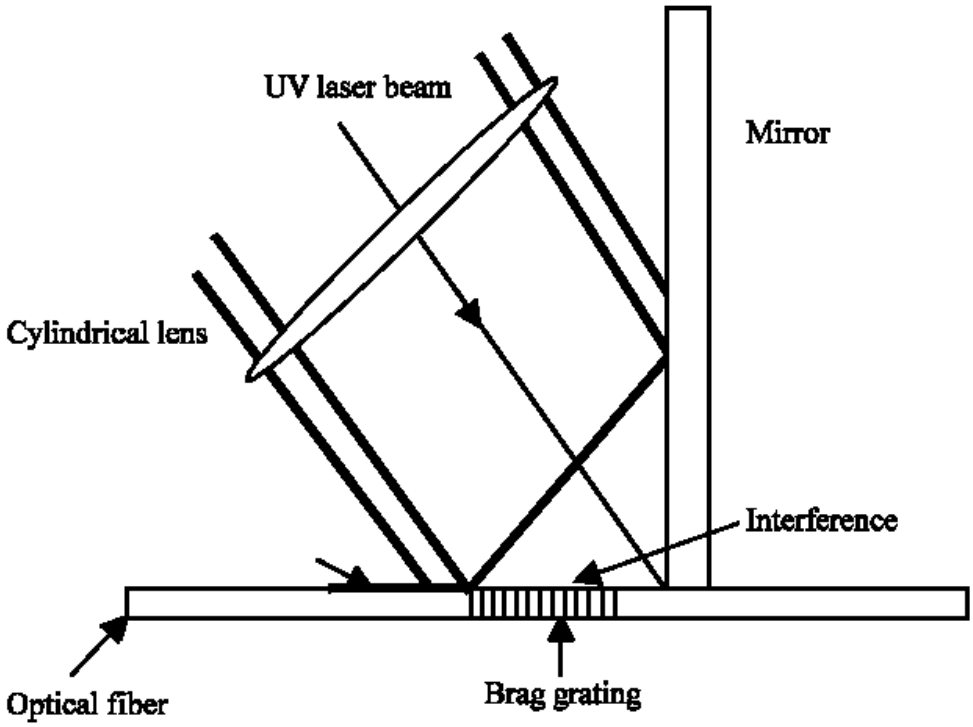

Figure 1.3: Experimental setup for Lloyd interferometer

This interferometer consists of a dielectric mirror, which directs half of the UV beam to a fiber that is perpendicular to the mirror. The UV beam is centered at the intersection of the mirror surface and fiber. The overlap of the direct and deviated portions of UV beam creates interference fringes normal to the fiber axis. As in the case of the previous interferometers, a cylindrical lens is usually placed in front of the system to focus the fringe pattern along the core of the fiber. A key advantage of the wave-front-splitting interferometers is that only one optical component is used. This greatly reduces the sensitivity to mechanical vibrations. In addition, the short distance where the UV beams are separated reduces the wave-front distortion induced by air currents and temperature differences between the two interfering beams [31]. Furthermore, this assembly can be rotated easily to vary the angle of intersection of the two beams for wavelength tuning. One disadvantage of this system is the limitation on the grating length, which is restricted

to half of the beam width. Another disadvantage is the range of Bragg wavelength tunability, which is restricted by the physical arrangement of the interferometers. That is, as the intersection angle increases, the difference between beam path lengths increases. Therefore, the beam coherence length limits the Bragg wavelength tunability [36].

Laser sources used for inscribing Bragg gratings via the above interferometric techniques must have good temporal and spatial coherence. The spatial coherence requirements can be relaxed in the case of the amplitude-split interferometer by simply making sure that the total number of reflections are the same in both arms. This is especially critical in the case where a laser with low spatial coherence, like an excimer laser, is used as the source of UV light. The temporal coherence has to be at least the length of the grating in order for the interfering beams to have a good contrast ratio, thus, resulting in good quality Bragg gratings. The above coherence requirement together with the UV wavelength range needed forced researchers to initially use very complicated laser systems [31]. One such system consisted of an excimer pumped tunable dye laser, operating in the range of 480–500 nm. The output from the dye laser was focused on a nonlinear crystal to double the frequency of the fundamental light.

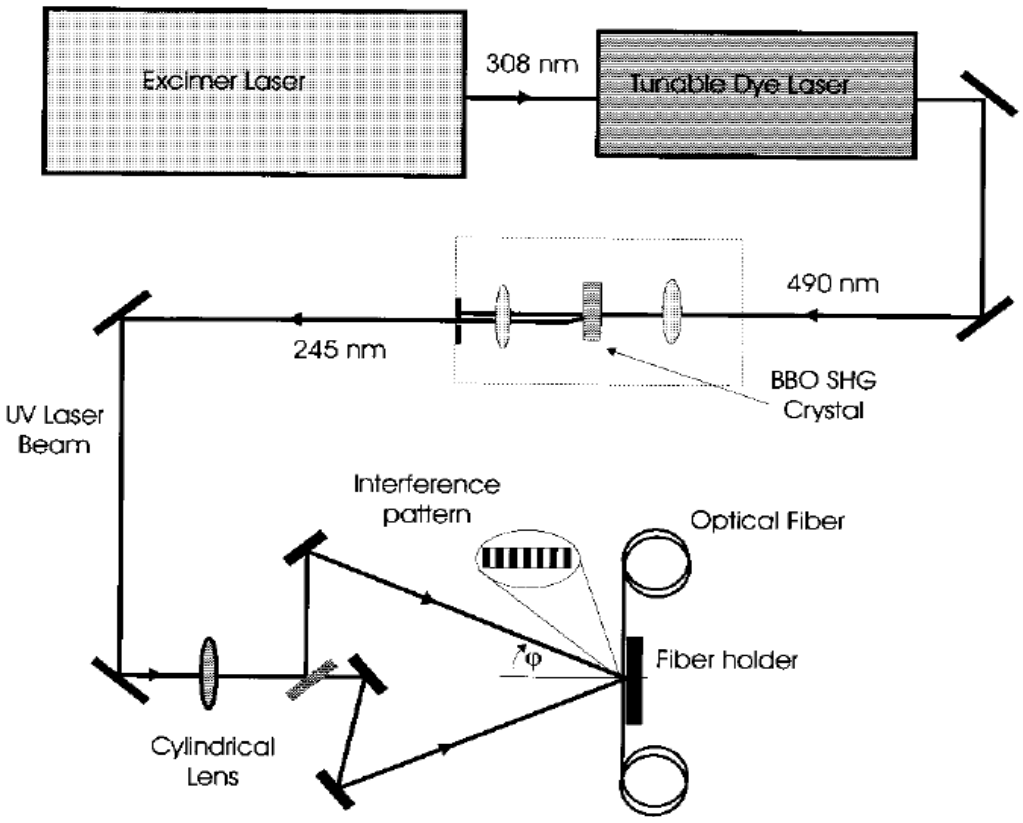

Figure 1.4 Experimental setup for Excimer Laser

Typically, this arrangement provided 10–20 ns pulses depending on the excimer pump laser [32], and of power 3–5 mJ with excellent temporal and spatial coherence. An alternative to this elaborate and often troublesome setup was a specially designed excimer laser that had a long temporal coherence length. These spectrally narrow linewidth excimer lasers could operate for extended periods of time on the same gas mixture with little changes in their characteristics. Commercially available narrow linewidth excimer systems were complicated oscillator amplifier configurations, which made them extremely costly. Othonos and Lee developed a low-cost simple technique where existing KrF excimer lasers may be retrofitted with a spectral narrowing system for inscribing Bragg gratings in a side written interferometric configuration. In that work, a commercially available KrF excimer laser Lumonics Ex-600 was modified to produce a spectrally narrow laser beam as shown in Figure 1.5 with a linewidth of approximately $4x10^{-12}$ m [33].

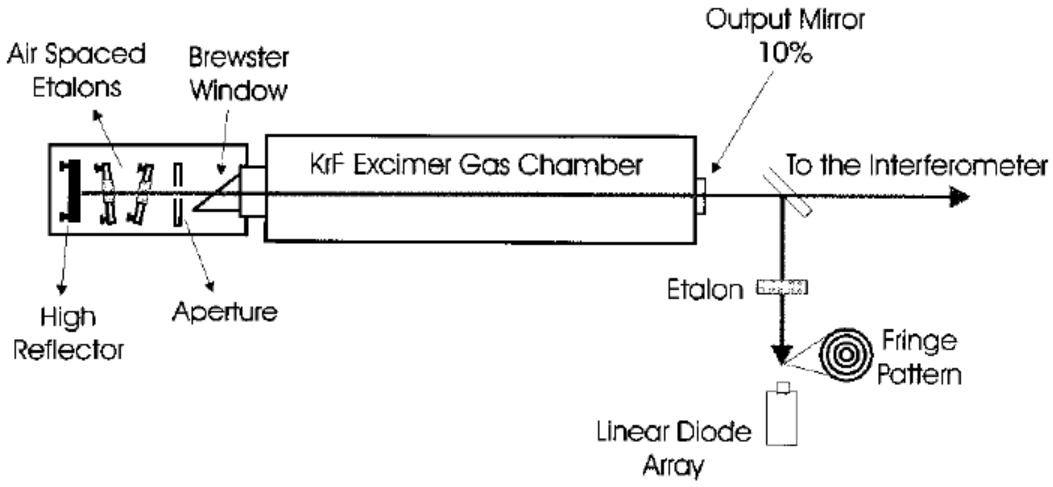

Figure 1.5 KrF excimer laser

This system was used to successfully inscribe Bragg gratings in photosensitive optical fibers. An alternative to the above system was the intracavity frequency-double argon ion laser that uses beta-barium borate. This system efficiently converted high-power visible laser wavelengths into deep ultraviolet 244 and 248 nm. The characteristics of these lasers include unmatched spatial coherence, narrow linewidth and excellent beam pointing

stability, which make such systems very successful in inscribing Bragg gratings in optical fibers [31].

1.3.2 Phase mask technique

One of the most effective methods for inscribing Bragg gratings in photosensitive fiber is the phase-mask technique. This method employs a diffractive optical element phase mask to spatially modulate the UV writing beam. Phase masks may be formed holographically or by electron-beam lithography [37].

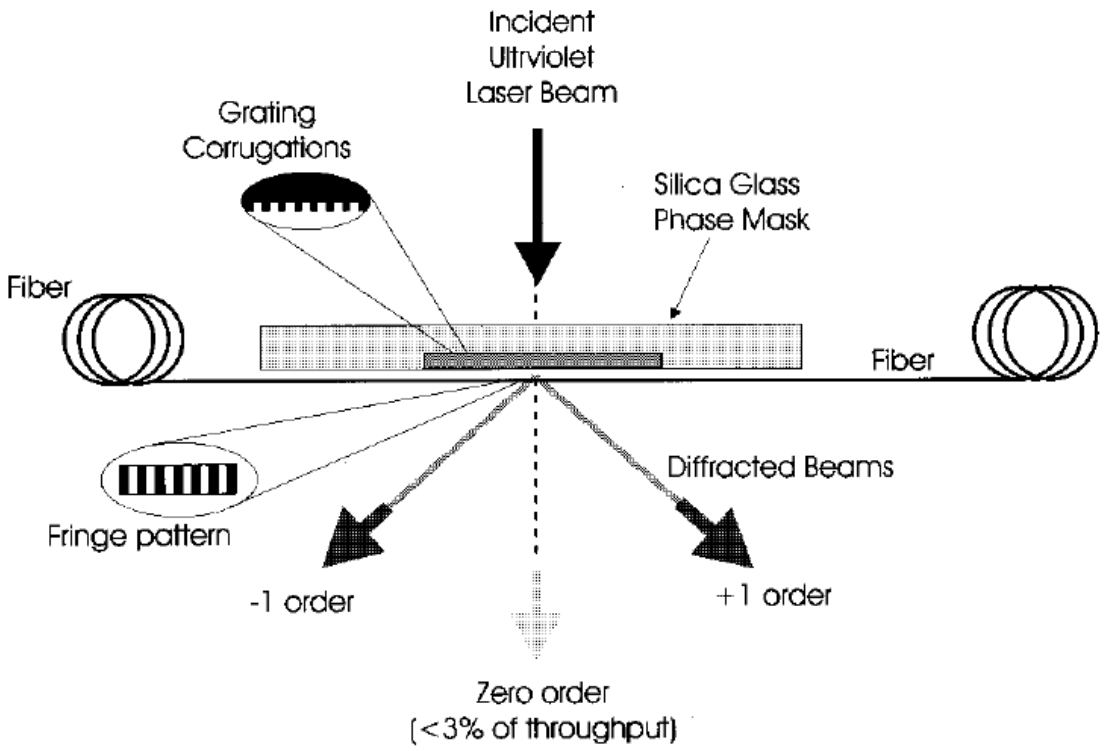

Figure 1.6 Phase mask technique

Holographically induced phase masks have no stitch error, which is normally present in the electron-beam phase masks. However, complicated patterns can be written into the electron beams fabricated masks quadratic chirps, Moire patterns, etc.

The phase-mask grating has a one-dimension surface-relief structure fabricated in a high-quality fused silica flat transparent to the UV writing beam. The profile of the periodic gratings is chosen such that when an UV beam is incident on the phase mask, the zero-order diffracted beam is suppressed to less than a few percent typically, less than 5% of

the transmitted power. In addition, the diffracted plus and minus first orders are maximized; each containing, typically, more than 35% of the transmitted power [36].
A near-field fringe pattern is produced by the interference of the plus and minus first-order diffracted beams. Experimental setup is of an excimer pump dye laser with a frequency doubled BBO crystal for generating UV light at 245 nm for inscribing Bragg gratings in an interferometer minus first-order diffracted beams. The period of the fringes are one-half that of the mask. The interference pattern photoimprints a refractive-index modulation in the core of a photosensitive optical fiber placed in contact with or in close proximity immediately behind the phase mask. A cylindrical lens may be used to focus the fringe pattern along the fiber core.

The phase mask greatly reduces the complexity of the fiber grating fabrication system. The simplicity of using only one optical element provides a robust and an inherently stable method for reproducing Fiber Bragg Gratings. Since the fiber is usually placed directly behind the phase mask in the near field of the diffracting UV beams, sensitivity to mechanical vibrations and, therefore, stability problems are minimized. Low temporal coherence does not effect the writing capability as opposed to the interferometric technique due to the geometry of the problem. KrF excimer lasers are the most common UV sources used to fabricate Bragg gratings with a phase mask.

The UV laser sources, typically, have low spatial and temporal coherence. The low spatial coherence requires the fiber to be placed in near contact to the grating corrugations on the phase mask in order to induce maximum modulation in the index of refraction. The further the fiber is placed from the phase mask, the lower the induced index modulation, resulting in lower reflectivity Bragg gratings. Clearly, the separation of the fiber from the phase mask is a critical parameter in producing quality gratings. However, placing the fiber in contact with the fine grating corrugations is not desirable due to possible damage to the phase mask. Improving the spatial coherence of the UV writing beam not only improves the strength and quality of the gratings inscribed by the phase-mask technique, it also relaxes the requirement that the fiber has to be in contact with the phase mask [36,37].

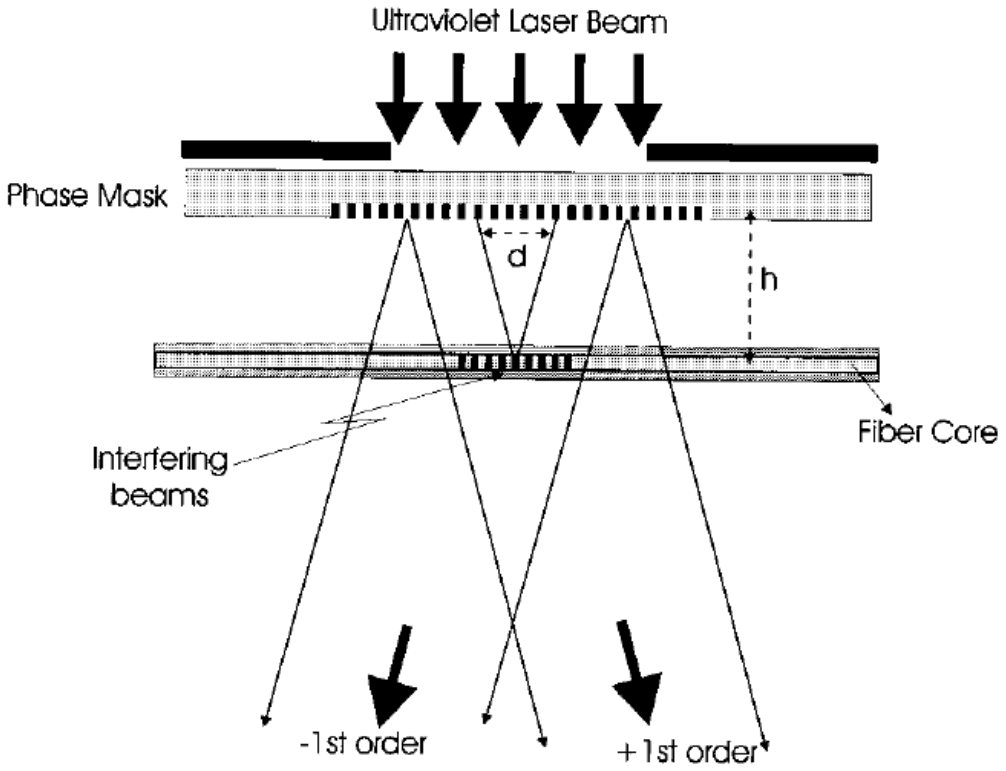

Figure 1.7: Schematic for Phase mask technique

To understand the significance of spatial coherence in the fabrication of Bragg grating using the phase-mask technique, it is helpful to consider a simple schematic diagram. Consider the fiber core to be at a distance h from the phase mask. The transmitted plus and minus first orders that interfere to form the fringe pattern on the fiber emanate from different parts of the mask separated by distance *d*. Since the distance of the fiber from the phase mask is identical for the two interfering beams, the requirement for temporal coherence is not critical for the formation of a high contrast fringe pattern [31].

On the other hand, as the distance *h* increases, the separation *d* between the two interfering beams emerging from the mask, increases. In this case, the requirement for good spatial coherence is critical for the formation of a high contrast fringe pattern. As the distance *h* extends beyond the spatial coherence of the incident UV beam, the interference fringe contrast will deteriorate, eventually resulting in no interference at all. The spatial coherence uses a KrF laser irradiated phase mask to form gratings in polyimide film. One of the advantages of not having to position the fiber against the phase mask is the freedom to be able to angle the fiber relative to the mask forming blazed gratings. Placing one end of the exposed fiber section against the mask and the

other end at some distance form the mask, it is possible to change the induced Bragg grating center wavelength. From simple geometry, one can derive a general expression for the tunability of the Bragg grating center wavelength [36], given by:

$$\lambda_B = 2n\Lambda\sqrt{1+\left(\frac{r}{l}\right)^2}, \tag{1.3}$$

where Λ is the period of the fiber grating, r is the distance from one end of the exposed fiber section to the phase mask, and l is the length of the phase grating. For a fixed phase mask period changing r will result in blazed gratings with changing center Bragg wavelength [31].

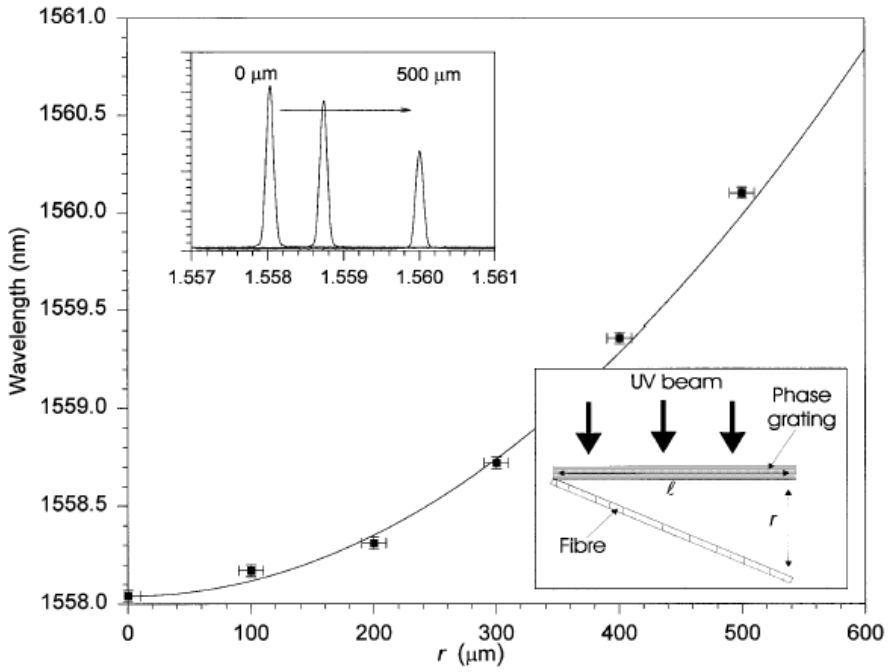

Figure 1.8 Theoretical curve for the tunability of the inscribed Bragg grating

Figure 1.8 shows the theoretical curve for the tunability of the inscribed Bragg grating as a function of distance r. The experimental values for the peak reflectivities of the Bragg gratings are also shown for different r values [31].

1.3.3 Point-by-point fabrication of Bragg gratings

The point-by-point technique for fabricating Bragg gratings is accomplished by inducing a change in the index of refraction a step at a time along the core of the fiber. Each grating plane is produced separately by a focused single pulse from an excimer laser. A single pulse of UV light from an excimer laser passes through a mask containing a slit. A

focusing lens images the slit onto the core of the optical fiber from the side, and the refractive index of the core in the irradiated fiber section increases locally. The fiber is then translated through a distance L corresponding to the grating pitch in a direction parallel to the fiber axis and the process is repeated to form the grating structure in the fiber core. Essential to the point-by-point fabrication technique is a very stable and precise submicron translational system [31].

The main advantage of the point-by-point writing technique lies in its flexibility to alter the Bragg grating parameters as the grating structure is built up a point at a time. Variations in grating length, grating pitch, and spectrum are possible. Experimental result of tuning a Bragg grating by tilting the writing fiber response can easily be incorporated. Chirped gratings can be produced accurately simply by increasing the amount of fiber translation each time the fiber is irradiated. The point-by-point method allows for the fabrication of spatial-mode converters and polarization-mode converters or rocking filters that have grating periods, L, ranging from tens of micrometers to tens of millimeters. Because the UV pulse energy can be varied between points of induced index change, the refractive-index profile of the grating can be tailored to provide any desired spectral response.

One disadvantage of the point-by-point technique is that it is a tedious process. Because it is a step-by-step procedure, this method requires a relatively long process time. Errors in the grating spacing due to thermal effects and/or small variations in the fiber's strain can occur. This limits the gratings to a very short length. Typically, the grating period required for first-order reflection at 1550 nm is approximately 530 nm. Because of the submicron translation and tight focusing required, first-order 1550 nm Bragg gratings have yet to be demonstrated using the point-by-point technique [32].

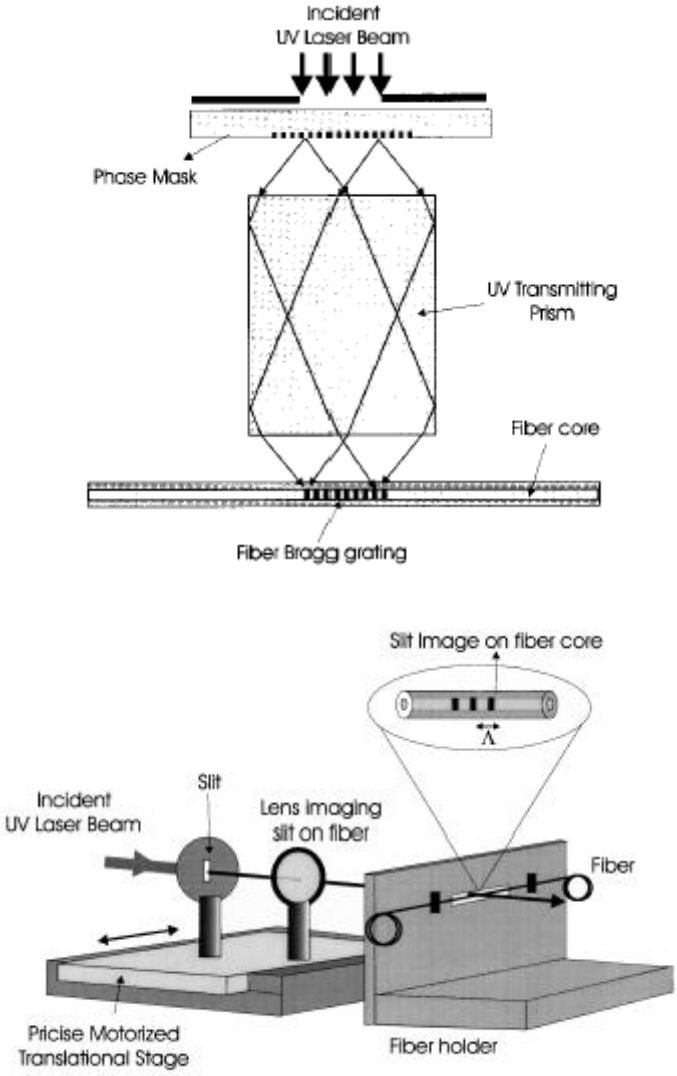

Figure 1.9 Point-by-point technique

1.3.4 Mask image projection

In addition to the above well-known techniques for fabricating Fiber Bragg Gratings, high-resolution mask projection has been demonstrated as a means of inscribing Bragg gratings in optical fiber using excimer laser pulses. The mass projection system consists of a excimer laser source generating an UV beam, which is incident on a transmission mask. In these experiments, the transmission mask consisted of a series of UV opaque line spaces. The transmitted beam was imaged onto the fiber core by a multi-component fused silica high-resolution system having a demagnification of 10:1. Using this technique, gratings with periods of 1, 2, 3, 4, and 6 μm have been written in single-mode Ge doped fiber using mask-imaging techniques. Because of the simplicity of the source and setup, the recording of coarse period gratings by mask-imaging exposures, in some

cases, may be more flexible than other techniques. Complicated grating structures like blazed, chirped, etc. can be readily fabricated with this method by implementing a simple change of mask [37].

1.4 Types of Fiber Bragg Gratings

There are several distinct types of Fiber Bragg Grating structures such as the common Bragg reflector, the blazed Bragg grating, and the chirped Bragg grating. These Fiber Bragg Gratings are distinguished either by their grating pitch, spacing between grating planes or tilt angle between grating planes and fiber axis. The most common Fiber Bragg Grating is the Bragg reflector, which has a constant pitch. The blazed grating has phase fronts tilted with respect to the fiber axis, that is, the angle between the grating planes and the fiber axis is less than 90°. The chirped grating has an aperiodic pitch, that is, a monotonic increase in the spacing between grating planes.

1.4.1 Common Bragg reflector

The common Bragg reflector was the first intracore fiber grating inscribed using the self-induced writing method. Depending on the parameters such as grating length and magnitude of induced index change, the Bragg reflector can function as a narrow-band transmission or reflection filter or a broadband mirror. In combination with other Bragg reflectors, these devices can be arranged to function as bandpass filters. Bragg reflectors are considered as excellent strain and temperature sensing devices because the measurements are wavelength encoded. This eliminates the problems of amplitude or intensity fluctuations that exist in many other types of fiber sensors. Since each Bragg reflector can be designated with its own wavelength-encoded signature, a series of these gratings can be written on the same fiber, each having a distinct Bragg resonance signal. This configuration can be used for wavelength division multiplexing or quasidistributed sensing. These gratings have also been demonstrated to be very useful components in tunable fiber or semiconductor lasers. It serves as one or both ends of the laser cavity, depending on the laser configuration, and it tunes the laser wavelength by varying the Bragg resonance feedback signal. Continuously tunable single-mode erbium fiber laser was made using these gratings. In this laser system, two Bragg reflectors were used in a Fabry–Perot configuration. Continuous tunability, without mode hopping, was achieved when both the gratings and enclosed fiber were stretched uniformly [31].

Bragg grating fiber lasers can also be used as sensors where the Bragg reflector serves the dual purpose of tuning element and sensor. A series of Bragg reflectors having distinct wavelength-encoded signatures can be multiplexed in a fiber laser sensor configuration for multipoint sensing.

1.4.2. Blazed Bragg gratings

Tilting or blazing the Bragg grating planes at angles to the fiber axis will result in light that is otherwise guided in the fiber, to be coupled out of the fiber core into loosely bound guided cladding modes or into radiation modes outside the fiber. The tilt of the grating planes and strength of the index modulation determines the coupling efficiency and bandwidth of the light that is tapped out. The criterion to satisfy the Bragg condition of a blazed grating is similar to that of the Bragg reflector that was analyzed earlier. Erbium-doped fiber amplifiers that use these gratings are now an integral part of long-haul high-bit-rate communication systems and are finding applications in areas of wide bandwidth amplification. Another interesting application of blazed gratings is in mode conversion. Mode converters are fabricated by inducing a periodic refractive-index perturbation along the fiber length with a periodicity that bridges the momentum mismatch between the modes to allow phase-matched coupling between the selected modes. Different grating periods are used for mode conversion at different wavelengths [31].

1.4.3. Chirped Bragg grating

A chirped Bragg grating is a grating that has a monotonically varying grating period. This can be realized by axially varying either the period of the grating L or the index of refraction of the core or both. Chirped gratings have been written in optical fibers using various methods. A double exposure technique has been used in forming a 1.5 cm long chirped grating. The effective mode index of the waveguide was modulated linearly over the grating length with radiation from an excimer laser and then the same length was re-exposed with a phase mask to produce a linearly chirped grating. A chirp of 0.4 nm was demonstrated at 1549 nm. The delay induced by the gratings was shown to be approximately 120 ps over the entire bandwidth of the grating.

A highly repeatable and simple technique for producing chirped gratings is based on the phase mask where the linear chirp is approximated by a step chirp. In this technique, a cascade of several gratings with increasing period is used to simulate a long chirped grating. The chirped structure is initially inscribed on the phase mask and then the mask is

used to fabricate the chirped Bragg gratings in the photosensitive fiber. Clearly, this is a highly repeatable and controllable technique for producing any type of chirped Bragg structure in fiber.

For forward propagating light, longer wavelengths travel further into the grating before being reflected. With the introduction of an erbium-doped amplifier in long-haul high-bit-rate communication systems, the main limitation in transmitting over such distance is the pulse broadening caused by chromatic dispersion. Dispersion induced pulse broadening can be eliminated by an element having a dispersion of opposite sign and equal magnitude to that of the optical fiber link. In a chirped grating, the resonant frequency is a linear function of the axial position along the grating so that different frequencies, present in the pulse, are reflected at different points and, thus, acquire different delay times. Chirped gratings, therefore, can be used as dispersion compensators to compress temporally broadened pulses.

In telecommunication systems, residual pump light emitted from an optical fiber amplifier can cause major problems. The performance of a receiver can be adversely affected by the residual pump power emitted from a preamplifier because it can cause excess noise and receiver saturation. The fiber amplifier performance can be improved by reflecting back the unabsorbed pump light at the amplifier output. Broadband chirped Fiber Bragg Grating can be used for pump rejection and recycling of unabsorbed pump light from an erbium-doped fiber amplifier [31].

1.4.4. Type II Bragg gratings and Novel Bragg gratings

In an experiment carried out to study the relationship between pulse energy and grating strength, a series of single pulse gratings were produced with an UV excimer laser beam. The UV beam was focused to an area of approximately 1530.3 mm^2 at the fiber. The peak-to-peak index modulation of each grating was estimated from its reflection spectrum using coupled-mode theory. It is apparent that there is a sharp threshold at a pulse energy of 30 mJ, above which the induced index modulation increases dramatically. Doubling the pulse energy from 20 to 40 mJ results in an increase in the photoinduced index modulation by almost three orders of magnitude. Below the threshold point, the index modulation seems to grow linearly with energy density, whereas above the index modulation it appears to saturate. The gratings formed with a low index of refraction modulation were labeled as type I and those formed with a high index of refraction modulation were called type II. There is a critical level of absorbed energy, which triggers off a highly nonlinear mechanism, initiating dramatic changes in the optical fiber.

Examination of a type II grating with an optical microscope revealed a damaged track at the core-cladding interface. This damage track appears only in type II gratings, which suggests that it may be responsible for the large index change. The fact that this damage is localized on one side of the core suggests that most of the UV light has been absorbed, most likely never reaching the other side. A characteristic of type II Bragg gratings is that they have a very high reflectivity and large bandwidth. The irregularities in the spectra are a sign of grating nonuniformity, which is because of the nonuniformities in the intensity profile of the excimer laser writing beam. In addition, type II gratings transmit wavelengths longer than the Bragg center wavelengths but strongly couple shorter wavelengths into the cladding, permitting the gratings to act as effective wavelength selective taps. Results of stability tests have shown type II gratings to be extremely stable at elevated temperatures. At 800 °C over a period of 24hrs, no degradation in grating reflectivity was evident. At 900 °C, the grating reflectivity decays quite slowly until a permanent component appears. At 1000 °C, most of the grating disappears after 4 hrs. The mechanism behind high-reflectivity type II single-pulse gratings differs from the usual type I mechanism [31]. The superior temperature stability of type II gratings make them useful for sensing applications in hostile environments. One of the most attractive features of type II gratings is that highly reflective gratings can be formed in just a few nanoseconds i.e. duration of a single excimer pulse. This is of great practical importance for large-scale mass production of strong gratings during the fiber drawing process before application of the protective polymer coating. One distinct advantage of producing Fiber Bragg Gratings during the draw process is that in-line fabrication avoids potential contact with the pristine outer surface of the glass. Whereas, off-line fabrication requires a section of the fiber to be stripped off its UV absorbing polymer coating, in order for the grating to be exposed. This drastically weakens the fiber at the site of the grating due to surface contamination, even if the fiber is subsequently recoated [31].

Superimposed multiple Bragg gratings basically perform a comb function, this device is ideally suited for multiplexing and demultiplexing signals. This device is that it does not require much space because all the gratings are written at the same location of the fiber. This lends itself to optical integrated technology, where the issue of size is always a concern, and can also be used for material detection where the multiple Bragg lines can be designed to match the signature frequencies of a given material. Another interesting observation is that the center wavelength of the existing Bragg gratings shifted to longer wavelengths each time a new grating was inscribed due to a change of the effective index

of refraction. Superstructure Bragg grating is referred to a grating fiber structure fabricated with a modulated exposure over the length of the gratings. One such approach was to translate the UV writing beam along a fiber and phase-mask assembly while the intensity of the beam was modulated. An excimer pumped dye laser was used with a frequency doubler to produce 2.0 mJ at 240 nm. Hydrogenated, single-mode, boron codoped fiber was placed in near contact with a phase mask, and the ultraviolet light was focused through the phase mask into the fiber core by a cylindrical lens, exposing a length of approximately 1 mm. To fabricate a 40 mm long superstructure, the excimer laser was periodically triggered at intervals of 15 s to produce bursts of 150 shots at a repetition rate of 10 Hz, while the ultraviolet beam was translated at a constant velocity of 0.19 mm/s along the mask. The resulting period of the grating envelope was approximately 5.65 mm, forming seven periods of the superstructure. These superstructure gratings can be used as comb filters for signal processing, and for increasing the tunability of the fiber laser grating reflector [31].

Bragg gratings generally act as narrow-band reflection filters centered at the Bragg wavelength because of the stop band associated with a one-dimensional periodic medium. Many applications, such as channel selection in a multichannel communication system, would benefit if the fiber grating could be designed as a narrow-band transmission filter. Although techniques based on Michelson and Fabry–Perot interferometers have been developed for this purpose, their use requires multiple gratings and may introduce additional losses. A technique commonly used in distributed feedback semiconductor lasers can be used to tailor the transmission spectrum to suit specific requirements. The technique consists of the introduction of phase shift across the fiber grating whose location and magnitude can be adjusted to design a specific transmission spectrum. One of the most obvious applications includes production of very narrowband transmission and reflection filters. Moreover, multiple phase shifts can be introduced to produce other devices such comb filters. They can also be used to obtain single-mode operation of DFB fiber lasers.

1.5 Properties of Bragg gratings

In its simplest form, a Fiber Bragg Grating consists of a periodic modulation of the index of refraction in the core of a single-mode optical fiber. These types of uniform fiber gratings, where the phase fronts are perpendicular to the fiber longitudinal axis and the

grating planes are of a constant period, are considered the fundamental building blocks for most Bragg grating structures[31].

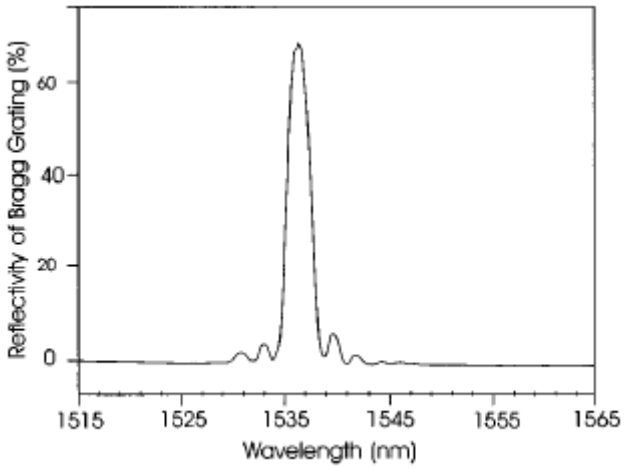

Figure 1.10 Spectral response of FBG

Light guided along the core of an optical fiber will be scattered by each grating plane. If the Bragg condition is not satisfied, the reflected light from each of the subsequent planes becomes progressively out of phase and will eventually cancel out. Where the Bragg condition is satisfied, the contributions of reflected light from each grating plane add constructively in the backward direction to form a back-reflected peak with a center wavelength defined by the grating parameters. The Bragg grating condition is simply the requirement that satisfies both energy and momentum conservation. Energy conservation requires that the frequency of the incident radiation and the reflected radiation is the same. Momentum conservation requires that the incident wave vector, $\mathbf{k}_i$, plus the grating wave vector, **K**, equal the wave vector of the scattered radiation $\mathbf{k}_f$, this is simply stated as

$$\mathbf{k_i}+\mathbf{K} = \mathbf{k_f} \qquad (1.4)$$

where the grating wave vector, **K**, has a direction normal to the grating planes and it has a magnitude 2 p/L, L is the grating spacing [31].

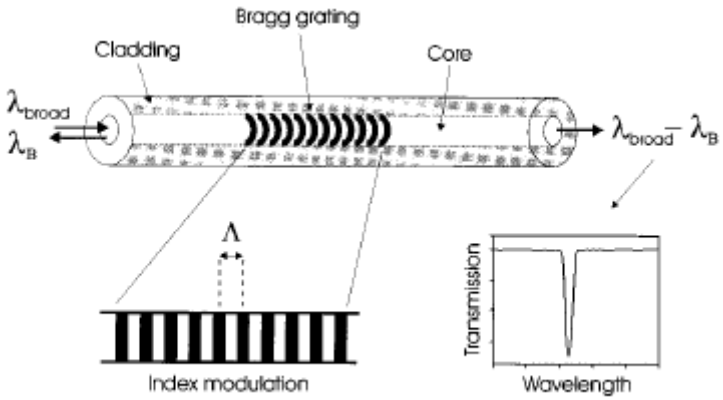

Figure 1.11Transmission Spectra of FBG

The diffracted wave vector is equal in magnitude but opposite in direction to the incident wave vector. Hence, the momentum conservation condition becomes [32]

$$2\left(\frac{2\pi n}{\lambda_B}\right) = \frac{2\pi}{\Lambda}, \tag{1.5}$$

which simplifies to the first-order Bragg condition

$$\lambda_B = 2n\Lambda, \tag{1.6}$$

where the Bragg grating wavelength, λ_B , is the free-space-center wavelength of the input light that will be back reflected from the Bragg grating, and n is the effective refractive index of the fiber core at the free-space-center-wavelength[37]. Software tools are available for simulating Fiber Bragg Gratings [38-41].

1.6 Features

- Bragg Gratings have low insertion losses and are compatible with existing optical fibers used in telecommunication networks.
- Bragg Gratings allow low-cost manufacturing of very high quality wavelength-selective optical devices.
- Phase masks used to photo-imprint the Gratings allow manufacturing that is relatively simple, flexible, low-cost and large-volume.

1.7 Applications

Bragg Gratings have proven attractive in a wide variety of optical fiber applications, such as [2-30]:

- Narrowband and broadband tunable filters
- Optical fiber mode converters
- Wavelength selective filters, multiplexers, and add/drop Mach-Zehnders
- Dispersion compensation in long-distance telecommunication networks
- Gain equalization and improved pump efficiency in erbium-doped fiber amplifiers
- Spectrum analyzers
- Specialized narrowband lasers
- Optical strain gauges in bridges, building structures, elevators, reactors, composites, mines and smart structures

It is evident that the demand for more bandwidth in telecommunication networks has rapidly increased the development of new optical components and devices. Current efforts of research and development are aiming at increasing the total capacity of optical fibers as a medium and improving long haul optical transmission systems using new innovative technologies such as ultra-dense wavelength division multiplexing (WDM). The advances in the optical communications have been synergised by development of efficient and powerful optical components which eliminate the need of costly conversions from optical to electrical signal and back. Fiber Bragg Gratings have been vital in the phenomenal growth of some of these products and are recognized as one of the most significant enabling technologies for fiber optic communications.

1.8 Gaps in Present Study

From the Literature Survey as presented in Chapter 2 it follows:

- No existing work has been done in which simulation of Fiber Bragg Gratings has been validated.
- No existing work has yet taken into account the effect of refractive index modulation profile in analysis of wavelength shift of Fiber Bragg Gratings.

- Design of Fiber Bragg Grating Interrogator is still in infancy. The existing solutions use bulky Optical components which are very expensive.

1.9 Problem Formulation

- Extensive literature survey has been conducted to study the literature available in the field of Fiber Bragg Gratings, their production techniques, characterisation and simulation.
- There is a need to study Wavelength Shift by simulating external perturbation to the Fiber Bragg Grating.
- Model has to be constructed and then coding for the simulation is required. Iterations have to be performed and the results have to be validated against practical experimental work to fine tune the simulation.

1.10 Objectives of proposed work

- To simulate Fiber Bragg Gratings and validate results using theoretical / experimental work
- To study wavelength shift in Fiber Bragg Gratings on simulated external perturbation using a wideband source.
- To design Fiber Bragg Grating Interrogator for Sensor/Communication systems.

1.11 Major contribution of Thesis

Although Fiber Bragg Gratings have many potential applications in the field of communications and sensors but without the interrogation unit it is not possible to offer Fiber Bragg Grating Based systems. Since the present work not only deals with the theoretical aspects of Fiber Bragg Gratings it also leads to the development of simulation tools and Interrogation System which can be used in the area of communications and sensors.

1.11.1 Contribution in the field of communications

The primary application of Fiber Bragg Gratings is in optical communications systems. They are specifically used as notch filters. They are also used in optical multiplexers and demultiplexers with an optical circulator, or Optical Add-Drop Multiplexer (OADM). A

demultiplexer can be achieved by cascading multiple drop sections of the OADM, where each drop element uses a FBG set to the wavelength to be demultiplexed. Conversely, a multiplexer can be achieved by cascading multiple add sections of the OADM. FBG demultiplexers and OADMs can also be tunable. In a tunable demultiplexer or OADM, the Bragg wavelength of the FBG can be tuned by strain applied by a piezoelectric transducer. The sensitivity of a FBG to strain is discussed below in Fiber Bragg Grating sensors.

1.11.2 Contribution in the area of Fiber Bragg Grating sensors

As well as being sensitive to strain, the Bragg wavelength is also sensitive to temperature. This means that Fiber Bragg Gratings can be used as sensing elements in optical fiber sensors. In a FBG sensor, the measurand causes a shift in the Bragg wavelength, $\Delta\lambda_B$. The relative shift in the Bragg wavelength, $\Delta\lambda_B / \lambda_B$, due to an applied strain (ε) and a change in temperature (ΔT) is approximately given by,

$$\left[\frac{\Delta\lambda_B}{\lambda}\right] = C_S\epsilon + C_T\Delta T \quad , \tag{1.7}$$

or,

$$\left[\frac{\Delta\lambda_B}{\lambda}\right] = (1 - p_e)\epsilon + (\alpha_\Lambda + \alpha_n)\Delta T \quad . \tag{1.8}$$

Here, C_S is the coefficient of strain, which is related to the strain optic coefficient p_e. Also, C_T is the coefficient of temperature, which is made up of the thermal expansion coefficient of the optical fiber, α_Λ, and the thermo-optic coefficient, α_n.

Fiber Bragg Gratings can then be used as direct sensing elements for strain and temperature. They can also be used as transduction elements, converting the output of another sensor, which generates a strain or temperature change from the measurand, for example Fiber Bragg Grating gas sensors use an absorbent coating, which in the presence of a gas expands generating a strain, which is measurable by the grating. Technically, the absorbent material is the sensing element, converting the amount of gas to a strain. The Bragg grating then transduces the strain to the change in wavelength.

Specifically, Fiber Bragg Gratings are finding uses in instrumentation applications such as seismology, and as downhole sensors in oil and gas wells for measurement of the effects of external pressure, temperature, seismic vibrations and inline flow measurement. As such they offer a significant advantage over traditional electronic gauges used for these applications in that they are less sensitive to vibration or heat and consequently are far more reliable. The Fiber Bragg Gratings can be used for measuring strain and temperature in composite materials for aircraft and helicopter structures. The Fiber Bragg Grating has to be interrogated in order to provide any sensor application. This thesis deals with not only the simulation of Fiber Bragg Gratings for application in communications and sensor systems abut also gives the design of low cost fiber optic interrogator for achieving this. The design of fiber optic interrogator is further upgraded to mitigate the effect of microbending losses caused in the optical fiber connecting the instrument to the sensor.

1.12 Organisation of Thesis Report

The thesis has been organized into nine chapters. Contents of each chapter are briefly described as under:

After introducing the Fiber Bragg Gratings in Chapter 1 comprehensive literature review and the theory of Fiber Bragg Gratings is presented in Chapter 2. Chapter 3 gives the work done in accomplishing the First Objective of the thesis i.e. Simulation of Fiber Bragg Gratings and Validation of Results using theoretical and experimental work. The theory of Fiber Bragg Gratings starting from the Maxwells condition to the derivation of Bragg Condition has been presented and then the simulation traces have been given. The simulation work has been performed using Matlab and GratingMOD. The traces of simulation have been given in this chapter. Chapter 4 presents the results of the study of wavelength shift in Fiber Bragg Gratings on application of external perturbation. This is the second objective of the thesis work. Three FBGs with different resonance wavelengths of 1549.576, 1548.426 and 1545.826 nm respectively were spliced together and connected to the interrogator in this order to demonstrate three different sensing elements. Chapter 5 covers the design of Fiber Bragg Grating Interrogator which is the third Objective of the thesis work. Chapter 6 presents the improvement in the design of Fiber Bragg Grating Interrogator by introducing the mitigation scheme for microbend losses in the fiber connecting the sensor to the interrogator unit. Chapter 7 describes one

application of the Fiber Bragg Grating System developed which is to detect the Landslides. Chapter 8 describes another application of Fiber Bragg Grating System developed which is to detect the Nitrate concentration in ground water and in the end Conclusion and Future Scope is given in Chapter 9.

Chapter 2
Literature Survey

The formation of permanent gratings in an optical fiber was first demonstrated by Hill *et al*. [32] in 1978 at the Canadian Communications Research Centre (CRC), Ottawa, Ont., Canada. They launched intense Argon-ion laser radiation into a germania-doped fiber and observed that after several minutes an increase in the reflected light intensity occurred which grew until almost all the light was reflected from the fiber. Spectral measurements, done indirectly by strain and temperature tuning of the fiber grating, confirmed that a very narrowband Bragg grating filter had been formed over the entire 1-m length of fiber. This achievement, subsequently called Hill gratings, was an outgrowth of research on the nonlinear properties of germania-doped silica fiber. It established an unknown photosensitivity of Germania fiber, which prompted other inquires, several years later, into the cause of the fiber photo-induced refractivity and its dependence on the wavelength of the light which was used to the form the gratings.

Detailed studies showed that the grating strength increased as the square of the light intensity, suggesting a two-photon process as the mechanism. In the original experiments, laser radiation at 488 nm was reflected from the fiber end producing a standing wave pattern that formed the grating. A single photon at one-half this wavelength, namely at 244 nm in the ultraviolet, proved to be far more effective. Meltz *et al*. [31] showed that this radiation could be used to form gratings that would reflect any wavelength by illuminating the fiber through the side of the cladding with two intersecting beams of UV light; now, the period of the interference maxima and the index change was set by the angle between the beams and the UV wavelength rather than by the visible radiation which was launched into the fiber core. Moreover, the grating formation was found to be orders-of-magnitude more efficient [31].

At first, the observation of photo-induced refractivity in fibers was only a scientific curiosity, but over time it has become the basis for a technology that now has a broad and important role in optical communications and sensor systems. Research into the underlying mechanisms of fiber photosensitivity and its uses is on-going in many

universities and industrial laboratories in Europe, North and South America, Asia, and Australia. Several hundred photosensitivity and fiber grating related articles have appeared in the scientific literature and in the proceedings of topical conferences, workshops, and symposia. FBG's are now commercially available and they have found key applications in routing, filtering, control, and amplification of optical signals in the next generation of high-capacity WDM telecommunication networks. Extensive literature survey was conducted to understand the fundamentals of FBG's, including a description of techniques for grating fabrication and a discussion of those fiber photosensitivity characteristics which underlie grating formation [31].

Kenneth *et al* [31] highlighted the salient properties of periodic, optical waveguide structures that are used in the design of grating filters and gave an overview of their key applications in optical telecommunications and quasidistributed, thermophysical measurement systems. Other articles and reviews of the technology that have appeared include a recent comprehensive article by Bennion *et al* [32]. and survey papers that discuss the physical mechanisms that are believed to be important in photosensitivity and applications of gratings to fiber optic sensors. Subhash *et al*. and Kashyap *et al* [33] demonstrated the use of multiple blazed gratings to flatten the gain spectrum of erbium-doped fiber amplifiers. Eggleton *et al* [32] demonstrated dispersion compensation by pulse compression with the use of a chirped grating.

Chtcherbakov *et al* [31] presented a chirped grating interrogator for Fiber Bragg Grating sensors. The interrogator uses the wavelength dependence of the phase group-delay response of a chirped Fiber Bragg Grating to determine the Bragg wavelength of the sensor. The sensitivity of the interrogator is determined by the selection of the grating length and the bandwidth. The experimental results demonstrated strain measurements over wide range per meter. It was also proposed by Chtcherbakov that multiplexing can be achieved by using an arrayed-waveguide grating that allows the interrogation of more than one grating sensor with a single chirped grating [31].

Lloyd *et al* [31] reported the first resonant-cavity time-division-multiplexed (TDM) Fiber Bragg Grating sensor interrogation system. This novel design uses a pulsed semiconductor optical amplifier in a cyclic manner to function as the optical source, amplifier, and modulator. Compatible with a range of standard wavelength detection

techniques, this optically gated TDM system allows interrogation of low reflectivity commodity sensors spaced just 2 m apart, using a single active component. Results demonstrate an exceptional optical signal-to-noise ratio of 36 dB, a peak signal power of over +7 dBm, and no measurable crosstalk between sensors. Temperature tuning showed that the system was fully stable with a highly linear response [31].

Sano *et al* [31] gave a new type of interrogator for distributed Fiber Bragg Grating (FBG) sensors that employs an arrayed waveguide grating (AWG) and presented its operating features in detail investigated both theoretically and experimentally. The remedy for achieving the linear characteristics of wavelength detection as well as for insuring the reliable and environmentally stable operation of interrogation were also proposed and its usefulness demonstrated in good agreement with the experimental results. The developed interrogator consisted of a fully passive, small, all-solid, rugged optical IC and could detect wavelengths. Chtcherbakov *et al* [31] reported a chirped Bragg grating interrogator for a uniform Bragg grating sensor. The wavelength of light reflected by the sensing grating is a function of strain. The position within the chirped Bragg gating the light is reflected from is a function of its wavelength. This position is determined by amplitude modulating the light source and measuring the phase of the reflected light and thus determining the value of the strain [32].

Geiger *et al* [42] gave a new technique for the interrogation of in-Fiber Bragg Grating sensors using an acousto-optic tunable filter (AOTF). The scheme involved frequency shift keying (FSK) of the RF drive to the AOTF to track the wavelength shifts of a Bragg grating. Experimental results were presented for temperature measurement. This technique provided a frequency-agile system, capable of rapid, random access and very wide tuning range.

Foote *et al* [43] presented work which indicated that the use of embedded Fiber Bragg Gratings as optical sensors for smart sensory structures could be a viable technology. It has been demonstrated that gratings can be embedded routinely without damage into carbon fiber composite material. The harsh embedding conditions do not significantly affect the optical characteristics of the gratings. Once embedded, the gratings act as strain sensors producing measurements consistent with predictions. In this work six embedded,

multiplexed grating sensors detected strain gradients in a loaded composite panel of complex structure.

Patrick *et al* [44] demonstrated a novel sensor which used the difference in strain and temperature response of Fiber Bragg Gratings and a long period fiber grating to discriminate between strain and temperature induced wavelength shifts. Sensor interrogation was performed entirely on the Fiber Bragg Grating reflection signals. Strain and temperature were simultaneously measured to ±9 μstrain and ±1.5°C .

Berkoff *et al* [45] described a multiplexing approach for high-resolution sensing with Bragg gratings. The scheme used a band-pass wavelength division multiplexer to separate the returned wavelengths from an array of gratings, and interferometric processing to attain high-strain resolution. A strain resolution of 1.5 nanostrain was demonstrated, with a sensor bandwidth of 10 Hz-2 kHz for four sensors.

Davis *et al* [46] reported the demonstration of an instrumentation system capable of monitoring a large number of Bragg gratings using a common source and scanning narrowband filter. The system described monitored five arrays of 12 Bragg gratings sensors for a total of 60 sensor elements with μstrain resolution.

Ferreira *et al* [47] presented a pseudoheterodyne, open-loop demodulation technique for detecting wavelength shifts in wavelength encoded Fiber Bragg Grating sensors. The scheme used a processing Bragg grating that is identical to one used as a sensor. When the processing fiber grating was stretched periodically, the system of two gratings produced a carrier at this frequency with its phase modulated by the measurand signal applied to the sensing grating. The demodulation technique was intrinsically immune to fluctuation of optical power in the system and independent of the source spectral profile characteristics. A resolution of ≈1 με/√(Hz) for static axial strain was achieved.

Ezbiri *et al* [48] published that in-fiber written Bragg gratings (FBGs) have been shown to offer many advantages over conventional interferometric and polarimetric sensors in particular for applications requiring embedded sensors. In certain implementations, robust

readout systems were necessary requiring immunity to vibration and the ability to operate at changing temperatures and pressure levels.

These requirements may sometimes rule out the use of established demodulation schemes, or the use of passive optical fibers that are inherently susceptible to temperature fluctuations. Another important parameter of signal processing techniques is the possibility of addressing more than one single sensor. In this article, a passive WDM multiplexed technique for high resolution detection of the wavelength of peak reflection from FBGs was reported. The approach was based on overcoming the low spectral resolution associated with inexpensive grating and linear array CCD detector combinations, which is typically 0.1 nm. Initial results obtained in the laboratories indicated that a resolution of 1 pm could easily be achieved. A demodulation technique based on curve fitting algorithms, that uses short broadband gratings and that can be used with low levels of light at the detector was also reported.

Ferreira *et al* [49] gave a demodulation scheme for Fiber Bragg Grating (FBG) sensors. It was based on the generation of an electrical carrier by using a modulated multimode laser diode to illuminate the fiber grating. The change in Bragg wavelength was measured by tracking the phase of the carrier at the detector output in either an open or a closed-loop scheme. A theoretical analysis of the interrogation technique in terms of linearity and dynamic range was presented. Experimental data were obtained for both strain and temperature measurements. Sensitivities of 0.7 με/√Hz and 0.05°C/√Hz were obtained over a dynamic range of 60 dB. The application of this demodulation scheme to a multiplexed sensing system was also demonstrated.

Gang *et al* [50] demonstrated the higher temperature sensitivity of a Fiber Bragg Grating (FBG) sensor when it is clad with a metal of a large thermal expansion coefficient. With lead (solder) cladding, the sensitivity of Bragg wavelength shift could be enhanced by about five (four) times. A theoretical model was adopted to show quite consistent results. It was found that thermal annealing was crucial for preparing high-quality Fiber Bragg Grating sensors with metal claddings.

Sung *et al* [51] experimentally demonstrated a new approach for the demodulation of a Fiber Bragg Grating (FBG) strain sensor by combining a tilted FBG demodulator with a temperature-independent property and a dual head FBG sensor with a temperature-discriminating property. This technique guaranteed a stable measurement independent of temperature perturbation at both sides of sensor and demodulator without any additional temperature-isolation or temperature-referencing process and had the minimum resolvable strain of 10 μstrain. The ranges of operating temperature at the sensor and at the demodulator which guaranteed a dynamic range of 1800 μstrain corresponding to the wavelength difference 2.2 nm between two notches of the tilted FBG spectrum were from room temperature to 180°C and 140°C, respectively.

Cavaleiro *et al* [52] gave a description of hybrid fiber optic current sensor combining a metal-coated Fiber Bragg Grating with a standard current transformer. Measurements of the RMS current of power lines at 50 Hz with a resolution of 2 mA were demonstrated.

Chan *et al* [53] showed that the wavelength detection accuracy of Fiber Bragg Grating (FBG) sensors was limited by various types of optical noises. For systems which used broadband sources, the received signal power was usually low, resulting in a low signal-to-noise ratio, especially when time-division multiplexing was used to multiplex a large number of sensors. In sensor systems using laser sources, although the signal power was relatively much higher, residual reflections in the system caused interferometric noise, which would limit the wavelength detection resolution. In this paper, Chan *et al* reported the results of their recent investigations on using a digital filtering technique for improving the wavelength detection accuracy in FBG sensors.

Sung *et al* [54] experimentally demonstrated a tilted Fiber Bragg Grating (FBG) demodulator that had a simple and compact scheme. Using this, wavelength-encoded information from a dual head strain sensor was demodulated with high stability and accuracy, independent of temperature perturbation at both sensor and demodulator FBG.

Jaehoon *et al* [55] enhanced the temperature sensitivity of a Fiber Bragg Grating sensor by attaching two metals with different expansion coefficients to it. The temperature sensitivity could be changed by varying the metal lengths. The proposed temperature sensor could be applicable as a high sensitivity temperature sensor .

Spammer *et al* [56] evaluated and use of fiber sensors in civil structures. Fiber Bragg Grating sensors have proved to be very well suited for applications such as structural health and performance monitoring. This paper reported on the use of Bragg gratings for strain measurements in concrete embedded civil structures. Sensors, attached to steel rebar, were characterized and subsequently embedded into the concrete deck of a steel truss bridge.

Sung *et al* [57] introduced a Mach-Zehnder interferometer whose optical path difference was controlled by a tunable optical delay line. Using the interferometer as a demodulator for Fiber Bragg Grating sensors, intensity-based measurement of dynamic strain with a wide range of 0~1880 μstrain and 0~1 kHz was experimentally demonstrated.

Shenping *et al* [58] presented a highly sensitive fiber temperature sensor based on a gain-switched Fabry–Perot semiconductor laser self-seeded from a linearly chirped Fiber Bragg Grating. A temperature resolution of better than 0.1°C was demonstrated. This sensor not only has the advantage of robustness against fluctuating light levels, but also obviates the need for fine wavelength discrimination.

Rochford *et al* [59] showed that the peak reflectance wavelengths of gratings with reflectance maxima separated by less than 2 nm can be accurately determined through a demultiplexing method based on Hilbert transforms of interferograms. It was demonstrated that a wavelength demultiplexing of three Fiber Bragg Gratings (FBG's) with less than 4 pm crosstalk and repeatability and less than 19 pm uncertainty was possible. It was anticipated that a large number of gratings could be demultiplexed with a single broadband source and a single receiving interferometer, provided that the interferogram is sampled at accurate intervals slightly above the Nyquist rate.

Wei *et al* [60] proposed a novel and short (5 mm long) fiber grating based sensor with a fiber grating Fabry-Perot cavity (GFPC) structure was fabricated and tested for simultaneous measurement of strain and temperature. The sensor exhibited unique properties that it possessed two spectral peaks within its main reflection band and the normalized peak power difference, in addition to its peak wavelength shift, it changed linearly with strain or temperature. The accuracy of this particular sensor in measuring

strain and temperature was estimated to be ±30 μs in a range from 0 to 3000 μs and ±0.4°C from 20°C to 60°C, respectively.

Moreira *et al* [61] gave a signal processing scheme for Fiber Bragg Grating sensors based on the utilization of adjacent modes of a multimode laser diode light source which allowed high sensitivity to be obtained over a large measurement range. For strain measurements, a range of 4800 μ; was achieved with a resolution of 0.08 μ;/Hz, yielding a dynamic range of 95 dB.

Chan *et al* [62] reported on the use of a frequency-domain reflectometry technique for multiplexing Fiber Bragg Grating (FBG) sensors. This technique was based on the modulation of light intensity from a broadband source by a swept-frequency RF carrier. Signals from the FBG sensors located at different positions in an array were separated in the frequency-domain and demodulated using a tunable optical filter. A three FBG sensor system was experimentally demonstrated. The potential of the technique for multiplexing a large number of FBG sensors was also discussed.

Youlong *et al* [63] presented a novel Fiber Bragg Grating displacement sensor. Using a uniform density and thickness overlapped dual-isosceles triangular cantilever beam as a strain agent, it was demonstrated both experimentally and theoretically that this sensor is able to automatically compensate for wavelength shifts induced by temperature. The measured sensitivity of this sensor was 0.1051 nm/mm within the working range of -18-18 mm.

Koo *et al* [64] were instrumental in the dense wavelength division multiplexing of Fiber Bragg Grating sensors by combining code division and wavelength division multiplexing schemes. This approach allowed close spectral spacing among Bragg grating sensors without sensor spectral dynamic range limitation.

Koo *et al* [65] also demonstrated dense-wavelength-division multiplexing (DWDM) of Fiber Bragg Grating sensors without sensor spectral dynamic range limitation by combining code-division and wavelength-division multiplexing schemes.

Sung *et al* [66] introduced a novel scheme to obtain the I/Q signals optically using a dual head Fiber Bragg Grating (FBG) sensor and an optical-path-controlled Mach-Zehnder interferometer. Using this scheme as a demodulator for the FBG sensor, intensity-based measurement of dynamic strain was experimentally demonstrated.

Chi *et al* [67] carried out an investigation of the performance of a time-division-multiplexed (TDM) Fiber Bragg Grating (FBG) sensor array using a tunable laser source. The system performance was found limited by the extinction ratio of the optical pulse modulator used for pulse amplitude modulation. Formulas that relate the crosstalk to the extinction ratio of the optical pulse modulator, the modulation parameters of the tunable laser, and the optical path differences among sensing channels were derived. Computer simulation showed that an array of 20 FBG sensors with 3 με resolution could be realized with a commercially available single Mach-Zehnder type optical pulse modulator of -35-dB extinction ratio.

Chan *et al* [68] also reported on the use of frequency-modulated continuous wave (FMCW) techniques for multiplexing Fiber Bragg Grating (FBG) sensors. This technique was based on the modulation of light intensity from a broadband source by a linear swept-frequency RF carrier. Signals from the FBG sensors located at different positions in an array were separated in frequency domain and demodulated using a tunable optical filter. The potential and limitation of the technique were discussed. A three-sensor FMCW multiplexed FBG array of parallel topology and a six-sensor hybrid FMCW/WDM system were experimentally demonstrated with -30 dB crosstalk between sensors and 2 με resolution in terms of root mean square (RMS) strain value.

Jaehoon *et al* [69] in their paper, employed a novel demodulation scheme to monitor the dynamic perturbation of a Fiber Bragg Grating (FBG) sensor using an long-period grating (LPG) pair with erbium-doped fiber (EDF) inserted between the two LPGs. The experimental results showed that the proposed technique features high resolution and much more immunity to temperature perturbation compared to the conventional unbalanced Mach-Zehnder interferometer (MZI).

Sennhauser *et al* [70] modeled mechanical and optical reliability of fibers and Bragg gratings at elevated temperature of up to 250°C and determined parameters in an

extended test program. Stress corrosion and grating decay were investigated for two commercially available Bragg grating types.

Jaejoong *et al* [71] introduced a Fiber Bragg Grating (FBG) laser sensor using a semiconductor optical amplifier (SOA) as gain medium. Experimental results showed good performance of the proposed laser sensor for multi-point sensing.

Seungwoo *et al* [72] proposed a novel Fiber Bragg Grating (FBG) sensor demodulator using fiber birefringence. The demodulator was composed of a polarizing beam splitter (PBS), a polarization controller (PC), and a chirped fiber grating (CFG). In the sensor application of this paper, the CFG was used as a broadband reflection mirror. The experimental results showed that the demodulator had good performance for measuring static and dynamic strain.

Youlong *et al* [73] gave a wavelength-division-multiplexing technique for interrogating 10-cascaded Fiber Bragg Grating sensing elements based on a ring-compounded-cavity fiber laser. A feedback control technique was introduced to a tunable Fabry-Perot filter that tracked the wavelength-shift of the sensor. The sensors were demodulated using an unbalanced scanning Michelson interferometer and a sensitivity of 1.682°/με was demonstrated.

Sungchul *et al* [74] described a Fiber Bragg Grating (FBG) sensor demodulator using a chirped fiber grating. The demodulator used UV-induced birefringence of chirped fiber grating to interrogate the wavelength shift of a sensor FBG. The demodulator was composed of a polarizing beam splitter, a polarization controller, a single-mode fiber, and a chirped fiber grating. The proposed demodulator was immune to light power fluctuation and was cost-effective.

Seunghwan *et al* [75] proposed and experimentally demonstrated a simple, passive, and self-referencing wavelength shift detection scheme for use in Fiber Bragg Grating sensing systems. The demodulation system was based on the interference between two modes in a polarization maintaining fiber loop mirror. Although it involved the use of an interference technique, it was stable as compared with other conventional interference demodulators.

Ying *et al* [76] demonstrated a novel high-sensitivity pressure sensor, which was based on the use of a Fiber Bragg Grating (FBG) embedded in a polymer-filled metal cylinder with an opening on one side to enhance the pressure sensitivity. The measured pressure sensitivity of the fractional change in the Bragg wavelength of the experimental sensor was -3.41×10-3 MPa-1 which is approximately 1720 times higher than that can be achieved with a bare FBG. The linearity of the sensor was also good. This sensor could find applications in the area of low-pressure measurement.

Wait *et al* [77] reported on a Brillouin optical time domain reflectometer-based distributed temperature sensor utilizing a Fiber Bragg Grating notch filter to suppress the Rayleigh backscatter in order to separate the Brillouin signal. The Brillouin light path was thus subject to minimum attenuation and was frequency independent. A 2-m spatial resolution was achieved over a range of 25 km with the temperature resolution rising from 1°C at the near end to 7°C at the far end in a measurement time of 10 min. This was reduced to <1°C over ~20 km if the measurement time was increased to 180 min.

Boulet *et al* [78] described a novel technique to provide demultiplexing of Fiber Bragg Grating sensors, interrogated using interferometric wavelength shift detection. Amplitude modulation of multiple radio frequency driving signals allowed an acoustooptic tunable filter to provide wavelength demultiplexing. A noise limited strain resolution of 150 nanostrain/√(Hz) and a crosstalk better than -50 dB has been demonstrated.

Chan *et al* [79] gave the use of gas absorption lines as multi-wavelength references to enhance the measurement accuracy of Fiber Bragg Grating sensors. Experiments with a three-FBG-sensor array interrogated by a tunable laser demonstrated an overall measurement accuracy of ~2 pm.

Cooper *et al* [80] found that the sensitivity of measuring time multiplexed Fiber Bragg Grating (FBG) sensors could be improved by amplifying the signal returning from the sensors. This could be used to either improve the system performance or reduce the power, and hence the cost of the optical source. In the experiments, the addition of the amplifier allowed a reduction of >120 times in the source power.

Da Silva *et al* [81] carried out strain studies in samples of power transmission cables by means of multiplexed optical Fiber Bragg Gratings. Calibration processes were presented. Strain was analyzed in individual wire conductors of the cable.

Barbosa *et al* [82] initially inscribed a uniform Fiber Bragg Grating in a multimode fiber. It was observed that the phase matching condition was approximately satisfied by a few modes, causing the appearance of lateral lobes. Then they experimentally analyzed the dependence of these lobes upon variations in temperature. This study may lead to the construction of multimode temperature sensors.

Seunghwan *et al* [83] discussed a simple, passive, and self-referencing wavelength shift detection scheme, for use with Fiber Bragg Grating sensing systems. The system was based on the use of a polarization maintaining fiber loop mirror.

Wade *et al* [84] presented a fiber optic sensor device was developed incorporating a short length of erbium doped fiber fused in close proximity to a single-Fiber Bragg Grating, to measure both the fluorescent lifetime decay and the wavelength shift in these respective elements, for temperature and strain determination. Calibration results obtained from this simple, low cost, intrinsic sensor scheme showed standard deviation errors of 20.4 μ and 1.2°C over strain and temperature ranges of 22–1860 μ and 25–120°C, respectively.

Arregui *et al* [85] presented a novel sensor capable of simultaneously measuring temperature and humidity fabricated and demonstrated using optical fiber waveguides. The sensor head was composed of a Fiber Bragg Grating and a low-finesse Fabry-Perot interferometric cavity. The Fabry-Perot cavity was fabricated using the electrostatic self-assembled monolayer process for the molecular-level deposition of materials of different thicknesses that form a humidity-sensitive coating on the end of the fiber, while the in-line Bragg grating fiber element was used to monitor temperature. Experimental results for a humidity range from 11% to 97% RH and for a temperature range from 10°C to 85°C were shown.

Gong *et al* [86] reported a minimum variance shift technique for wavelength detection in Fiber Bragg Grating (FBG) sensors. The technique was demonstrated to offer high

detection accuracy even when the spectrum of the FBG was in partial overlap with a neighboring FBG within a wavelength division multiplexed sensor array.

Frazao *et al* [87] came up with a new scheme for simultaneous measurement of strain and temperature using a sampled Fiber Bragg Grating based on a long period structure written using the electric arc technique. The temperature and strain measurement resolutions were estimated to be ±0.50°C/√Hz and ±3.38 με/√Hz, respectively.

Murphy *et al* [88] demonstrated a spatially-scanned interferometric technique for demodulation of Bragg grating sensors, overcoming the 'moving parts' and measurement bandwidth limitations associated with temporally scanned interferometric schemes. The wavelength measurement was derived from the phase of the complex analytic signal of spatial interferograms, in contrast to spectral measurement by FTS. The technique incorporated precise delay mapping based on the analytic signal of a laser interferogram, thus overcoming limitations of conventional spatial interferometers caused by nonuniformities in optical surfaces and in the imaging array. Murphy *et al* achieved a resolution of 25 pm for a limited OPD scan of 200 mm. This result compared favourably to reported temporally-scanned schemes and indicated potential for far higher resolutions and measurement bandwidth in larger spatial interferometer designs using long high-speed imaging arrays. Murphy *et al* [88] have further reported the investigation of the fundamental limits of the accuracy of the approach when using sampling densities close to the Nyquist limit.

Teunissen *et al* [89] highlighted that based on the changes occurring in the electricity market, online monitoring of h-v transformers becomes an important aspect to supervise the actually operating conditions of old devices and to assess the residual lifetime. The use of optical sensors based on Fiber Bragg Gratings offers the possibility to measure the temperature and the partial discharges directly at the active part of h-v transformers. For a successful integration of the FBGs inside the transformer the long-term stability and optical fiber's influence on the dielectric strength of transformer oil was investigated.

Fernandez *et al* [90] presented that Fiber Bragg Grating sensors were being evaluated by the nuclear industry for structural integrity and temperature monitoring. Radiation effects

on FBG sensors have been reviewed and in-reactor core irradiation of FBG temperature sensors has been discussed.

Betz, *et al* [91] published that the field test has shown the great potential of fiber-optic Bragg gating sensors. They were suitable for load monitoring of aviation structures under real-world conditions. The results obtained with the Bragg gratings showed excellent consistency with the strain gage results. This indicated that both the sensor installation technique of gluing the sensors to the surface and the sensor interrogation technique using a tunable laser-based system, both of which were studied in the field test, were well-suited for these measurements. In addition, the fiber-optic sensor network had several advantages: it was immune to electromagnetic interference and had high multiplexing capability, for hundreds of these sensors could be aligned along a single optical fiber, if desired. This significantly reduced the effort needed for wiring and also lead to a considerable decrease in weight compared to standard electrical sensor networks.

Hua *et al* [92] have successfully demonstrated the application of Fiber Bragg Grating sensors to detect the solder interconnect debounding between flip chip ball grid array and printed circuit board in four-point bend tests. Four sensors, due to their small size, were surface-mounted on the four-corners of the ball grid array substrate, about 1 mm from the solder balls that allow more sensitive strain measurement under board flexure. The measured strain data was compared with the data from strain gauge, daisy chain resistance, and dye and pry test. The preliminary results showed that the fiber sensors were capable of detecting the onset of solder joint fracture, strain relaxation, and extent of the failure.

Ping *et al* [93] gave a new fiber-optic sensor for simultaneous measurement of water-soluble analytes and temperature with polymer-coated Fiber Bragg Gratings (FBGs). As an application of the approach, simultaneous monitoring of the concentration of sugar or potassium chloride (KCl) and temperature was achieved. Changes in these environmental parameters resulted in different extents of either red- or blue-shifts of the Bragg resonance wavelengths of the gratings. It was found that polyimide-coated FBG responds to variations of both temperature and concentrations of soluble analytes, while acrylate-coated FBG was sensitive to environmental temperature only.

The experimental results [93] showed that the temperature sensitivity of the acrylate-coated FBG, temperature, sugar, and KCl concentration sensitivities of the polyimide-coated FBG were 0.0102 nm/degC , 0.0094 nm/degC, 0.0012 nm/degBx , and 0.0126 nm/M, respectively. The sensing mechanism of the polyimide-coated FBG was in the hygroscopic properties of the polyimide coating, which resulted in the change of the strain of the fiber and, thus, the optical properties of the grating. Since the sensor detected the analytes that swell the polyimide coating and different analytes induced different swelling effects, the sensor could detect different analytes without prior knowledge once a calibration curve was developed.

Peng *et al* [94] proposed a Fiber Bragg Grating (FBG) sensor system with a two-level ring architecture. The survivability and capacity of a FBG for a multipoint sensor system were enhanced by adding remote nodes and optical switches in the two-level ring architecture. Additionally, to enhance the signal-to-noise ratio (SNR) of the sensor system, a fiber ring laser approach was utilized to construct the proposed two-level ring architecture. The fiber ring laser adopted herein yielded the high SNR of the sensor system. The proposed system could increase the reliability of FBG sensor systems for multipoint smart structures.

Song *et al* [95] presented a novel pressure sensor structure comprising a carbon fiber ribbon-wound composite cylindrical shell. Based on this mechanical structure combined with a Fiber Bragg Grating (FBG), an accurate low-pressure sensor was developed. Theoretical analysis and first-principle investigations were conducted. Further, experimental results indicated that the pressure sensitivity and measurement range could reach 0.452 nm/MPa and 8 MPa, respectively.

Yinping *et al* [96] described a relative humidity (RH) sensor based on tilted Fiber Bragg Grating (TFBG) by utilizing polyvinyl alcohol (PVA) as the sensitive cladding film. RH increasing in the PVA coating would result in reduction of refractive index. Due to the TFBG's sensitivity to ambient refractive index, the spectral properties of PVA-coated TFBG were modified under exposure to different ambient humidity levels ranging from 20% to 98% RH. The transmission power of TFBG had different linear behaviors for two different humidity ranges (20%-74% RH and 74%-98% RH), and the sensitivity for each humidity range reached as high as 2.52 and 14.947 dBm/%RH, respectively. Combining

the advantages of optical fiber grating and PVA as a smart material, this design involved simple configuration, low cost, compactness, a small degree of hysteresis, stability, and wide dynamic sensing range as well. Therefore, the sensor could be applied in real-time RH monitoring for normal as well as extremely humid environments.

Muller *et al* [97] presented that an embedded Fiber Bragg Grating could be subjected to arbitrary states of strain including shear strain. Such perturbations could cause coupling between polarization modes. Coupled-mode theory in Bragg gratings so far neglected this effect and only considered forward-backward coupling. Polarization mode coupling within a Bragg grating lead to interdependencies between Bragg reflection peaks which had so far been unaddressed. A full strain tensor treatment of Fiber Bragg Gratings, considering the coupling of the polarization modes within the grating was formulated. Muller *et al* [97] gave an approximation for the coupling coefficients affecting the polarization mode coupling and numerically solved the coupled-mode equations for representative states of strain. Muller *et al* [97] showed in which way shear strain affects the optical response of a grating and demonstrated how the fiber's beat length influenced this characteristic.

Seongmin *et al* [98] presented a highly sensitive Fiber Bragg Grating temperature sensor using a temperature-sensitive Pb/Ge-codoped fiber experimentally with the average temperature sensitivity of the resonance wavelength shift about 0.0176 nm/degC.

Han *et al* [99] gave a simple and practical scheme for a directional bending sensor based on a sampled chirped Fiber Bragg Grating. The proposed sensing method had temperature insensitivity. The wavelength spacing in the reflection spectrum of a sampled chirped Fiber Bragg Grating was changed by bending because of the modification of the chirp ratio. As positive or negative bending was applied to the sampled chirped Fiber Bragg Grating embedded on a flexible cantilever beam, the wavelength spacing increased or decreased because of the induction of the tension and the compression strain gradient along the fiber grating. However, the wavelength spacing did not change by the applied temperature. Since the effect of the temperature variation along the grating length remained the same, the chirp ratio was independent of the applied temperature change. Regardless of temperature change, it was therefore possible to measure the direction and the variation of bending.

Ambrosino *et al* [100] in their work showed the dependence of the magnetostrictive response on the prestress used to improve and fit the performance of Terfenol-D based Fiber Bragg Grating magnetic sensor. The possibility to tune sensitivity allowed to work at different operative conditions and to develop advanced sensors with reconfigurable sensitivity. Performance improvements in terms of magnetic resolution up to 0.0116 A/m were demonstrated.

Grobnic *et al* [101] presented a narrowband multiple high-order Bragg resonances from a single Bragg grating structure inscribed using a femtosecond IR laser and a 4.28 mum pitched phase mask were used to demonstrate a multiparameter sensor in standard low cutoff wavelength optical fiber. Six high reflectivity resonances that are observed in the wavelength range from 1 to 2 mum can be used to monitor up to six sensing parameters. Temperature and strain coefficients of the grating at each of the high-order Bragg resonances were evaluated.

Dong *et al* [102] came up with a novel technique for chirp control of a uniform Fiber Bragg Grating (FBG) based on the special strain function modulation. A cylinder taper cantilever beam (CTCB) was specially designed and capable of providing special position-dependent strain function gradients along an originally uniform FBG, which allowed tunable quasi-triangular and quasi-Gauss-gradient FBG filter. Furthermore, the feasibility of the tunable chirped FBG based on the strain function modulation as sensor was validated. This state-of-art technique was expected to be applied in fiber filter, FBG sensor and multiwavelength fiber laser.

Fu *et al* [103] presented and demonstrated a novel Fiber Bragg Grating (FBG) sensor configuration using three broadband light sources of different wavelength bands for the interrogation of FBG sensors distributed over 75 km of fiber. Rayleigh backscattering was reduced and a 60-dB effective dynamic range was demonstrated.

Suleiman *et al* [104] showed an innovative investigation of optical feedback or self-mixing interference within the cavity of a single-longitudinal-mode laser as an integral part of a novel interrogation scheme to be employed in a Fiber Bragg Grating-based sensor for strain measurement. The entire sensor device simply consisted of a laser diode

with an integrated photodiode which was coupled to a Fiber Bragg Grating under strain. A small percentage of the injected lightwave resonantly reflected off the grating structure reentered the laser cavity and modified the emission properties of the laser, resulting in the formation of characteristic sawtooth fringes which contained the embedded strain information. The feasibility of demodulating the induced small wavelength shifts of Fiber Bragg Gratings under dynamic mechanical loading by self-mixing interferometry was thus presented analytically and experimentally verified. A relatively good corroboration was achieved.

Caucheteur *et al* [105] presented the explosion risk linked to the use of hydrogen as fuel requiring low-cost and efficient sensors. A multipoint in-fiber sensor capable of hydrogen leak detection in air as low as 1% concentration with a response time smaller than a few seconds was presented. This solution made use of Fiber Bragg Gratings (FBGs) covered by a catalytic sensitive layer made of a ceramic doped with noble metal which, in turn, induced a temperature elevation around the FBGs in the presence of hydrogen in air.

Qizhen *et al* [106] presented and demonstrated a novel time-division-multiplexing Fiber Bragg Grating (FBG) sensor for multipoint temperature warning sensor. A multiwavelength pulsed laser based on a multichannel matched FBG was employed. The sensor array consisted of multiple uniform FBGs at different positions and with different nominal wavelengths. When the temperature exceeded the threshold at a certain position, the light at the corresponding time slot and wavelength could be detected. The sensor provided a simple and flexible solution to locate the abnormal temperature increase with different tolerable thresholds at different locations.

Yong *et al* [107] described a double-arched-beam-based Fiber Bragg Grating (FBG) sensor for displacement measurement. Unlike most FBG sensors that measured the resonance wavelength shifts to detect the measurand, this kind of FBG sensor was proposed to measure the displacement based on the demodulation of the FBG's reflective spectra bandwidth. According to the strain distribution on the novel double-arched beam surface, the positive and negative strain would act on only one FBG, which was stuck on the beam surface. Thus, the positive and negative strain would make the spectra broaden as the displacement increases. The problem of cross-sensitivity in the FBG sensor was solved because temperature only affects the wavelength shift, but not the spectra

bandwidth. Simulation and preliminary experimental results indicated the feasibility of the proposed idea and a fairly good linearity of the measurement characteristic.

Wei *et al* [108] gave a simple anisotropic structure made by carbon fiber laminated composite for fabricating a high pressure sensor. A pressure sensor with good sensitivity over a broad measurement range was fabricated by using Fiber Bragg Grating and the anisotropic carbon fiber laminated composite structure. The characteristic responses of pressure and temperature of the new pressure sensor were analyzed. Experimental data showed that when the pressure changes from 0 to 70 MPa, the wavelength shift of the Fiber Bragg Grating pressure sensor was up to 7 nm, corresponding to a sensitivity of 10 kPa/pm.

Fu *et al* [109] presented a novel high-speed Fiber Bragg Grating (FBG) sensor interrogator using dispersion-compensating fiber. The wavelength shift measurement of the FBG sensor was converted to time-domain measurement. The high-speed potential of this scheme was investigated experimentally, demonstrating an effective sampling speed of 2.44 megasamples per second.

Tosi *et al* [110] innovated a novel interrogation technique for Fiber Bragg Gratings, based on the self-mixing effect in strong feedback regime and intensity detection, through experimental measurements. The application of an appropriate spectral estimator permitted transferring the analysis into the frequency domain, leading to the realisation of a power drift-tolerant strain sensor.

Yong *et al* [111] described the dynamic testing and control results obtained with an exoskeletal robot finger with embedded fiber optical sensors. The finger was inspired by the designs of arthropod limbs, with integral strain sensilla concentrated near the joints. The use of Fiber Bragg Gratings (FBGs) allowed for embedded sensors with high strain sensitivity and immunity to electromagnetic interference. The embedded sensors were useful for contact detection and for control of forces during fine manipulation. The application to force control required precise and high-bandwidth measurement of contact forces. A nonlinear force control approach that combined signals from an optical interrogator and conventional joint angle sensors to achieve accurate tracking of desired contact forces has been presented.

Wei *et al* [112] improved the performance of FBG sensors in a wavelength-division multiplexed sensor network using genetic algorithm. Simulation and experiment showed that computed speed and capability of multiplexing are enhanced, and the measurement range of sensors in FBG sensor network is increased while using improved genetic algorithms with proper parameters.

Haibin *et al* [113] demonstrated a novel wireless sensors network available for multi-dimension and multi-parameter measurement based on Fiber Bragg Grating sensing units. The combination of wireless communication with the Fiber Bragg Grating sensors obtained obvious advantages including inherent immunity to electromagnetic interference, compact size and high sensitivity compared with conditional wireless sensing network based on electronic elements. Additionally, data collection, processing and transmission of sensing information were achieved by forming a multi-jump and self-organized network via wireless communication. Considering its unique advantages, this kind of wireless sensors network has wide application in many harsh environments, such as desert, wasteland and the health monitoring of some complicated buildings.

Myonghwan *et al* [114] gave a precise information on spatial distributions of temperature important for diagnosing power transformers and evaluating its life because a power system failure results in an enormous loss in tangible as well as social. The optical Fiber Bragg Grating (FBG) sensors, which have been studied intensively for last decade, could be very efficient tools for applications to above mentioned purpose because these are immune to EMI and can be highly multiplexed, which enables efficient quasi-distributed temperature sensing along tens of km range. A fiber-optic temperature monitoring system with an array of over 4 sensor gratings was proposed. The temperature-induced Bragg wavelength variations were accurately monitored by a scanned tunable wavelength filter. Differential measurement with temperature-stabilized reference gratings and a Gaussian curve-fitting algorithm were used to enhance measurement accuracy, which obtained temperature resolution of ~0.6degC, and linearity error less than 0.4 %.

Kunzler *et al* [115] showed that optical Fiber Bragg Grating sensors exhibit specialized sensing characteristics for harsh environments. The most common interrogation methods for FBGs require high resolution spectrometers that are not well suited to some embedded

test situations. A compact, high speed, Ethernet-enabled interrogator that consumed less than 10 Watts was developed. The conventions used to convert from the optical domain to a sensor network have been introduced and an integrated system test data acquired from sensors in dynamic temperature and strain environments has been presented. Fiber optic system and sensor performance has been tested to be capable of mainstream usability.

Hwa *et al* [116] highlighted that railway is an important part of the transportation systems in many parts of the world. Results obtained from a FBG sensor network installed on 26-km rail track and several train-borne monitoring systems demonstrated that FBG has the potential to revolutionize the railway industry.

Wild *et al* [117] presented an intensiometric detection system for Fiber Bragg Grating sensors. The system is designed to directly detect intensity modulated signals, or to convert spectrally modulated signals into intensity modulated signals.

Foo *et al* [118] presented a novel non-intrusive respiratory monitoring system for detection of life threatening situations in bedridden or bed bound patients, and for monitoring of sleep disorders in elderly or patients. Specifically, the subtle design and implementation of a system using Fiber Bragg Grating pressure sensors to monitor the respiratory rate without requiring the patients or elderly to wear any probes has been presented. The special packaging design of the sensors allows them to be blended into the natural settings of a normal bed for continuous 24x7 respiratory rate monitoring.

Canning *et al* [119] regenerated gratings seeded by type I gratings to withstand temperatures beyond 1000degC. A new approach to increasing temperature resistance of ultra high T stable gratings was presented.

Franke *et al* [120] gave more advanced robotic applications requiring high accuracy positioning of the robot manipulator. They introduced a novel approach to measure the elastic deformations of robot links in order to improve its pose accuracy using Fiber Bragg Gratings. They developed a model of the fiber Bragg sensors that locally measure strain. In conjunction with a finite model of the link geometry this information enabled the prediction of the arm deformation. The approach opens an avenue for more advanced

position control, which considers the elastic link deformations. Both models provide the basis for a systematic analysis and optimization of the spectrometer, signal processing and sensor configuration. An evolutionary algorithm optimizes the sensor locations in order to minimize the predicted deformation error. The proposed scheme is verified experimentally on an industrial manipulator.

Arkwright *et al* [121] designed and clinically tested performance of Fiber Bragg Grating based pressure sensing catheters for the diagnosis of gastrointestinal motility disorders. The fiber optic design allowed catheters with multiple sensing regions but small overall diameters to be fabricated, which was advantageous for nasal intubation into patients. The fiber optic catheters have been compared to a commercially available solid-state device both in-vitro and in-vivo, and results demonstrated that they are suitable for diagnosis of gastrointestinal motility disorders.

Xinyong *et al* [122] described a novel intensity-modulated Fiber Bragg Grating (FBG) sensor system employing fiber dispersion. A RF signal is generated at a photodetector by two modulated optical signals reflected from a sensing and a reference FBG. Bragg wavelength shift of the sensing FBG changes intensity of the RF signal due to a fiber dispersion-induced phase change, with temperature effect being compensated automatically by the reference FBG. Strain measurement with a maximum sensitivity of -0.34 muV/muepsiv has been achieved.

Mondal *et al* [123] described an embedded dual Fiber Bragg Gratings sensor for temperature and strain discriminatio. Two nearly identical gratings were mounted opposite side of an arch-shape steel strip. The gratings in concave and convex position experienced equal blue and red shift due to bending of the strip under compressive and tensile strains respectively. The thermal response and strain response were separated by addition and subtraction of the resultant shifts from two gratings. The thermal and strain sensitivity of the sensor was improved to 30 pm/degC and 2.6 pm/muepsiv. The sensor could measure strain and temperature with a permissible error of plusmn 1 muepsiv and plusmn 1.5degC respectively.

Qizhen *et al* [124] demonstrated a Fiber Bragg Grating (FBG)-based multi-point temperature warning sensor using a multi-channel matched FBG. The sensor provided

simple, flexible, and cost-effective solutions to locate abnormal temperature increase with different thresholds at different locations.

Xinlong *et al* [125] undertook first step experimental researches about embedded Fiber Bragg Grating (FBG) sensors network for health monitor of solid rocket motors (SRM. In the experiment, the FBG sensors networks were embedded in composites plane with simulative delamination and scale SRM models. The results of the plane bend test indicated that damage could be identified by detecting concentration strain field, and the results of the scale SRM shells internal hydraulic pressure test indicated that the complex strain and deformation could be monitored by the sensors network, leading to the possibility to develop FBG sensors network systems for composites SRM health monitor. These researches would extend missile weapons reliability and safety in serving lifetime, enhance maintenance procedures to maximize serving time and improve reliability.

Ke *et al* [126] presented a temperature sensor based on fibers Bragg grating in photonic crystal fibers. The temperature property of uniform fibers Bragg grating in photonic crystal fibers was studied. By finite element method, the relation between the birefringence in photonic crystal fibers and the temperature was analyzed. Numerical results showed that the birefringence in photonic crystal fibers is in proportion to the temperature. Still, a new measurement dependent on polarization was also presented. This measurement was proved that it is applicable for the proposed temperature sensor.

Yanliang *et al* [127] analyzed the strain-temperature cross sensitive characteristic of optical Fiber Bragg Grating (FBG) theoretically, designed and made a novel FBG strain sensor. It had a temperature-compensated function, and it improved the effect of being sensitive to strain. To a certain extent, this sensor overcame the traditional temperature-compensated methods easy to have a creep and aged phenomenon. The experimental results showed that the sensor realized the temperature sensitivity reduces to 1/10 before the seal, and the strain sensitivity increases to 1.4 pm/uepsiv over the temperature range from -10degC to 50degC.

Hongyan *et al* [128] described a microchannelled chirped Fiber Bragg Grating (MCFBG) fabricated using femtosecond laser processing and HF-etching. Intrinsical refractive-

index sensitivity induced by the microchannel made MCFBGs ideal for biochemical sensing.

Men *et al* [129] presented an in-line one-fiber approach to realize simultaneous measurement of salinity and temperature. The sensor system, which consisted of multiplexed polymer-coated Fiber Bragg Gratings, showed that the polyimide-coated grating responds to variations of both temperature and salinity, while the acrylate-coated grating is only sensitive to the environmental temperature. The experimental results indicated that the temperature sensitivity of the acrylate-coated grating in water was 0.0102 nm/°C for redshifted Bragg wavelength with increasing temperature, and the temperature and the salinity sensitivities of the polyimide-coated grating were 0.0094 nm/°C (redshifted) and 0.0165 nm/M (blueshifted), respectively, which are in excellent agreement with the theoretical analysis.

Espejo *et al* [130] gave a new method for measuring transverse stress with 10.2-mum spatial resolution in a Fiber Bragg Grating sensor, without the use of polarization-maintaining fiber, by combining a four-state polarization analysis with a layer-peeling algorithm. Measurements of the externally induced birefringence agreed well with predicted values. It was also demonstrated that the measurement is insensitive to temperature changes and spatial gradients, making it ideal for nonisothermal applications.

Saini *et al* [131] demonstrated that the etched-core Fiber Bragg Grating sensor could be used to detect down to a monolayer of biological and chemical agents immobilized on the surface of the fiber. Theoretical models based on calculating the effective index of the surrounding medium in the presence of immobilized layers were developed and confirmed experimentally by immobilizing a monolayer of 3-aminopropyl-monoethoxydimethyl-silane (APMDS) and polymers of 3-aminopropyl-triethoxysilane (APTES) on the surface of the fiber. The immobilization of APMDS and APTES is confirmed by carrying out hybridization of DNA. It was also demonstrated that the sensor could be used to understand and optimize biological and chemical processes.

Shengchun *et al* [132] presented a time-division multiplexed Fiber Bragg Grating (FBG) sensor system capable of real-time monitoring. It was based on an unbalanced Michelson interferometer, a delay signal generator, and a tree-structured single-pole-double-throw

switch array. Realization of real-time monitoring was because the arriving time of sensing signals was synchronized with the controlling signals of the switches. A phase meter was used to measure the strain of FBG sensors.

Saitoh *et al* [133] presented a long-distance Fiber Bragg Grating (FBG) sensor system developed using a wavelength-swept light source with output power turned on-off and timing synchronized to the sweep signal to reduce optical noise caused by Rayleigh scattering generated from the transmission fiber. This system could detect changes in the FBG reflection wavelengths even if the FBG is 120 km from the sensing position.

Binfeng *et al* [134] presented a highly sensitive liquid-level sensor based on etched Fiber Bragg Grating (FBG). The transmission dips of FBG spectra were affected by the fraction of the length of the etched FBG that was surrounded by the liquid. The experiments showed that for a liquid-level variation of 24 mm, the transmission dip difference changed about 32 dB. Also in the linear region, a high sensitivity of 2.56 dB/mm was achieved.

Ambrosino *et al* [135] demonstrated a magnetic field sensor based on the integration of a Fiber Bragg Grating (FBG) with a magnetic shape memory alloy (MSMA). MSMA is a new kind of material able to show extremely large strains in response to a magnetic field. Moreover, differently from classical shape memory alloys, which were actuated by temperature, MSMAs normally show quite fast responses. The basic features of the proposed device were illustrated, and field range and sensitivity of the device were also discussed. Moreover, comparison with Terfenol-based FBG sensor performances was reported showing results with a sensitivity (DeltalambdaB/lambdaB)/(DeltaH/Hm) of 1.81middot10-4, where lambdaB was the Bragg wavelength and Hm the mean magnetic field in the considered range.

Michael *et al* [136] found the use of liquid hydrogen as a fuel requires low-cost multipoint sensing of hydrogen gas for leak detection and location well below the 4% explosion limit of hydrogen and presented a multipoint in-fiber hydrogen sensor capable of hydrogen detection below 0.5% concentration with a response time of less than 10 s. This solution entailed use of a Fiber Bragg Grating (FBG) coated with a layer of hydrogen-absorbing palladium which, in turn, induced strain in the FBG in the presence

of hydrogen. Infrared power laser light was used to induce heating in the palladium coating which dramatically decreased sensor response time and increased the sensor's sensitivity at low temperatures. This technology promised an inexpensive fiber solution for a multipoint hydrogen detection array with only one fiber feed-through.

Huang *et al* [137] presented a demodulation algorithm for Fiber Bragg Grating (FBG) sensor. The proposed demodulation algorithm evaluated the wavelength shift in the reflected spectrum of an FBG sensor. It computed the cross-correlation between the perturbed spectrum and the undisturbed spectrum. The proposed algorithm was compared with another three reported algorithms and the experimental results in respect of the reflective index of FBGs and other factors that may influence the sensing resolution were discussed. The strain resolutions of 0.4 and 1.5 muepsiv in high reflective gratings and low reflective gratings, respectively have been reported.

Yiping *et al* [138] gave a measurement method developed to determine the full-field deformation of a simply supported plane plate under transverse load. The method utilized strain information provided by a set of four Fiber Bragg Grating sensors mounted on the plate in a way that all sensors measured strains along one certain direction. The sensors were interrogated using a wavelength swept fiber laser. Utilizing the strain information and the first four terms of Navier solution of simply supported rectangular plate, the necessary parameters for determining the deflection could be computed. By substituting the values of x- and -y- coordinates of each position on the rectangle plate, the full-field deformation information could be obtained. Single-point loading tests were experimentally performed to verify the accuracy of the method.

Bowei *et al* [139] innovated Fiber Bragg Grating temperature sensor and sensor arrays were applied widespread particularly in harsh environments. Although FBGs were often referring to permanent refractive index modulation in the fiber core, exposure to high-temperature environments usually resulted in the bleach of the refractive index modulation. The maximum temperature reported for the conventional FBG temperature sensor was around 600 degC due to its weak bonds of germanium and oxygen. Bowei *et al* reported design and development of a novel high-temperature resistance FBG temperature sensor, based on the hydrogen-loaded germanium-doped FBG. The refractive index modulation in the FBG was induced by the molecular water. The results of the

experiments showed that the stability of the device was substantially increased at high temperature range. Due to the high bonds energy of hydroxyl and the low diffusivity of the molecular water, the thermal testing results of this temperature sensor showed the thermal stability of hydrogen-loaded FBG could be increased by using annealing treatment; moreover, the highest erasing temperature for the device could reach to 1100 degC or more. The reflectivity of this new FBG depended on the concentration of Si-OH and indirectly related to the reflectivity of hydrogen-loaded FBG. Furthermore, the experimental results provided a better understanding of the formation of the hydrogen-loaded FBGs and the chemical transfers at elevated temperatures in the fiber core.

Guo *et al* [140] gave a technique for temperature-immune pressure measurement using a strain-induced quadratic-chirped Fiber Bragg Grating by differential optical power detection. Linear pressure measurement up to 20 kPa with a resolution of 0.05 kPa and thermal stability less than 2% full-scale for a temperature range from 0 to 80degC were achieved using pin photodiodes detection, without any temperature compensation.

Thus the ability to inscribe intracore Fiber Bragg Gratings (FBGs) in germanosilicate core photosensitive fibers in the recent years has revolutionized the fields of telecommunication and optical fiber sensor technology. Fiber Bragg Gratings are realized by permanently changing the index of refraction in a periodic pattern along the core of the fiber by exposing them to intense UV radiation. This periodic modulation of the index of refraction in the fiber core acts like a selective mirror for the Bragg wavelength of the structure. As the spectral properties of FBGs are highly dependent on the grating period, the FBG properties are very sensitive to changes in the length of the fiber into which they are inscribed. This property makes FBGs excellent all optical sensors for smart structures, process control, geophysical research and mining applications.

Fiber optic sensitivity has, indeed, opened a new era in the field of fiber optics based devices. Fiber Bragg Gratings are versatile and robust devices and novel & innovative Bragg grating structures are finding myriad of applications in telecommunication, fiber sensors, fiber lasers & fiber amplifiers and in multiple disciplines in science and engineering. As FBGs are an integral part of the fiber itself, they offer a high level of mechanical convenience, simplicity, and economy to the user and these characteristics have made them very attractive for telecommunication and sensors applications.

Compared with other fiber optic sensors, FBG sensors offer a number of distinct advantages such as (1) They can give an absolute measurement that is insensitive to fluctuations in the irradiance of the illuminating source, as the information is usually obtained by detecting the wavelength shift induced by the measurand, (2) They can be directly written into the fiber with out changing the fiber diameter, making them compatible with a wide range of situations where small diameter probes are important, such as in advanced composite materials for strain mapping or the human body for temperature profiling, (3) FBG sensors are small in diameter, lightweight and can be unintrusively embedded/bonded in a wide variety of materials, including concrete and polymer based components (4) they can be mass produced at low cost, making them potentially competitive with conventional electrical sensors, (5) They can be multiplexed using similar techniques that have been applied for use with fiber-optic sensors, including wavelength-division-multiplexing (WDM), spatial-division-multiplexing (SDM), time-division-multiplexing (TDM), and their combination making quasi-distributed sensing feasible in practice. One of the most important applications of FBG sensors that has been demonstrated to date is for the fiber-optic smart structures, where FBGs are embedded into the structure to monitor its strain distribution. Fiber-optics smart structure technology could in the future lead to structures that are self-monitoring and even self-scheduling of their maintenance and repair by the marriage of fiber-optic sensor technology and artificial intelligence with material science and structural engineering.

Fiber Bragg Grating sensing systems have emerged to be a practical technology for strain sensing, and are now deployed in a wide variety of applications including health monitoring of civil structures (highways, bridges, buildings, and dams), longterm fatigue assessment in ship hulls, and oil well pressure/temperature monitoring. Moreover, myriad potential applications are under active development, such as smart structures for aerospace vehicles, remote monitoring applications in nuclear plants, power cables, pipelines, and tow-arrays, as well as bio-medical and chemical sensing for trace pollutants, toxic gases, and in vivo temperature profiling in human bodies.

From the extensive literature survey it can be concluded that there is a definite need to carry out research in the area of Fiber Bragg Gratings. The investigations required in the field of Fiber Bragg Gratings for communication systems should encompass the area of simulation of Fiber Bragg Gratings and its validated using theoretical and experimental

work. The wavelength shift in Fiber Bragg Gratings on simulated external perturbation using a wideband source also needs to be observed leading to the design of Fiber Bragg Grating Interrogator for Sensor/Communication systems.

Chapter 3

Simulation of Fiber Bragg Gratings and Validation of Results using theoretical / experimental work

3.1 Theoretical Analysis of Fiber Bragg Gratings

To analyze the wave propagation in optical fibers, the Maxwell equations have been solved with appropriate boundary conditions. To solve them the weak guidance which allows the decomposition of modes into orthogonal set of transversely polarized modes has been considered. The solutions provide the basic field distributions of the bound and radiation modes of the waveguide. These modes propagate without coupling in the absence of any perturbation. If the waveguide has a phase and/or amplitude perturbation that is periodic with a perturbation phase/amplitude-constant close to the sum or difference then only that propagating modes will couple. The technique applied for solving this problem is coupled-mode theory. This method assumes that the mode fields of the unperturbed waveguide remain unchanged in the presence of weak perturbation. This approach provides a set of first-order differential equations for the change in the amplitude of the fields along the fiber, which have analytical solutions for uniform sinusoidal periodic perturbations [141].

A Fiber Bragg Grating of a constant refractive index modulation and period therefore has an analytical solution. Complex grating may be considered to be a concatenation of several small sections, each of constant period and refractive index modulation. The modeling of Fiber Bragg Grating becomes simple and the application of the transfer matrix method provides a clear and fast technique for analyzing more complex structures. Another technique for solving the transfer function of Fiber Bragg Gratings is by the calculation of the reflected and transmitted fields at an interface between two dielectric slabs of dissimilar refractive indices. The reflection and phase response can be evaluated using a matrix method. By using the analytical solution of a grating with a uniform period and refractive index modulation as in the previous method, the field reflection and transmission coefficients of a single period may be used instead. However, the thin-film approach does allow a refractive index modulation of arbitrary shape to be modeled with ease and can handle effects of saturation of the refractive index modulation.

The complex grating can also be analysed using eigen mode solutions of the periodic structures. With this approach the deeper physical insight can be explored into the dispersion characteristics of gratings. Coupled integral equations can also be used to exactly solve the inverse scattering problem for the design of a desired filter. It combines the characteristics of the Fourier transform technique, local reflection method and optimization of the inverse scattering problem which allows the design of gratings with required features in both phase and reflection. This method can also be applied to fabricate near top-hat reflectivity filters with low dispersion. The method has been recently applied to fabricate near top-hat reflectivity filters with low dispersion. Other methods such as the effective index method, useful for planar waveguide applications, discrete-time, Hamiltonian and variation are also useful. The generalized matrix approach has been used for nonlinear gratings. The matrix method can be modified to avoid the problems of the slowly varying approximation for ultra strong gratings. The transfer matrix method provides high accuracy for modeling in frequency domain and to analyze the practically realizable gratings.

3.2 Wave Propagation

To develop the theory of Fiber Bragg Gratings by considering the propagation of modes in optical fiber and guided wave optics, allows us to get the relationship between mode and the refractive index perturbation which plays an important role on overall efficiency of the Fiber Bragg Grating. Here the wave propagation in optical fiber by theory of mode coupling has been considered [141].

By Maxwell equations

$$D = \varepsilon_o E + P \tag{3.1}$$

$$B = \mu_o H \tag{3.2}$$

Where D is the electric displacement vector**;** **E** is the applied electric; $\boldsymbol{\varepsilon_0}$ is the dielectric constant and $\boldsymbol{\mu_0}$ is the magnetic permeability, both scalar quantities B and H are the magnetic flux and magnetic field vectors .

And the induced polarization P is given by

$$P = \varepsilon_o \chi_{ij} E \tag{3.3}$$

Here χ_{ij} is the linear susceptibility which is second rank tensor having two laboratory frame polarization susceptibilities ***ij*** and these are related to permittivity tensor ε_{ij} ***as*** follows

$$\varepsilon_{ij} = 1 + \chi_{ij} \tag{3.4}$$

By assuming the dielectric wave guide is source free

$$\nabla . D = 0 \tag{3.5}$$

and in the absence of ferromagnetic materials

$$\nabla . B = 0 \tag{3.6}$$

The electric field distribution in complex form given by

$$E = \frac{1}{2}[Ee^{i(\omega t - \beta z)}E + Ee^{-}i(\omega t - \beta z) \tag{3.7}$$

Induced polarization vector is defined by Maxwell equation

$$\nabla * E = \frac{-\partial B}{\partial t} \tag{3.8}$$

$$\nabla * H = \frac{-\partial H}{\partial t} + J \tag{3.9}$$

Here J is the displacement current.

With J = 0, by using Eq. (3.1), Eq. (3.9) becomes

$$\nabla * H = \frac{\partial}{\partial t}[\varepsilon_0 E + P] \tag{3.10}$$

Taking the curl of Eq. (3.8) and using Eqs. (3.2)-(3.5) and the time derivative of Eq. (3.10),

the wave equation is

$$\nabla^2 E = \mu_0 \varepsilon_0 \frac{\partial^2 E}{\partial t^2} + \mu_0 \frac{\partial^2 P}{\partial t^2} \tag{3.11}$$

By using eq (2.3),(2.4),(2.5) ,it follows

$$\nabla^2 E = \mu_0 \varepsilon_0 \frac{\partial^2}{\partial t^2}[1 + \chi_{ij}]E \tag{3.12}$$

Or

$$\nabla^2 E = \mu_0 \varepsilon_0 \varepsilon_{ij} \frac{\partial^2 E}{\partial t^2} \tag{3.13}$$

By introducing guided modes in optical fiber into the wave equation, the modes can be described as a summation of *l* transeverse guided mode amplitudes ,$A_\mu(z)$, along with a continuum of radiation modes $A_\rho(z)$ with corresponding propagation constants, $\beta_\mu$and β_ρ.

$$E_t = \frac{1}{2}\sum_{\mu=1}^{\mu=1}[A_\mu(z)\xi_{\mu t}e^{i(wt-\beta_\mu z)} + cc] + \sum\int_{\rho=0}^{\rho=\infty} A_\rho\,(z)\xi_{\rho t}\,e^{i(wt-\beta_\rho,z)}d\rho \qquad (3.14)$$

Where $\xi_{\mu t}$ and $\xi_{\rho t}$ are the radial transverse field distributions of the ρth guided and ρth radiation modes, respectively. Here *t* is the trasverse subscript of the polarization modes. The summation in the integral represents the different types of radiation modes accounting for transverse electric (TE), transverse magnetic (TM) , as well as the hybrid modes (EH and HE). If the power carried in the μth mode in watts is $|A_{\mu t}|^2$ by following orthogonality condition [141].

$$\frac{1}{2}\int_{-\infty}^{+\infty}\int_{-\infty}^{+\infty}\widehat{e_z}.[\,\xi_{\mu t} * \xi_{\vartheta t}^{*}\,]dxdy = \frac{1}{2}\left[\frac{\beta_\mu}{\omega\mu_0}\right]\int_{-\infty}^{+\infty}\int_{-\infty}^{+\infty}\xi_{\mu t}.\xi_{\vartheta t}^{*}dxdy = \delta_{\mu\vartheta} \qquad (3.15)$$

Here, $\widehat{e_z}$ is a unit vector along the propagation direction z. $\delta_{\mu\vartheta}$ is Kronecker's delta and is unity for μ=ν, otherwise it is zero.This result is identical to integrating Poynting's vector (power-flow density) for the mode field transversely across the waveguide. $\delta_{\mu\vartheta}$ is the Dirac delta function which is infinite for μ= ν and zero for μ≠ ν. By applying the eq(2.15) to the weakly guiding modes for which the longitudinal component of the electric field is much smaller than the transverse component, rendering the modes predominantly linearly polarized in the transverse direction to the direction of propagation , the transverse component of the magnetic field is given by

$$H_t = \sqrt{\frac{\varepsilon_0\varepsilon_r}{\mu_0}}[\widehat{e_z}\frac{\partial}{\partial z} \times \xi_t \qquad (3.16)$$

The fields which are bounded by the waveguide will satisfy the wave equation Eq. (3.13) in the cladding of a cylindrical waveguide are given by K-Bessels and in the core J-Bessels solutions. These solutions are two sets of orthogonal modes in general. The transverse fields for the μth x-polarized mode that satisfy the wave equation Eq. (3.13) are then given as

$$\xi_x = C_\mu J_\mu\left(u\frac{r}{a}\right)\begin{Bmatrix}cos\mu\emptyset\\ sin\mu\emptyset\end{Bmatrix} \qquad (3.17)$$

$$H_y = n_{eff}\sqrt{\frac{\varepsilon_0}{\mu_0}}\xi_x \qquad (3.18)$$

The corresponding fields in the cladding are

$$\xi_x = C_\mu\frac{J_\mu(u)}{K_\mu(w)}K_\mu\left(w\frac{r}{a}\right)\begin{Bmatrix}cos\mu\emptyset\\ sin\mu\emptyset\end{Bmatrix} \qquad (3.19)$$

$$H_y = n_{eff}\sqrt{\frac{\varepsilon_0}{\mu_0}}\xi_x \qquad (3.20)$$

Where the following normalized function have been used

$$v = \frac{2\pi a}{\lambda}\sqrt{n_{core}^2 - n_{clad}^2} \tag{3.21}$$

$$u = \frac{2\pi a}{\lambda}\sqrt{n_{core}^2 - n_{eff}^2} \tag{3.22}$$

$$\omega^2 = v^2 + u^2 \tag{3.23}$$

And

$$n_{eff} = n_{clad}\left[b\left(\frac{n_{core} - n_{clad}}{n_{clad}}\right) + 1\right] \tag{3.24}$$

where n_{eff} is the effective index of the mode and

$$b = \frac{\omega^2}{u^2} \tag{3.25}$$

By assuming a single polarization the y-polarized mode,

$$\xi_x = H_x = 0 \tag{3.26}$$

For perfectly circularly polarized modes the choice of sine or cosine term is somewhat arbitrary. These sets of modes become degenerate from poynting's vector theory of eq (3.15), the normalized constant C_μ can be expressed as

$$C_\mu = \frac{2\omega}{av}\left[\frac{\sqrt{\mu_0/\varepsilon_0}}{n_{eff}\pi e_\mu |J_{\mu-1}(u)J_{\mu+1}(u)|}\right]^{1/2} \tag{3.27}$$

Where e_μ= 2 when μ = 0 (fundamental mode) and 1 for $\mu \neq 0$. By matching and solving the core cladding boundary fields by considering waveguide characteristic eigenvalue equation, to calculate the propagation constant of the modes:

$$u\frac{J_{\mu\pm1}(u)}{J_\mu(u)} = \omega\frac{K_{\mu\pm1}(\omega)}{K_\mu(\omega)} \tag{3.28}$$

2.3 Coupled-mode theory

The waveguide modes satisfy the unperturbed wave equation Eq. (3.13) and have solutions described in Eqs. (3.17) through (3.20). The effects of perturbation have to be included in order to derive the coupled mode equations, assuming that the modes of the unperturbed waveguide remain constant. This equation can be the starting point [141]

$$\nabla^2 E = \mu_0\varepsilon_0(\partial^2 E/\partial t^2) + \mu_0(\partial^2 P/\partial t^2) \tag{3.29}$$

The total polarization response of the dielectric medium can be separated in two terms : Perturbed and unperturbed polarization and it is assumed that wave propagation takes place in a perturbed system with a dielectric grating

$$P = p_{unper} + p_{grating} \tag{3.30}$$

Where $$p_{unpert} = \varepsilon_0 \chi^1 E_\mu \tag{3.31}$$

Eq. (3.29) becomes:

$$\nabla^2 E_{\mu t} = \mu_0 \varepsilon_0 \varepsilon_r (\partial^2 E_{\mu t} / \partial t^2) + \mu_0 (\partial^2 P_{grating,\mu} / \partial t^2) \tag{3.32}$$

Where the subscripts represent to transverse mode number μ

Now by putting the modes in Eq. (3.14) into (3.32) the following relationship can be obtained:

$$\nabla^2 \left[\frac{1}{2}\sum_{\mu=1}^{\mu=l}\left[A_\mu(z)\xi_{\mu t}e^{i(\omega t-\beta_\mu z)} + cc\right] + \sum\int_{\rho=0}^{\rho=\infty} A_\rho(z)\xi_{\rho t}e^{i(\omega t-\beta_\rho z)}d\rho\right] - \mu_{0\varepsilon_0\varepsilon_r}\frac{\partial^2}{\partial t^2}\left[\frac{1}{2}\sum_{\mu=1}^{\mu=1}\left[A_\mu(z)\xi_{\rho t}e^{i(\omega t-\beta_\mu z)} + cc\right] + \sum\int_{\rho=0}^{\rho=\infty} A_\rho(z)\xi_{\rho t}e^{i(\omega t-\beta_\rho z)d\rho)}\right] = \mu_0\frac{\partial^2}{\partial t^2}P_{grating,\mu} \tag{3.33}$$

The left side of Eq. (3.13) can be expanded by ignoring the coupling to the radiation modes. In weak coupling, further simplification is possible by applying the slowly varying envelope approximation. This needs that the amplitude of the mode changes slowly over the distance of the wavelength of the light as:

$$\frac{\partial^2 A_\mu}{\partial z^2} \ll \beta_\mu \frac{\partial A_\mu}{\partial z} \tag{3.34}$$

$$\nabla^2 E_t = \frac{1}{2}\sum_{\mu=1}^{\mu=1}\left[-2i\beta_\mu\frac{\partial A_\mu}{\partial z}\xi_{\mu t}e^{i(\omega t-\beta_\mu z)} - \beta_\mu^2 A_\mu \xi_{\mu t}e^{i(\omega t-\beta_\mu z)} + cc\right] \tag{3.35}$$

Expanding the second term in (3.33), and noting that $\omega^2\mu_0\varepsilon_0\varepsilon_r = \beta_{\mu,}^2$ and combining with (3.35), the wave equation becomes

$$\sum_{\mu=1}^{\mu=l}\left[-i\beta_\mu\frac{\partial A_\mu}{\partial z}\xi_{\mu t}e^{i(\omega t-\beta_\mu z)}+cc\right]=\mu_0\frac{\partial^2}{\partial t^2}P_{grating,\mu} \quad (3.36)$$

Here, the subscript t on the polarization Pgrating,t reminds us that the grating has a transverse profile. Multiplying both sides of Eq. (3.36) by ξ_μ^* and integrating over the wave-guide cross-section leads to

$$\sum_{\mu=1}^{\mu=1}\int_{-\infty}^{+\infty}\int_{-\infty}^{+\infty}\left[-i\beta_\mu\frac{\partial A_\mu}{\partial_\mu}\xi_{\mu t}\xi_{\mu t}^*e^{i(\omega t-\beta_\mu z)}+cc\right]dxdy=\int_{-\infty}^{+\infty}\int_{-\infty}^{+\infty}\mu_0\frac{\partial^2}{\partial t^2}P_{grating,}\xi_\mu^*dxdy. \quad (3.37)$$

now Eq. (3.37) is used to see how mode coupling occurs by introducing forward- and backward-propagating modes. It is fundamentally the wave propagation equation, . The total transverse field may be described as a sum of both fields, not necessarily composed of the same mode order

$$E_t=\frac{1}{2}(A_v\xi_{vt}e^{i(\omega t-\beta_\mu z)}+cc+\beta_\mu\xi_{\mu t}e^{i(\omega t+\beta_\mu z)}+cc) \quad (3.38)$$

$$H_t=\frac{1}{2}(A_vH_{vt}e^{i(\omega t-\beta_\mu z)}+cc-\beta_\mu H_{\mu t}e^{i(\omega t+\beta_\mu z)}-cc) \quad (3.39)$$

Here –ve sign justfies forward and the +ve sign backward propagating mode.The modes of a waveguide form an orthogonal set and they do not couple in an ideal fiber unless there is a perturbation in the fiber using Eq. (3.38) and (3.39) in (3.37) leads to

$$\left[\frac{\partial A_v}{\partial z}e^{i(\omega t-\beta_v z)}+cc\right]-\left[\frac{\partial B_\mu}{\partial z}e^{i(\omega t+\beta_\mu z)}+cc\right]=+\frac{i}{2\omega}\int_{-\infty}^{+\infty}\int_{-\infty}^{+\infty}\frac{\partial^2}{\partial t^2}P_{grating,t,}\xi_\mu^*dxdy. \quad (3.40)$$

The total polarization with the perturbed permittivity in which the dielectric constant varies perdiocally along the wave propagation direction $\nabla\varepsilon(z)$ and the applied field is

$$P=\varepsilon_0[\varepsilon_r-1+\Delta\varepsilon(z)]E_{\mu.} \quad (3.41)$$

Where $\chi=[\varepsilon_r-1+\Delta\varepsilon(z)]\ and\ \varepsilon_r$ is the relative permittivity of the unperturbed core. The relation between the permittivity of the material and the refractive index n is

$n^2 = \varepsilon_r$. By considering this equation in case of periodically varying refractive index perturbation can be obtained

$$[n + \delta n(z)]^2 = \varepsilon_r + \Delta\varepsilon(z) \quad (3.42)$$

If the perturbation is small the equation becomes

$$\Delta\varepsilon(z) \approx 2n\,\delta n(z) \quad (3.43)$$

Defining the refractive index modulation of the grating as

$$\delta n(z) = \overline{\Delta n}\left\{1 + \frac{v}{2}\left(e^{i[(2\pi N/\Lambda)z + \emptyset(z)]} + cc\right)\right\} \quad (3.44)$$

Where Δn is the refractive index change averaged over a single period of the grating, v is the visibility of the fringes, and the exponent term along with the complex conjugate cc describe the real periodic modulation in complex notation. An arbitrary spatially varying phase change of $\emptyset(z)$ has been included.

Λ is the period of the perturbation, while N is an integer($-\infty$ < N < $+\infty$) that signifies its harmonic order. The period-averaged change in the refractive index has to be taken into account since change in the refractive index alters the effective index n_{eff} of a mode.

Combining Eqs. (3.42) and (3.44), the total material polarization alters.

$$P = \varepsilon_0\left\{n^2 - 1 + 2n\overline{\Delta n}\left[1 + \frac{v}{2}\left(e^{i[(2\pi N/\Lambda)z + \emptyset(z)]} + cc\right)\right]\right\}E_\mu, \quad (3.45)$$

where the first term on the RHS is the permittivity, the second term is the dc refractive index change, and the third term is the ac refractive index modulation. Finally, defining a new modulation amplitude by incorporating the visibility,

$$\delta n(z) = 2n\left\{\overline{\Delta n} + \frac{v}{2}\left(e^{i\left[\left(\frac{2\pi N}{\Lambda}\right)z + \emptyset(z)\right]} + cc\right)\right\} \quad (3.46)$$

With $\Delta n = v\overline{\Delta n}$ as the amplitude of the ac refractive index modulation. Eq. (3.46) describes the UV-induced refractive index change due to a grating written into the fiber core. Figure 3.1 shows the refractive index modulation for a uniform grating on a background index of the core

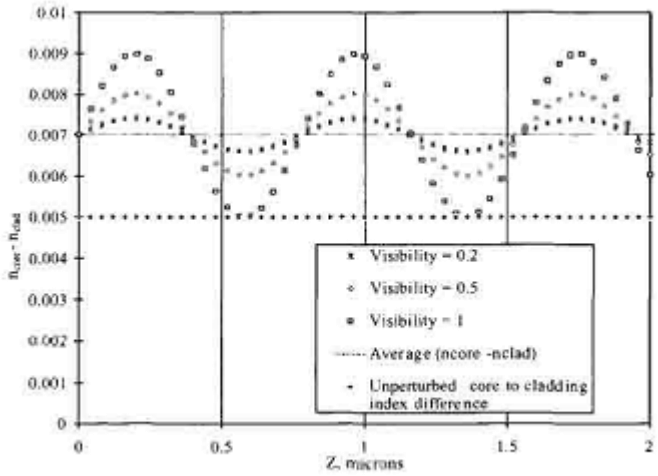

Figure 3.1 Refractive index modulation in the core of a fiber for different visibilities of the fringe pattern.

The change in the average index in the core is constant, irrespective of the visibility of the fringes, although it remains a function of δn. In the example shown, however, both the average index and the refractive index modulation δn increase with UV exposure time. The perturbed polarization can now be related to refractive index change shown in Eq. (3.46) to give

$$P_{pert} = 2n\varepsilon_0 \left\{\overline{\Delta n} + \frac{\Delta n}{2}\left(e^{i\left[\left(\frac{2\pi N}{\wedge}\right)z+\emptyset(z)\right]} + cc\right)\right\} E_\mu \qquad (3.47)$$

Including Eq. (3.47) in Eq. (3.40) results in

$$\left[\frac{\partial A_v}{\partial z} e^{i(\omega t-\beta_v z)} + cc\right] - \left[\frac{\partial B_\mu}{\partial z} e^{i(\omega t+\beta_\mu z)} + cc\right]$$

$$= +\frac{i\varepsilon_0}{2\omega}\int_{-\infty}^{+\infty}\int_{-\infty}^{+\infty}\frac{\partial^2}{\partial t^2}\delta n(z)\left[A_v\xi_{vt}e^{i(\omega t-\beta_\mu z)} + \beta_\mu\xi_{\mu t}e^{i(\omega t+\beta_\mu z)}\right]\xi^*_{\mu,vt}\,dxdy + cc$$

$$= -in\omega\varepsilon_o A_V\int_{-\infty}^{+\infty}\int_{-\infty}^{+\infty}\left[\overline{\Delta n} + \frac{\Delta n}{2}\left(e^{i\left[\left(\frac{2\pi N}{\wedge}\right)z+\emptyset(z)\right]} + cc\right)\right]\xi_{vt}e^{i(\omega t-\beta_v z)}\xi^*_{\mu,vt}dx$$

$$-in\omega\varepsilon_o B_\mu\int_{-\infty}^{+\infty}\int_{-\infty}^{+\infty}\left[\overline{\Delta n} + \frac{\Delta n}{2}\left(e^{i\left[\left(\frac{2\pi N}{\wedge}\right)z+\emptyset(z)\right]} + cc\right)\right]\xi_{\mu t}e^{i(\omega t+\beta_\mu z)}\xi^*_{\mu,vt}dxdy + cc \qquad (3.48)$$

According to the orthogonality relationship of eq (3.15), $\xi^*_{\mu,vt}$ is choosen as multiplier and μ *and* v can be used to determine the rate of variation of either A_v *or* B_μ. Once the term on the LHS has been chosen, the next question is the choice of the terms on the RHS. Before this is examined, consider the terms on the RHS in general.

The RHS of Eq. (3.48) has two generic components for both A and B modes as:

RHS = -in$\omega\varepsilon_0 B_\mu e^{i(\omega t+\beta_\mu z)} \times \int_{-\infty}^{+\infty}\int_{-\infty}^{+\infty} \overline{\Delta n}\, \xi_{\mu t}\xi_{\mu t}^{*} dxdy.$

$$- in\omega\varepsilon_0 A_\mu e^{i(\omega t-\beta_p z+\phi(z))} \times \int_{-\infty}^{+\infty}\int_{-\infty}^{+\infty} \frac{\Delta n}{2}\xi_{vt}\xi_{\mu t}^{*} dxdy + cc \qquad (3.49)$$

The left hand side of eq (3.48) has dependence on the refractive index change which must agree with the first exponent term of the eq(3.49) because any other phase-velocity dependence will not remain in synchronism with the generated wave. The first part of the second term in eq (3.49) is dependent on the phase-synchronous factor

$$\beta_p = \frac{2\pi N}{\wedge} \pm \beta_v \qquad (3.50)$$

From the right hand side of Eqs. (3.48) and (3.49) the interactions of modes can be determined. The aspects taken into account are the following: first, the phase constants on the LHS and the RHS of Eq. (3.49) be identical to Eq. (3.50) for the conservation of the momentum and hence it influences the coupling between copropagating or counterpropagating modes. Secondly, the transverse integral on the RHS of Eq. (3.49), determines the strength of the mode interactions.

3.4 Phase matching

In the Eq. (3.50) the phase factor is the sum or difference between the phase factor of the perturbation and the magnitude of the driving electric field mode propagation β_v. The resultant $\beta_p$is the phase constant of the induced polarization wave. This is the propagation constant of the bounded wave in the presence of sources which is generated by the polarization response of the material. The generated and the polarization waves must remain in phase over a significant distance, z for significant transfer of energy from the driving field amplitude A_v to the generated fields on the LHS of Eq. (3.49).

For the continuous transfer of the energy:

$$\beta_\mu = \beta_p \qquad (3.51)$$

It gives the phase matching condition. The phase mismatch $\Delta\beta$ is given by

$$\Delta\beta = \beta_\mu - \beta_p \qquad (3.52)$$

Including (3.50) in (3.52) it can be obtained

$$\Delta\beta = \beta_\mu \pm \beta_v - \frac{2\pi N}{\wedge} \qquad (3.53)$$

If β_v and β_μ have same sign then the interaction is between the counter propagating modes; if they have opposite signs, then the interaction is between copropagating modes . Finally, energy conservation requires that the frequency of the generated wave remains unchanged. This is thus the theory of Bragg Condition.

Let us consider an optical fiber with a refractive index profile $n^2(x,y)$ in which there is a periodic z-dependent perturbation given by Δn^2(x,y,z) this perturbation could correspond to periodic index variation as in a Fiber Bragg Grating .

If $\Psi_1(x,y)$ and Ψ_2(x,y) are two modes of the fiber, then the periodic perturbation can, under certain conditions couple power among the modes. Thus for the total field at any value of z as

$$\Psi(x,y,z) = A(z)\Psi_1(x,y)e^{-i\beta_1 z} + \text{B(z)}\,\Psi_2(x,y)e^{-i\beta_2 z} \qquad (3.54)$$

Here β_1 and β_2 are the absence of the perturbation and A(z) and B(z) are the corresponding amplitudes. In the absence of the perturbation A and B would be constants. The perturbation couples power among the modes and hence A and B are z-dependent.

Since Ψ_1 and $\Psi_2$are the modes of the fiber in the absence of any perturbation they satisfy the following equations.

$$\nabla_t^2\Psi_1 + (k^2n^2(x,y) - \beta_1^2)\,\Psi_1 = 0 \qquad (3.55)$$

$$\nabla_t^2\Psi_2 + (k^2n^2(x,y) - \beta_2^2)\Psi_2 = 0 \qquad (3.56)$$

Where

$$\nabla_t^2 = \nabla^2 - \partial^2/\partial z^2 \qquad (3.57)$$

They also satisfy the following orthogonality conditions

$$\iint_{-\infty}^{\infty} \Psi_1^*(x,y)\,\Psi_2\ (x,y)\,dxdy = 0 \qquad (3.58)$$

The wave equation to be satisfied by $\Psi(x,y,z)$is

$$\nabla_t^2\Psi\ + \frac{\partial^2\Psi}{\partial z^2} + k_0^2[n^2(x,y) + \Delta n^2(x,y,z)]\Psi = 0 \qquad (3.59)$$

Substituting from eq (3.54)

$\nabla_t^2[A(z)\Psi_1(x,y)e^{-i\beta_1 z} + \text{B(z)}\,\Psi_2(x,y)e^{-i\beta_2 z}] + \partial^2/\partial z^2[A(z)\Psi_1(x,y)e^{-i\beta_1 z} + \text{B(z)}$

$\Psi_2(x,y)e^{-i\beta_2 z}] + k_0^2[n^2(x,y) + \Delta n^2(x,y,z)]\,[A(z)\Psi_1(x,y)e^{-i\beta_1 z} + \text{B(z)}\,\Psi_2(x,y)e^{-i\beta_2 z}] = 0$

$\nabla_t^2[A(z)\Psi_1(x,y)e^{-i\beta_1 z} + \text{B(z)}$

$\Psi_2(x,y)e^{-i\beta_2 z}] + \Psi_1(x,y)[\partial^2A/\partial z^2(e^{-i\beta_1 z}) - 2i\beta_1.(dA/dz)(e^{-i\beta_1 z}) - A\beta_1^2(e^{-i\beta_1 z})] +$

$\Psi_2(x,y)[\partial^2B/\partial z^2(e^{-i\beta_2 z}) - 2i\beta_2.(dB/dz)(e^{-i\beta_2 z}) - B\beta_2^2(e^{-i\beta_2 z})] +$

$k_0^2[n^2(x,y) + \Delta n^2(x,y,z)]\,[A(z)\Psi_1(x,y)e^{-i\beta_1 z} + \text{B(z)}\,\Psi_2(x,y)e^{-i\beta_2 z}] = 0$

neglecting second derivative of A(z) and B(z) with z i.e slowly varying envelope approximation

$$A(z)e^{-i\beta_1 z}\left[\nabla_t^2\Psi_1(x,y)+\left(k_0^2\ \ n^2(x,y)-\beta_1^2\right)\Psi_1(x,y)\right]+$$

B(z) $e^{-i\beta_2 z}[\nabla_t^2\Psi_2(x,y)+(k_0^2n^2(x,y)-\beta_2^2)\Psi_2(x,y)]+[-2i\beta_1.(dA/dz)$

$\Psi_1-2i\beta_2(\frac{dB}{dz})\Psi_2]e^{-i\Delta\beta z}+[k_0^2\Delta n^2(x,y,z)\left[A\,\Psi_1+B\Psi_2\right]e^{i\Delta\beta z}]=0$

By using eq(3.55)and(3.56) it follows

$$-2i\beta_1.(dA/dz)\,\Psi_1-2i\beta_2(\frac{dB}{dz})\Psi_2e^{-i\Delta\beta z}+[k_0^2\Delta n^2(x,y,z)\left[A\,\Psi_1+B\Psi_2e^{i\Delta\beta z}\right]=0 \qquad (3.60)$$

Where

$$\Delta\beta=\beta_1-\beta_2 \qquad (3.61)$$

Multiplying eq(3.60) by Ψ_1^* (complex conjugate of Ψ_1) and integrating

$-2i\beta_1.(dA/dz)\iint\Psi_1^*\ \Psi_1dxdy-2i\beta_2(\frac{dB}{dz})\iint\Psi_1^*\ \Psi_2dxdy\,e^{-i\Delta\beta z}+$

$k_0^2[A\iint\Psi_1^*\,\Delta n^2\,\Psi_1dxdy+B\iint\Psi_1^*\,\Delta n^2\,\Psi_2dxdye^{i\Delta\beta z}]=0$

By using eq(3.58)

$$-2i\beta_1.\left(\frac{dA}{dz}\right)\iint\Psi_1^*\ \Psi_1\,dxdy=-k_0^2[A\iint\Psi_1^*\,\Delta n^2\,\Psi_1\,dxdy+B\iint\Psi_1^*\,\Delta n^2\,\Psi_2dxdye^{i\Delta\beta z}]$$

Then

$$\frac{dA}{dz}=-ic_{11}A-ic_{12}Be^{i\Delta\beta z} \qquad (3.62)$$

Where the orthogonality condition has been used and

$$c_{11}(z)=\left(\frac{k_0^2}{2\beta_1}\right)\iint\Psi_1^*\,\Delta n^2\,\Psi_1dxdy/\iint\Psi_1^*\ \Psi_1\,dxdy \qquad (3.63)$$

$$c_{12}(z)=\left(\frac{k_0^2}{2\beta_1}\right)\iint\Psi_1^*\,\Delta n^2\,\Psi_2dxdy/\iint\Psi_1^*\ \Psi_1\,dxdy \qquad (3.64)$$

Similarly ,multiplying (3.60) by $\Psi_2^*$and integrating

$$\frac{dB}{dz}=-ic_{22}B-ic_{21}Ae^{-i\Delta\beta z} \qquad (3.65)$$

Where

$$c_{22}(z)=\left(\frac{k_0^2}{2\beta_2}\right)\iint\Psi_2^*\,\Delta n^2\,\Psi_2dxdy/\iint\Psi_2^*\ \Psi_2dxdy \qquad (3.66)$$

$$c_{21}(z)=\left(\frac{k_0^2}{2\beta_2}\right)\iint\Psi_2^*\,\Delta n^2\,\Psi_1dxdy/\iint\Psi_2^*\ \Psi_2dxdy \qquad (3.67)$$

Eqs. (3.62) and (3.65) together present the coupled mode equations and describe the z-dependence of A and B.

In the presence of a periodic z-dependent perturbation

$$\Delta n^2(x,y,z) = \Delta n^2(x,y)\sin Kz \qquad (3.68)$$

Where K=2π/Λ, and Λ represents the spatial period of the perturbation .Eq. (3.68) represents the refractive index perturbation in Fiber Bragg Grating. For $\Delta n^2(x,y,z)$ given by Eq. (3.68).

$$c_{12}(z) = \left(\frac{k_0^2}{2\beta_1}\right)\left[\frac{\iint \Psi_1^* \Delta n^2(x,y)\Psi_2 dxdy}{\iint \Psi_1^* \Psi_1 dxdy}\right] sinkz \quad = 2k_{11} sinkz \qquad (3.69)$$

Where

$$k_{11} = \left(\frac{k_0^2}{4\beta_1}\right)\left[\frac{\iint \Psi_1^* \Delta n^2(x,y)\Psi_2 dxdy}{\iint \Psi_1^* \Psi_1 dxdy}\right] \qquad (3.70)$$

Similarily from (3.64, 3.66 and 3.67)

$$C_{11}=2K_{11}SinKz$$

$$C_{22}=2K_{22}SinKz$$

$$C_{21}=2K_{21}SinKz \qquad (3.71)$$

With K_{11} , K_{22} and K_{21} being z-independent and given by Eq. (3.70).
Substituting from Eqs. (3.69) and (3.71) in Eq. (3.62)

$$\frac{dA}{dz} = -2iK_{11}A\ \sin Kz - k_{12}Be^{i(\Delta\beta+K)z} + K_{12}Be^{i(\Delta\beta-K)z} \qquad (3.72)$$

for weak perturbation K_{12} and K_{21} are small and hence, the typical length scale over which the mode amplitudes change appreciably $\approx 1/K_{12} \approx 1/K_{21}$,which is large if Eq. (3.72) is integrated over distance L, small compared with the distance over which A and B change appreciably.

$$\int_{z-\frac{L}{2}}^{z+\frac{L}{2}} \frac{dA}{dz}dz = \int_{z-\frac{L}{2}}^{z+\frac{l}{2}} [-2ik_{11}\ \ A\sin Kz - k_{12}Be^{i(\Delta\beta+K)z} + k_{12}Be^{i(\Delta\beta-K)z}]\,dz$$

$$A(z+\tfrac{L}{2}) - A(z-\tfrac{L}{2})$$

$$= 2iK_{11}\cos k\left[\left(z+\frac{L}{2}\right)-\left(z-\frac{L}{2}\right)\right]/K - \frac{k_{12}B\left[e^{i(\Delta\beta+K)\left[\left(z+\frac{L}{2}\right)-\left(z-\frac{L}{2}\right)\right]}\right]}{i(\Delta\beta+K)} + \frac{k_{12}B\left[e^{i(\Delta\beta-K)\left[\left(z+\frac{L}{2}\right)-\left(z-\frac{L}{2}\right)\right]}\right]}{i(\Delta\beta-K)}$$

$A(z+\frac{L}{2})-A(z-\frac{L}{2})=$

$+4\acute{i}K_{11}A\cos Kz\frac{\sin(K\frac{L}{2})}{K}-2i\frac{k_{12}B\left[e^{i(\Delta\beta+K)z}\right]}{i(\Delta\beta+K)}\{[e^{\frac{i(\Delta\beta+K)L}{2}}+e^{\frac{-i(\Delta\beta+K)L}{2}}]/2\}+2i$

$\frac{k_{12}B\left[e^{i(\Delta\beta-K)z}\right]}{i(\Delta\beta-K)}\{[e^{\frac{i(\Delta\beta-K)L}{2}}+e^{\frac{-i(\Delta\beta-K)L}{2}}]/2\}$

That is

$A(z+\frac{L}{2})-A(z-\frac{L}{2})=+4\acute{i}K_{11}A\cos Kz\frac{\sin(K\frac{L}{2})}{K}$

$$-2\acute{i}K_{12}Be^{i(\Delta\beta+K)z}\{\frac{\sin(\Delta\beta+K)(L/2)}{\Delta\beta+K}\}$$

$$+2\acute{i}K_{12}Be^{i(\Delta\beta-K)z}\{\frac{\sin(\Delta\beta-K)(L/2)}{\Delta\beta-K}\} \quad (3.73)$$

Now,

$$\Delta\beta=(2\pi/\ \lambda_0)\Delta n_{eff} \quad (3.74)$$

Where Δn_{eff} is the effective index difference between the modes. As a typical value Δn_{eff} is approximately the index difference between core and cladding which if assumed to be about 0.005, gives for λ_0=1µm

$\Delta\beta\approx 3*10^4\ m^{-1}$

Thus, if K is chosen so that K≈Δβ and L≈$2*10^{-3}m$, then from (3.73)

$|\frac{\sin(\Delta\beta-K)\frac{L}{2}}{\Delta\beta-K}|\approx\frac{L}{2}=10^{-3}m$

$|\frac{\sin(\Delta\beta+K)\frac{L}{2}}{\Delta\beta+K}|\leq\frac{1}{(\Delta\beta+K)}\approx\frac{1}{2\Delta\beta}\approx 1.7*10^{-5}m$

$|\frac{\sin\frac{KL}{2}}{K}|\leq\frac{1}{K}\approx\frac{1}{\Delta\beta}\approx 3*10^{-5}m$

Hence for K≈Δβ, the contribution from the first and the second terms in the RHS of Eq. (3.73) is negligible compared with the last term and hence can be neglected.

The second term would have made significant contribution if $\Delta\beta=\beta_1-\beta_2=-K$ that is if $\beta_2\approx\beta_1+K$.

Thus, in the presence of a periodic perturbation, coupling takes place mainly among modes for which $\Delta\beta$ is close to either K or to –K. This justifies the two term expansion of Eq. (3.54). The approximation corresponds to the rotating wave approximation used in time-dependent perturbation theory in quantum mechanics.

Thus, if

$$K=\frac{2\pi}{\Lambda}\approx\Delta\beta=\beta_1-\beta_2 \tag{3.75}$$

Then Eq. (3.72) can be approximated by

$$\frac{dA}{dz}=k_{12}Be^{i\Gamma z} \tag{3.76}$$

Where $\Gamma=\Delta\beta-K$. similarly, Eq. (3.65) leads to

$$\frac{dB}{dz}=-K_{21}Ae^{i\Gamma z} \tag{3.77}$$

3.5 Bragg Condition

If the modes Ψ_1 and Ψ_2 are normalized to carry unit power, then under the weakly guiding approximation [33]

$$\frac{\beta_1}{2\omega\mu_0}\int\int \Psi_1^{*}\Psi_1 dxdy=1 \tag{3.78}$$

And similar equation for Ψ_2 then $|A|^2$ and $|B|^2$ would directly give the power carried by both modes. Using Eq. (3.78) in Eq. (3.70)

$$K_{12}=\frac{\omega\varepsilon_0}{8}\iint\Psi_1^{*}\Delta n^2(x,y)\Psi_2 dxdy \tag{3.79}$$

By using the orthonormality relation for Ψ_2, one can show that

$$K_{21}=K_{12}=K \tag{3.80}$$

Thus, the two coupled equations become

$$\frac{dA}{dz}=KBe^{i\Gamma z} \tag{3.81}$$

$$\frac{dB}{dz} = -KAe^{-i\Gamma z} \qquad (3.82)$$

Where K is given by eq(3.79)

Eqs. (3.81) and (3.82) describe the coupling among the two modes propagating along the same direction .that is β_1 and β_2 both positive or negative. This is referred to codirectional coupling.

Another important coupling is contradirectional coupling. In this the total field at any value of z is given by

$$\Psi(x,y,z)=A(z)\Psi_1(x,y)e^{-i\beta_1 z}+B(Z)\Psi_2(x,y)e^{i\beta_2 z} \qquad (3.83)$$

Thus, the mode with propagation constant β_1 is propagating in the +z direction and that with the propagation constant $\beta_2$is propagating in –z direction. If they correspond to the same mode, then

$\beta_1 = \beta_2 = \beta$.

For this coupling if the identical procedure described earlier is followed, then following two coupled mode equations can be obtained

$$\frac{dA}{dz} = KBe^{i\Gamma z} \qquad (3.84)$$

$$\frac{dB}{dz} = KAe^{-i\Gamma z} \qquad (3.85)$$

With

$$\Gamma = \beta_1 + \beta_2 - K \qquad (3.86)$$

Note that the signs on the RHS of Eqs. (3.84) and (3.85) are the same, which is opposite in the case of codirectional coupling. Because of this, the solutions for the contradirectional case are not oscillatory.

Here if the coupling between two modes which are propagating in opposite directions are considered, for phase matching condition it is required that $\Gamma=0$.

Implying $\beta_1 + \beta_2 = K$ (3.87)

If the coupling is between two identical modes travelling in opposite directions, then

$$\beta_1 = \beta_2 = (2\pi/\lambda_0)n_{eff} \quad (3.88)$$

Where n_{eff} is the effective refractive index of the mode and $K=\frac{2\pi}{\Lambda}$ (3.89)

Then by eq(3.87)

$$2\left(\frac{2\pi}{\lambda_0}\right)n_{eff} = \frac{2\pi}{\Lambda} \quad (3.90)$$

$$\text{i.e.} \quad \lambda_0 = 2n_{eff}\Lambda \quad (3.91)$$

which is known to be bragg condition.

3.6 Uniform Bragg grating reflectivity

Consider a uniform Bragg grating formed within the core of an optical fiber with an average refractive index n_0. The index of refractive profile can be expressed as

$$n(x) = n_0 + \Delta n \cos\left(\frac{2\pi x}{\Lambda}\right) \quad (3.92)$$

Where Δn is the amplitude of the induced refractive-index perturbation typically $10^{-5}-10^{-2}$and x is the distance along the fiber longitudinal axis. Using the coupled-mode theory, analytical description of the reflection properties of Bragg gratings may be obtained. The reflectivity of a grating with constant modulation amplitude and period is given by the following expression:

$$R = \frac{k^2 \sinh^2(sl)}{\delta^2 \sinh^2(sl) + s^2 \cosh^2(sl)} \quad (3.93)$$

where R(l ,λ) is the reflectivity, which is a function of the grating length l , and wavelength λ. *k* is the coupling coefficient, δ is the detuning wave vector, $k=2\pi n_0/\lambda$ is the propagation constant and $s=\sqrt{k^2-\delta^2}$.

3.7 Coupling Coefficient for Contradirectional Coupling

For contradirectional coupling between two LP01 modes propagating in opposite directions, $\varphi_1 = \varphi_2$ and Eq. (3.79) becomes

$$k = \frac{\omega\varepsilon 0}{8} \iint \Delta n^2(x,y)|\varphi|^2 dxdy \tag{3.94}$$

If the Gaussian approximation for φ is used, then

$$\varphi = \frac{2}{\omega_0}\sqrt{\frac{\omega\mu_0}{\pi\beta}}\, e^{-r^2/\omega_0^2} \tag{3.95}$$

Where the multiplying constant will satisfy Eq. (3.94)

For Fiber Bragg Grating, it may be assumed that the periodic refractive index perturbation is uniform inside the core and zero outside so,

$$\Delta n^2(x,y) = \Delta n^2; \qquad x^2 + y^2 < a^2$$

$$= 0; \qquad otherwise \tag{3.96}$$

And Eq. (3.94) becomes

$$k = \frac{\omega\varepsilon_0}{8}\Delta n^2 \frac{4}{\omega_0}\frac{\omega\mu_0}{\pi\beta}\int_0^a r\, dr \int_0^{2\pi} d\emptyset\, e^{-2r^2/w_0^2}$$

$$= \frac{k_0\Delta n^2}{4\, n_{eff}}\left(1 - e^{-2a^2/w_0^2}\right)$$

If $\Delta n^2 \cong 2n\Delta n$ and assume n$\cong n_{eff}$,

$$k = \frac{\pi\Delta n}{\lambda_0}\left(1 - e^{-2a^2/w_0^2}\right) \tag{3.97}$$

One can, in general, evaluate Eq. (3.94) for any given perturbation $\Delta n^2(x,y)$ and modal field profiles $\varphi_1(x,y)$ and $\varphi_2(x,y)$.

For the sinusoidal variation of index, perturbation along the fiber axis is given by

$$k = \frac{\pi\,\Delta n\, I}{\lambda} \tag{3.98}$$

Where *I* is given by $\left(1 - e^{-2a^2/w_0^2}\right)$ under the Gaussian approximation and is called as integral overlap. For sinusoidal variation it is given by

$$I = 1 - \frac{1}{V^2} \tag{3.99}$$

a function of the fiber parameter V that represents the fraction of the integrated fundamental-mode intensity, contained in the core. At the Bragg grating center wavelength, there is no wave-vector detuning and ($\delta = 0$), therefore, the expression for the reflectivity becomes

$$\text{R (l, } \lambda) = tanh^2(kl) \tag{3.100}$$

The reflectivity increases as the induced index of refraction change increases. Similarly, as the length of the grating increases so does the resultant reflectivity. A calculated reflection spectrum as a function of the wavelength detuning is shown in Figure 3.2. The side lobes of the resonance are due to multiple reflections to and from opposite ends of the grating region

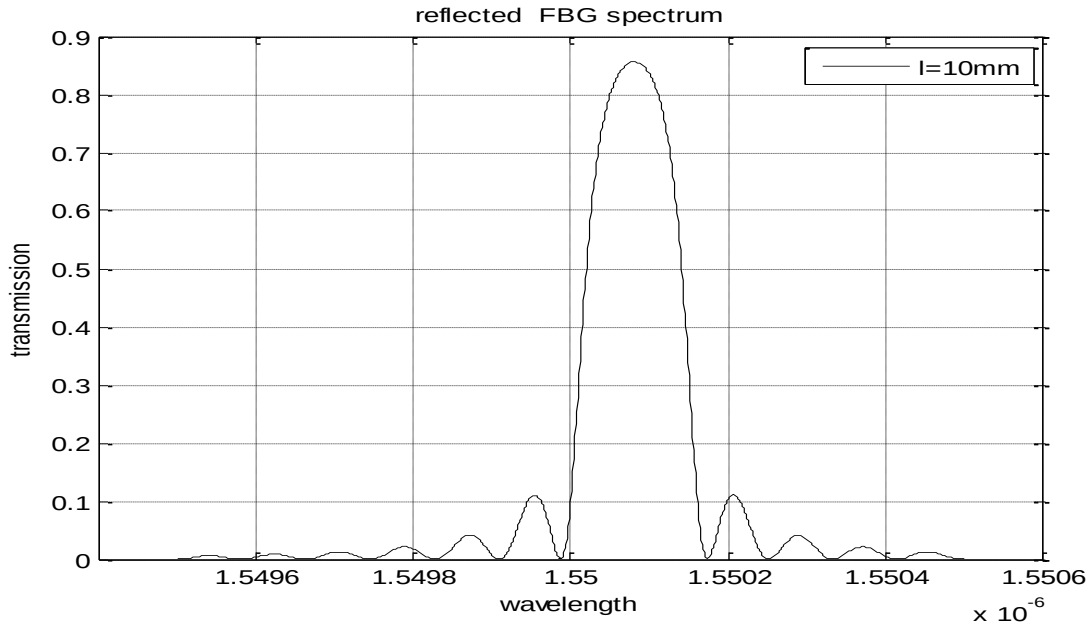

Figure 3.2 Calculated Reflected FBG spectrum

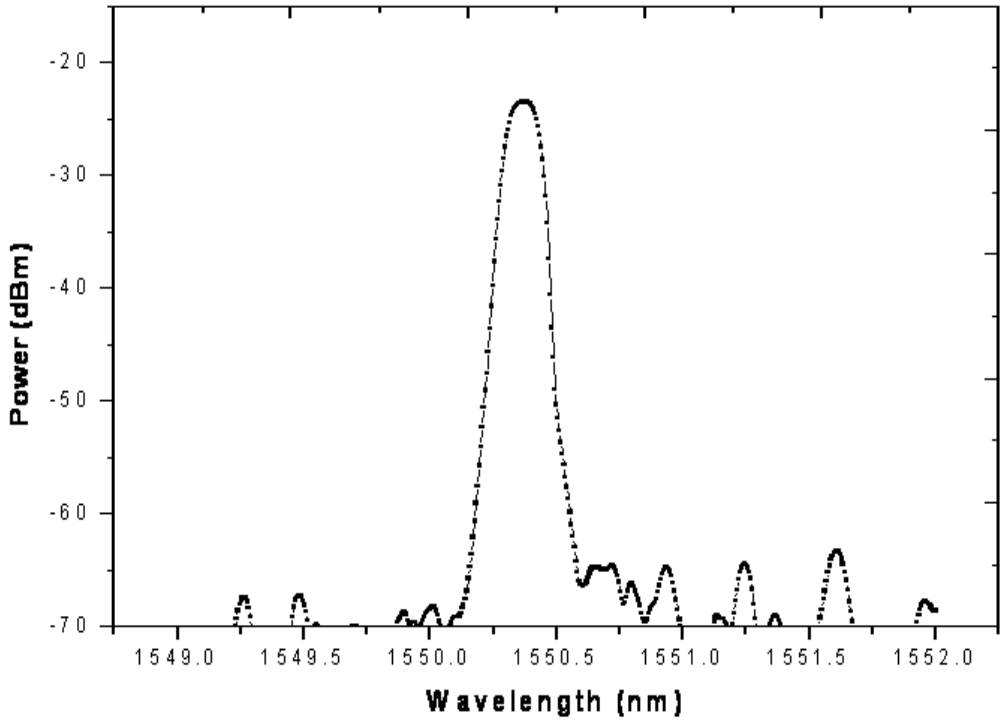

Figure 3.3 Experimental spectrum of FBG

A general expression for the approximate full width at half-maximum bandwidth of a grating is given by

$$\Delta\lambda = \lambda_B \alpha \sqrt{\left(\frac{\Delta n}{2n_0}\right)^2 + \left(\frac{1}{N}\right)^2}, \qquad (3.101)$$

where N is the number of the grating planes. The parameter is ≈1 for strong gratings (for grating with near 100% reflection) and a≈ 0.5 for weak gratings.

3.8 Effects of strain and temperature on Fiber Bragg Gratings

The core effective index of refraction and the periodicity of the grating determine its centre wavelength so that the change of fiber with strain and temperature will affect its core refractive index. The shift in the Bragg grating centre wavelength due to strain and temperature changes is given by [11]

$$\Delta\lambda_B = 2\left(\Lambda\frac{\partial n_{eff}}{\partial l} + n_{eff}\frac{\partial \Lambda}{\partial l}\right)\Delta l + 2\left(\Lambda\frac{\partial n_{eff}}{\partial T} + n_{eff}\frac{\partial \Lambda}{\partial T}\right)\Delta T \qquad (3.102)$$

where T is temperature. The first term in Eq. (3.102) represents the strain effect on an optical fiber. The change of grating length, which is caused by a strain on the fiber, will also affect the period of grating and the strain-optic induced refractive index.

3.8.1 Strain sensitivity

The strain effect term could also be expressed by

$$\Delta\lambda_{B(s)} = \lambda_B(1 - p_e)\varepsilon_z \qquad (3.103)$$

where ε_z is the applied strain on the fiber grating longitudinal axis, and p_e is an effective strain optic constant defined by

$$p_e = \frac{n_{eff}^2}{2}[p_{12} - v(p_{11} + p_{12})] \qquad (3.104)$$

where p_{11} and p_{12} are components of the strain-optic tensor, n_{eff} is the index of the core, and v is Poisson's ratio. For a typical optical fiber p_{11} = 0.113, p_{12} = 0.252, v= 0.16 andn_{eff} = 1.482. By using these parameters and the above equations, the sensitivity of the Fiber Bragg Grating at 1550 *nm* is about 1.2 *pm* of the wavelength shift for 1 μe applied to the grating. Figure 3.4 shows the experimental results of wavelength dependence on applied strain for a 1550.08 *nm* Fiber Bragg Grating.

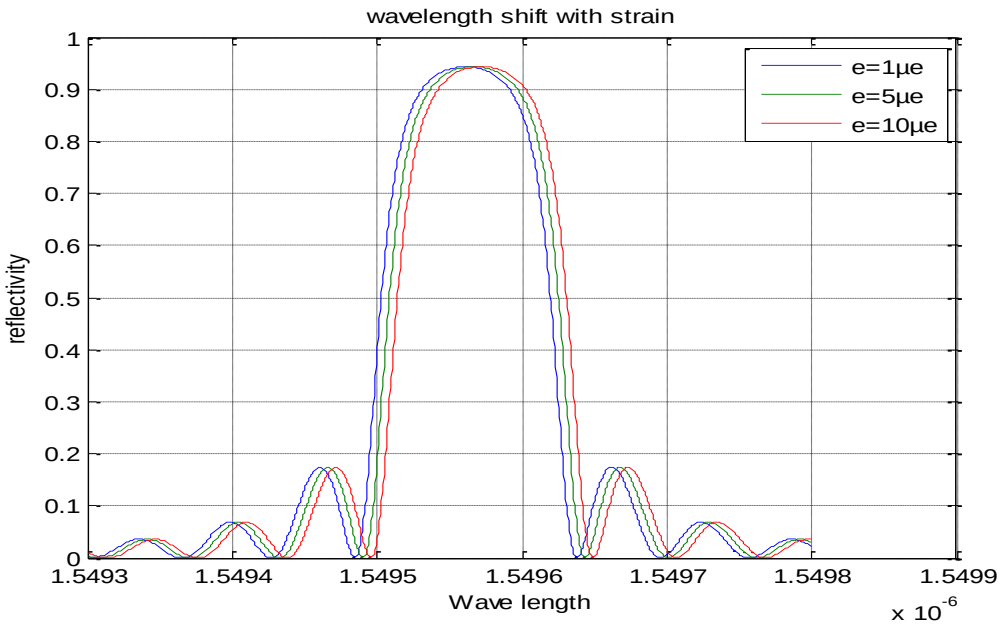

Figure 3.4 Spectrum showing Wavelength Shift with strain

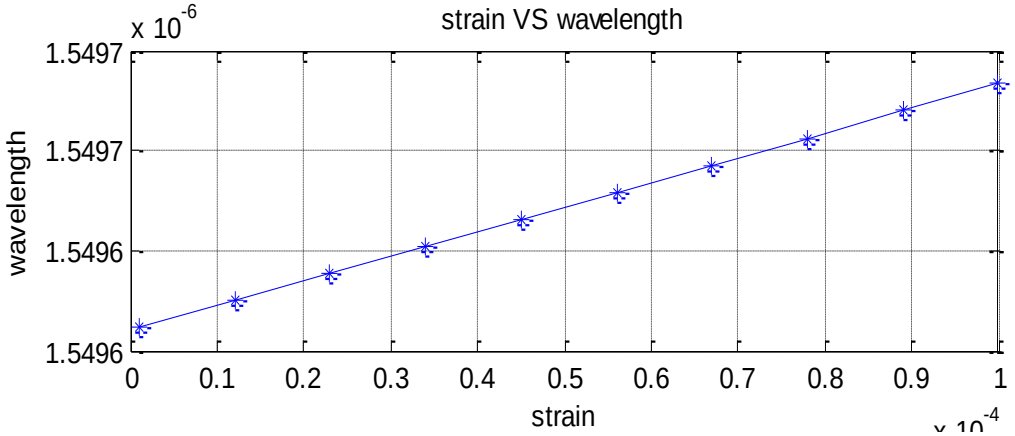

Figure 3.5 Wavelength variation with strain

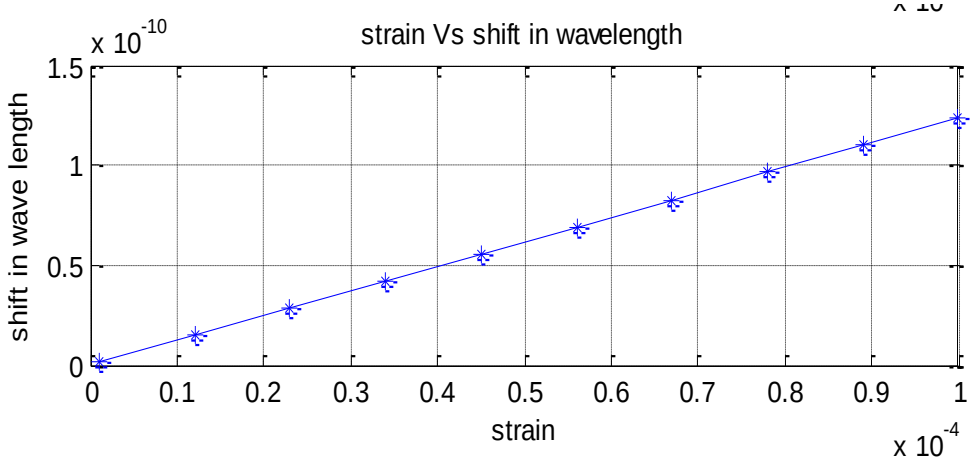

Figure 3.6 shift in wave length with respect to the applied strain

3.8.2 Temperature sensitivity

The second term in Eq. (3.15) represents the temperature effect on an optical fiber. There is a shift in the Fiber Bragg Grating centre wavelength because the thermal expansion changes the grating period and the index of refraction. This fractional wavelength shift for a temperature change (ΔT) could be written as

$$\Delta\lambda_{B(t)} = \lambda_B(\alpha + \zeta)\Delta T \qquad (3.105)$$

Where $\alpha = \left(\frac{1}{\Delta}\right)\left(\frac{\partial \Lambda}{\partial T}\right)$, is the thermal expansion coefficient for the fiber (approximately $0.55*'10^{-6}$ for silica and $\zeta = \left(\frac{1}{n_{eff}}\right)\left(\frac{\partial n_{eff}}{\partial T}\right)$, represents the thermo-optic

coefficient and it is approximately equal to $8.6*10^{-6}$ for the germania-doped silica core fiber. From Eq. (3.18) the expected sensitivity at a ~ 1550 *nm* Bragg grating is approximately 13.7 *pm*/ ^{o}C . Figure 3.7 provides the experimental results of a Fiber Bragg Grating centre wavelength shift as a function of temperature.

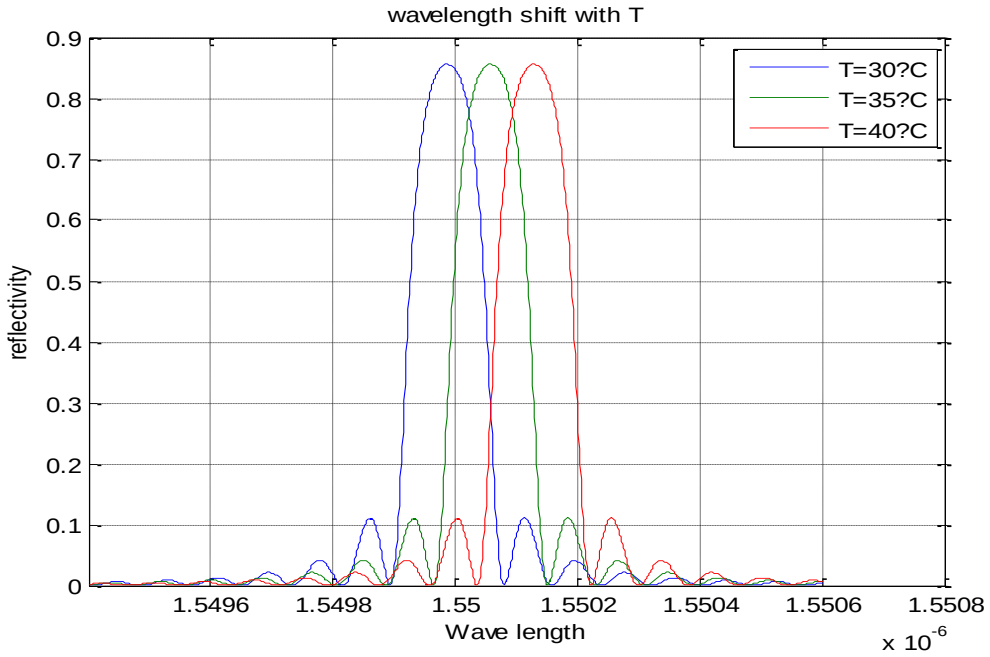

Figure 3.7 Spectrum showing shift in wavelength with varying temperature

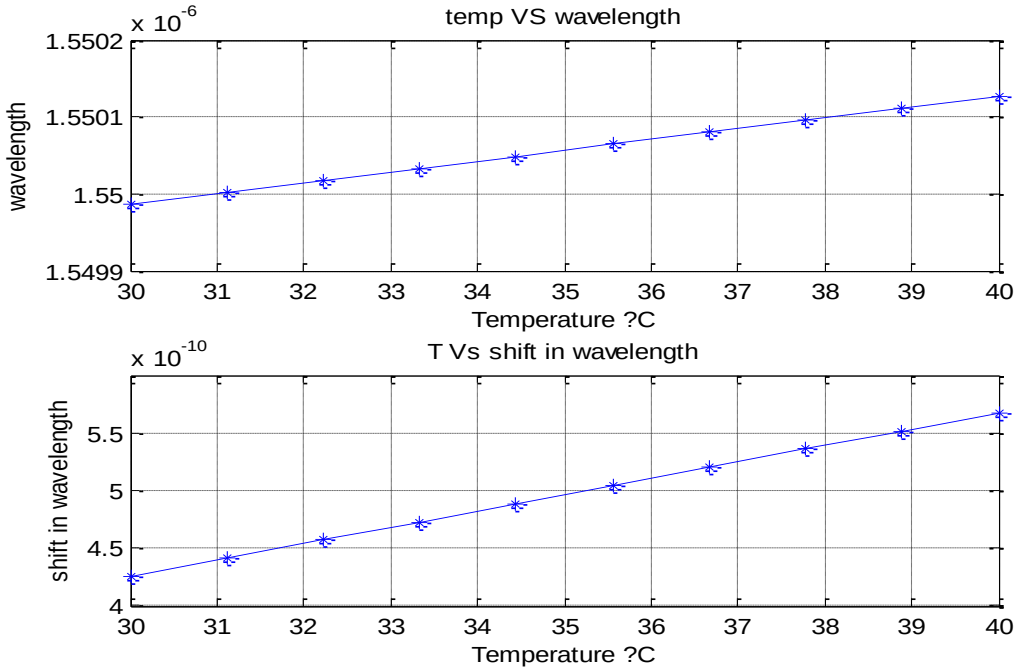

Figure 3.8: Shift in wavelength with varying temperature

3.9 Spectral response of Fiber Bragg Gratings

3.9.1 T-matrix formalism:

An analytical solution for a grating of length *Lg*, with an arbitrary coupling constant *K(Z)* and chirp *A(z)*, is desirable but no simple form exists. The variables cannot be separated since they collectively affect the transfer function. In the T-matrix method, the coupled mode equations are used to calculate the output fields of a short section of grating for which the three parameters are assumed to be constant. Each may possess a unique and independent functional dependence on the spatial parameter *z*. For such a grating with an integral number of periods, the analytical solution results in the amplitude reflectivity, transmission, and phase. These quantities are then used as the input parameters for the adjacent section of grating of length $S(\delta l/2)$ (not necessarily = $\pm\delta l$). The input and output fields for a single grating section are shown

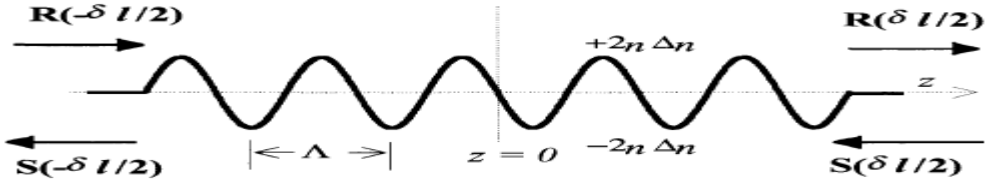

Figure 3.9 Refractive index modulation in the core of a fiber.

Shown in this schematic are the fields at the start of the grating on the LHS and the fields at the output on the RHS. The grating may be considered to be a four-port device with four fields: input fields $R(-\delta l_1/2)$ and $R(\delta l_1/2)$ output fields $S(-\delta l_1/2)$ and $S(\delta l_1/2)$. A transfer matrix T^{1} represents the grating amplitude and phase response. For a short uniform grating, the two fields on the RHS of the following equation are transformed by the matrix into the fields on the LHS

$$\begin{bmatrix} R(-\delta l_1/2) \\ S(-\delta l_1/2) \end{bmatrix} = [T^1] \begin{bmatrix} R(\delta l_1/2) \\ S(\delta l_1/2) \end{bmatrix}. \qquad (3.106)$$

The boundary conditions applied to Eq. (3.106) lead directly to the reflectivity and transmissivity of the grating. These conditions depend on whether the grating is a contradirectional or a codirectional coupler.

3.9.2 Reflection grating

For a reflection grating, the input field amplitude $R(-\delta l_1/2)$ is normalized to unity, and the reflected field amplitude at the output of the grating $S(\delta l_1/2)$ is zero, since there is no perturbation beyond the end of the grating.

Writing the matrix elements into Eq. (3.106) and applying the boundary conditions leads to

$$\begin{bmatrix} 1 \\ S(-\delta l_1/2) \end{bmatrix} = \begin{bmatrix} T_{11} & T_{12} \\ T_{21} & T_{22} \end{bmatrix} \begin{bmatrix} R(\delta l_1/2) \\ 0 \end{bmatrix} \tag{3.107}$$

The transmitted amplitude is easily seen to be

$$R(\delta l_1/2) = \frac{1}{T_{11}}. \tag{3.108}$$

The reflected amplitude follows from Eqs. (3.107) and (3.108) as

$$S(-\delta l_1/2) = \frac{T_{21}}{T_{11}}. \tag{3.109}$$

Consequently, these are now the new fields on the RHS that can be transformed again by another matrix, *T2* and so on, so that for the entire grating after the *Nth* section, where

$$L = \sum_{j=1}^{N} \delta l_j$$

$$\begin{bmatrix} R(-L/2) \\ S(-L/2) \end{bmatrix} = [T^N] \cdots [T^3][T^2][T^1] \begin{bmatrix} R(L/2) \\ S(L/2) \end{bmatrix} \tag{3.110}$$

Replacing the *N* multiplied 2 x 2 matrices in Eq. (3.110) by a single 2 x 2 matrix, the transfer function of the whole grating is,

$$\begin{bmatrix} R(-L/2) \\ S(-L/2) \end{bmatrix} = [\mathbf{T}] \begin{bmatrix} R(L/2) \\ S(L/2) \end{bmatrix} \tag{3.111}$$

where the matrix T is

$$[\mathbf{T}] = \prod_{j=1}^{N} [T^j]. \tag{3.112}$$

Now reflectivity *p*,

$$\rho = \frac{S(-L/2)}{R(-L/2)} = \frac{T_{21}}{T_{11}} \tag{3.113}$$

From the solution to the coupled-mode Eqs. (3.112) and (3.113),
The transfer matrix elements for the y'th section are

$$T_{11} = \cosh(\alpha \delta l_j) - \frac{i\delta \sinh(\alpha \delta l_j)}{\alpha}$$

$$T_{22} = \cosh(\alpha \delta l_j) + \frac{i\delta \sinh(\alpha \delta l_j)}{\alpha}$$

$$T_{12} = -\frac{i\kappa_{ac} \sinh(\alpha \delta l_j)}{\alpha}$$

$$T_{21} = \frac{i\kappa_{ac} \sinh(\alpha \delta l_j)}{\alpha}. \tag{3.114}$$

From these expressions the reflectivity of the grating can be simulated by combining with Eq. (3.113)

3.9.3 Spectral reflectivity dependence on grating length:

The reflection spectral response for uniform Fiber Bragg Gratings could be calculated by using the *T*-matrix formalism described above. The simulations are to demonstrate how the spectral response of a grating is affected as the length of the grating is altered. The change of index of refraction is assumed to be uniform over the grating length However, the value of the change is reduced accordingly with increasing grating length such that the maximum grating reflectivity remains constant. Figure 3.10 shows the spectral profiles uniform Fiber Bragg Gratings with different lengths. Clearly, the bandwidth of the gratings decreased with increasing length. The 15 *mm* long uniform grating has a bandwidth of approximately 0.1 *nm*, and the 10 *mm* long grating has a bandwidth of 0.13 *nm*. Theoretically, Fiber Bragg Gratings can be constructed with extremely small bandwidths by simply increasing the grating length. However, in practice, such devices are not easy to manufacture. The error associated with the spacing between the periods of a grating (during manufacturing) is cumulative therefore, by increasing the length of the

grating, the total error will increase, resulting in out-of-phase periods (leading to broadening of the Fiber Bragg Grating).

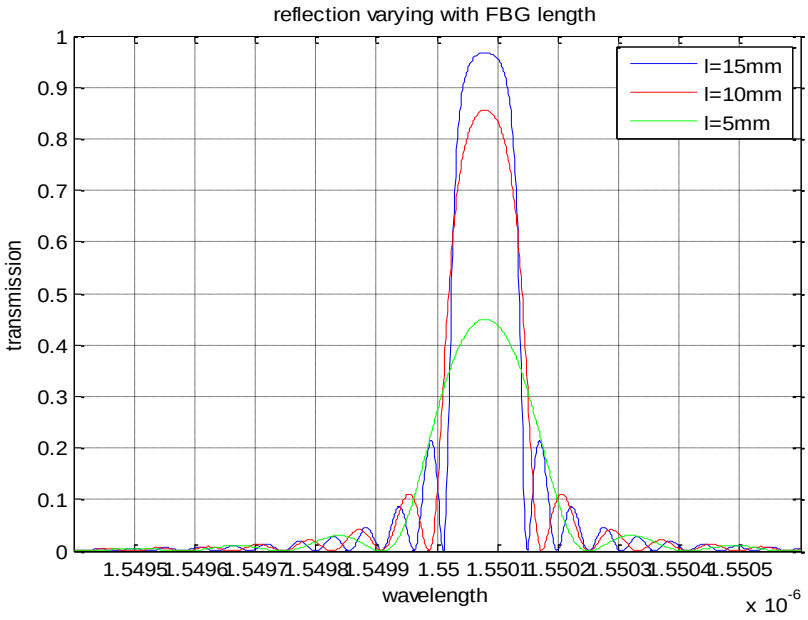

Figure 3.10 shows the spectral profiles uniform Fiber Bragg Gratings with different lengths of grating.

Furthermore, if a long perfect Fiber Bragg Grating is constructed, the effects of the environment have to be considered very carefully. For example, any strain or temperature fluctuations on any part of the grating will cause the periods to move out of phase, resulting in the broadening of the spectrum of the Fiber Bragg Grating.

3.9.4 Spectral reflectivity dependence on refractive index:

Figure 3.11 shows a set of simulations assuming a uniform Fiber Bragg Grating of 20 *mm* in length. In these simulations, the index of refraction changes are varied. For the first grating with $\Delta neff = 0.5 * 10$ -4 the reflectivity is 90% and the bandwidth is approximately 0.086 *nm*. By reducing the change of the index of refraction to half the value of the first grating (Δn_{eff} = 1 $*10^{-4}$), the refractivity decreases to 45% and the bandwidth to 0.049 *nm*. A further decrease in the index of refraction change (Δn_{eff} = 2$*10^{-4}$) results in a reflectivity of 95% and a bandwidth of 0.039 *nm*. It appears that the bandwidth approaches a minimum value and remains constant for further reduction in the index of refraction change.

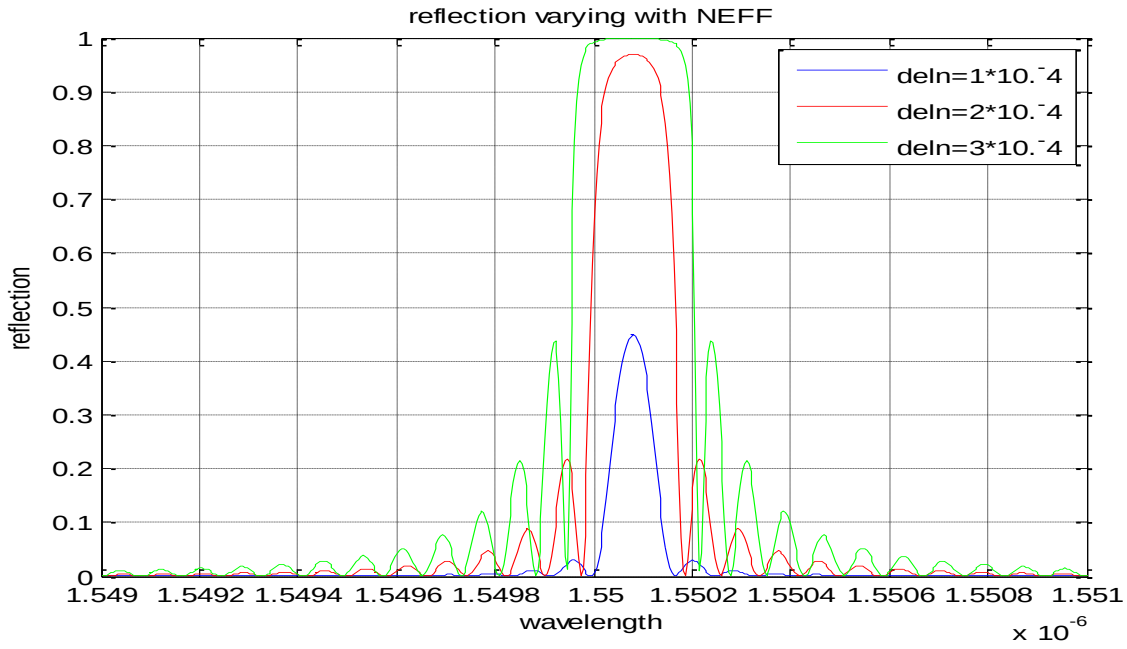

Figure 3.11 Reflectivity v/s index modulation

In this chapter, the uniform Fiber Bragg Grating, which is the simplest type of Fiber Bragg Grating, was introduced. By using the coupled-mode theory, the properties of uniform Fiber Bragg Grating could be explained easily and clearly. The applied strain and surrounding temperature are two main factors that can significantly affect the properties of Fiber Bragg Gratings. There are several techniques for simulating Fiber Bragg Gratings, and all the techniques have varying degrees of complexity. However, the simplest method is the straight forward numerical integration of the coupled-mode equations. This method is direct and capable of simulating the transfer function accurately. This chapter introduced a fast and accurate technique that is based on the T-matrix formalism for calculating the input and output fields for a short section of the grating. The outputs of the first matrix were used as the input fields to the second matrix, not necessarily identical to the first matrix. The process was continued until an entire complex profile grating is modelled. This method was capable of accurately simulating both strong and weak gratings, with or without chirp and apodization. It has the advantage of handling a single period of grating as the minimum unit length for the matrix in the case when the period or amplitude is a slowly varying function of length. The reliability of Fiber Bragg Gratings, which is discussed at the end of this chapter, is essential for long-term usage in optical communications and sensing system.

3.10 Simulation of Fiber Bragg Gratings

This chapter presents the results of simulation of Optical Fiber Bragg Grating (FBG) sensors for stress, strain measurement and demonstrates the methodology to arrive at optimal grating pitch dimensions for a given interrogating wavelength. The wavelength chosen for interrogation of the Fiber Bragg Grating is from the Third window so as to minimize attenuation of the light signal in the communication link from Fiber Bragg Grating sensor to the electronic instrumentation. Before actually inscribing the grating in the fiber, simulation tools provide valuable help in optimizing the design parameters.

Generally, Optical Fibers are used for communication. However, these days Optical Fibers are being increasingly used in sensing applications in the area of civil structures, novel materials, medicines, aerospace, power generation, transportation, military and scientific research[142-150]. Their insensitivity to electromagnetic radiations offers wide usage in places where other instruments are unable to function properly due to effects of radiations. Besides being EMI/RFI immune optical fibers are electrically inert and its flexibility and small size makes routing easy.

Nuclear environments are one such place where optical fiber sensors are being used. However, when optical fibers are exposed to ionizing radiations it results in a wavelength-dependent attenuation increase [151-154]. The use of Fiber Bragg Grating sensors can circumvent this problem.

A FBG consists of a periodic modulation of the index of refraction along the core of an optical fiber as shown in Figure 3.12. FBGs are created by exposition of a photosensitive fiber to an intensity pattern of UV light. In its basic form, the resulting grating reflects selectively the light guided by the optical fiber at the Bragg wavelength $\lambda = 2n\Lambda$, where n and Λ are the effective index of refraction of the fiber and the pitch of the grating in the fiber respectively [155].

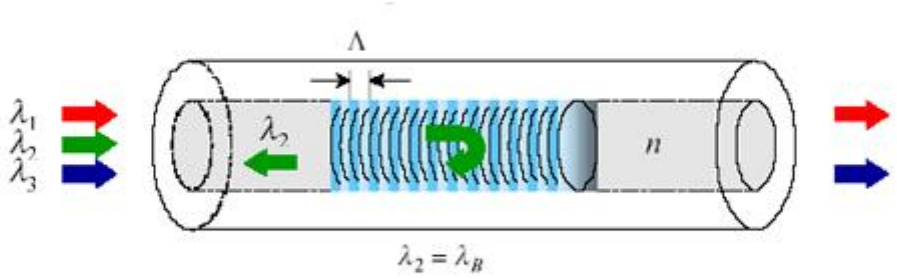

Figure 3.12 Principle of operation of Fiber Bragg Grating

FBG sensors are based on the fact that the Bragg wavelength changes with change in the pitch of the grating and the change in the refractive index. Thus, any physical parameter (like temperature, stress, strain) which causes change in the above mentioned parameters can be sensed using a FBG, by measuring the shift in the Bragg wavelength or the change in reflection coefficient of a particular wavelength. When the Fiber Bragg Grating is interrogated with a light of given wavelength, the reflection coefficient changes with the change in the grating pitch and/or refractive index induced by the physical parameter to be measured.[156]

The manufacturing techniques for Fiber Bragg Gratings are still evolving. The earliest and still one of the most popular, sidewriting methods for producing fiber gratings is the UV holographic [157-159]. This uses two beam interference from amplitude splitting mirror interferometer to fabricate the gratings. The UV holographic method has the advantage of being a flexible system which allows gratings to be written over a wide range of wavelengths, but does require a mechanically stable experimental set-up for CW or multipulse writing. The Bragg wavelength is controlled by adjusting the angle of intersection between the two writing beams. Another common method of grating

fabrication is to use a phase mask. In the usual near field configuration the diffracted first order beams from the phase mask interfere at the optical fiber placed in close proximity to the phase mask surface. In the far field version the +/-1 order beams are reflected off the sides of a fused silica block before they are recombined at the optical fiber. The phase mask techniques are less sensitive to environmental disturbances and produce gratings with highly repeatable characteristics.

Manufacturing facility for Fiber Bragg Gratings involves huge infrastructure and financial involvement. Simulation is an important tool which helps us in optimal design of Fiber Bragg Grating sensors before fabricating.

3.11 Simulation details

Following parameters were chosen for the construction of FBG model. Single mode optical fiber of core diameter 7um was chosen. Index of refraction of the core was fixed as 1.46 and index difference as 0.01. The length of the grating was taken as 1mm under unperturbed conditions. The approximate number of grating pitches in this length is 2000. Care was taken to ensure that the simulated strain induced is well within the limits of the breaking strain which is approximately 4%.

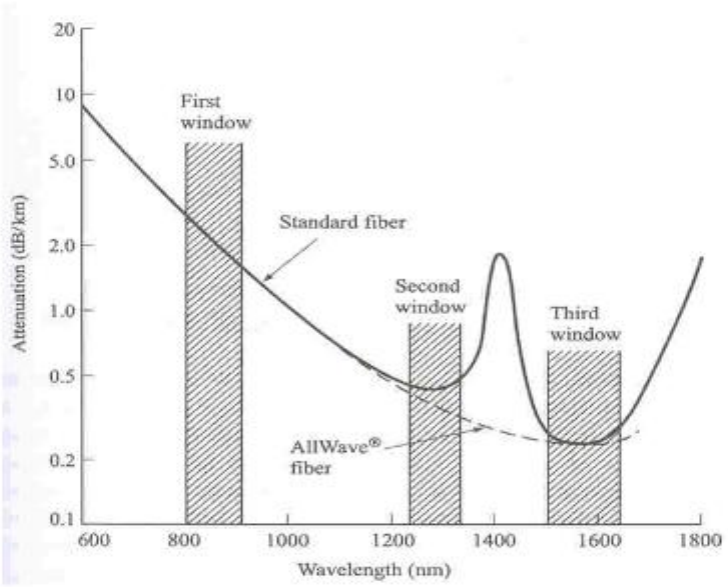

Figure 3.13: Optical Fiber Attenuation as a function of Wavelength

The wavelength of the interrogating light signal was chosen as 1550nm since it falls in the Third window and suffers minimum attenuation during communication from Fiber Bragg Grating sensor to the electronic instrumentation [157]. Optical fiber attenuation as a function of wavelength is show in Figure 3.13.

Iterations were performed to arrive at the optimal pitch for this wavelength and it was found out that for a grating pitch of 0.5325μm, the interrogating wavelength of 1550nm underwent maximum reflection of 94.69% as shown in Figure 3.14.

3.12 Simulation Results

The Figures 3.14 - 3.19 depict the simulation results in the form of graphs of reflected power as a function of wavelength. From iterations it has been established that at a grating pitch of 0.5325μm, maximum reflected power is recorded at wavelength of 1550nm. The effect of strain in elongating the optical fiber and thus the grating pitch has been simulated by taking the output graphs by varying the grating pitch from 0.5323μm to 0.5327μm in regular intervals of 0.0001μm.

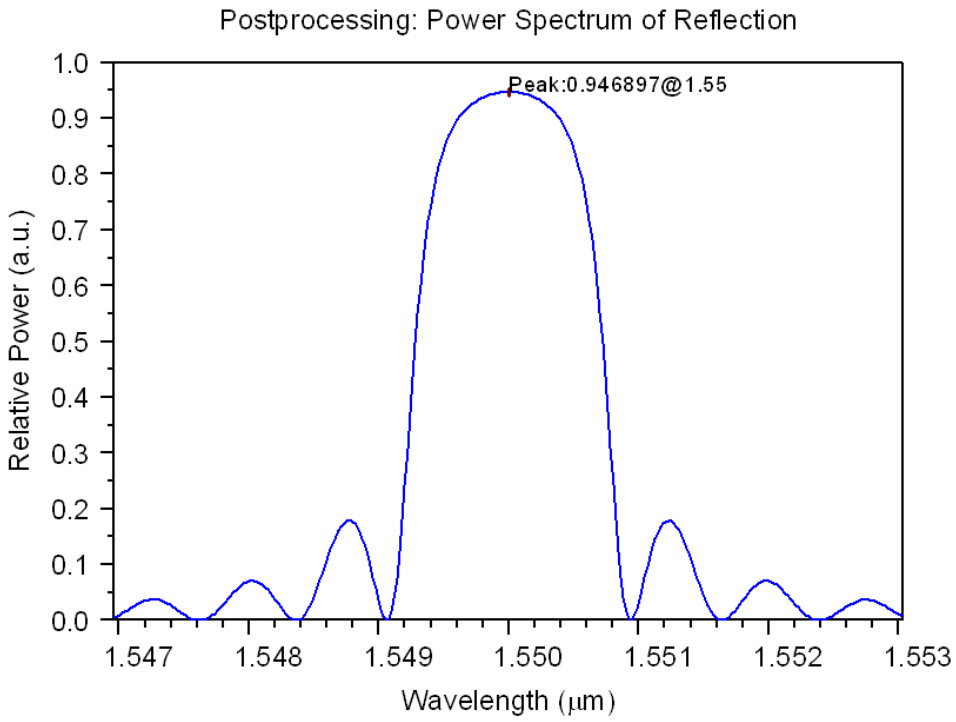

Figure 3.14 Reflected power as a function of wavelength at 1550 nm

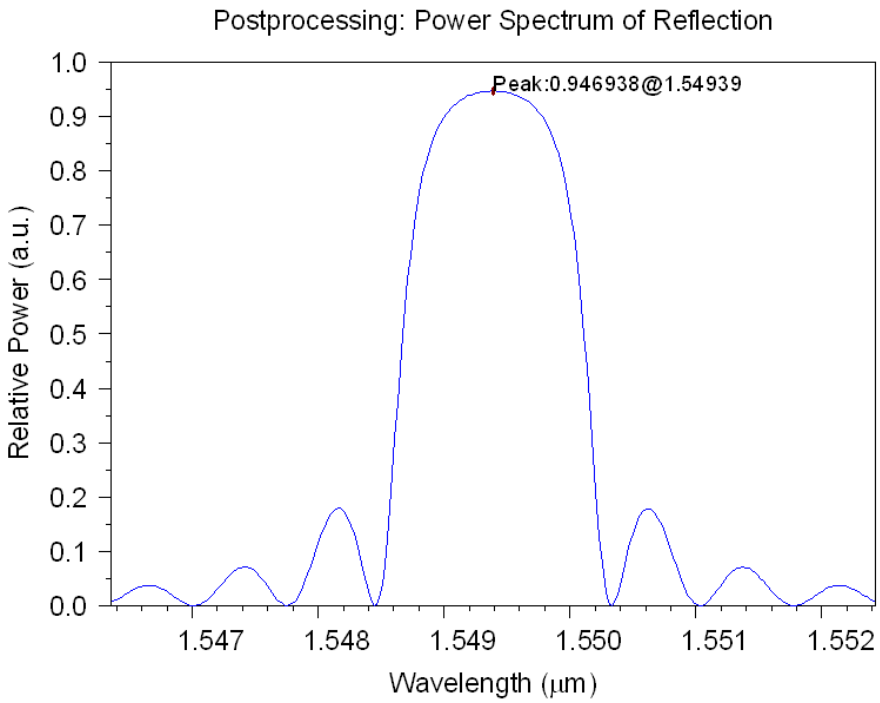

Figure 3.15 Reflected power as a function of wavelength with fiber having pitch 0.5323 um

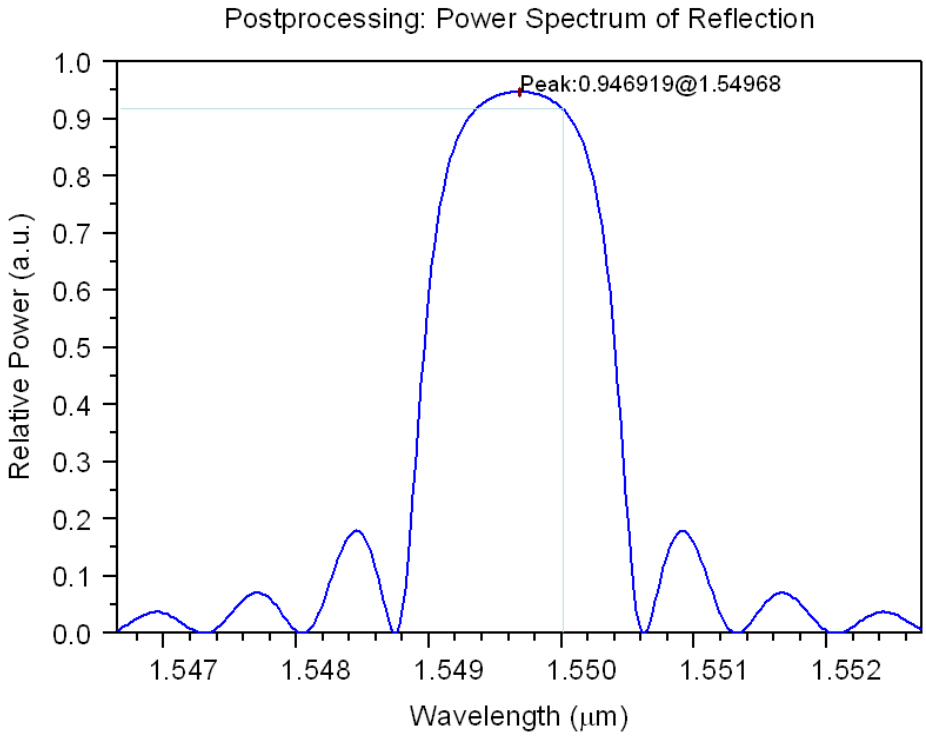

Figure 3.16 Reflected power as a function of wavelength with fiber having pitch 0.5324 um

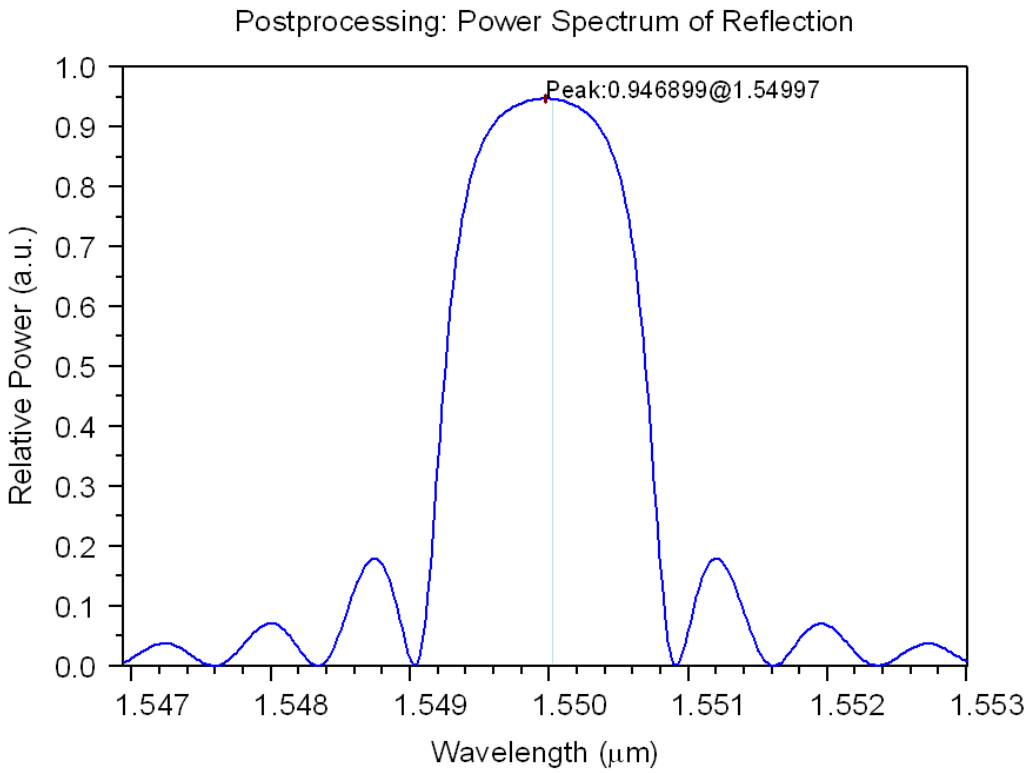

Figure 3.17 Reflected power as a function of wavelength with fiber having pitch 0.5325 um

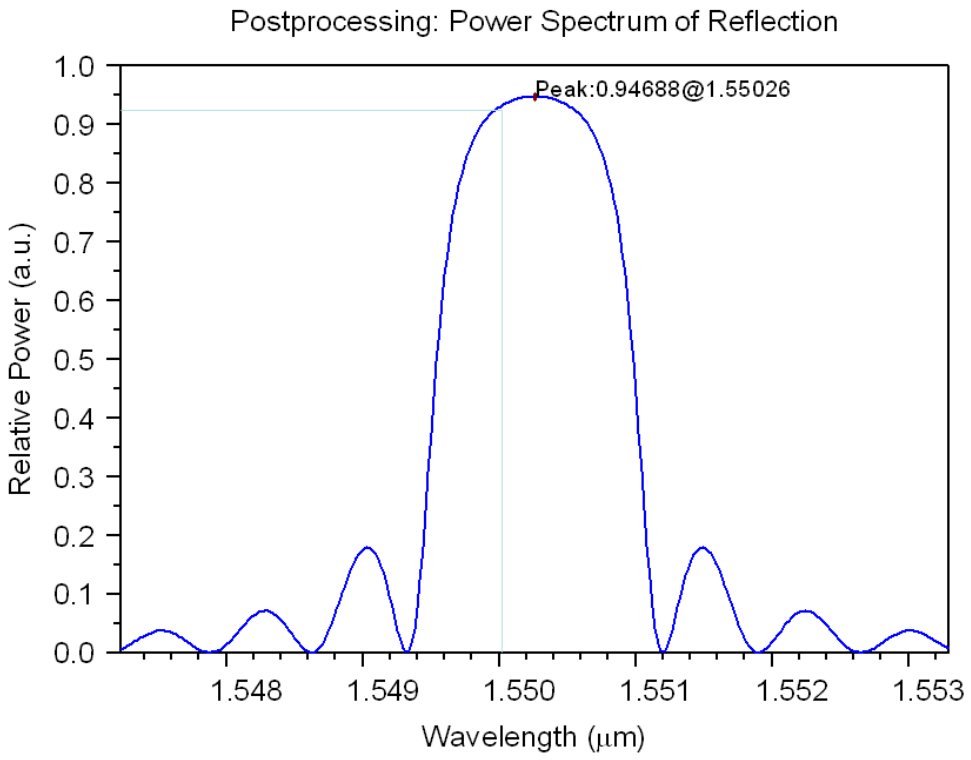

Figure 3.18 Reflected power as a function of wavelength with fiber having pitch 0.5326 um

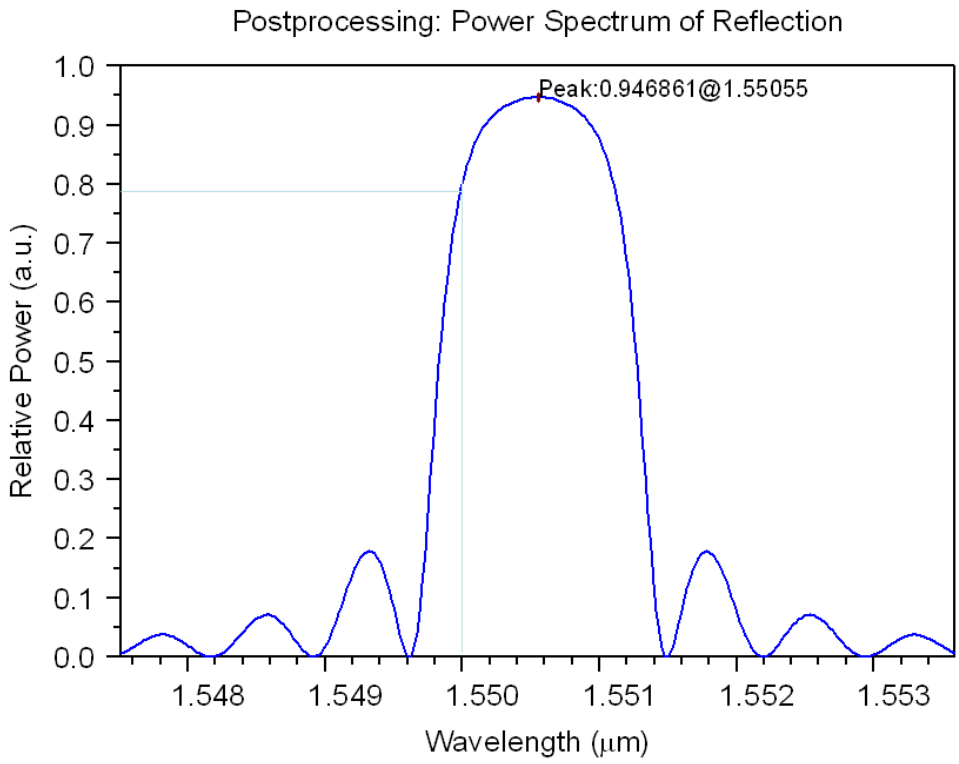

Figure 3.19 Reflected power as a function of wavelength with fiber having pitch 0.5327 um

It can be observed that change in the pitch of the grating changes the reflection coefficient of the interrogating wavelength 1550nm. By observing this change, the strain in the fiber can be calculated and the corresponding measurements can be made.

In Figure 3.16, it can be seen that for a grating pitch of 0.5324μm, the reflectivity of the chosen wavelength of 1550nm had reduced to approximately 93% from 94.6% earlier. In Figure 3.18, it can be observed that for a grating pitch of 0.5236μm, the reflectivity of the chosen wavelength of 1550nm had reduced to approximately 91.5%. for a grating pitch of 0.5237μm, the reflectivity has further reduced to 79%. Thus it can be concluded that change in the pitch, changed the reflectivity of the interrogating wavelength.

It can be observed from the graphs that the reflection coefficient at interrogating wavelength of 1550nm can be same for two different pitches, one lesser and one greater than the grating pitch of 0.5325μm (which gives Bragg wavelength of 1550nm). Therefore, before measuring any physical parameter, it has to be determined in which direction the pitch would change.

3.13 Marginal Change proposed in theoretical model for FBGs

A TeraXion Grating Writing Station at CSIO was used to write the grating as per the specifications of the grating element simulated and experimental data was acquired and compared with the simulated data. The plot below shows the reflectivity curves obtained after simulations superimposed on the actual experimental data.

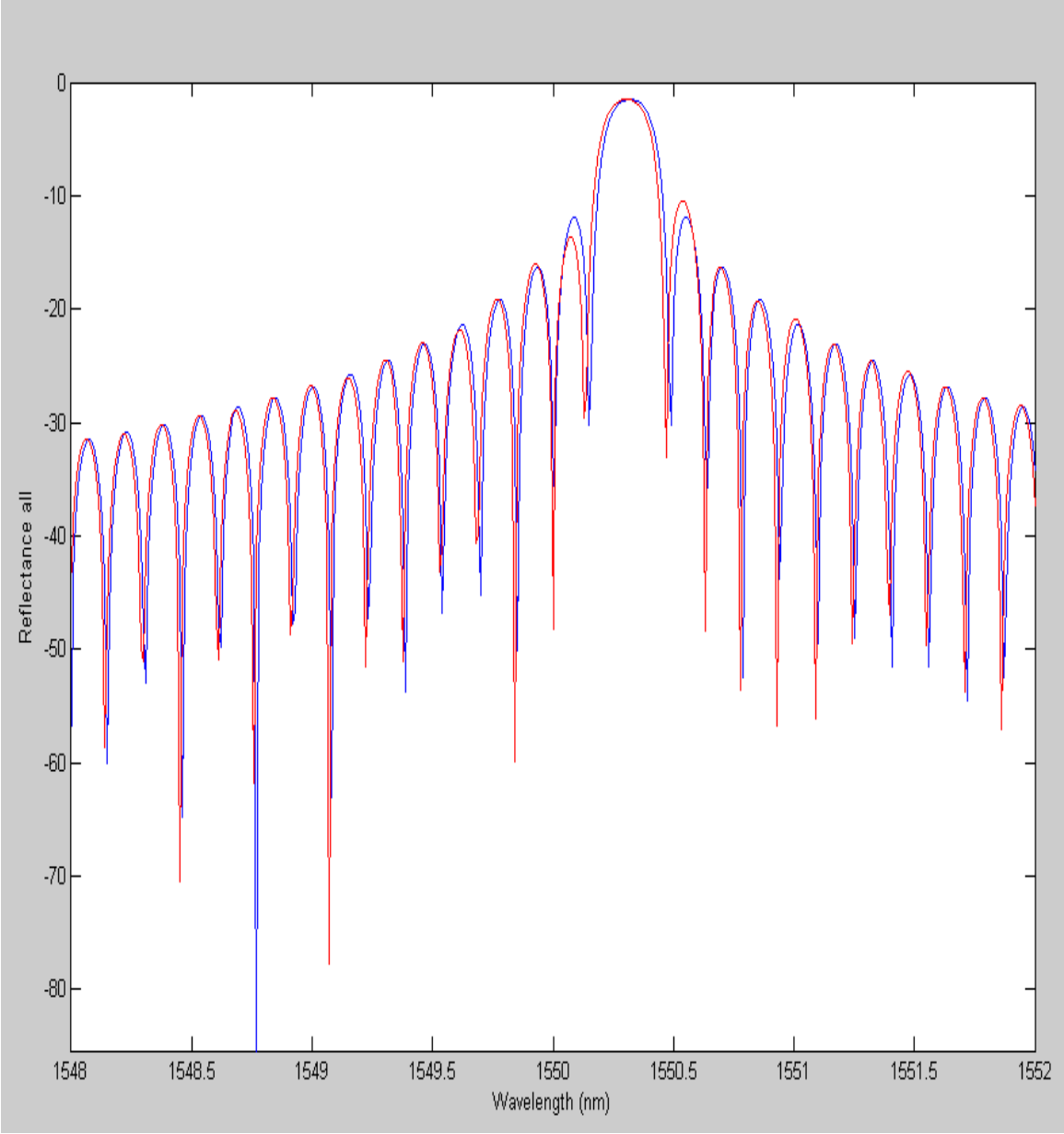

Figure 3.19 Reflected power as a function of wavelength for simulated and experimental data

It was observed that there was a difference in the simulated and experimental data. The grating actually fabricated and the one simulated had the difference that there were small

imperfections in the refractive index modulation depths in the ideal simulated Fiber Bragg Grating model and the actual fabricated Fiber Bragg Grating. The Figure 3.20 highlights the difference

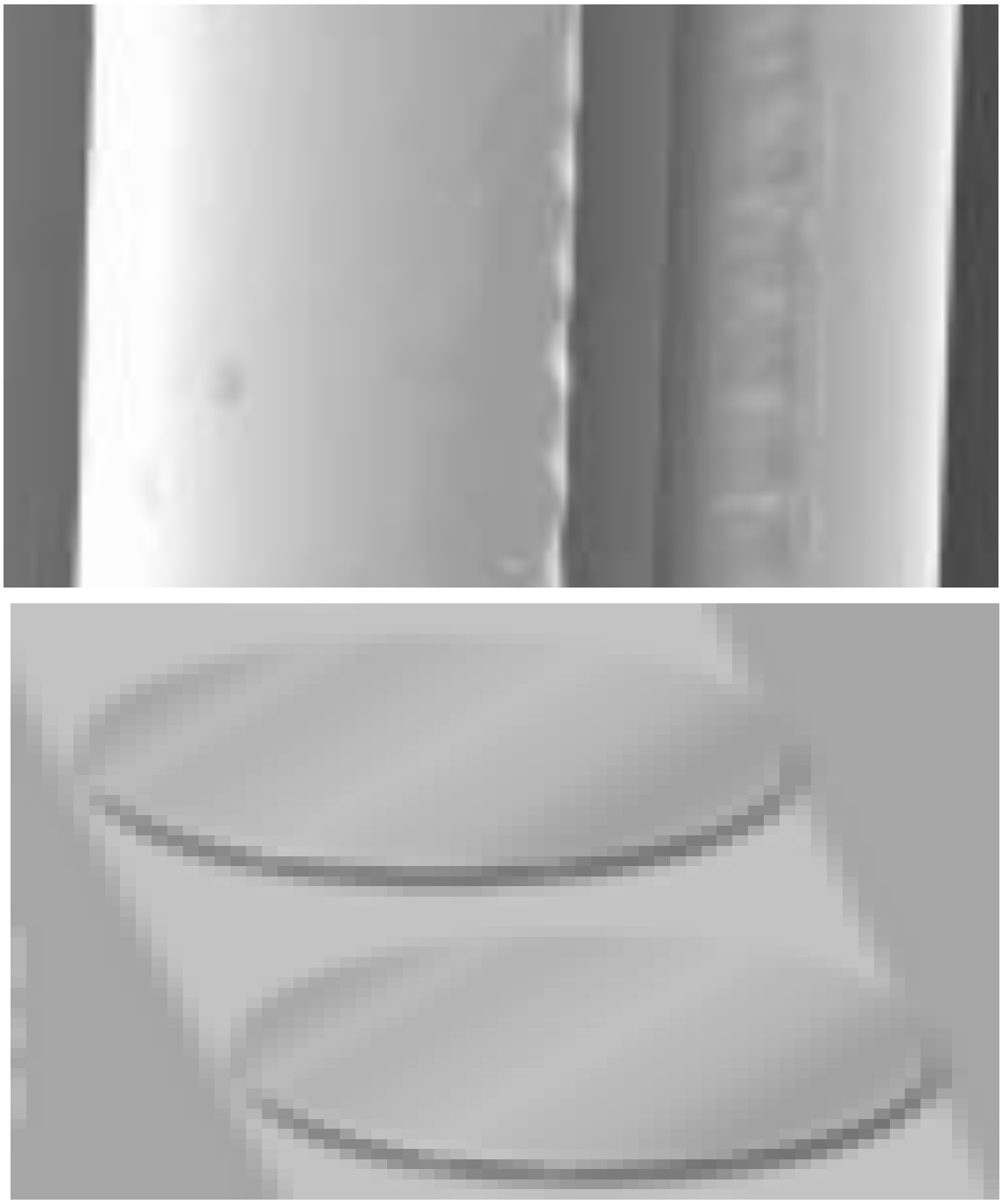

Figure 3.20 Difference in the Simulated Model of Ideal Fiber Bragg Grating and Experimental Actual Fabricated Fiber Bragg Grating

This difference arises due to the practical limitation of the Grating Writing System of not being able to expose the complete depth of the optical fiber to uniform excimer laser light for refractive index modulation. When laser beam is scanned across the length of a phase

mask the part of the fiber nearer to the phase mask tends to get broader refractive index modulation than the part away from it leading to a small drift in the pitch of the grating inscribed.

To mitigate this error the change in the model has been proposed as described below.

Since the refractive index modulation is not uniform so instead of the expression as given in eq (3.114) the actual FBG tends to be non uniform in grating pitch. Therefore, what the light wave encounters along the FBG would be a periodic, non-uniform grating. For the sake of simplicity, it is assumed that the drift in refractive index modulation depth is alternate along the length of the FBG in a periodic fashion as shown in Figure. 3.21

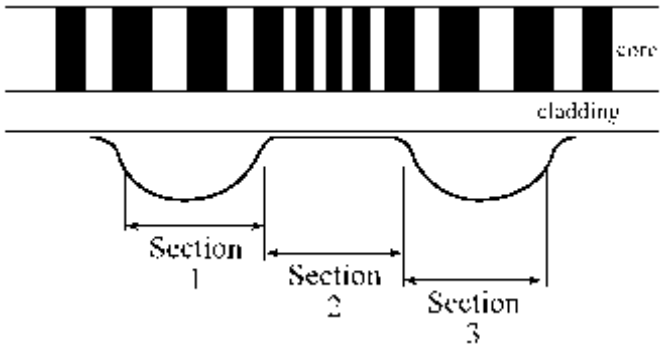

Figure 3.21 Concept of change in pitch of FBG due to Refractive index modulation depth drift

The numerical method used to simulate the FBG model is the Transfer Matrix model (TMM). In the TMM method, it is assumed that entire grating is made up of sections of ABCD matrices. The coupled mode equations are modified for the FBG sensor as in Eq. (3.115) for one section, with V1 representing the incident wave and V2 representing the reflected wave.

$$\begin{bmatrix} V_1(z_1) \\ V_2(z_1) \end{bmatrix} = \begin{bmatrix} A & B \\ C & D \end{bmatrix}_1 \begin{bmatrix} V_1(0) \\ V_2(0) \end{bmatrix} \tag{3.115}$$

In a similar fashion to Eq. (3.115), the other sections can be written out as follows,

$$\begin{bmatrix} V_1(z_2) \\ V_2(z_2) \end{bmatrix} = \begin{bmatrix} A & B \\ C & D \end{bmatrix}_2 \begin{bmatrix} V_1(z_1) \\ V_2(z_1) \end{bmatrix}$$

$$\vdots$$

$$\begin{bmatrix} V_1(z_{n+1}) \\ V_2(z_{n+1}) \end{bmatrix} = \begin{bmatrix} A & B \\ C & D \end{bmatrix}_{(n+1)} \begin{bmatrix} V_1(z_n) \\ V_2(z_n) \end{bmatrix}$$

By cascading these matrices, the entire grating response can be modeled.

$$\begin{bmatrix} V_1(L) \\ V_2(L) \end{bmatrix} = \begin{bmatrix} A & B \\ C & D \end{bmatrix}_{(n+1)} \begin{bmatrix} A & B \\ C & D \end{bmatrix}_n \cdots \begin{bmatrix} A & B \\ C & D \end{bmatrix}_1 \begin{bmatrix} V_1(0) \\ V_2(0) \end{bmatrix}$$

The entire grating can represented by one sum ABCD matrix.

$$\begin{bmatrix} V_1(L) \\ V_2(L) \end{bmatrix} = \begin{bmatrix} A' & B' \\ C' & D' \end{bmatrix} \begin{bmatrix} V_1(0) \\ V_2(0) \end{bmatrix}$$

The new expression for the intensity reflectance is

$$|\rho|^2 = \left| \frac{-C'}{D'} \right|^2 \tag{3.116}$$

A program in Matlab was made to construct the model of the FBG based on this new equation and the result of the simulation is as shown in Figure 3.21

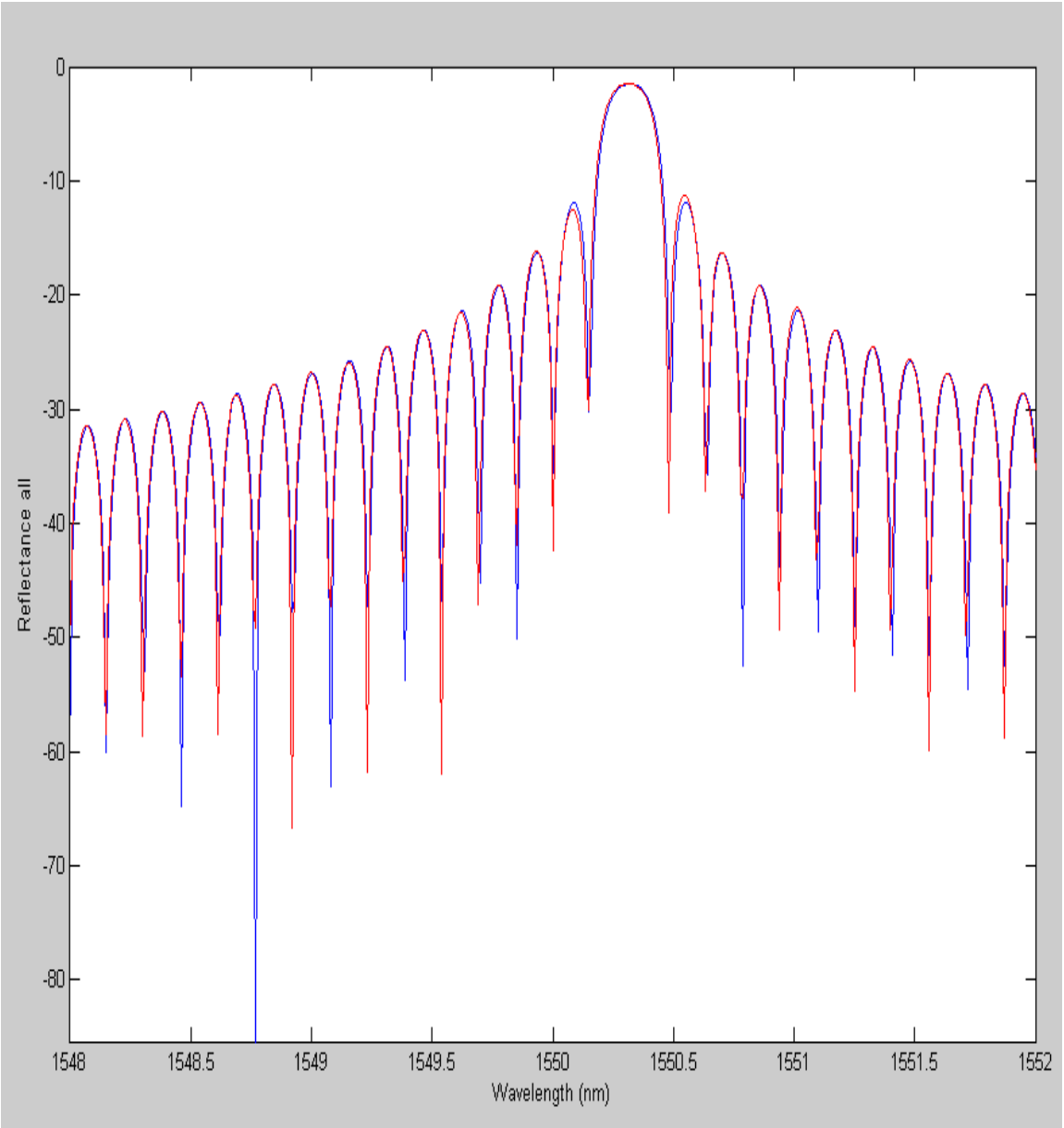

Figure 3.22 Reflected power as a function of wavelength for new proposed model simulated and experimental data

3.14 Conclusion

Using simulation tools it is possible to design the Fiber Bragg Grating sensor for strain measurement by first estimating approximately the grating pitch for maximum reflective power for a given interrogating wavelength and then characterizing the sensor by varying the grating pitch as it would change on application of stress and noting the decrease in reflected power for the chosen wavelength.

Chapter 4

Study of Wavelength Shift in Fiber Bragg Gratings on Simulated External Perturbation using a Wideband Source

4.1 Introduction

This chapter focuses on the study of Wavelength Shift in Fiber Bragg Gratings on Simulated External Perturbation using a Wideband Source, which is related to the second objective of the research work.

In an optical fiber with a refractive index profile $n^2(x,y)$ in which there is a periodic z-dependent perturbation given by Δn^2(x,y,z) this perturbation could correspond to periodic index variation as in a Fiber Bragg Grating [33] .

The coupled mode equation from Eq. (3.84) becomes

$$\frac{dA}{dz}=k_{12}Be^{i\Gamma z} \tag{4.1}$$

where $K=\frac{2\pi}{\Lambda}\approx\Delta\beta=\beta_1-\beta_2$

Where $\Gamma=\Delta\beta-K$. Similarly, Eq. (3.1) leads to

$$\frac{dB}{dz}=-K_{21}Ae^{i\Gamma z} \tag{4.2}$$

If the modes Ψ_1 and Ψ_2 are normalized to carry unit power, then under the weakly guiding approximation

$$\frac{\beta_1}{2\omega\mu_0}\int\int \Psi_1^{*}\Psi_1 dxdy=1 \tag{4.3}$$

And similar equation for Ψ_2 then $|A|^2$ and $|B|^2$ would directly give the power carried by both modes. It can be obtained

$$K_{12}=\frac{\omega\varepsilon_0}{8}\iint\Psi_1^{*}\Delta n^2(x,y)\Psi_2 dxdy \tag{4.4}$$

By using the orthonormality relation for Ψ_2, one can show that

$$K_{21}=K_{12}=K \tag{4.5}$$

Thus, the two coupled equations become

$$\frac{dA}{dz}=KBe^{i\Gamma z} \tag{4.6}$$

$$\frac{dB}{dz}=-KAe^{-i\Gamma z} \tag{4.7}$$

Where K is given by eq(4.5)

Eqs. (4.6) and (4.7) describe the coupling among the two modes propagating along the same direction that is β_1 and β_2 both positive or negative. This is referred to codirectional coupling.

Another important coupling is contradirectional coupling. In this the total field at any value of z as

$$\Psi(x,y,z)=A(z)\Psi_1(x,y)e^{-i\beta_1 z}+B(Z)\Psi_2(x,y)e^{i\beta_2 z} \tag{4.8}$$

Thus, the mode with propagation constant β_1 is propagating in the +z direction and that with the propagation constant $\beta_2$is propagating in –z direction. If they correspond to the same mode, then

$$\beta_1 = \beta_2 = \beta.$$

For this coupling if the identical procedure described earlier is followed, then following two coupled mode equations can be obtained

$$\frac{dA}{dz} = KBe^{i\Gamma z} \tag{4.9}$$

$$\frac{dB}{dz} = KAe^{-i\Gamma z} \tag{4.10}$$

With

$$\Gamma= \beta_1 + (\pm\beta_2) - K \tag{4.11}$$

Note that the signs on the RHS of Eqs. (4.9) and (4.10) are the same, which is opposite in the case of codirectional coupling. Because of this, the solutions for the contradirectional case are not oscillatory.

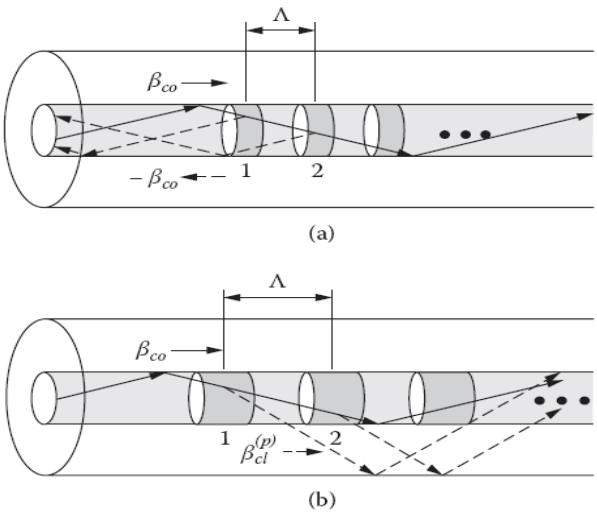

Figure 4.1 Mode couplings: (a) contradirectional coupling; (b) codirectional coupling.

Coupling of modes can be explained by considering the coupled mode theory.

The intuitive illustration of mode couplings is shown in Figure 4.1: (a) illustrates a contradirectional coupling for reflection-type gratings and (b) a codirectional coupling for transmission-type gratings. By means of the refractive index perturbation, diffracted modes can be excited. For the diffracted mode to be accumulated constructively, each diffracted radiation from the series of the perturbation should be in phase; that is, the following equation should be satisfied:

$$\beta_i - (\pm \beta_d) = (2\pi m) / \Lambda \qquad (4.12)$$

Where β_i and β_d, respectively, are the propagation constants for the incident and diffracted modes; Λ is the period of the grating; and m stands for an integer number. It is noteworthy that a minus sign before the propagation constant describes the case wherein the mode propagates in the –z direction. The optical path difference between lights diffracted from the adjacent grating positions (Figure 4.1) should be an integer multiple of the wavelength for a resonant coupling of modes, as in the case of a constructive interference in dielectric multilayers . In most cases, first-order diffraction is dominant, and hence m is assumed to be unity . Thus, the resonant wavelength can be obtained as follows:

$$\lambda = [n_{i,eff} - (\pm n_{d,eff})] \Lambda \qquad (4.13)$$

In the case of a single-mode fiber, $n_{i,eff}$ and $n_{d,eff}$ can be the effective indices of both the core and cladding modes. In the case of contradirectional coupling, the nominal Bragg wavelength of the core mode is given by

$$\lambda = 2\, n_{co,eff}\, \Lambda \qquad (4.14)$$

Where $n_{co,eff}$ is the effective index of the core mode. When the core mode becomes coupled to the counter propagating cladding mode, the $n_{d,eff}$ in Eq.(4.13) is given by the effective refractive index of a cladding mode with a minus sign, which is possible in the case of strong Bragg gratings and blazed gratings.

In the case of codirectional coupling, the resonant wavelength for coupling between the core and cladding modes is given by

$$\lambda = (n_{co,eff} - n^{(m)}_{cl,eff})\,\Lambda \qquad (4.15)$$

Where $n^{(m)}_{cl,eff}$ is the effective index of the pth cladding mode. The differences in effective indices between the core and cladding modes are much smaller than unity, and hence the grating period for codirectional coupling at a given wavelength is much longer than that for contradirectional coupling. Typically, the grating period for the codirectional coupling is hundreds of micrometers in length.

The Bragg grating is a periodic variation in the refractive index of the fiber core in the sensing part of an optical fiber. When a wideband light is guided through an optical fiber, the peak of a certain wavelength is reflected at the Bragg grating. The Bragg wavelength is defined by the Bragg equation:

$$\lambda_B = 2nd \qquad (4.16)$$

Where,

λ_B- wavelength of radiation reflected at the Bragg grating

n - refraction index of Bragg grating

d - period of Bragg grating

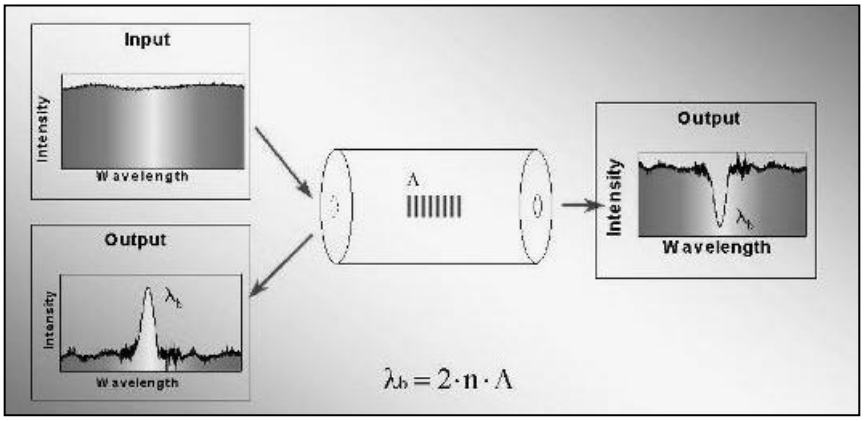

Figure 4.2. Bragg grating sensor principle

When a strain is applied to the optical fiber, the period of grating and index of refraction will change. By measuring the shift in Bragg wavelength, applied deformation can be determined according to Eq. (4.16).

$$\frac{\Delta\lambda_B}{\lambda_B} = (1-P)\frac{\Delta L}{L} \qquad (4.17)$$

Where,

L - length of the sensor (Bragg grating)

P - optical strain coefficient (typical 0,22 for axial strain)

$\Delta\lambda_B$ - Bragg wavelength shift

λ_B - Bragg wavelength before applied strain

The Bragg grating sensor principle is shown in Figure 4.2.

The FBG resonance wavelength will vary accordingly with temperature or strain changes experienced by the fiber. For a temperature change ΔT, the corresponding wavelength shift is given by:

$$\Delta\lambda_B = \lambda_B\left(\frac{1}{\Lambda}\frac{\partial\Lambda}{\partial T} + \frac{1}{n}\frac{\partial n}{\partial T}\right)\Delta T = \lambda_B(\alpha + \xi)\Delta T, \qquad (4.18)$$

where α is the fiber thermal-expansion coefficient, and ξ is the fiber thermo-optic coefficient. The wavelength shift, induced by a longitudinal strain variation $\Delta\epsilon$ is given by,

$$\Delta\lambda_B = \lambda_B\left(\frac{1}{\Lambda}\frac{\partial\Lambda}{\partial\varepsilon} + \frac{1}{n}\frac{\partial n}{\partial\varepsilon}\right)\Delta\varepsilon = \lambda_B(-p_e)\Delta\varepsilon, \qquad (4.19)$$

where p_e is the photoelastic coefficient of the fiber. For a silica fiber, the wavelength-strain and wavelength-temperature sensitivities are ~13pm^{o}C-1 and ~1.15pmϵ-1, for a Bragg wavelength centred at 1555nm [32].

3.2 Experimental Setup

Measurement at multiple points is possible with an optical fiber with many gratings placed at desired locations. Up to 100 Bragg gratings may be written in the single optical fiber. The Bragg gratings have different periodicity, which makes it possible to

distinguish the measurement location. Figure 4.3 shows principle of measuring system with multiple Bragg gratings.

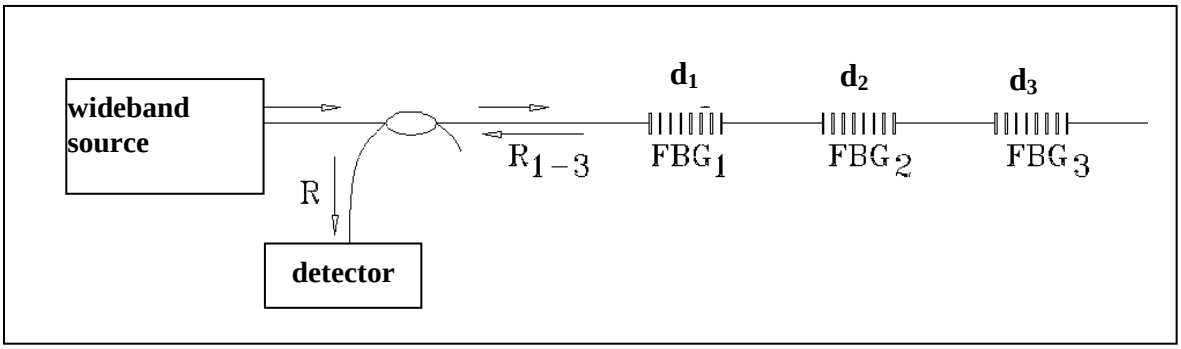

Figure 4.3. Principle of sensor with multiple Bragg gratings

Three FBGs indicated as FBG1, FBG2 and FBG3 with different resonance wavelengths of 1549.576, 1548.426 and 1545.826 nm respectively are spliced together and connected to the interrogator in this order to demonstrate three different sensing elements. The three Bragg wavelengths are observed on the monitor under conditions of zero loading. The schematic and photograph of the experimental set up implemented are depicted in Figure 4.4.

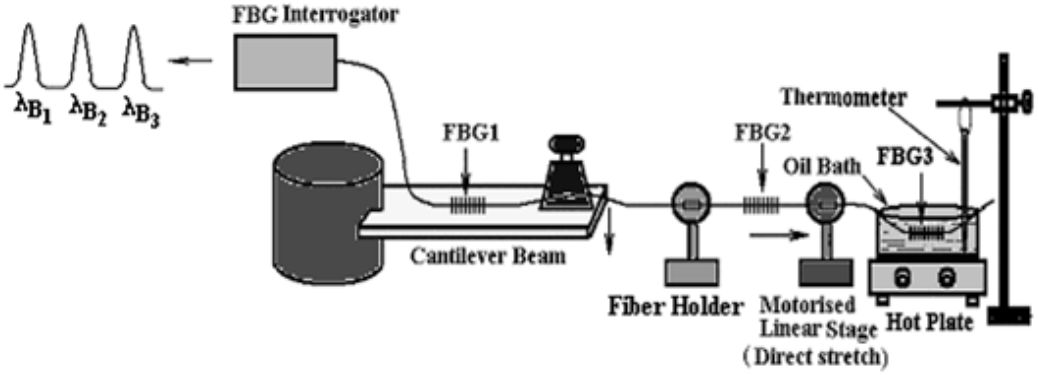

Figure 4.4: Schematic of setup for study of wavelength shift

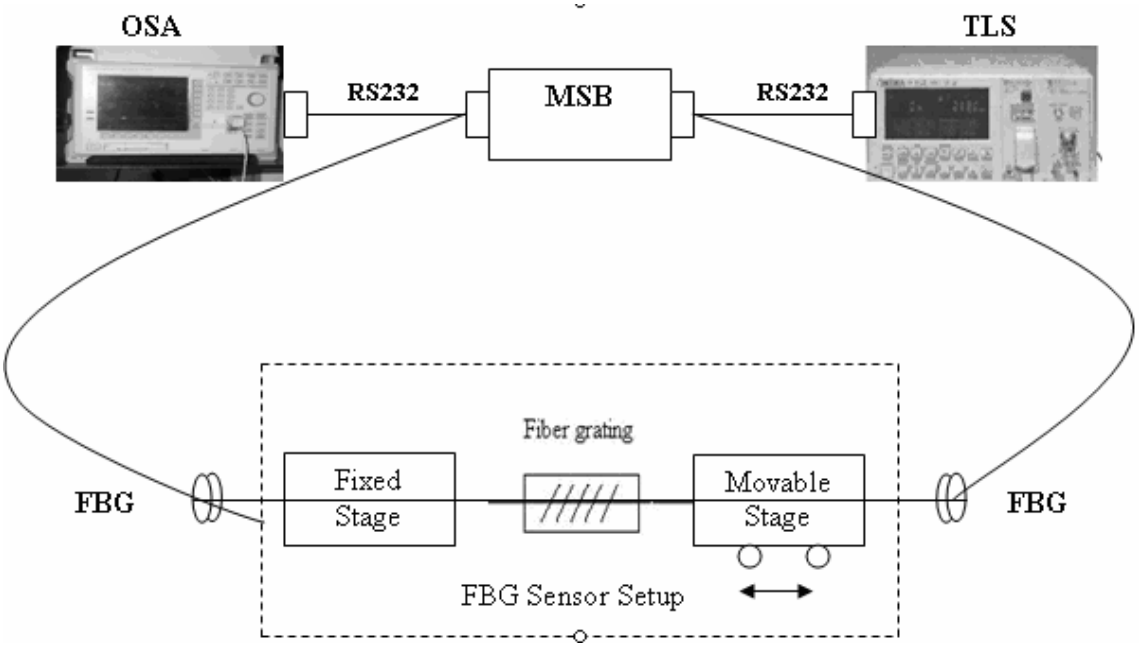

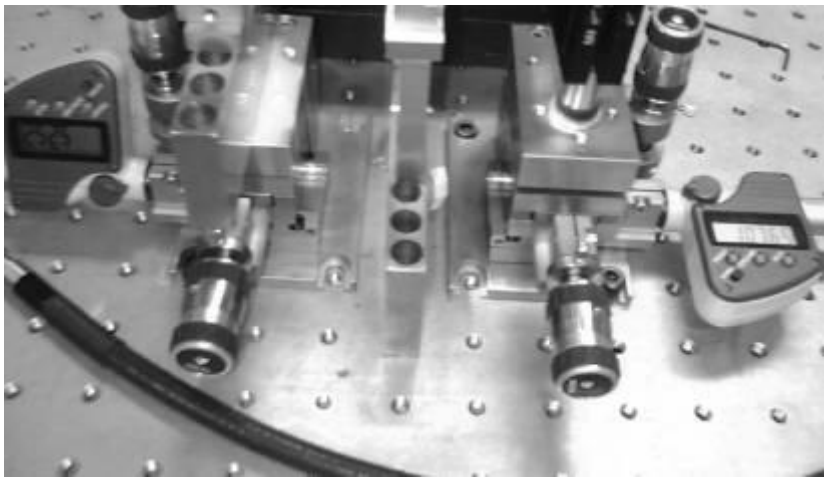

Figure 4.5: Experimental setup for study of wavelength shift

The first grating FBG1 is bonded to a metallic cantilever (39.5cm x 4.2cm) at a location of 12cm from the fixed end using araldite epoxy. It acts as a pressure sensor with different weights applied on the cantilever tip and the results obtained for different loading are quite linear as shown in Figure 4.6. The second grating FBG2 is used as a strain sensor and it is held tight between two fiber holders and stretched longitudinally using a motorized linear precision stage with a pitch of 0.5 mm i.e. one complete rotation of the motor screw results in 0.5 mm movement of the linear stage which is the change in length of the fiber (Δl as in equ.4.6). A 30 cm length of the fiber with a grating element located in the middle position is stretched by the movement of the stage. Thus, for each rotation value of the screw Δl is known and resulting strain is calculated using the simple formula for strain $\Delta l/L$, where L is 30 cm in this case. A maximum strain of ~2333 με was thus produced using this technique. The effect of the pulling strain on the Bragg wavelength is quite linear as shown in Figure 4.7. The third grating FBG3, which demonstrates the effect of temperature on Bragg wavelength, is immersed in a glycerol bath kept in a second bigger bath containing water. The grating is heated indirectly to avoid rapid temperature rise. The temperature of the glycerol bath varied from 15^{o}C to 70^{o}C is measured using thermometer immersed in the glycerol bath and the corresponding Bragg wavelength shift was recorded which has also shown a good linearity as depicted in Figure 4.8.

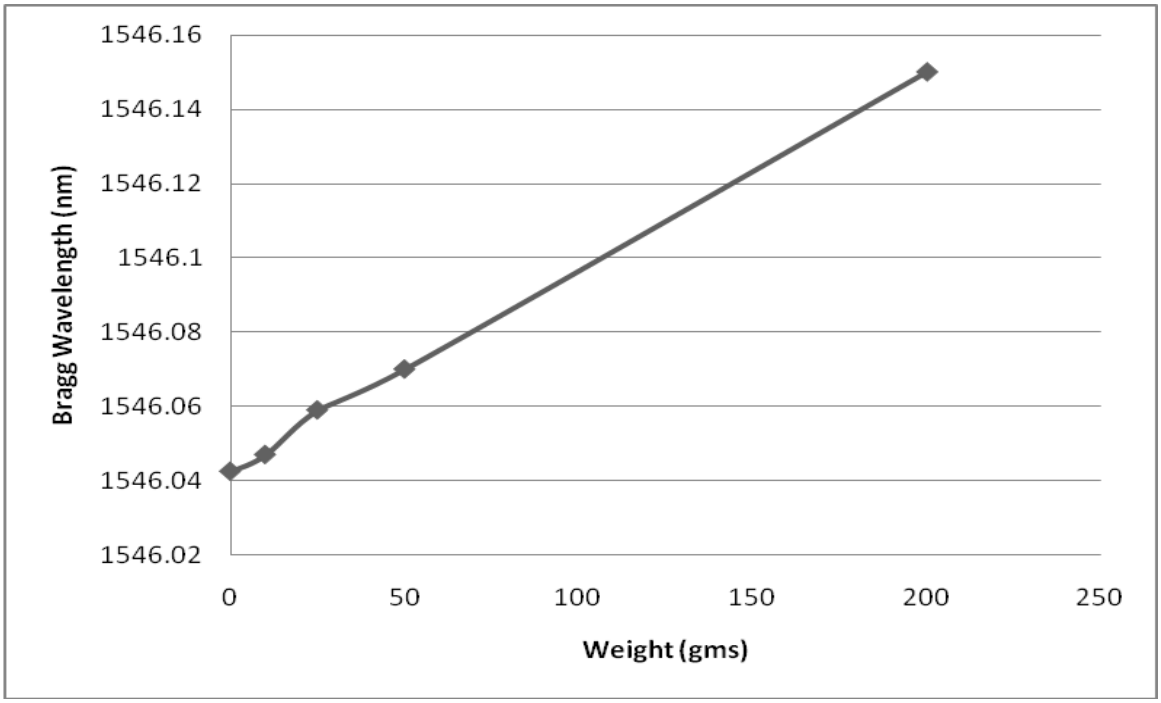

Figure 4.6: Wavelength shift caused by external perturbation of bending strain

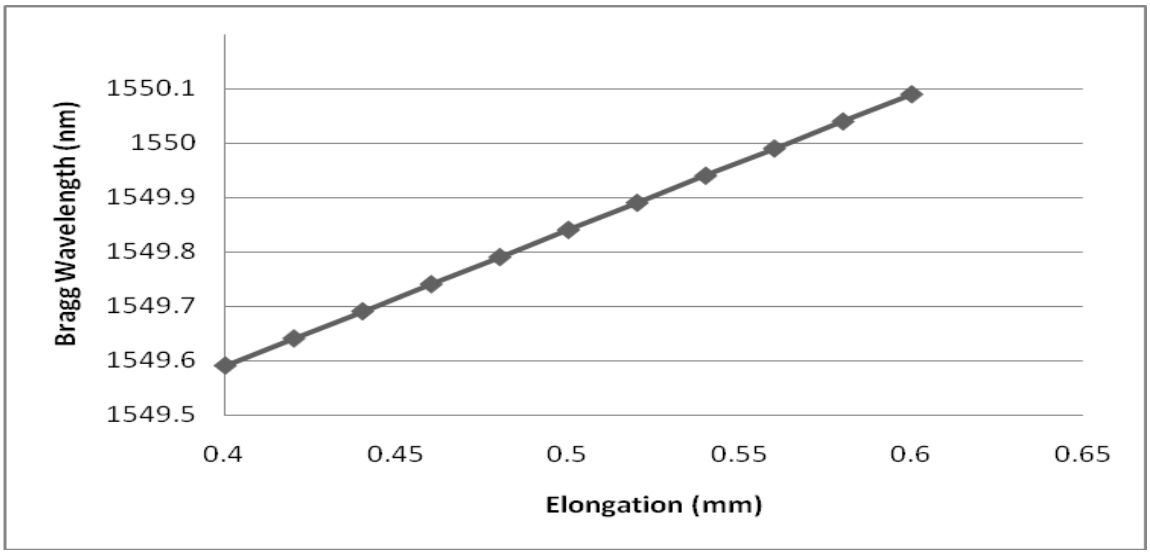

Figure 4.7: Wavelength shift caused by external perturbation of direct pull strain

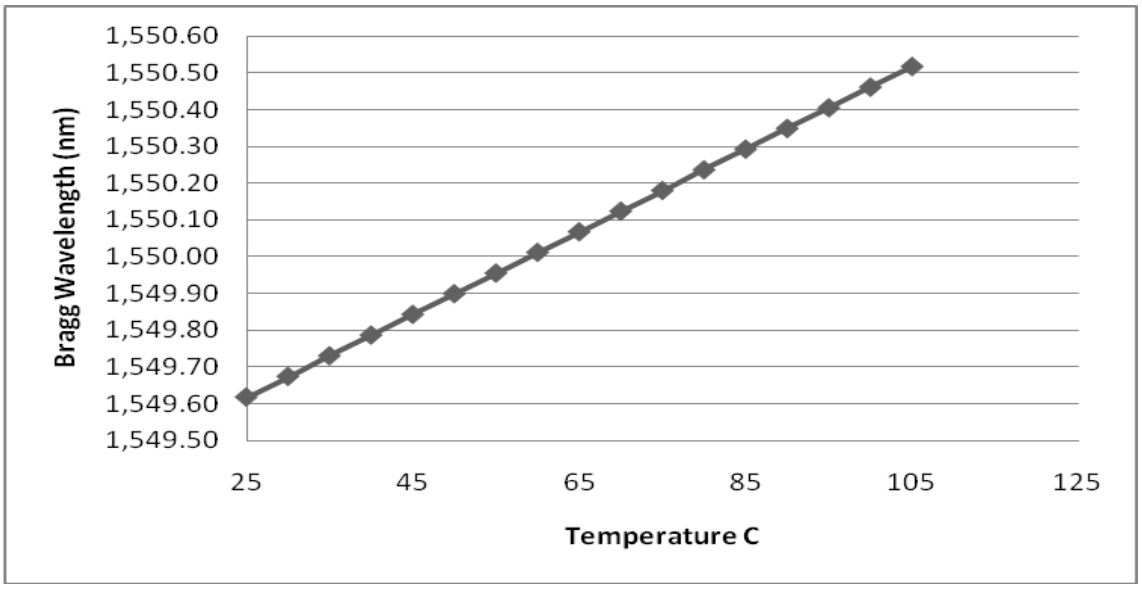

Figure 4.8 : Wavelength shift caused by external perturbation of temperature

4.3 Results and Discussion

The wavelength shift in FBGs on application of external perturbation, realized by splicing three Fiber Bragg Grating elements, is demonstrated for simultaneous measurement of strain and temperature. The three sensors have exhibited a good linear performance as expected. The experiment has been performed in a controlled temperature laboratory environment but in actual applications, suitable compensation technique will have to be employed for variation in environmental temperature to obtain the realistic mechanical

strain data. One approach is to use athermal coating on the FBG that can be embedded as strain sensor, or alternatively, two FBGs can be used; one bonded with the structure while the other is unbonded so that there is no strain effect. Thus the first grating senses both strain and temperature and the second one is just a temperature sensor. For the second FBG sensor, strain results from the direct pull, and its sensitivity has been estimated to be approximately 0.39 pm/με. The third grating which is used as temperature sensor has exhibited a sensitivity of 11.1 pm / ^{0}C. The first grating bonded to a cantilever has exhibited a response of 4.8 pm/gm. In this case bending the cantilever with pressure applied at its free end produces strain in the grating. Apart from being lightweight, low cost, immune to EMI/RFI, chemically inert; this device offers other advantages as well. For example, a good linear response is obtained in all the three cases and the sensed parameter namely strain and temperature are wavelength encoded, and hence they are independent of fluctuations in the light source, connector or fiber losses etc. Another point that is crucial for structural health monitoring and sensing in hazardous environment is the feasibility of remote sensing. It is because the commercial fibers have very low loss in the operating wavelength range used in the present investigations and they are able to transmit sensed information to distant monitoring locations. Besides, the narrow bandwidth of FBG allows multiplexing of many sensing elements, which work independently without interfering each other. Thus, this study offers an efficient and inexpensive technique for structural health monitoring such as civil and aerospace structures and other applications involving hazardous environmental conditions such as oil and gas exploration wells and monitoring of load of power transmission lines in snow covered areas and hot zones.

4.4 Enhancement of Sensitivity due to External Perturbation

Since the coefficient of thermal expansion of FBG made of silica is quite small, investigations were made to enhance temperature sensitivity of FBG sensors. For this purpose, a suitable metallic encapsulating fixture was designed and fabricated & its performance investigated. The fixture has a central hole of appropriate diameter along its length and an FBG was kept inside the hole with its ends bonded to the metal cap. The transducer was dipped in a hot water bath and the effect of heating on the Bragg wavelength was monitored and an improvement of sensitivity from 11 pm/ ^{0}C to 20pm/ ^{0}C was realized in the temperature range of 25 to 65 ^{0}C used. Further, the design of the

fixture is being modified to realise a still higher multiplier effect of longitudinal expansion of the FBG. The experimental set up implemented and the results obtained are indicated in Figures 4.9 and 4.11 respectively.

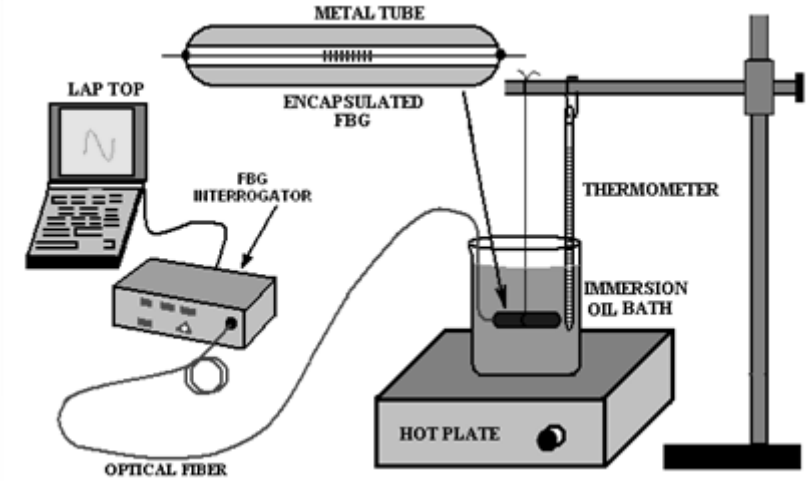

Figure 4.9 Schematic of sensitivity enhancement of FBG sensor

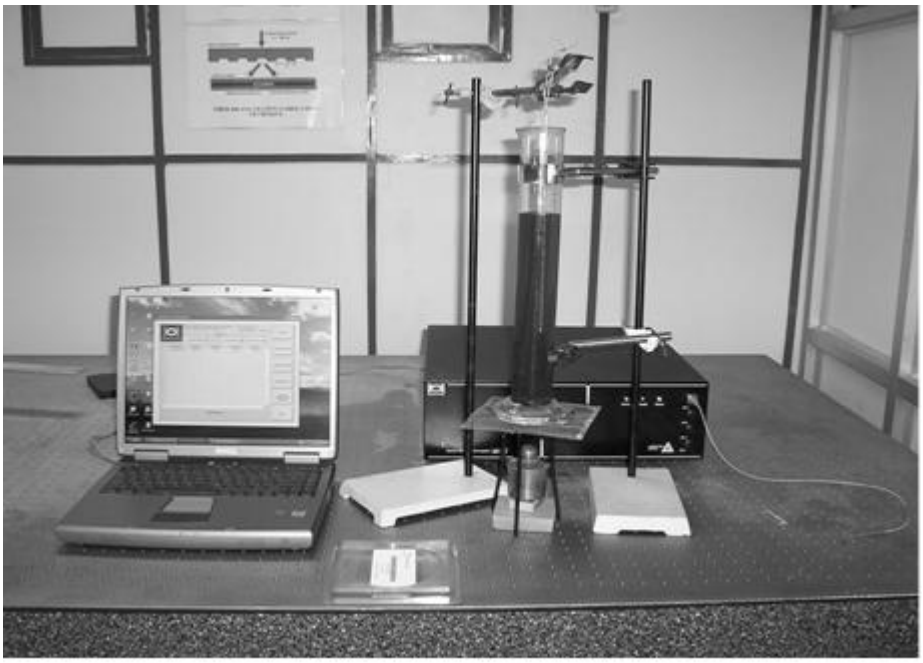

Figure 4.10: Experimental set-up for sensitivity enhancement of FBG sensor

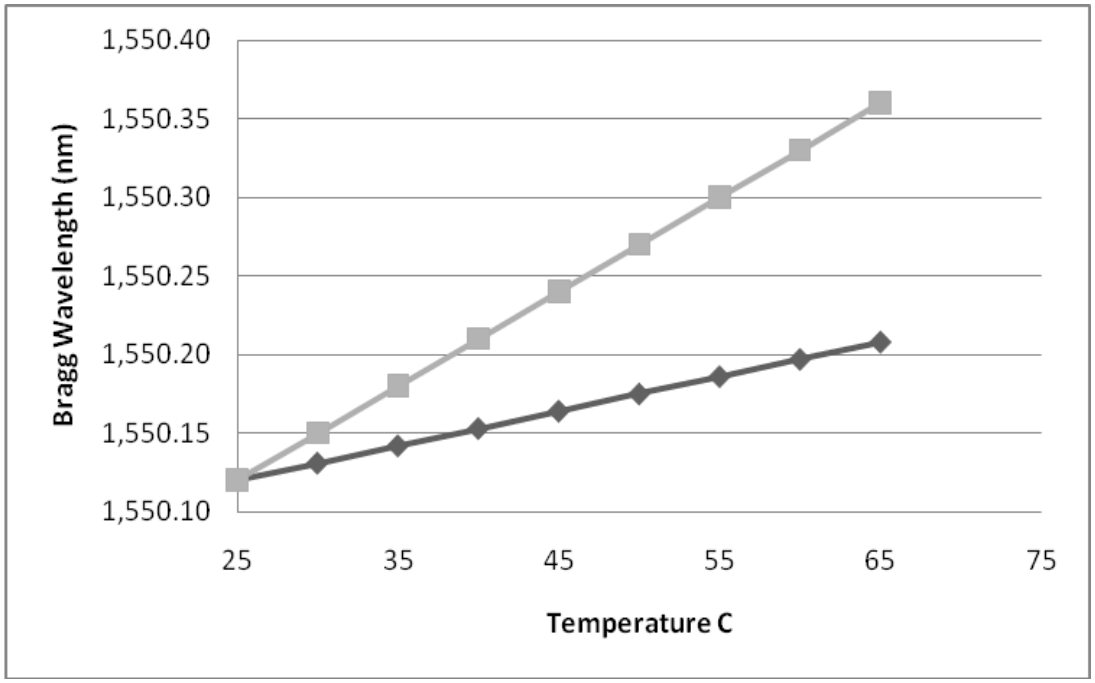

Figure 4.11: Results of sensitivity enhancement of FBG sensor

Other than grating sensors technique all techniques are based on change in either intensity or the phase of the inputted signal that may be degraded due to noise induced in it. But with significant discovery of photosensitivity in optical fibers a new class of In-fiber component based on non-intensity types of fiber optic sensor has been developed, called the Fiber Grating sensor. It has more advantages than all other fiber optic sensor as are following;

- Measured information is wavelength encoded.
- Immune to source power.
- Independent to fluctuation of light levels.
- Immune to connector losses.
- In-fiber sensing
- Self-referencing capability.
- Remote signal processing abilities.
- Multiplexing capabilities.
- Fabricated on most commercially available fibers.
- No need for coherent light source, simple diode is enough.

Fiber Grating sensor became most common and most promising fiber optic sensors. In it a part of fiber core itself is the sensing element which comprise of grating lines that have a

slightly different index of refraction than the rest of the fiber core. With the above review of optical fiber and optical sensors as a background, this thesis endeavors to examine the grating structure when subjected to physical parameters like temperature, pressure and also chemical sensing applications.

Multiplexed Fiber Bragg Grating (FBG) sensor systems have been successfully developed and utilized in structural health monitoring applications measuring various measurands such as strain, temperature, and pressure. These mesuarands are transferred to the bragg wavelength shifts, which Can be detected using one of many well established demodulation techniques. However, in field of applications, integration of FBG sensors often limits the performance of the sensor systems. FBG sensors are embedded into composite structures or bonded on the surface of structures. In many cases, improper embedding or environmental influences causes substantial distortion or broadening of FBG spectra, which leads to increased system noise and false measurements with demodulation techniques.

4.5 Effective refractive index of FBG sensor

The theory of Fiber Bragg Gratings may be developed by considering the propagation of modes in an optical fiber. Wave propagation in optical fibers is analyzed by solving Maxwell's equations with appropriate boundary conditions. The solutions provide the basic field distributions of the bound and radiation modes of the waveguide. These modes propagate without coupling in the absence of any perturbation (e.g., bend). Coupling of specific propagating modes can occur if the waveguide has a phase and/or amplitude perturbation that is periodic with a perturbation ‘phase/amplitude-constant’ close to the sum or difference between the propagation constants of the modes. Although guided wave optics is well established, the relationship between the mode and the refractive index perturbation in a Bragg grating plays an important role on the overall efficiency and type of scattering allowed by the symmetry of the problem. Here, wave-propagation in optical fiber is given, followed by the theory of mode coupling [141].

Considering the constitutive relations

$$\mathbf{D} = \varepsilon_0 \mathbf{E} + \mathbf{P} \tag{4.20}$$

$$\mathbf{B} = \mu_0 \mathbf{H} \tag{4.21}$$

Where ε_0 is the dielectric constant and μ_0 is the magnetic permeability, both scalar quantities; **D** is the electric displacement vector; **E** is the applied electric; **B** and **H** are the magnetic flux and field vectors, respectively; and **P** is the induced polarization,

$$\mathbf{P} = \varepsilon_0 \chi_{ij}^{(1)} \mathbf{E} \tag{4.22}$$

The linear susceptibility $\chi_{ij}^{(1)}$ is in general a second-rank tensor with two laboratory frame polarization subscripts ij and is related to the permittivity tensor ε_{ij} with similar subscripts as

$$\varepsilon_{ij} = 1 + \chi_{ij}^{(1)} \tag{4.23}$$

Using Maxwell's equations,

$$\nabla \times \mathbf{E} = -\partial \mathbf{B}/\partial t \tag{4.24}$$

$$\nabla \times \mathbf{H} = \partial \mathbf{D}/\partial t + \mathbf{J} \tag{4.25}$$

Where **J** is the displacement current, and using Eq. (4.20) in Eq. (4.25) and with **J** = 0,

$$\nabla \times \mathbf{H} = \partial/\partial t \, [\varepsilon_0 \mathbf{E} + \mathbf{P}] \tag{4.26}$$

Taking the curl of Eq. (4.24) and the time derivative of Eq. (4.26), the wave equation is shown to be

$$\nabla^2 \times \mathbf{E} = \mu_0 \varepsilon_0 \partial^2 \mathbf{E}/\partial t^2 + \mu_0 \partial^2 \mathbf{P}/\partial t^2 \tag{4.27}$$

Using Eq. (4.22) and (4.23) in (4.27),

$$\nabla^2 \times \mathbf{E} = \mu_0 \varepsilon_0 \varepsilon_{ij} \partial^2 \mathbf{E}/\partial t^2 \tag{4.28}$$

The next step in the analysis is to introduce guided modes of the optical fiber into the wave equation.

Consider a simple three layer step index fiber geometry with core radius a_1,refractive index n_1,cladding radius a_2 and RI n_2 and surrounding medium of RI n3. Linearly polarized approximation has been used to describe core guided modes while the cladding modes fields have been obtained using exact vector field treatment since the interface between the cladding and its surrounding might have large index difference. LP

approximation to calculate both core and cladding fields. The difference in the result due to use of scalar approximation would be shift in peak position of the resonances. However to design gratings for any practical application , scalar approximation would be sufficient since behavior of the transmission spectra can be well described by this approximation and also the peak position of resonance experimentally obtained would be sensitive to index fluctuation or radius fluctuation in the fiber spool and exact match in peak position is not expected even if vector calculation of the fields are performed.

Core mode are supported by the total internal reflection at the core cladding boundary and have a propagation constant β such that , $n_2^2\kappa_0^2 < \beta^2 < n_1^2\kappa_0^2$ where κ_0 Is the wave vector in vacuum. The transverse modal fields are oscillatory in the core and decay outside it. The transverse dependence of the core modal field is given by

$$\Psi(r,\emptyset) = A_{co}\frac{J_l(U_r/a_1)}{J_l(U)}\begin{bmatrix}\cos(l\emptyset)\\ \sin(l\emptyset)\end{bmatrix} \qquad r < a_1 \qquad (4.29)$$

$$A_{co}\frac{k_l(U_r/a_1)}{k_l(U)}\begin{bmatrix}\cos(l\emptyset)\\ \sin(l\emptyset)\end{bmatrix} \qquad r > a_2$$

$$U = a_1(\kappa_0^2 n_1^2 - \beta^2)^{1/2}$$

$$W = a_1(\beta^2 - \kappa_0^2 n_2^2)^{1/2} \qquad (4.30)$$

Where continuity of φ is assumed at r = a_1. The interface at r = a_2 is neglected since the decaying field has negligible strength at this point continuity of $\frac{\partial\varphi}{\partial r}$at r =$a_1$ leads to ,

$$U\frac{J'_l(U)}{J_l(U)} = W\frac{k'_l(W)}{k_l(W)} \qquad (4.31)$$

where J_l is a Bessel function of the first kind; K_l a modified Bessel function of the second kind; r_{co} the core radius; λ the wavelength in vacuum; and n_1, n_2 and n_{eff} the core refractive index, the cladding refractive index, and the effective refractive index of the core, respectively. With respect to the cladding modes, their derivation is more complicated, since the waveguide geometry includes two boundaries.

By using recursion formulas

$$U\frac{J_{l+1}(U)}{J_l(U)} = W\frac{K_{l+1}(W)}{K_l(W)} \qquad (4.32)$$

Above equation can be used to study the guided modes in step index fiber. For *l*=0 it can be obtained

$$U\frac{J_1(U)}{J_0(U)} = W\frac{K_1(W)}{K_1(W)} \tag{4.33}$$

Here that the boundary conditions used in deriving the eigen value equation are consistent with the approximation involved in scalar value wave equation.

To solve the above equation it is convenient to define the normalized propagation constant

$$b = (\frac{\beta}{k_0^2} - n^2_{cl})/(n^2_{co} - n^2_{cl}) = \frac{W^2}{V^2} \quad \text{where} \tag{4.34}$$

$$V = 2\pi\, r_{co}\sqrt{(n^2_{co} - n^2_{cl})}/\lambda \tag{4.35}$$

thus $W = V\sqrt{b}$ and $U = V\sqrt{1-b}$.

for guided modes $n_2^2\kappa_0^2 < \beta^2 < n_1^2\kappa_0^2$ i.e $0 < b < 1$.

$$V\sqrt{1-b}\frac{J_1(V\sqrt{1-b})}{J_0(V\sqrt{1-b})} = V\sqrt{b}\frac{K_1(V\sqrt{b})}{K_0(V\sqrt{b})} \tag{4.36}$$

The solution of the above equation will give us universal curves describing the dependence of b on V. For a given value of *l* ,there will be a finite number of solutions and the *m*th solution is referred to as the LP_{0m} mode.

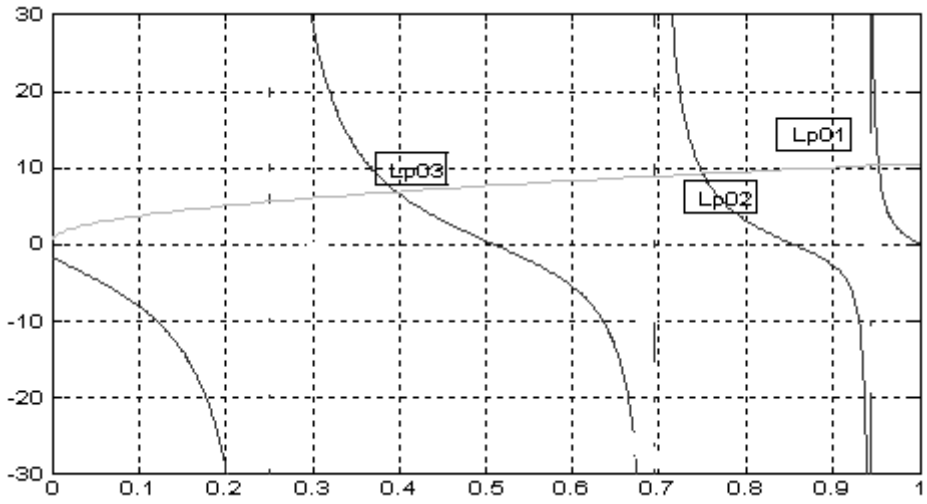

Figure 4.12.Normalized propagation constant

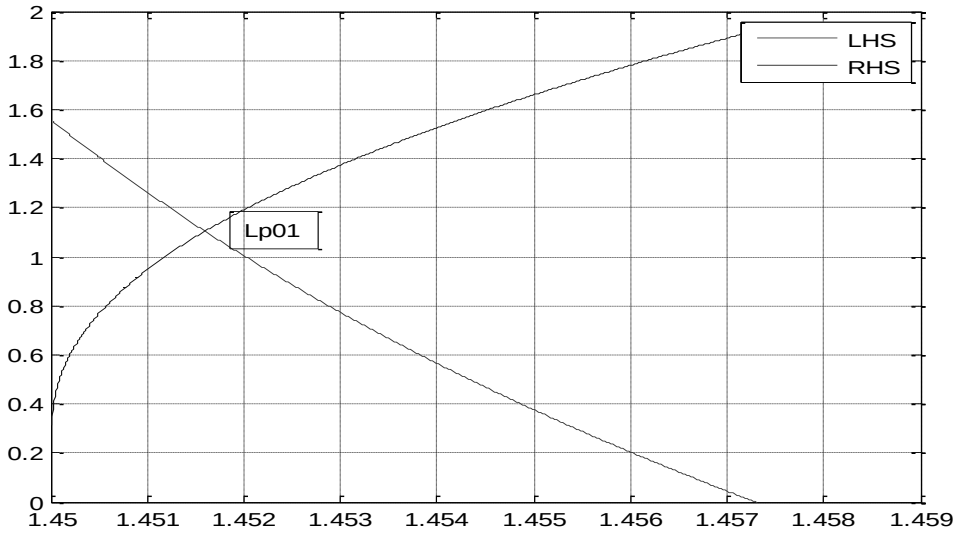

Figure 4.13 Effective refractive index Lp01

By knowing the b values the effective refractive index of the mode can be calculated as following

$$n_{eff}^{co} = \frac{\beta}{k_0} = \sqrt{n_2^2 + b(n_1^2 - n_2^2)} \qquad (4.37)$$

Solving this numerically one gets the allowed values corresponding to different guided modes supported by core. For a single mode fiber(for a concerned wavelength range) there would be only one β values . that is allowed as a solution to Eq. (4.37). For example consider a fiber of n_1 = 1.4573, n_2= 1.45, n_3= 1.0, a_1 = 2.5μm and a_1 = 62.5μm . At λ= 1.55 μm , this fiber supports only one core mode whose propagation constant can be obtain by solving Eq. (4.37) as core β (LP_{01}) = 5.88432/micrometer

Cladding mode are those modes which propagate by total internal reflection at the cladding air interface. They have propagation constant β such that $n_3^2\kappa_0^2 < \beta^2 < n_2^2\kappa_0^2$ the transverse field is oscillatory in both core and cladding and decays outside the cladding . the transverse dependence of the cladding mode field is given by

$$\Psi(r,\emptyset) = A\, J_l((U_1 r/a_1) \begin{bmatrix}\cos(l\emptyset)\\ \sin(l\emptyset)\end{bmatrix} \qquad r < a_1$$

$$(B\, J_l((ur/a_2\ ) + CY_l(ur/a_2) \begin{bmatrix}\cos(l\emptyset)\\ \sin(l\emptyset)\end{bmatrix} \qquad a_1 < r < a_2$$

$$DK_l((wr/a_2) \begin{bmatrix}\cos(l\emptyset)\\ \sin(l\emptyset)\end{bmatrix} \qquad r > a_2 \qquad (4.38)$$

$$U_1 = a_1(\kappa_0^2 n_1^2 - \beta^2)^{1/2}$$

$$u = a_2\left(\kappa_0^2 n_2^2 - \beta^2\right)^{\frac{1}{2}}$$

$$w = a_2(\beta^2 - \kappa_0^2 n_1^2)^{1/2} \quad (4.39)$$

Continuity of the field at the boundaries at r = a_1 and r = a_2 leads to the following equations:

$$A J_l(U_1) = B J_l((U_1 a_1/a_2) + C Y_1(u a_1/a_2) \quad (4.40)$$

$$B J_l(u) + C Y_l(u) = D K_l(w) \quad (4.41)$$

Continuity of the derivative of the field at the two boundaries r = a_1 and r = a_2 leads to

$$A\frac{U_1}{a_1} J_l(U_1) = B\frac{u}{a_2} J_l(U_1 a_1/a_2) + C\frac{u}{a_2} Y_l(u a_1/a_2) \quad (4.42)$$

$$B\frac{u}{a_2} J_l(w) + C\frac{u}{a_2} Y_l(u) = D\frac{w}{a_2} K_l(w) \quad (4.43)$$

If the modes are normalized and carry unit power then under the weakly guiding approximation it can be written,

$$\frac{\beta}{2\omega\mu_0}\iint_0^{2\pi\infty} \Psi^2(r)\cos^2(l\emptyset)\mathrm{rdrd}\emptyset = 1 \quad (4.44)$$

for a frequency component ω and free space permeability μ_0, the four equations(4.40-4.43) form a set of coupled equations. For given values of a_1, a_2, n_1, n_2 and λ, β can be found such that such that the determinant formed by the coefficients of A,B,C,D form the four equations as shown in Figure 4.14.

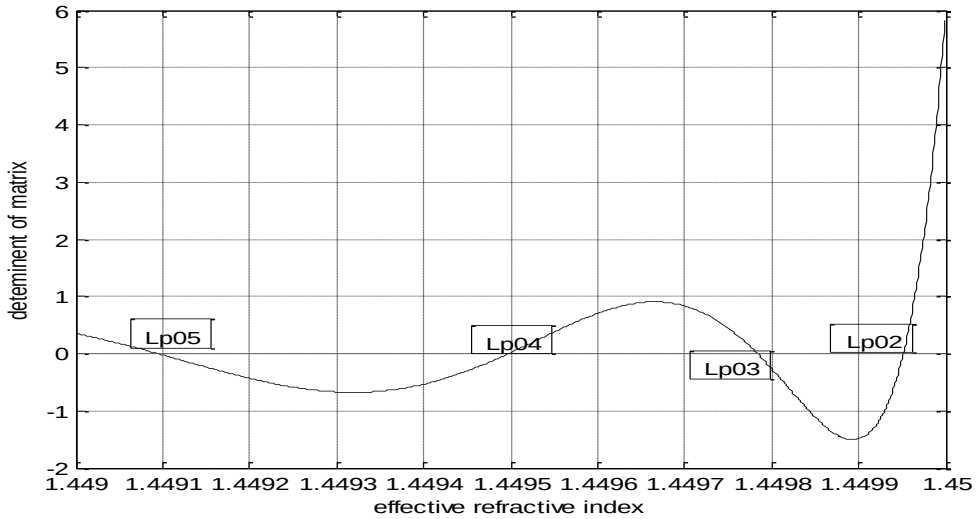

Figure 4.14 Determinant of matrix vs effective refractive index

If it is considered that fiber has n_1 = 1.4573, n_2= 1.45, n_3= 1.0, a_1 = 2.5μm and a_2 = 62.5μm . At λ= 1.55micro meter, the β values of four lowest order modes are given by Lp02= 5.8776217/ μm ,Lp03= 5.87694/ μm, Lp04= 5.875783 / μm, Lp05= 5.87414 / μm.

In the two-layer approximation used by various authors, the refractive index profile used to evaluate the propagation characteristics of cladding modes is given by

$$n = n_2 \qquad r < a_{cl}$$
$$= n_a(air) \qquad r > a_{cl}$$

whereas for the core-guided mode it is given by

$$n = n_1 \qquad r < a_{co}$$
$$= n_2 \qquad r > a_{co} \tag{4.45}$$

where a_{co} and a_{cl} are the core and cladding radii, respectively, and n_1, n_2, and n_a are the respective refractive indices of the core, cladding, and ambient.

The complete eigenvalue equation for HE modes in a step index optical fiber can be employed to determine the cladding mode propagation constant using the same eigen value equation if the fiber is modeled as a circular dielectric two-layer waveguide composed of an inner layer with radius and refractive index, and an external layer with infinite radius and refractive index (that of the external medium) . Then, the eigen value equation takes the form

$$\frac{J_{l-1}(u)}{uJ_l(u)} = -\left(\frac{n_2^2+n_3^2}{2n_2^2}\right)\frac{K_l'(w)}{wK_l(w)} + \left\{\frac{l}{u^2} - \left[\left(\frac{n_2^2-n_3^2}{2n_2^2}\right)^2\left(\frac{K_l'(w)}{wK_l(w)}\right)^2 + \left(\frac{l\beta_{cl,i,m}}{n_2k_0}\right)^2\left(\frac{1}{w^2}+\frac{1}{u^2}\right)^2\right]^{1/2}\right\} \tag{4.46}$$

For frequency components ω and free space permeability μ_0 the four equations form a set of coupled equations.

If there are some perturbations in the fiber, the modes can be coupled to other modes. The main coupling directions can be determined as contradirectional or codirectional based on whether the traveling directions of modes coupled to each other are opposite or the same. Based on the direction of the mode coupling, fiber gratings can be classified in two types.

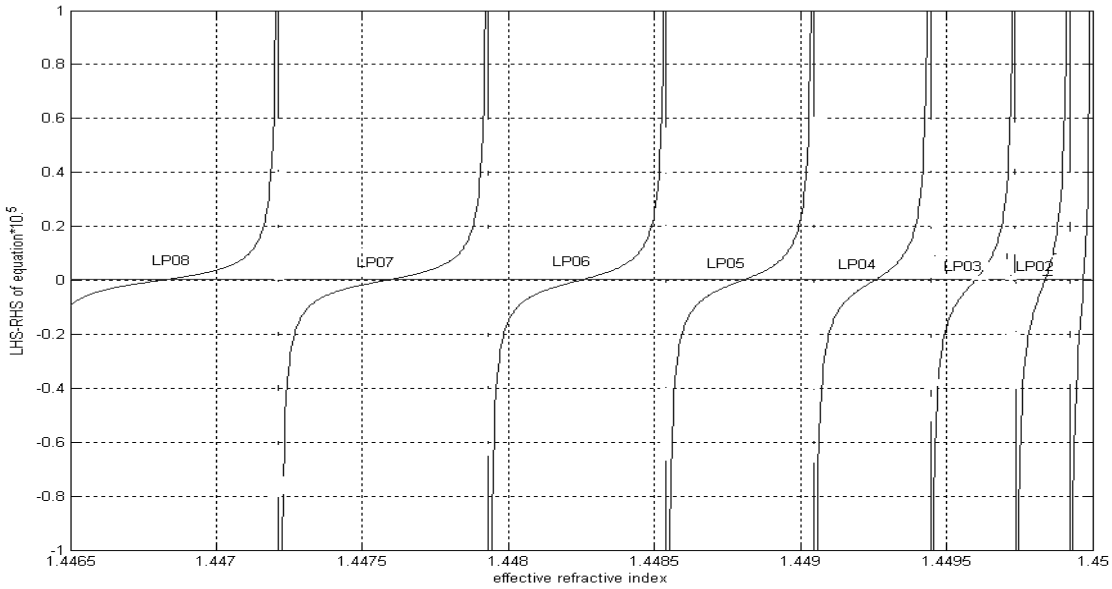

Figure 4.15 Effective refractive index (Lp02-Lp08)

One type is a short-period or reflection grating, where coupling occurs between modes in opposite directions. The FBGs (Fiber Bragg Grating), chirped gratings, and tilted short-period gratings belong to this category. The other type is a transmission grating, represented by LPFGs (Long Period Fiber Grating), where coupling occurs between modes traveling in the same direction .

4.6 Conclusion

This study is important for realizing fire safety sensors for aircrafts, railways, industrial and building complexes and also as tunable components for sensors and communication applications.

Chapter 5
Design of Fiber Bragg Grating Interrogator for Sensor/Communication systems

.

5.1 Introduction

The Bragg wavelength is changed with a change in the effective refractive index or grating period. Strain applied to an FBG elongates it (or compresses it for negative strain); hence, the grating period is increased (or decreased), which results in a shift of the Bragg wavelength to longer (or shorter) wavelengths. With temperature change, the grating period also changes due to thermal expansion (or compression) of the fiber, but the effect of the change in the refractive index is about one order of magnitude larger than that of the thermal expansion (or compression). Hence, with the temperature change, the Bragg wavelength shifts mainly due to the change of n_{eff}.

Interrogators or demodulators in fiber grating sensor systems are the measurand-reading units that extract measurand information from the light signals coming from the sensor heads. The measurand is typically encoded spectrally, and hence the interrogators are usually meant to measure the Bragg wavelength shifts and convert the results to measurand data. The challenge in this design is that since the wavelength shift to be measured is in picometers the electronics required to process it should be obviously very high speed by virtue of sampling theorem. Although many techniques have been reported to provide fast and reliably interconnecting MIN architectures but still it is yet not possible to take processing in the domain of THz [74]. Spectrum analyzers are not appropriate for real sensor systems, not only because of their high prices but also because their slow scanning speed limits dynamic sensing. Precise wavelength measurement using FBG sensors has been a challenging problem since the early stage of FBG sensing work.

5.2 Passive Detection Schemes

Passive detection scheme interrogators refer to those that do not use any electrical, mechanical, or optical active devices. Interrogators using linearly wavelength-dependent devices, performing measurand monitoring by detecting optical power, using identical

chirped grating pairs, and known as the charge-coupled device (CCD) spectrometer are discussed in this chapter.

5.2.1 Linearly Wavelength-Dependent Optical Filters

The concept of the wavelength demodulator is that, light transmittance of the filter is linearly dependent on wavelength. According to the linear response range, this type of filter is sometimes called an edge filter (which has a narrow linear range with a sharp slope) or a broadband filter (which has a wide range with a less sharp slope). There is a trade-off between the measurable range and the sensitivity. Figure 5.1 shows the schematic of such wavelength demodulator. This wavelength-change interrogator is based on intensity measurement; that is, information relative to wavelength change is obtained by the intensity monitoring of the light at the detector.

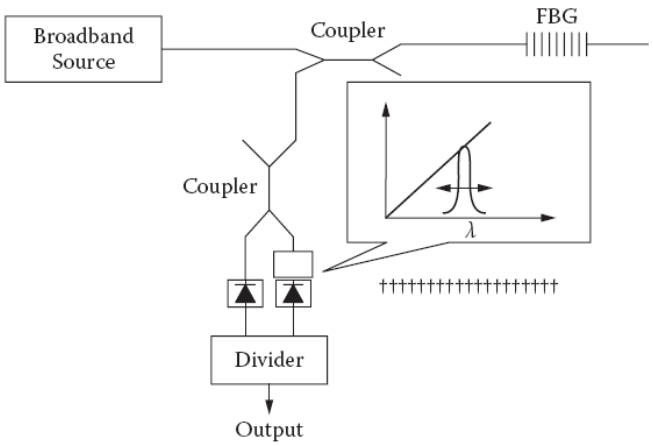

Figure 5.1 Schematic of edge filter-based FBG sensor interrogation.

The intensity-based measurement has the advantage that it had a simple structure. It does not use the fact that the information of the measurand is contained in the reflection light wavelength.

5.2.2 Power Detection

In some applications of fiber grating sensors, a simple detection of reflected or transmitted power is sufficient for the measurand interrogation. Instead of using a linearly wavelength-dependent optical filter, a light source that has intensity linearly dependent on wavelength can be used. An example is to use the amplified spontaneous emission (ASE) profile of an erbium-doped fiber amplifier (EDFA). Kim *et al*. [75] recently proposed a

chirped fiber grating strain sensor that is immune to temperature change. A chirped fiber grating has a position-dependent grating period (or pitch) and a wide reflection bandwidth. With temperature increase, the overall reflection band moves to a longer wavelength, but the bandwidth remains unchanged because the entire chirped grating experiences the same thermo-optic effect. However, with strain, the bandwidth becomes narrower because the reflection band due to the shorter period grating part moves to a longer wavelength with an elongation in the grating period, and the band becomes partially overlapped with the reflection band of the fixed grating part. Therefore, if a broadband light is launched to the fiber sensor system, the strain can be measured independently of temperature by monitoring the light power reflected by the fiber grating.

5.2.3 CCD Spectrometer Interrogator

One of the wavelength-change interrogators suitable for multipoint fiber grating sensors is to use parallel detection using a detector array such as a CCD. Lights reflected from FBGs are given to a fixed diffractive element such as finely ruled diffraction gratings and then focused to a CCD. For a light incident to the diffraction grating, the diffraction angle is dependent on the wavelength of the light. Lights with different wavelengths illuminate different areas of pixels. The change in the light wavelength results in the shift of the light at the detector array of the CCD. Therefore, this system can be used as a wavelength-change interrogator for multipoint fiber grating sensors. This demodulator can interrogate spatial and wavelength multiplexed sensors. And also there are other different techniques like identical chirped grating pair interrogating system.

5.3 Active Detection Schemes

The active detection scheme interrogators are that usually involve tracking, scanning, or modulating mechanisms to monitor Bragg wavelength shifts from single or multiple FBGs. In general, although the active detection schemes require more complex systems compared to the passive detection schemes, the active schemes show better resolution.

5.3.1 Fabry–Perot Filter Interrogator

The Fabry–Perot filter (FPF) consists of two partially reflecting surfaces with a spatial separation. When a light is incident on this cavity, due to multiple reflections inside the cavity and interference of the multiply reflected lights, the transmittance of light through

this cavity has a periodic characteristic with the variation of optical frequency or the spacing between the two reflecting surfaces. One of the most successful techniques for wavelength-change interrogators of FBG sensors is based on the use of the tunable bandpass filter. The most commonly used technique employs a fiber-pigtailed Fabry–Perot tunable filter as a narrow bandpass filter. The filter is sometimes referred to as a fiber Fabry–Perot interferometer. If the phase difference is a multiple of 2π radians, then the transmittance becomes maximum due to the constructive interference. The phase difference is inversely proportional to the wavelength, the small change in the phase difference is proportional to the small wavelength change shows that the phase difference is proportional to the cavity length.

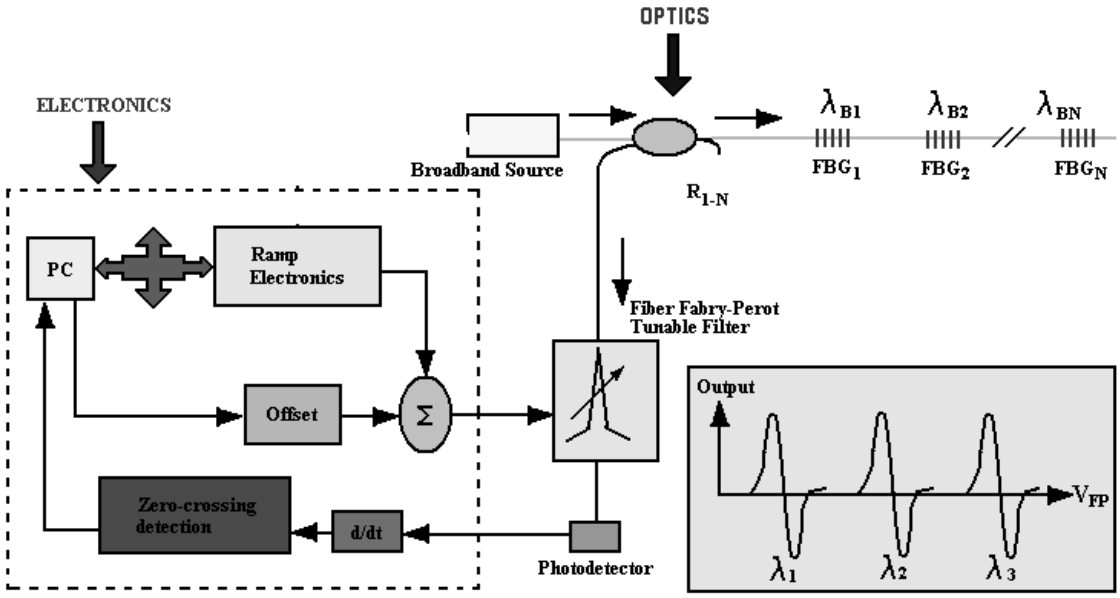

Figure 5.2 Schematic diagram of the Fabry–Perot filter interrogator sensor system.

Figure 5.2 shows the schematic diagram of the tunable fiber FPF for demodulating the wavelength shift from a single FBG. In this case the demodulator is working in a tracking or closed-loop mode.

5.3.2 Acousto-Optic Tunable Filter Interrogator

The acousto-optic tunable filter (AOTF) is a device for detection, over a wide spectral range, of a small wavelength change in light reflected from an FBG. The acousto-optic interaction between a light and an acoustic wave in a photoelastic medium exhibits very

useful performances, which include signal access at high speed, a wide tuning range in wavelength, and a narrow bandwidth filtering.

The Bragg condition can be satisfied for a fixed light wavelength with an appropriate grating vector, the magnitude of which is determined by the acoustic frequency. The wavelength tuning of the AOTF is obtained by varying the frequency of the RF (radiofrequency) signal that generates the sound wave via the transducer. As a result, by changing the RF of the AOTF, it is possible to interrogate a sensor grating. It can also be extended to multipoint grating sensors. It is possible to change the acoustic wave frequency from tens of hertz to hundreds of megahertz, thereby extending spectral tuning range. Thus, it is suitable for use in both dynamic and quasi-static detection of wavelength change in a broadband spectral range that may include multiplexed sensors. Furthermore, the AOTF technique has several advantages. It can be accessed at multiple wavelengths simultaneously as well as at random wavelengths. This is obtainable by applying multiple RF signals of different frequencies. The AOTF can offer a parallel interrogation and a reduction of interrogation time in a multiplexed sensor array system.

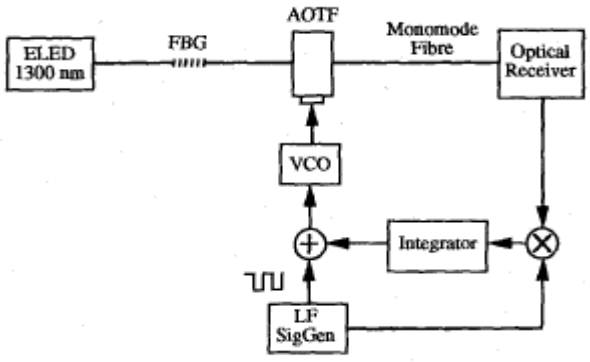

Figure 5.3 Schematic of Bragg wavelength tracking loop

The AOTF is operated in two principal modes: the scanning mode and the lock-in mode. In the scanning mode, the light wavelength is gradually scanned over the range of interest by means of varying the applied RF signal frequency. In the lock-in mode, the AOTF is dithered with a feedback loop, and the lock-in signal with the dithering frequency is detected. The dithering frequency is much lower than that of the RF signal. The lock-in regime is relatively immune to the intensity noise compared with the scanning mode.

And also other available techniques are Fourier Transform Spectrometer Interrogator, Unbalanced Mach–Zehnder Interferometer Interrogator, Michelson Interferometer Interrogator

5.3.3 Wavelength Tunable Sources

Most of the broadband sources are not high-power devices, and the receivable optical powers are reduced considerably after the broadband lights are reflected from the narrow-band sensor gratings. The low power leads to low SNRs, which might reduce the reliability of the interrogation and increase the interrogation time. To increase the SNR, active high-power interrogation has been proposed [90,91]. Rather than a superfluorescent broadband source, this technique utilizes a wavelength tunable source that has a relatively high power and a narrow linewidth. It is possible to fully interrogate the spectral change in the sensor grating by tuning the wavelength of the laser source over a spectral range of interest.

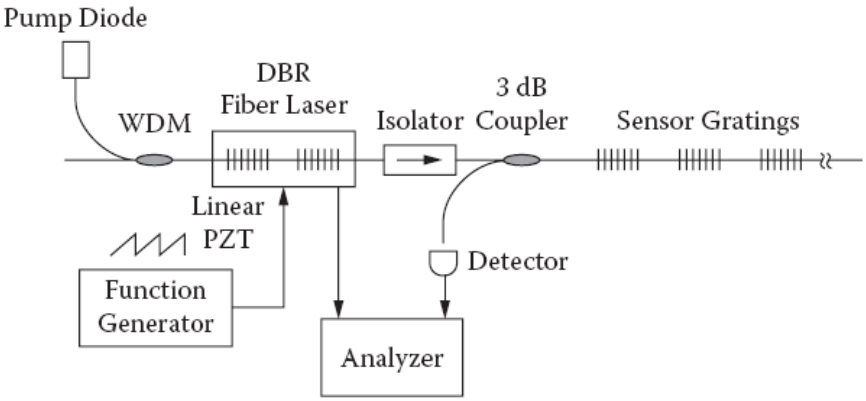

Figure 5.4 Schematic diagram of an interrogation by wavelength tunable source.

The wavelength tunable EDF laser has been demonstrated for the interrogation of a three-FBG sensor in Figure 5.4. If the wavelength of the line source is known and is launched to a sensor grating, the detected optical power reflected from the sensor grating indicates the spectral response of the sensor at the given wavelength.

The fabry perot tunable filters interrogating system for multiplexing FBG sensor systems is more commonly used because of its

- wide dynamic range
- Narrow band width
- High tuning speed.

5.4 Fabry-Perot Tunable Filter Design for FBG Interrogator

The Fabry-Perot interferometer is an optical instrument which uses multiple-beam interference, first constructed by Charles Fabry and Alfred Perot. In recent years, much effort has been devoted to the development of tunable optical filters based on Fabry-Perot Interferometers (FPI).

In principle, the device consists of two planes, parallel, highly reflecting surfaces that are precisely aligned to satisfy the boundary conditions to support constructive interference. Incident light enters the Fabry-Perot cavity and undergoes multiple reflections between the mirrors so that the light can interfere with itself many times. The condition for constructive interference within a Fabry-Perot interferometer is that the light forms a standing wave between the two mirrors $2nl\cos\theta = m\lambda$, m an integer, λ the wavelength of light, n refractive index of the material between two mirrors.. Otherwise, destructive interference will not allow any light through the Fabry-Perot interferometer.

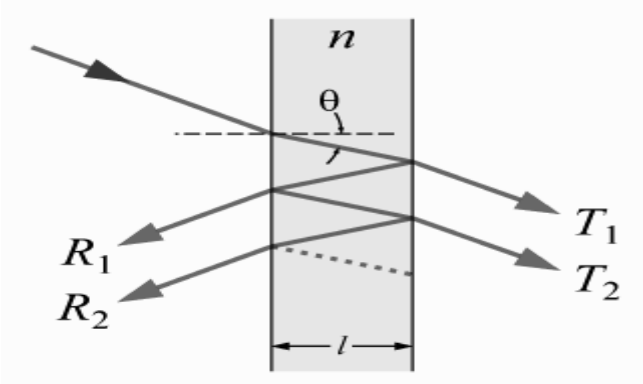

Figure 5.5 : Operating principle of tunable filter

A Fabry-Pérot etalon is shown in Figure 5.5. Light enters the etalon and undergoes multiple internal reflections. Whether the multiply-reflected beams are in-phase or not, depends on the wavelength (λ) of the light, the angle the light travels through the etalon (θ), the thickness of the etalon (*l*) and the refractive index of the material between the reflecting surfaces (*n*).

The phase difference between each succeeding reflection is given by δ:

$$\delta = \left(\frac{2\pi}{\lambda}\right) 2nl\cos\theta \qquad (5.1)$$

5.5 Transmission of Fabry-Perot Etalon

The transmitivity of a Fabry-Perot etalon is dependant of the wavelength of the incident radiation. The interference created between mirrors creates standing waves. These standing waves will generate constructive interference when they will fit exactly with the cavity length. In other word, the optical cavity length is an integer number times the resonant wavelengths. So there are a discrete number of resonant wavelengths.

The transmitted intensity can then be expressed by the following equation:

If the incident angle(ɵ) is taken to be very small the transmission function of an etalon is given by

$$T_e = I_t/I_i = T^2/(1+R^2-2R\cos\delta)$$

Or equalently

$$T_e = \left(\frac{\left(\frac{T}{1-R}\right)^2}{1+\left[\frac{4R}{(1-R)^2}\right]sin^2\left(\frac{\delta}{2}\right)}\right) \qquad (5.2)$$

If the absorption of the plates is negligible then T+R=1

Then eq(5.2) becomes

$$T_e = \left[1 + Fsin^2\left(\frac{\delta}{2}\right)\right]^{-1} = \boldsymbol{A}(ɵ) \qquad (5.3)$$

Where A(ɵ) is known as AIRY function. Here F is the co-efficient of finesse, given by

$$F = \frac{4R}{(1-R)^2} \qquad (5.4)$$

From eq(5.2) to get maximum transmission peak the phase difference is given by

$\delta = 2\pi m$ where m is an integer.

Then from eq(5.1) it can be obtained $m\lambda = 2nlcosɵ$.. (5.5)

The wave length which satisfies the above condition for that transmission is maximum.

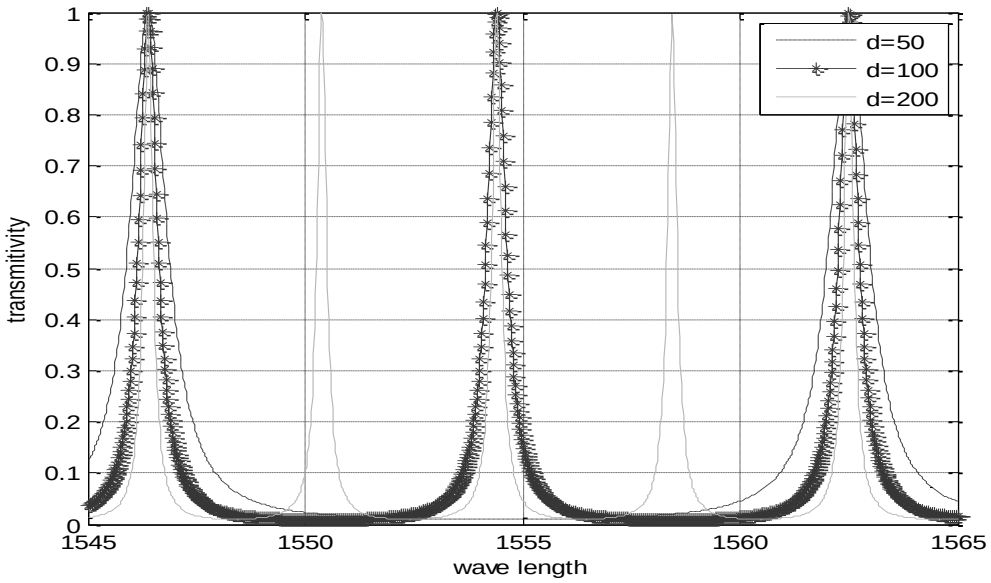

Figure 5.6 the transmission of a particular wavelength in different orders for d=50μm,100 μm,200 μm and R=0.98,n=1.5.

5.6 Characteristics of Interferometer:

5.6.1 Full Width Half Maxima(FWHM):

It is a measure of sharpness of the fringes that is how rapidly the irradiance drops off on either side of the maxima. It is the width of the peak where irradiance will drop half of its maximum value. That is A(ɵ)=1/2.

From eq(5.3) it follows that

$$\delta_{1/2} = 2sin^{-1}(\frac{1}{\sqrt{F}}) \backsimeq 2/\sqrt{F}$$ since usually F is large.

From eq(5.4) it can be concluded that if reflectivity of the mirrors(R) is high then the sharpness of the transmission peaks will increase.

5.6.2 Finesse:

It is the ratio of separation of adjacent maxima to the FWHM. Given by

$$\mathcal{F} = \frac{2\pi}{FWHM}$$

That is given by $\mathcal{F} = \frac{\pi\sqrt{F}}{2}$

Also it can be written as $\mathcal{F} = \frac{\pi\sqrt{R}}{1-R}$

That is as the reflectivity increases the finnese also increases that is sharpness of peaks will increase. By using high reflectivity mirrors Finesse of about 10,000 can be acheved. The below graph shows the relation between Finesse and the reflectivity of the mirror.

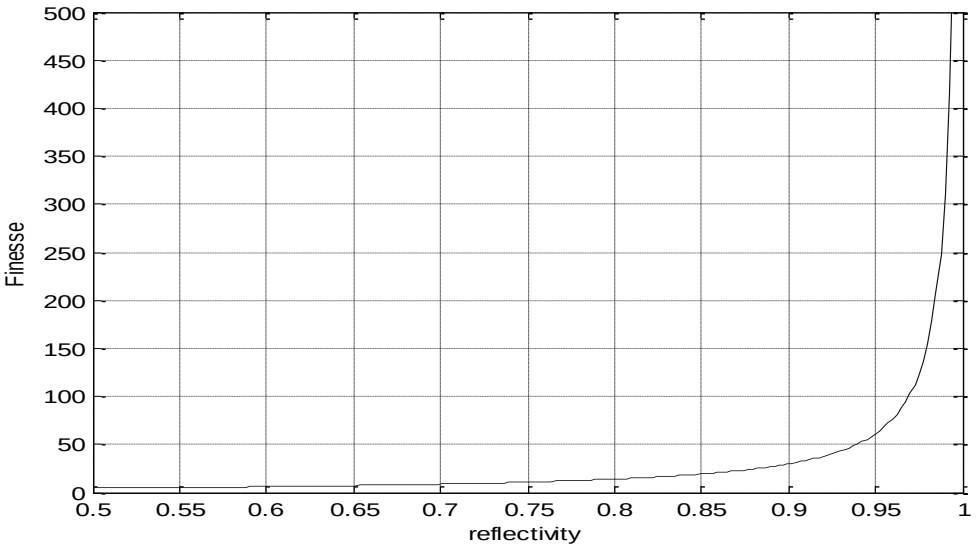

Figure 5.7: reflectivity Vs Finesse of the tunable filter

5.6.3 Spectral Resolution

A purely monochromatic light wave generates a particular fringe system. But δ is a function of λ, so that if the source is made up of two such monochromatic waves two superimposed fringe system would result. When the individual fringe systems partially overlap, a certain amount of ambiguity exists eve when they are said to be resolved. According to Rayleigh criteria two peaks will be considered to be resolvable if their separation is greater than their FWHM – that is 2Δm. This will give a dip which is about 80 % of maximum in most cases.

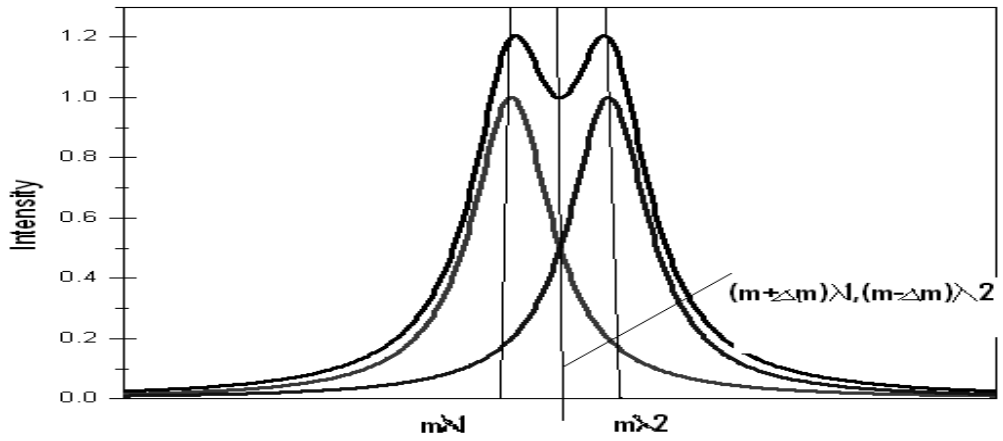

Figure 5.8:Normalized transmitted intensity Vs wavelength

For normal incidence resolving power is given by

$$\Re = \frac{\lambda_o}{\Delta\lambda_{omin}} \backsimeq \mathcal{F}2nl/\lambda_o$$

Or $\Re \backsimeq \mathcal{F}m$ .In frequency terms

$$(\Delta\vartheta)_{min} = c/\mathcal{F}2nl$$

As the two components present in the source become increasingly different in wavelength, the peaks overlap separates.

5.6.4 Free Spectral Range (FSR):

Taking Eq. (5.4), the resolution of a Fabry-Perot plate can be improved by increasing d_n, the optical path difference between the two reflecting surfaces. But by doing this the interference order is also increased, leading to more problems with overlapping orders. As a measure for the useful working range (no overlapping orders) the Free Spectral Range of an instrument is defined. It is calculated by equating the phase shift for a certain wavelength λ , order m+ 1 with that for λ + FSR, order m:

$$\frac{2ln}{\lambda} = 2\text{nl}/(\lambda + \text{FSR}) + 1$$

$FSR = \Delta\lambda_{fsr} \approx \lambda^2/2\text{ln}$ and similarly

$$(\Delta\vartheta)_{fsr} \approx c/2nl$$

On comparison with resolution $\Delta\lambda_{fsr}/\Delta\lambda_{res} = \mathcal{F}$

From above equations it can be concluded that to increase the resolving power by merely increasing *l*, the FSR will decrease, bringing with it the resulting confusion from the overlapping of orders. Need is that $\Delta\lambda_{res}$ *be* as small as possible and $\Delta\lambda_{fsr}$ be as large as possible.

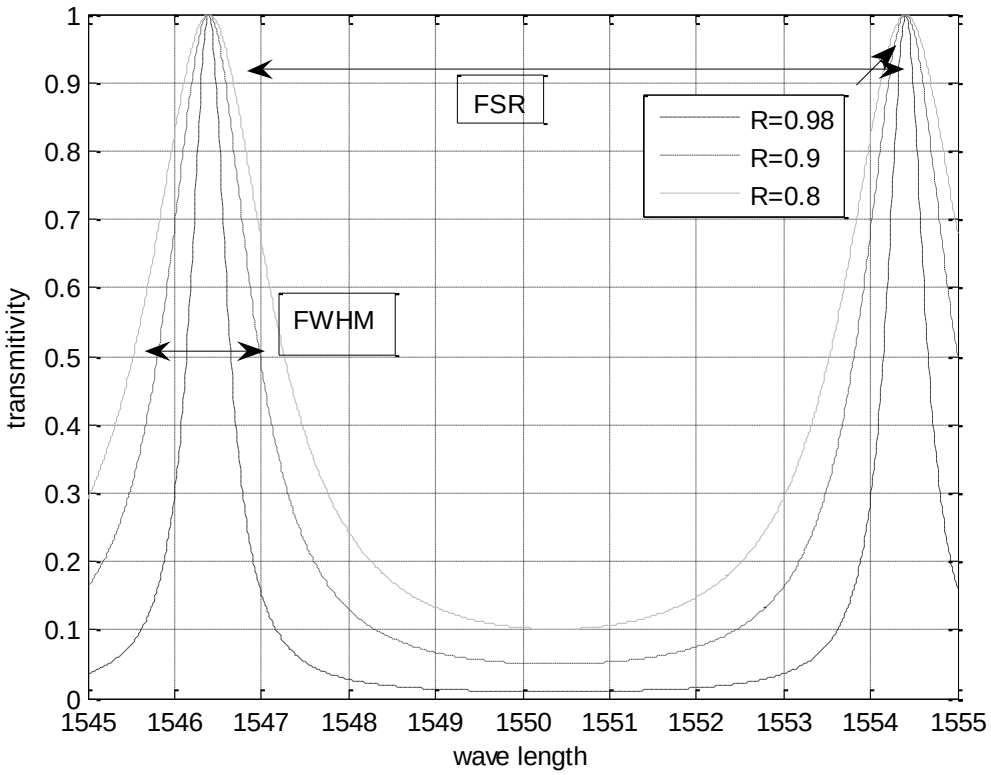

Figure:5.9 Simulated spectrum of FPTF for R=0.98,0.9,0.8,d=100 μm,n=1.5

5.6.5 Contrast

To rate the suppression between maxima, the Contrast is defined as ratio of peak height to the minimum intensity. The transmission minimum at $\delta = \pi$ and at equivalent phases define a Contrast value C of

$$C=F+1$$

5.7 Tunable Fabry Perot Interferometres

A Fabry-Pérot interferometer differs from a Fabry-Pérot etalon in the fact that the distance *l* between the plates can be tuned in order to change the wavelengths at which transmission peaks occur. Due to the angle dependence of the transmission, the peaks can also be shifted by rotating the etalon with respect to the beam**.**

5.7.1 The Air-Spaced Fabry-Perot Interferometer

Nearly all tuning schemes use interferometers where two highly reflective glass plates are separated by a plane-parallel 'plate' of air. The scheme is complementary to the plane-parallel plate discussed and obeys the same equations. Figure 5.10 shows the principle, the two plates usually are slightly wedge-shaped to suppress interference due to the outer surfaces.

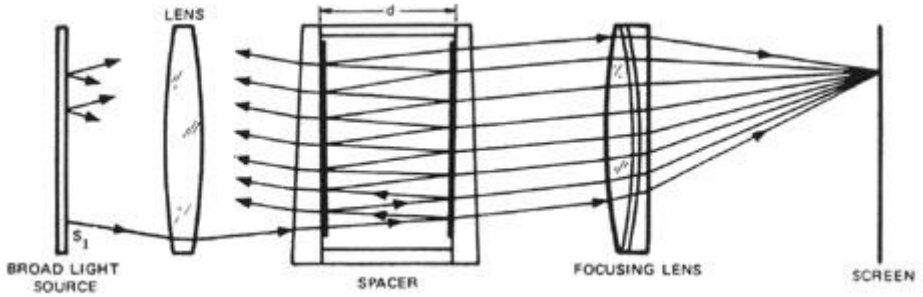

Figure 5.10 : Schematic diagram of air spaced scanning interferrometre

Parallel light is achieved using a broad light source in the focus of the illuminating lens in Air-spaced Fabry-Perot interferometer.

As the optical distance between the two plates is dn, a convenient way to change it is to vary the air pressure. That was classically used, keeping the distance d constant by mechanical spacers and varying the refractive index n of the air by changing the pressure. Nowadays, this technique is not used and piezoelectric transducers are used.

5.7.2 The Scanning Fabry-Perot Interferometer

The preferred method used for scanning is to move one of the two reflecting plates mechanically. The principle is shown in Figure 5.11 As the mechanical scanning distance necessary is in the order of the light wavelength this scanning can be done by piezoelectric actuators.

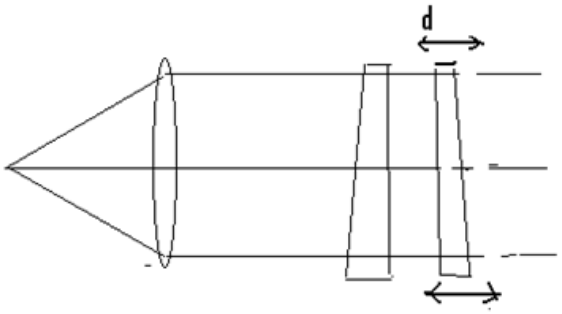

Figure 5.11: Scanning Fabry-Perot interferometer, principle.

The space d between the two reflecting surfaces is varied by moving on of the plates. The actuators can be driven at moderate voltages (100. . . 500 V), to get linear scans, usually saw tooth waveforms are used.

Piezoelectric scanning has a variety of advantages compared to other scanning techniques:

- Both slow and fast scanning modes are possible. In fast scanning modes, the interferogram may be displayed online on an oscilloscope.
- The scanning voltage can be directly used as measure for the plate position.
- The final adjustment can be easily done by automatically or manually adjusting the drive voltages of the (usually three) piezo stacks.
- Stabilization schemes can be easily included by controlling the drive voltages of the piezo stacks. The controller, e. g., can try to hold a constant position and height of the peaks

There is also one disadvantage of piezoelectric actuators that they often show a large temperature drift thus they have to be driven in a controlled mode.

5.8 Fiber based FP filter

When the fibers are coated at the ends with the gold then they act as reflectors that are wavelength dependent. Hence they serve the purpose of traditional mirrors in the FP filter along with providing the certain advantages.

- Miniaturization
- Simplicity
- Less stringent stable alignment conditions
- Less weight
- Free from EMI interference

Achieving the space tunability.

The space tunability can be achieved as follows.

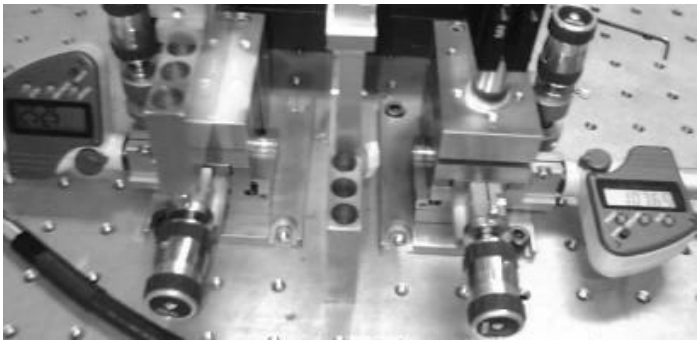

Figure 5.12: Changing of the gap between fibers

One end of the fiber is attached to the one end of the peizoelectric crystal. The second goldplated fiber end side is attached to another end of the peizoelectric crystal. One of the ends of peizoelectric crystal is fixed on its mount and the other is let to move free.

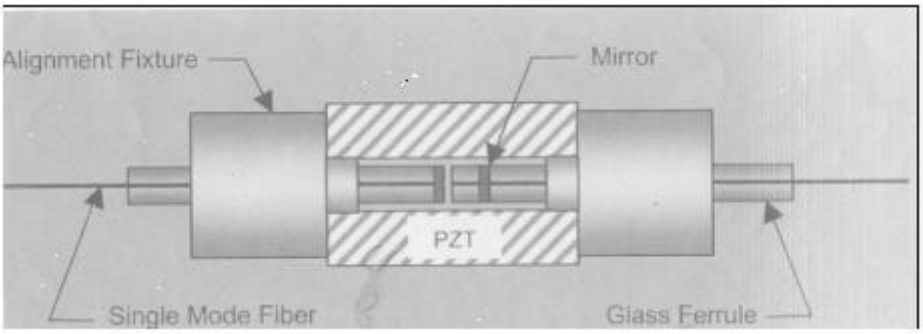

Figure 5.13: FP filter using fibers

As the ramp electronics increases its voltage, this value is applied to PZT, which changes its dimensions accordingly. Along with this PZT movement moves the free end of the fiber. Hence the distance between the fiber ends changes. This achieves the neccesary spacing tuning and corresponding to the different spacings the different wavelengths emerge.

5.9 Design of tunable filter:

INPUT

FILTER SPECIFICATIONS			CHANNEL SPACING		
Bandwidth(BW)	10.000	GHz		50	GHz
Finesse(F)	650	(unitless)			
			MINIMUM		
Free Spectral Range(FSR)	6500	GHz	BANDWIDTH	10	GHz
Free Spectral Range(FSR)	52	nm	=function of (Bit Rate)		

with these parameters by studying the behavior FPTF it was observed that:

operating wave length =1550nm

FILTER SPECIFICATIONS		
Loss		3.0dB
Polarize Sensitivity		No
CONTRAST FACTOR	52	dB
=function of (Finesse)		
CAVITY LENGTH	15.7	um
=function of (FSR)	0.02	mm
MIRROR REFLECTIVITY	99.5	%
=function of (Finesse)		

BAND WIDTH	10GHz	
Finesse	650	
ISOLATION BAND WIDTH(GHz)	10	(3dB)
	30	(10dB)
	100	(20dB)

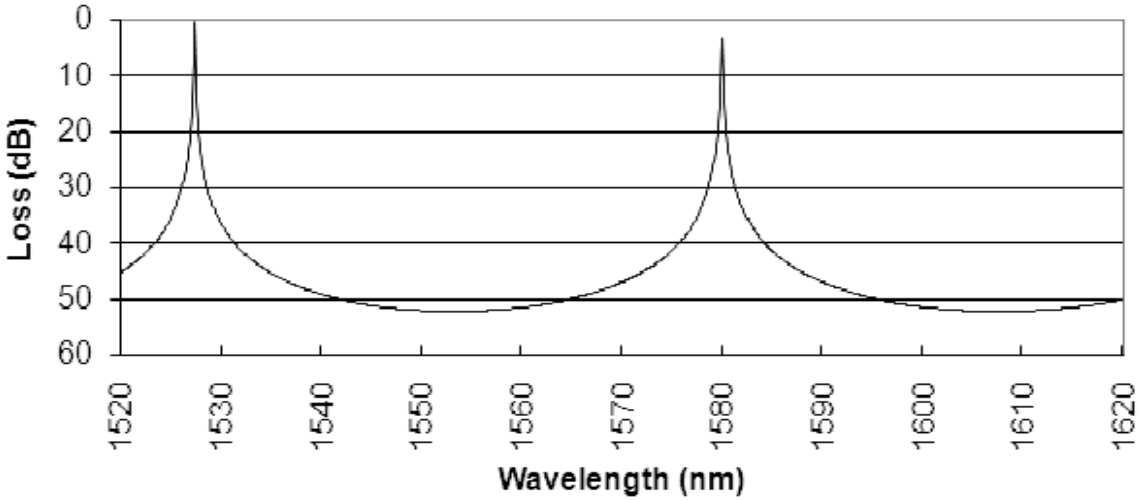

Figure 5.14 Airy Functions for given finesse and BW

5.10 Peak Detection System

Multiplexed Fiber Bragg Grating (FBG) sensor systems have been successfully developed and utilized in structural health monitoring applications measuring various measurands such as strain, temperature, and pressure. These measurands are transferred to the Bragg wavelength shifts, which can be detected using one of many well established demodulation techniques. However, in field of applications, integration of FBG sensor s often limits the performance of the sensor sytems. FBG sensors are embedded into

composite structures or bonded on the surface of structures. In many cases, improper embedding or environmental influences causes substantial distortion or broadening of FBG spectra, which leads to increased system noise and false measurements with demodulation techniques.

A Fiber Bragg Grating peak detection system has a broadband source that provides a broad band optical signal, a Fiber Bragg Grating and a variable threshold and Grating profile Peak detection unit. The FBG responds to the broadband optical signal, and further responds to a physical parameter, for providing a Fiber Bragg Grating optical signal containing information about the physical parameter.

The variable threshold or grating profile peak detection unit responds to the Fiber Bragg Grating optical signal, or providing a variable threshold detection unit signal containing information about a peak detected in the Fiber Bragg Grating optical signal that is used to determine the physical parameter. During the variable threshold peak detection unit determines a local threshold value for each wavelength over a spectral band of the Fiber Bragg Grating optical signal.

In this FBG sensor the broad band source having the spectral range 1520-1570 has been used.

In operation, the broadband source illuminates the FBG. The FBGs provide reflected optical signals containing reflected spectral information that is then directed by the coupler into the optical detection unit, which performs an optical to electrical signal conversion and is responsible for determining each of the wavelengths reflected by FBGs.

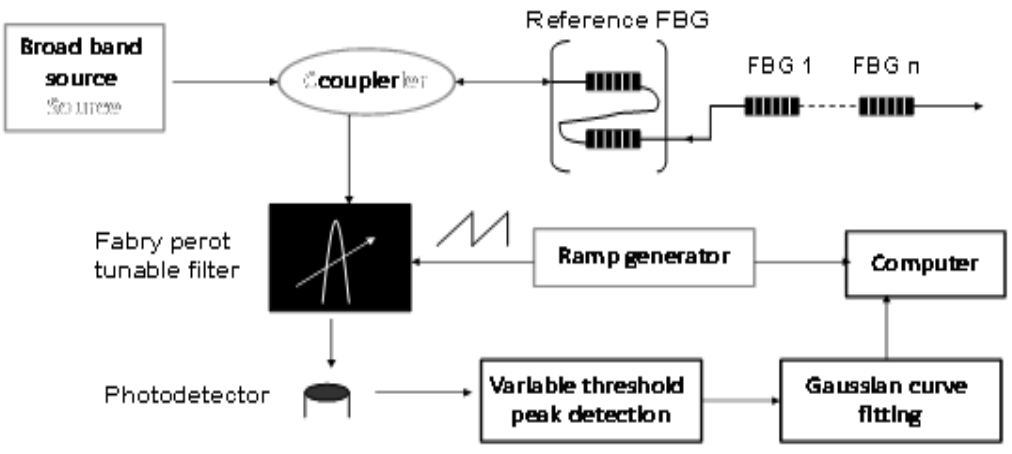

Figure 5.15 Basic Block Diagram of Peak Detection System

Several techniques for optical detection have been developed including methods which effectively read the optical spectrum range of interest and present this information for processing. Also present on the return spectrum is an overall background signal which can be present in the returned spectra when reflections are present in the optical path. Once this spectra is detected, the FBG peaks can be identified and the wavelengths of each FBG reflected signal is calculated. However, as shown, a background signal will be present in the returned spectra often due to optical connectors, splices or imperfections in the FBG itself. Also, small Fabry perot cavities can create modulations on the reflected signals which can appear to be very similar to the reflections from the FBG sensors of interest. These background and unwanted signals can often make it very difficult for a system to determine the location of a valid FBG signal from the unwanted background signals. Because of this, a fixed threshold cannot be accurately used across the entire wavelength band due to potential back reflected spectral signals.

The apparatus for detecting a valid FBG signal includes a Fiber Bragg Grating detection system having a Fiber Bragg Grating parameter sensing and detection system in combination with a variable threshold or grating profile peak detection system as shown in Figure 5.16.

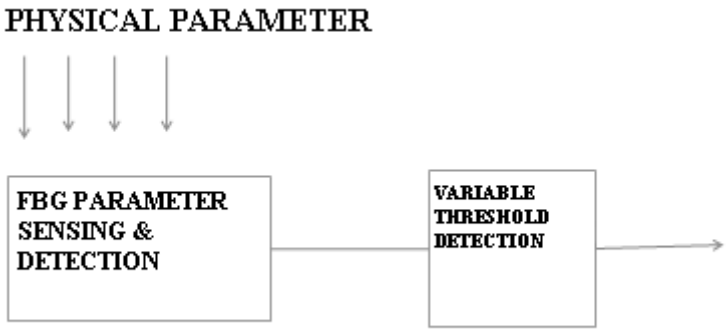

Figure 5.16 Bock diagram for threshold value calculating

As shown, the Fiber Bragg Grating parameter sensing and detection system responds to a physical parameter, such as pressure or temperature depending on application, for providing a Fiber Bragg Grating parameter sensing and detecting signal containing information about the physical parameter being sensed.

The broad band source includes a narrow source swept over a broad band, and provides a broadband optical signal via the coupler to one or more Fiber Bragg Gratings.

The one or more Fiber Bragg Gratings responds to the broadband optical signal, and further responds to a physical parameter, including temperature or pressure, for providing a Fiber Bragg Grating optical signal containing information about the parameter via the coupler to the optical detection unit. The information communicated by the Fiber Bragg Grating optical signal is in the form of the peak associated with each Fiber Bragg Grating wavelength.

The variable threshold detection unit responds to the optical detection unit signal, for providing a variable threshold peak detection unit signal containing information about the one or more peaks detected in the Fiber Bragg Grating optical signal that is used to determine the physical parameter being measured as shown in Figure 5.17.

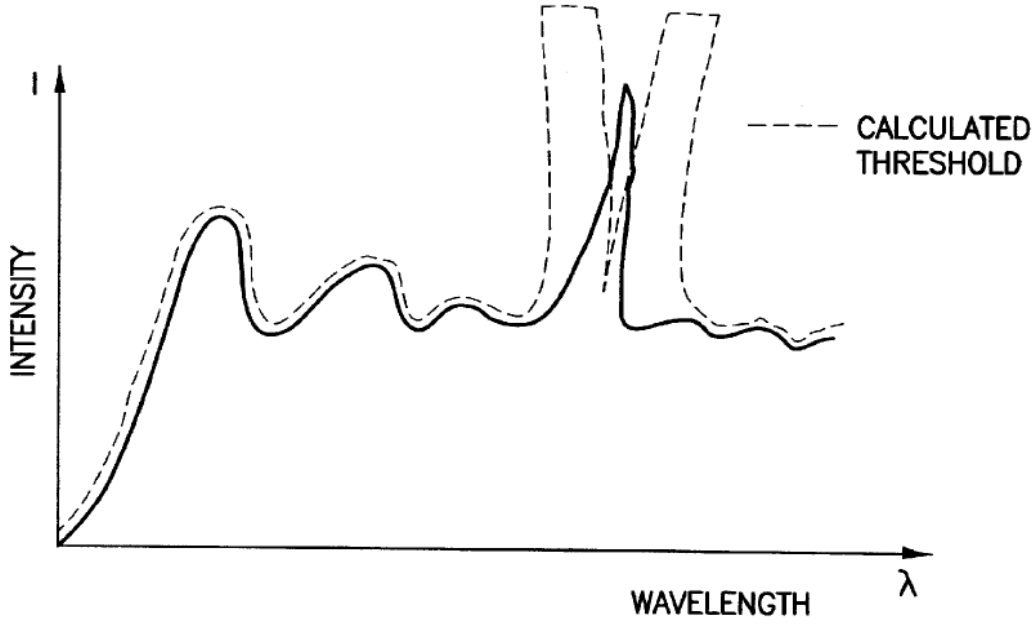

Figure 5.17 Variable Detection response curve

5.11 Variable Local Thresholds:

The operation of peak detection is based on the use of a local variable threshold, where the optical spectrum peaks above the threshold value. The local threshold value is the combination of the underlying DC component of the back ground signal and the factor of the standard deviation of the local noise of that location.

The DC component of the background signal is determined by performing two running averages along the spectral trace which resulting in a threshold number used that it will still maintain overall shape of the background signal while also averaging out the small features .

A running average span that is about four times the full width half maximum (FWHM) of the FBG signals should average out oscillations and features about which are potential peaks but still maintain background shape.

The variable threshold peak detection unit determines the local threshold value by following formula

Threshold=[(Forward running average(-offset) + Backward running average(+offset))/2]

+ [N*(Forward standard deviation(-offset) + Backward standard deviation(+offset))/2]

+ minimum noise level.

In this calculation, the running average points used should are points which are derived for locations offset before and after the peak to assure that the overall threshold term does not match the FBG itself and prevent peak detection.

If one then takes the case of a FBG peak on a steep slope of the background signal as shown in Figure 5.18. In that case a single forward running average will not work since the running average for the values on the high side of the peak will outweigh the peak itself. However by also taking a running average in the reverse direction and averaging this term with the component in the forward direction, this problem is corrected.

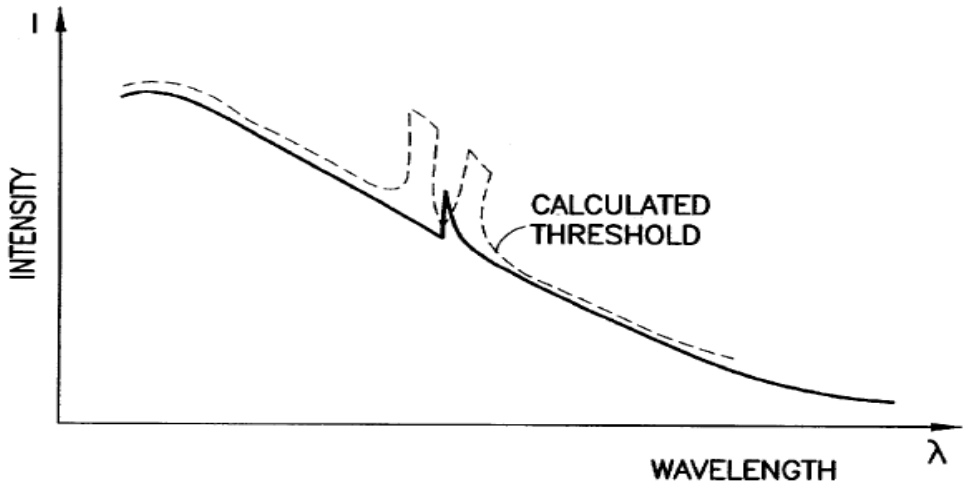

Figure 5.18 Ideal threshold values for a sample FBG

An ideal threshold values for a sample FBG signal is shown in Figure 5.18 above. The dashed lines in the figure represents the intensity of calculated local threshold variable values, and the solid lines represent the intensity of the fiber optic Bragg grating signal with some back ground signal.

The local threshold is located just above the background signal except in the region of the FBG signal, where the local threshold value is relatively high except for a window located directly over the FBG. This window is a function of the offset used in the average calculations and the set of points used for each running average. The offset should be constant with the number of points used in the running average. A value of half the average points will permit the window to dip sufficiently low in the middle of a grating profile to consistently detect the signal.

The factor of the standard deviation of the local noise to that location is determined using the same operation with standard deviation calculations. An additional multiplication term (N) is used to amplify the standard deviation term dependent on the noise present on the back reflected signal. The additional multiplication term (N) will depend on the particular system in use. It also could change with different gain settings possible on the optical detection system.

In addition, an overall minimum level term can be used which is comparable to the noise level of the variable threshold and grating profile peak detection unit.

This threshold stage will permit the detection of peaks which are extremely small and are almost vanishing into the noise or structures on the spectral profile.

The Figure 5.19 shows the graph of wavelength (nm) versus intensity (arbitrary units) of a return spectrum from two Fiber Bragg Gratings with some background spectrum and an intensity threshold.

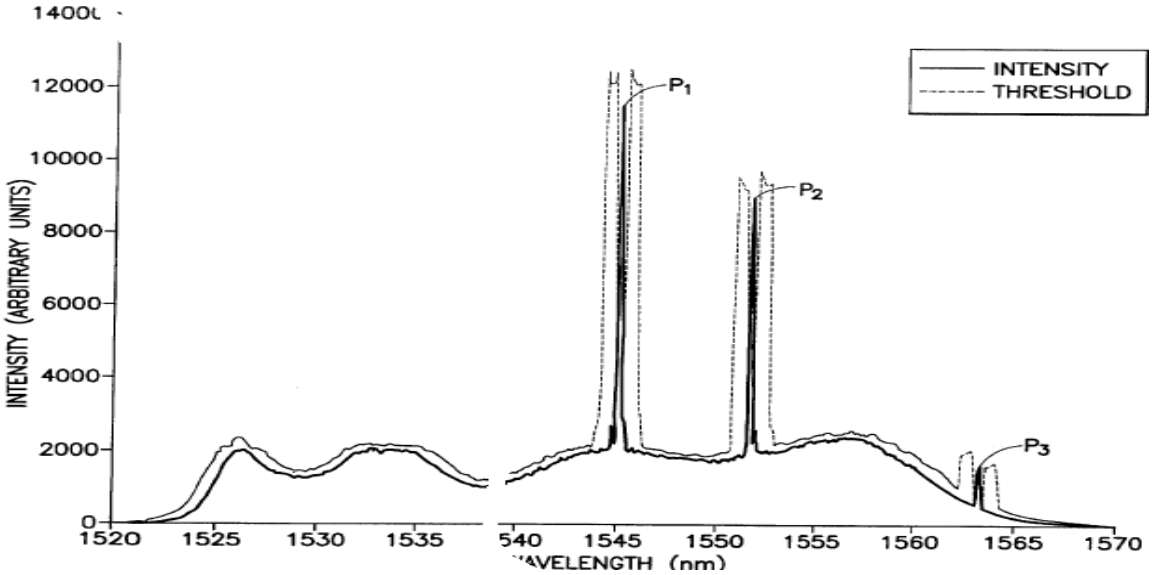

Figure 5.19 Graph of wavelength versus intensity of a return spectrum from two Fiber Bragg Gratings with some background spectrum and an intensity threshold.

The magnified part of the above Figure 5.19 is shown below in the range 1543 to 1547nm. It shows the intensity of the local variable threshold and the fiber optic Bragg grating signal in relation to peak P1.

Practical data was taken to perform simulation for the above algorithm .

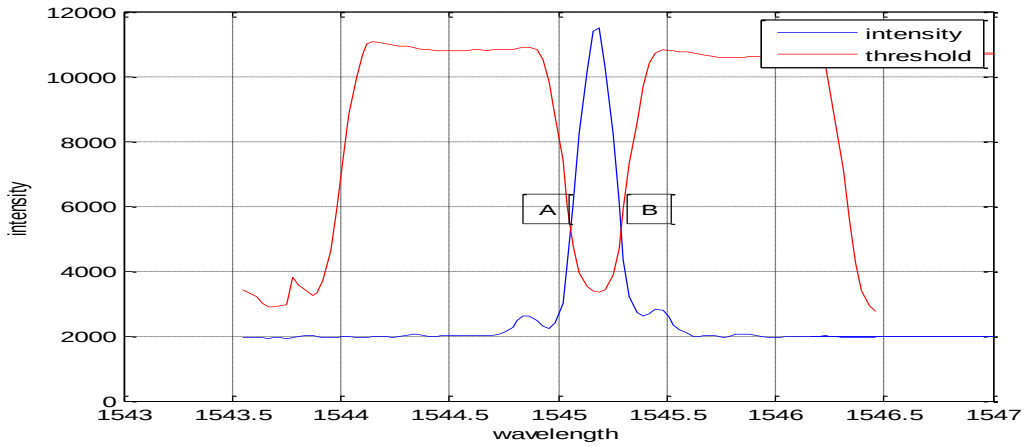

Figure 5.20 Wavelength Vs Intensity and calculated threshold values.

In figure 5.20 the points A,B shows the end of the peak P1.

This threshold stage will permit the detection of peaks which are extremely small and are almost vanishing into the noise or structures on the spectral profile.

Algorithm and coding to calculate the threshold value is described below.

STEP1: Store the data in excel file coming from sensor in file name "nav.xls'.

x-wavelength , y-intensity, n-is the size of the array.

STEP2: access the data in MATLAB through the command.

STEP3:To calculate the Full Width Half Maximum

FWHM=The width of the peak at which the intensity value is half of the maximum value(Imax/2).

STEP4:calculating the span by calculating the moving averages.

Span=4*FWHM.

STEP5: Caleculating forward moving averages in the forward direction in the span.

for i=1;i ≤ n;i++

If i≤ span then Forward average at ith point is given by

$$F.avg_i = \sum_{s=1}^{i} y(s)/i$$

If i>span then forward average at that point is given by

$$F.avg_i = \sum_{s=i}^{i+span} y(s)/span$$

Step6: calculating backward moving average

For i=1 : i≤n : i++

If i ≤(n-span) then backward average at ith point is given by

$$ba_i = \sum_{s=i}^{i+span-1} \frac{y(s)}{span}$$

If i> (n-span) then the backward average is given by

$$ba_i = \sum_{s=i}^{n} \frac{y(s)}{n-i+1}$$

STEP 7: Calculating forward standard deviation in the span as same as in calculating averages

For i=1 : i≤n : i++

If i ≤ span the forward standard deviation is given by

$$sfa_i = \sqrt{\frac{1}{i-1}\sum_{s=1}^{i}(y(s) - fa_i)^2}$$

If i> span then the forward standard deviation is given by

$$sfa_i = \sqrt{\frac{1}{span-1}\sum_{s=i-span+1}^{i}(y(s) - fa_i)^2}$$

STEP 8: Calculating backward standard deviation

for i=1 : i≤n : i++

if i ≤(n-span) then the backward standard deviation at i^{th} point is given by

$$sba_i = \sqrt{\frac{1}{span-1}\sum_{s=i}^{i+span-1}(y(s) - ba_i)^2}$$

If I > (n-span) then the backward standard deviation is given by

$$sba_i = \sqrt{\frac{1}{n-i+1}\sum_{s=i}^{n}(y(s) - ba_i)^2}$$

the threshold value is calculated using Eq. (4.1)

Flow chart for algorithm given by

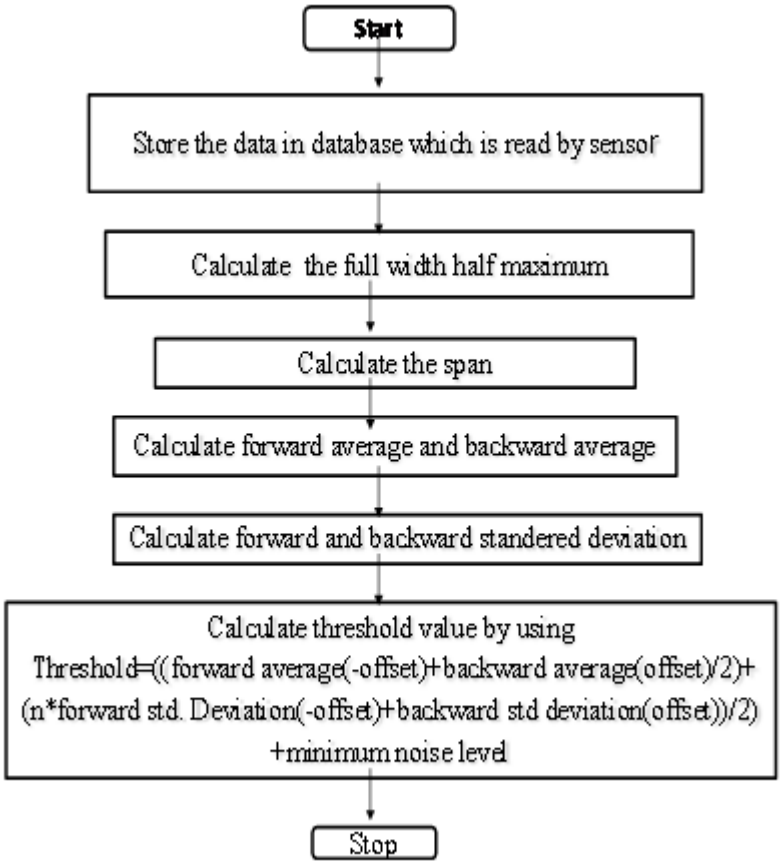

Figure 5.21 Flow chart for peak detection algorithm

5.12 Accuracy improvement in peak positioning:

In structural health monitoring applications measuring various measurands such as strain, temperature, and pressure by using multiplexed Fiber Bragg Grating sensor systems have been successfully developed. In many cases improper embedding or environmental influences causes substantial distortion or broadening of FBG spectra, which leads to false measurements with demodulation techniques.

Here the measurement accuracy of Fabry Perot band pass filter demodulation can be considerably improved by curve fitting the distorted FBG spectra to Gaussian line shapes and using their centre wavelengths. The algorithm has developed in reducing the noise of the spectral distortion, obtaining better resolution with severely distorted FBG sensor.

5.13 Gaussian line fitting:

The experimental set up is shown in Figure 5.22. A broad band source with 1550±20 nm center wavelength is used to illuminate a FBG sensor array. Two temperature shielded reference gratings are used for differential measurements, minimizing the effect of nonlinearities in the band pass filters wavelength tuning mechanism. The light reflected from the sensor array passes through a fiber optic Fabry Perot filter that is tuned by a ramp signal, and the wavelength shifts of the sensor gratings are determined by comparing peak positions in the photo detector signal with those of reference gratings, hence it is very important to locate the exact peak positions of sensor gratings. Zero crossing detection of the PD signal's derivative has been widely used for locating peaks. However, When a large amount of strain or stress gradient applies to gratings, the spectrum broadens and may develop more than one reflection peak. Then the peak search algorithm detects one or more unstable zero crossings, which increases the level of measurement noise and false readings.

To minimize uncertainties, curve fitting was employed to the reflected spectra of grating sensors. The Gaussian, which is inherently the closest profile to the FBG reflection spectrum, was used as a curve fitting profile and, in each step of iterative process, the MSE was calculated and compared to find the best matching curve .

After acquisition of the PD signal from the variable threshold peak detection system the peaks are saved in arrays and fitted to Gaussian shapes by using

$$Y_i = a_i \exp\left[-\left(\frac{x_i - c_i}{b_i}\right)^2\right]$$

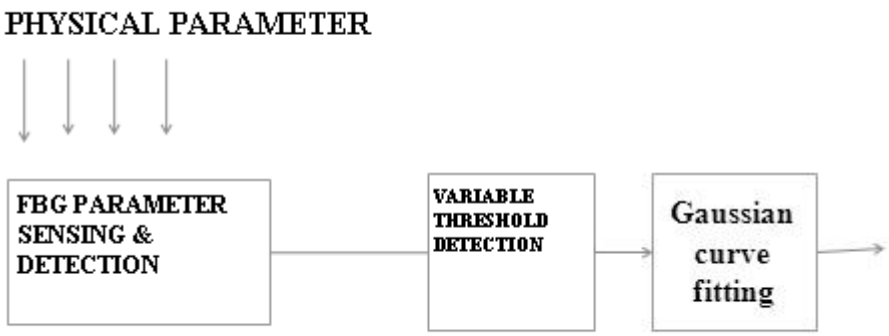

Figure 5.22 Block diagram of the Gaussian curve fitting

At a fixed centre position c_i ,the coefficients a_i , b_i represent the maximum amplitude, width of the Gaussian curve at 1/e of maximum value of amplitude respectively. The coefficients can be calculated that make Y_i match best with the profile are determined by finding the least MSE as the following equation.

$$MSE = \frac{1}{n}\sum_{i-1}^{n}(Y_i - y_i)^2$$

Where n is the array size, $y_i$is the PD signal, and Y_i is the fitted signal. The minimum MSE is recorded, this process is repeated for every centre position c_i in the array, and finally the peak position is assigned to be C_{min}, where MSE has smallest value.

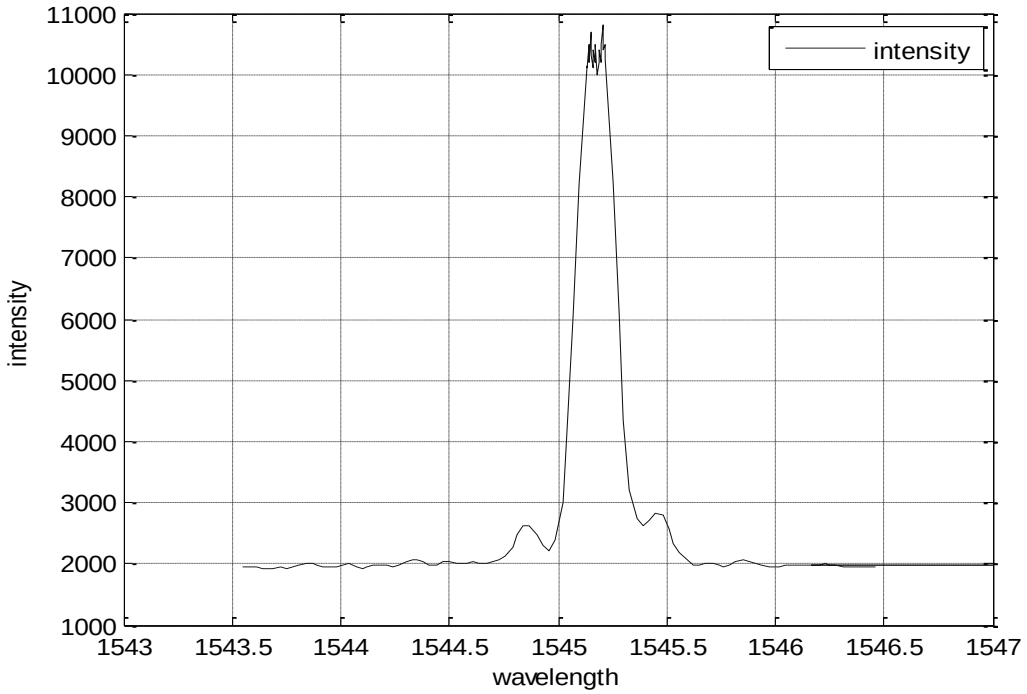

Figure 5.23 Wave length Vs Intensity .noise created randomly at the centre of the peak.

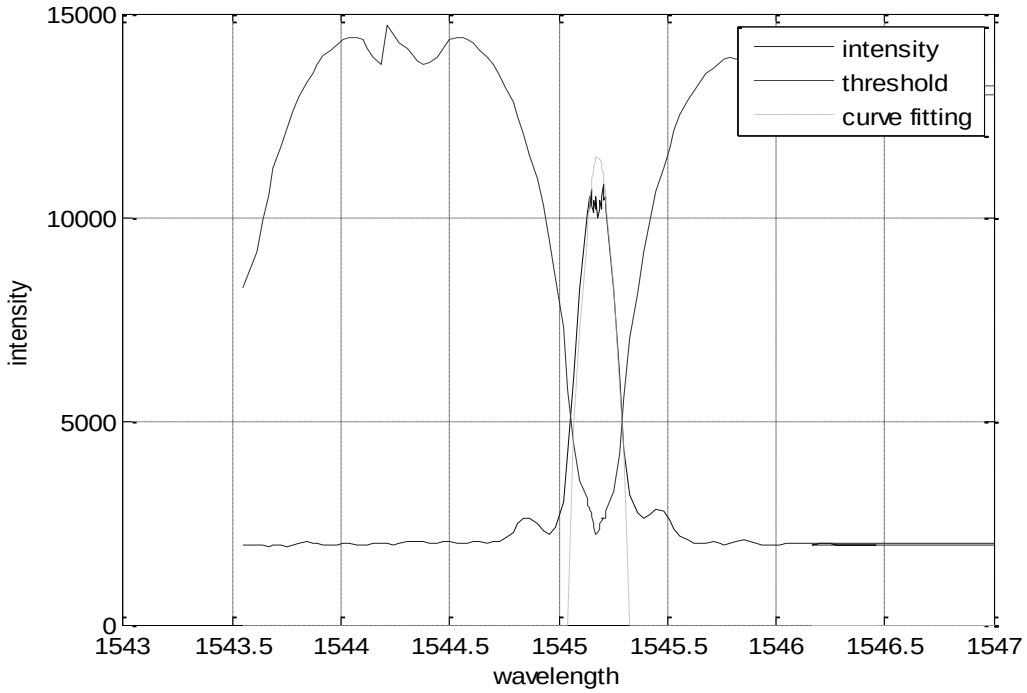

Figure 5.24 Wave length Vs Intensity and Gaussian curve fitted

By using these algorithm Gaussian curve was fitted on the randomly given noise data and exact location of peak where it is without noise was obtained. The simulated result is shown in Figure 5.24.

To obtain the better resolution in the result in curve fitting, a step size was used which was one tenth of original one. This process substantially simplified by employing a binary search algorithm that calculates and compares MSE value at only logically selected points. The initial centre position $c_i$of the Gaussian curve is set at the half position of the array , and MSE at c_1 -dx, $c_1, c_1 + dx$ are evaluated and compared ,where dx is an incremental step size and A,B are the initial and final positions of the search range respectively

Peak positioning:

If

$$MSE(c_i - dx) < MSE(c_i) < MSE(c_i + dx) \quad (5.6)$$

Then the centre position of the least MSE, C_{min} should satisfy $A_i < C_{min} < c_i$.

If $MSE(C_i - dx) > MSE(C_i) > MSE(C_i + dx)$

Then the centre position of the least MSE should satisfy $c_i < C_{min} < Bi$.

Then the new search range is set again following relations

$A_{i+1} = A_i, B_{i+1} = c_i$ or

$A_{i+1} = c_i,\ B_{i+1} = B_i$ And the next centre position c_{i+1} is set at the half position of the new range.

This process is repeated until a C_{min} is found that satisfies following relationship

$MSE(c_i - dx) > MSE(c_i) < MSE(c_i + dx)$

Then $C_{min}$is the peak centre position.

The flow chart algorithm is as follows

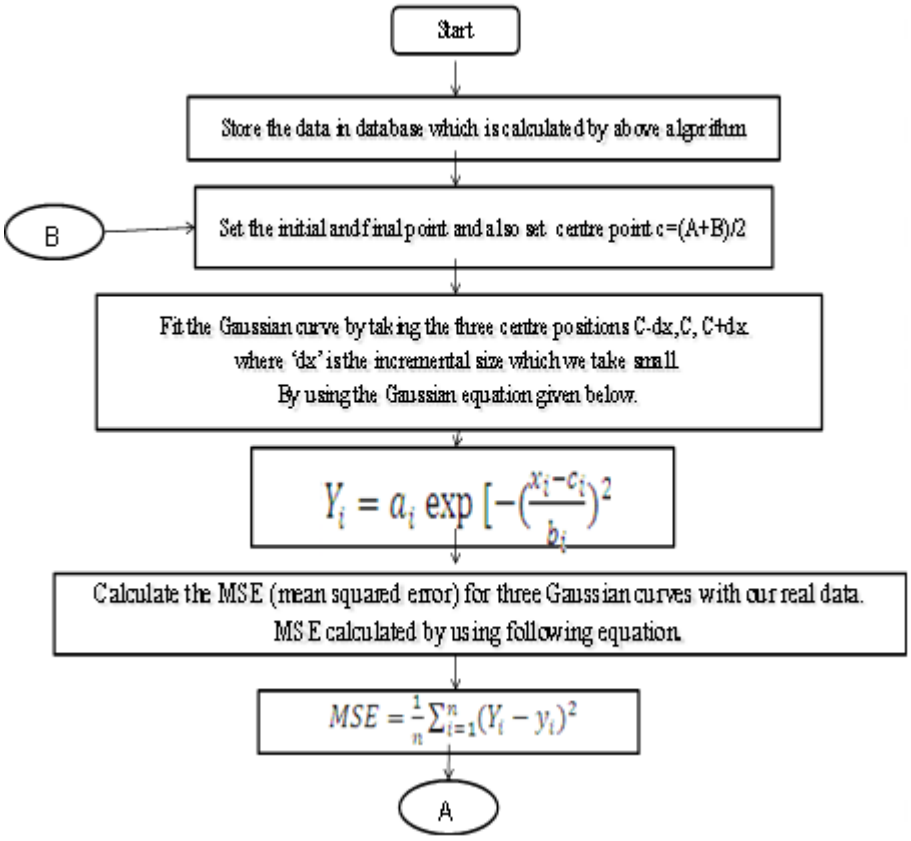

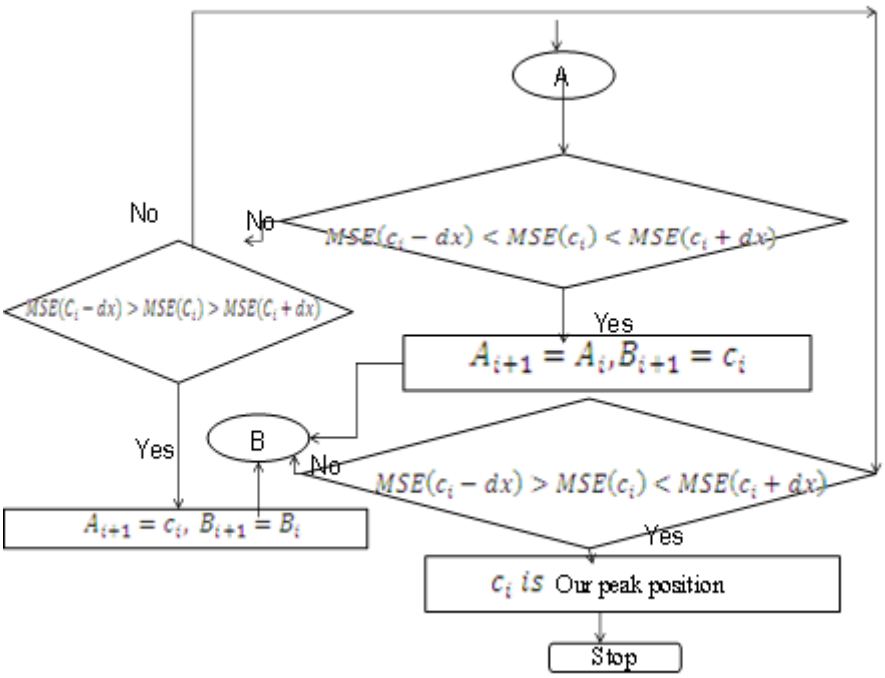

Figure 5.25 Flowchart for peak positioning

5.14 Summary

In this chapter the design of Fiber Bragg Grating Interrogator based on Fabry Perot Tunable Filter has been discussed. Also the design covered how to remove the side lobes and getting the peak from spectrally distorted data by using variable threshold and Gaussian fitting algorithm. Flow charts to calculate the threshold value and for Gaussian curve fitting to the spectrally distorted data have also been given. The design of tunable filter has also been implemented for the FBG interrogator. Although this design achieves detection of wavelength shift with considerable accuracy but it is expensive to implement since the filters and swept sources available in the market are proprietary items of micron Optics. So an alternate low cost Fiber Bragg interrogator has been designed in the next chapter.

Chapter 6

Fiber-Optic Bragg Grating Interrogator with Microbend Attenuation Compensated Edge Filtering Technique

This Chapter presents an edge filtering technique based interrogator for Fiber Bragg Grating sensors with microbend attenuation compensation system. The interrogator uses reference fiber along with the fiber in which the grating is inscribed to mitigate the effect of microbend attenuation in determining the Bragg wavelength of the sensor.

6.1 Introduction

There are many different types of Optical Fiber Sensor (OFS), working on many different principles: intensity modulation (e.g., microbending), interferometry, polarization effects, refractive index changes, reflectometry and so on. One relatively mature type which appears to be particularly attractive in many applications is the Fiber Bragg Grating (FBG).

Bragg gratings are made by illuminating the core of a suitable optical fiber with a spatially-varying pattern of intense UV laser light. Short-wavelength (<300 nm) UV photons have sufficient energy to break the highly stable silicon-oxygen bonds, damaging the structure of the fiber and increasing its refractive index slightly. A periodic spatial variation in the intensity of UV light, caused by the interference of two coherent beams or a mask placed over the fiber, gives rise to a corresponding periodic variation in the refractive index of the fiber.

This modified fiber serves as a wavelength selective mirror: light travelling down the fiber is partially reflected at each of the tiny index variations, but these reflections interfere destructively at most wavelengths and the light continues to propagate down the fiber uninterrupted. However, at one particular narrow range of wavelengths, constructive interference occurs and light is returned down the fiber.

Since the output of a Bragg grating sensor is present in the wavelength domain it requires sophisticated circuits to measure wavelength shift. A few approaches were developed to solve this problem [160]. One way of interrogating a Bragg grating sensor is to use a tunable filter. One example is the Fabry–Perot interferometer with a cavity length controlled by a piezoelectric actuator. Although this approach has a good resolution and is

independent of light intensity variations, it is relatively slow and expensive [161]. Chirped Fiber Bragg Grating (CFBG) can also be used as the wavelength-sensitive component [163]. A chirped Bragg grating can be used as a device that converts wavelength into delay [164]. For example, a typical grating of 10 cm in length corresponds to a maximum delay of 1 ns. By measuring this delay, the wavelength of light corresponding to the delay can be found [165]. Very fast electronic circuitry is required for resolving this delay and it proves to be very expensive.

To use an FBG as a sensor, it is illuminated by a light source with a broad spectrum and the reflected wavelength is measured and related to the local measurands of interest. Shifts in the Bragg wavelength can be monitored by any of the following techniques:

An interferometer may be used to convert wavelength shifts into phase shifts, which can be detected by measuring variations in the light intensity as the path difference in the interferometer is varied. This technique potentially allows for very high sensitivity, but the equipment to do it is expensive and prone to environmental interference. No commercial equipment employs interferometry [166].

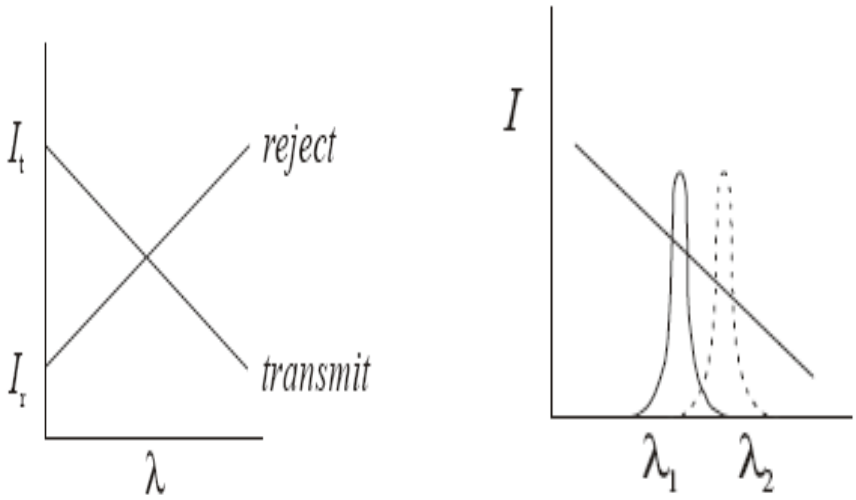

Figure 6.1: Wavelength shifts converted into intensity shifts

A sloped optical filter, which may be another Bragg grating, can be used to convert wavelength shifts directly into intensity changes. If the filter is designed to have a known pass/reject ratio which varies with wavelength, then the wavelength of a narrowband

reflection from a single grating can be determined simply by measuring and comparing the passed and rejected intensities. For the filter with a transmission spectrum shown on the left in the figure 6.1, as the Bragg wavelength increases from λ1 to λ2, the transmitted intensity I_t decreases and the reflected or rejected intensity I_r increases correspondingly. This technique referred to as edge filtering technique is the simplest and cheapest way of demodulating FBG.

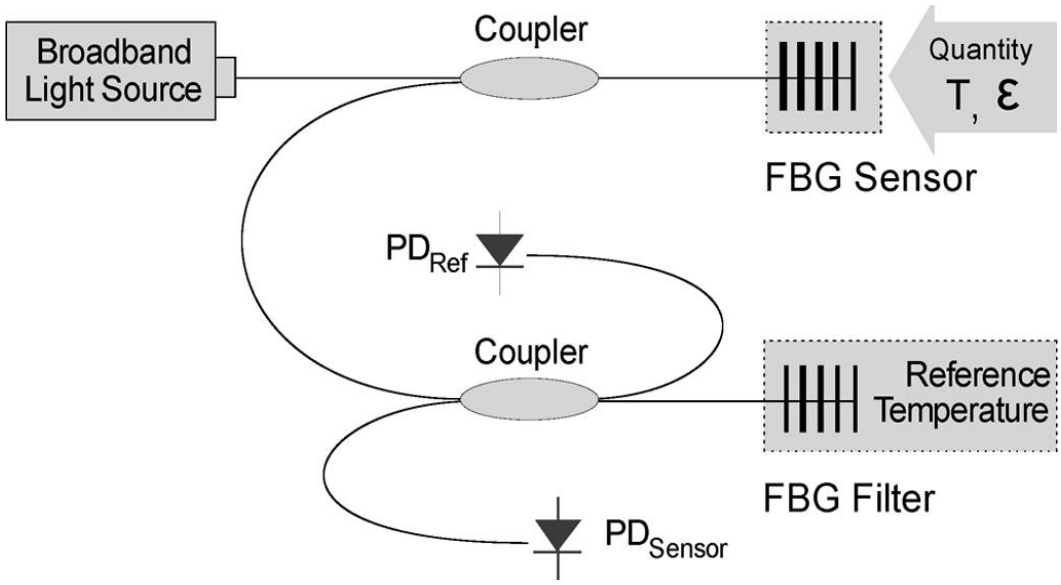

Figure 6.2: Edge Filter Technique for FBG Interrogation

This technique can be enhanced using Artificial Neural Networks to detect the edges and remove ambiguities [166-168] but so far no method has been proposed to mitigate the microbend loss errors.

The use of an edge filter is an inexpensive way of measuring Bragg wavelength shift but the accuracy is impaired by microbend losses that occur in the fiber connecting the Fiber Bragg Grating Interrogator to the Fiber Bragg Grating.

If a portion of fiber is deformed, the fiber would exhibit excess light loss. Such perturbation of fiber axis results in redistribution of guided power between modes of the fiber and also coupling of the fiber from one mode/mode group to another. In ray description due to sharp bends in the fiber, there will be some light rays falling at the core cladding interface at an angle less than the critical angle, thus preventing their total

internal reflection. These rays will thus be lost from the guiding structure. As the fiber is bent more and more sharply, so more and more number of rays will thus be lost and at a certain bend radius defined by the fiber geometrical characteristics, the bend loss becomes very steeply dependant on bend.

If /\, the spatial wavelength of periodic deformation, satisfies the following phase matching condition between pair of modes,

$$\beta_p - \beta_q = 2\pi/\backslash$$

where β_p and β_q represent modal propagation constants, then power transfer will occur from pth to qth mode. If qth mode happens to be a radiation mode, this transfer of power will result in a net transmission loss of the guided modes. From theory of coupled modes, it can be shown that for the case of step-index fiber of core radius 'a', core index n, and relative core-cladding difference, critical spatial frequency $/\backslash_{cr}$, of a deformer required to induce heavy transfer of power from highest order guided modes to radiation modes will be given by the expression

$$/\backslash_{cr} = \pi\alpha/\sqrt{\Delta} = \sqrt{\pi}.a.n_1/N.A.$$

The accuracy of an edge filter for measuring Bragg wavelength shift is impaired by these microbend losses that occur in the fiber connecting the Fiber Bragg Grating Interrogator to the Fiber Bragg Grating. This chapter presents the technique to circumvent this problem.

6.2 Experiment & Results

The errors induced due to intensity fluctuations because of microbending are reduced by employing corrections based on the intensity modulation in the reference fiber. The block diagram of the experimental arrangement is shown below

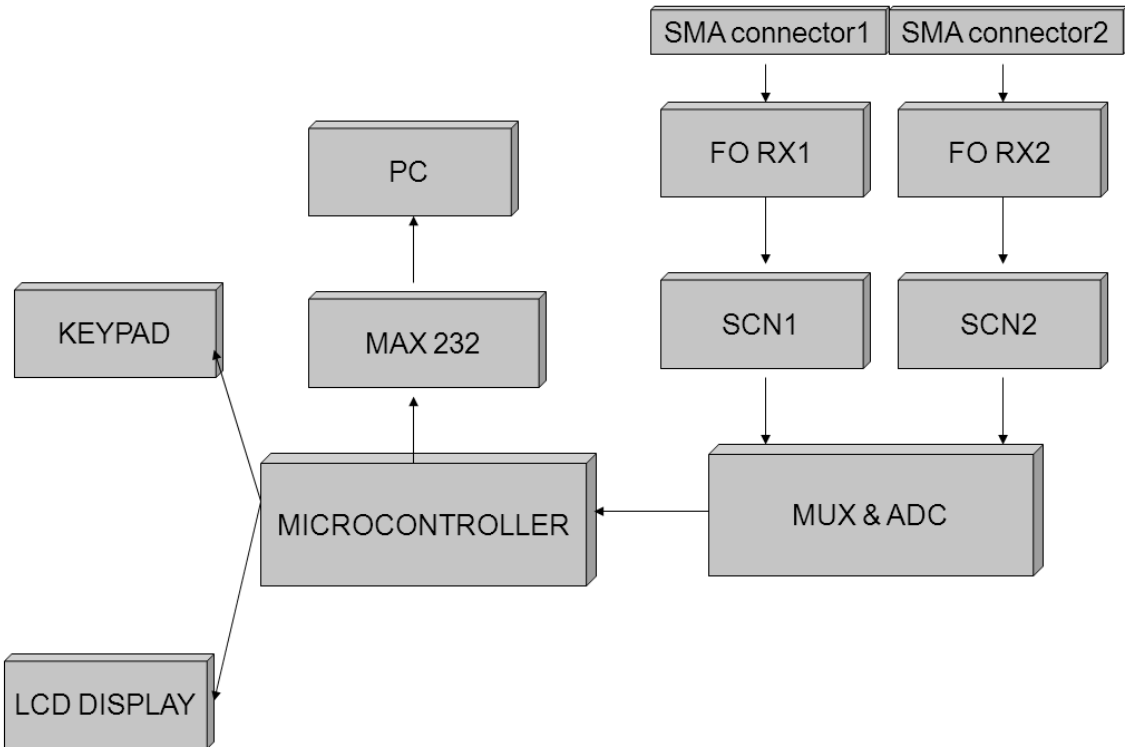

Figure 6.3: Block Diagram of FBG Interrogator

As shown in the Figure 6.3 the Fiber Optic Receiver converts the light intensity from the optical fiber coming from the Fiber Bragg Grating Sensor fixed at the SMA connector into an electrical signal. The broadband light from the source is initially filtered in the FBG sensor, which reflects a narrowband light to the second FBG filter. The portion now reflected by this filter corresponds to the convolution between both FBG reflectivity, and it is directed to the photodetector. So, the variation of the sensor Bragg wavelength is measured trough the intensity of the light that reaches the photodetector. This signal is then amplified and given to filter circuit which conditions the signal to be input to the Analog to digital converter (ADC). The ADC converts the analog signal into digital which is given to the microcontroller to be analyzed.

The microcontroller then uses a look up table or extended finite state machine [169] to introduce corrections in the readings induced due to microbending losses. The embedded

system can be further enhanced by Monotonic Partial Order Reduction as a Symbolic Partial Order Reduction Technique to enhance speed [170]. The microbend loss magnitude is determined using the reference fiber input. The multiplexer in the ADC has eight input lines, so four such sensors can be interrogated with the same circuit.

The microbend loss magnitude is determined using the reference fiber input. The multiplexer in the ADC has eight input lines, so four such sensors can be interrogated with the same circuit.

The software has been implemented in native MCS51 assembly language keeping it compact and modular. Separate routines have implemented to initialize the system, handshake with the ADC for multiplexing and acquire and display the results after suitable correction due to microbend compensation from a lookup table.

The experimental results demonstrate increased precision in the strain measurements using this technique. The graph below shows the comparison of strain measurements taken with the help of conventional strain gage sensor, edge filtering technique without microbend loss compensation and with microbend loss compensation. It can be seen from the graph that the results of interrogator with microbend loss compensation are closer to that of the conventional sensor.

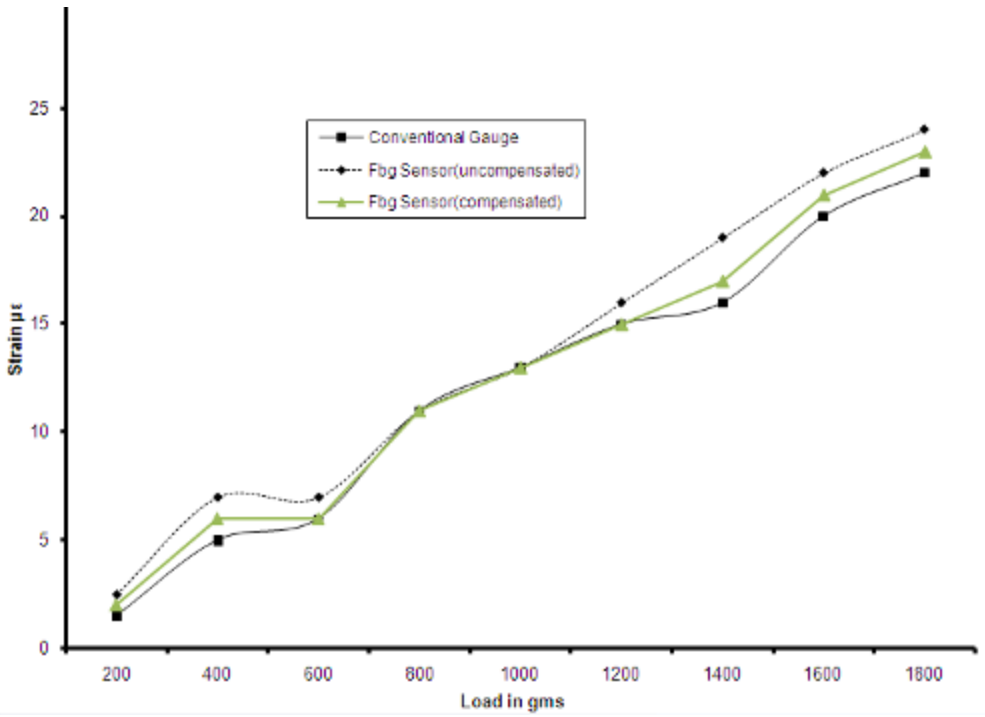

Figure 6.4: Comparison of results of FBG based microbend compensated sensor and uncompensated sensor along with conventional strain gage

6.3 Conclusion & Future Scope

Since the experimental results demonstrate increased precision by using this technique, compact, rugged and low cost Fiber Bragg Grating Interrogators can be designed using this technique. FBG sensors are passive and require no electrical power. Because of this, they are totally immune to interference from electrostatic or radio frequency sources. Furthermore, they are intrinsically safe and can be used to instrument the most hazardous explosive environments. Optical fiber is a very efficient signal carrier. Because of this, the electrical interrogation unit can be sited many kilometers away from the sensing location, whereas conventional electrical strain gauge systems require regular amplification to avoid signal to noise degradation. For monitoring large, remote structures such as sea-bed pipelines or a long rail tunnels, this is a unique and invaluable benefit. Optical sensors are immune from down-lead effects and, since the microbend compensation can be implemented using this technique it is not possible for the value of a remote sensor to be corrupted whilst being transmitted along a long fiber.

This approach can also be extended to mitigate errors in other intensity based fiber optic sensors also.

Chapter 7

Landslide Monitoring Using Fiber Optic Interrogator

In this chapter a system of monitoring landslide activity using an Fiber Optic Interrogator has been described. This system can prevent damage to life and property by issuing a warning if the landslide is impeding in an area. The unique feature of this system is that it is economical, easy to install and monitor. In this system a Fiber Optic Sensor Cable with anchors is lowered in a borehole where landslide activity has to be monitored. When there is relative slippage of soil due to landslide activity this sensor cable is perturbed. This perturbation causes modulation of light signal which can easily be detected by a Fiber Optic Interrogator installed at a remote site. This chapter presents the design details of this system along with the results of the field trials performed by installing this system in an active landslide test site.

7.1. Introduction

Landslide can paralyze the road communication network or cause damage to life and property. Lose sediments, rocks, weathered material etc remain stationary and stable on a slope. If due to natural reasons like an earthquake, excessive rainfall, toe erosion by the river, snow avalanche or anthropogenic reasons like road construction or any other such developmental work the material on the slopes is disturbed it moves. Gravity pulls it down and often water within acts as a lubricant and this causes landslide. Unlike other Geo Hazards Landslide can be predicted by employing technology.

7.2. Existing Technology for Monitoring Landslides

Many options are available for monitoring landslides. “In-place” inclinometers, entensometers and tiltmeters can detect new movement, an acceleration of movement, and the direction of movement. It is to be noted that Tiltmeters, Inclinometers are cumbersome to install, time consuming, have inadequate sensitivity and are susceptible to environmental hazards [171].

Another recent technique for landslide monitoring is based on Time Domain Reflectometry (TDR) [172]. This technology uses coaxial cable and a cable tester. This technique suffers from errors in readings caused by water seepage and electromagnetic interference.

Fiber Optic System based on optical time domain reflectometry tries to overcome these problems as optical fiber is inherently immune to electromagnetic interference and moisture ingress[173].

7.3. Design of Fiber Optic Interrogator

The Block Diagram of the Fiber Optic Interrogator is as shown below

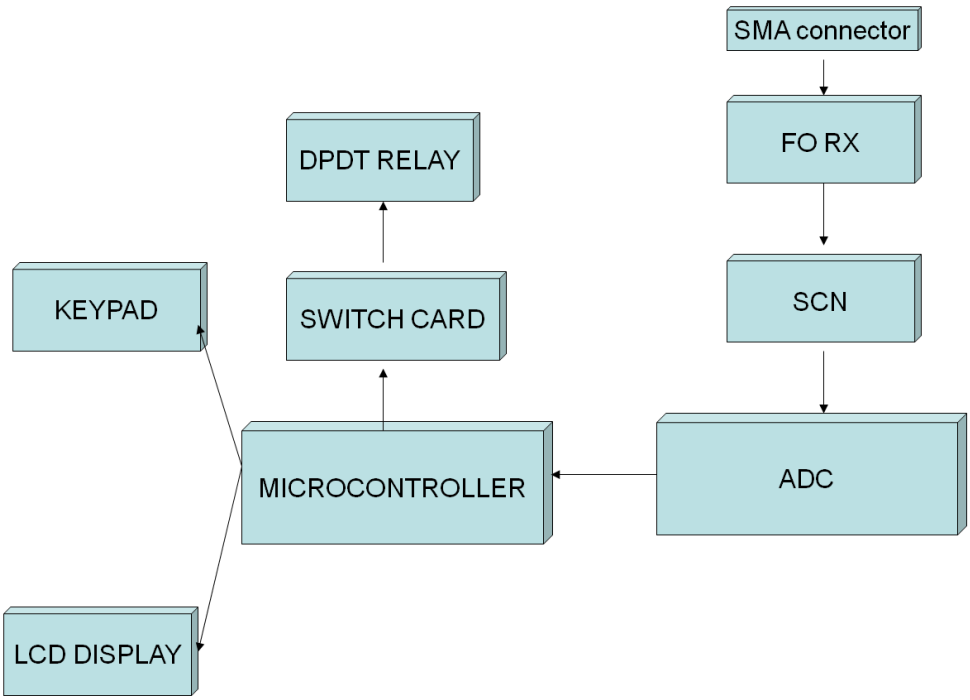

Figure 7.1 Block Diagram of Fiber Optic Interrogator

As shown in the Figure 7.1 the Fiber Optic Receiver converts the light intensity from the optical fiber fixed at the SMA connector into an electrical signal. This signal is then amplified and given to filter circuit which conditions the signal to be input to the ADC. The Analog to digital converter converts the analog signal into digital which is given to the microcontroller to be analyzed. The microcontroller then fixes the threshold dynamically and monitors the input signal. If the input falls below the threshold it issues a

warning through audio visual alarm enunciation by operating the relay. Software has been designed in assembly language. This has made possible to keep the code compact so that it can be flashed in the inbuilt memory of the 89c51 microcontroller.

7.4. Design of Fiber Optic Sensor Assembly

If a portion of fiber is deformed by movement of land mass, the fiber would exhibit excess light loss. Such perturbation of fiber axis results in redistribution of guided power between modes of the fiber and also coupling of the fiber from one mode/mode group to another. In ray description due to sharp bends in the fiber, there will be some light rays falling at the core cladding interface at an angle less than the critical angle, thus preventing their total internal reflection. These rays will thus be lost from the guiding structure. As the fiber is bent more and more sharply, so more and more number of rays will thus be lost and at a certain bend radius defined by the fiber geometrical characteristics, the bend loss becomes very steeply dependant on bend radius and the microbend sensor takes advantage of this very fact.

7.5. Field Experiments

The experiments were performed at an active landslide site on Haridwar byepass road near Mansa Devi Temple at Uttaranchal in India. Haridwar district, covering an area of about 2360 sq.km. is in the western part of Uttarakhand state of India. It's latitude and longitude are 29.58 degree north and 78.13 degree east respectively. The height from the sea level is 249.7 mts.

Fiber Optic Interrogation System was installed along with the conventional instrumentation at landslide prone locations. The idea is to fix the thresholds by comparing the data obtained from the Fiber Optic Interrogator with that obtained from conventional instrumentation like tiltmeter, inclinometer etc.

Figure 7.2 shows the close up view of the Fiber Optic Sensor installed along the hill slope. A microbender resolution enhancer comprising of a reel for holding about 10 m of fiber enclosed in a split hollow bi-conical casing was employed at the flagged points. Typically, a force of 5 kgf (where kgf is the unit of force i.e. kilogram-force) was applied

at the junction of the two microbend resolution enhancers to simulate effect of landslide. The sensor cable shown is 20 m in length so that it is sufficient to monitor the bulk movement of landslide. The cable length can be increased according to the area to be monitored.

]

Figure 7.2 Design of Fiber Optic Sensor

The Fiber Optic Interrogator was installed in the temporary shed equipped with solar panels for power source. The interrogator basically takes the digital input corresponding to the perturbation and sends it over serial port for logging. Figure 7.3 shows the Fiber Optic Interrogator installation.

Figure 7.3 Installation of FBG Interrogator

Testing of the system was carried out under stable conditions and by causing measured perturbation. The data logged was analyzed. As there were no short term variations in the slope, the data collected compares well with the conventional instrumentation. The graphs plotted have been shown in Figure 7.4

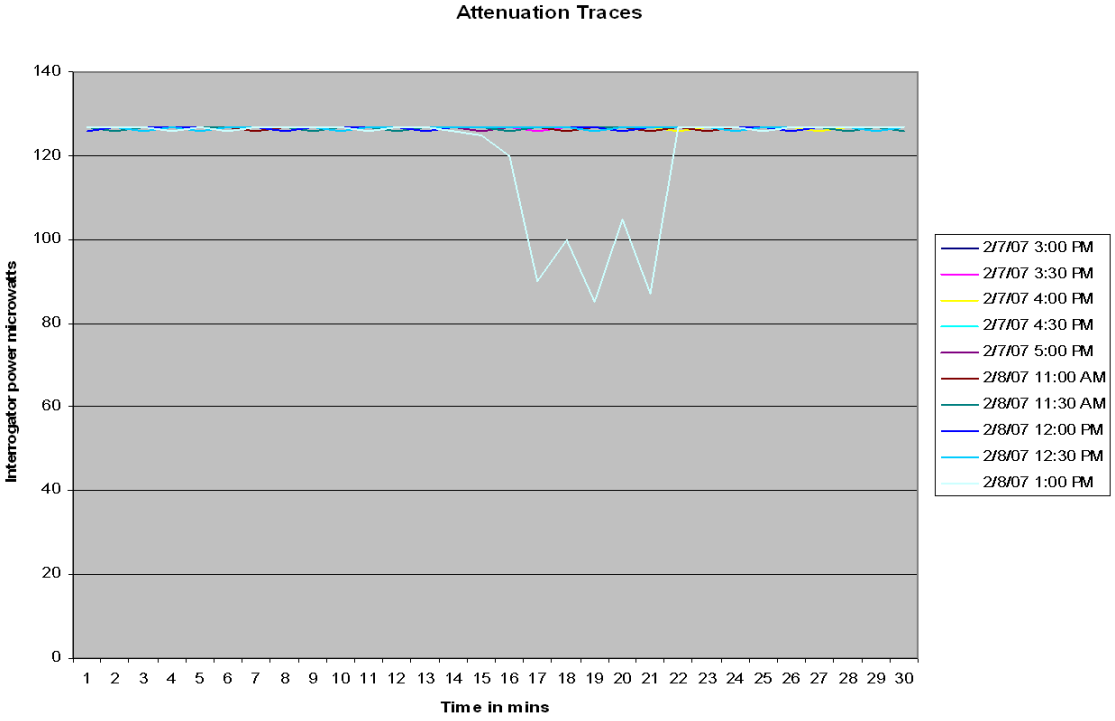

Figure 7.4 FBG Interrogator Traces

When the Fiber was subjected to perturbation the system enunciated an alarm and the data collected showed a corresponding change in the level of light intensity measured. The graph below shows how the attenuation trace showed a dip on perturbation.

7.6 Conclusion

Feasibility of a fiber optic system for monitoring landslides has been demonstrated and this promises to be an economical alternative to conventional instrumentation. The change in the rate of movement can be determined by plotting the fiber attenuation slope with time. Advantages of such a system over the traditional methods include: easy installation; less time consuming data collection; disposable cable; no need to clean debris from the inclinometer hole before taking measurements; EMI/EMC immunity and no effect of moisture ingress in cable and ability of remote monitoring at multiple locations using dataloggers and modern communication facilities.

Chapter 8

Fiber Optic Interrogator for In-Situ Nitrate Detection in Groundwater Based on Colorimetry Technique

Nitrate poisoning occurs when nitrite is absorbed into the blood where it changes the red-colored blood pigment, called hemoglobin, to methemoglobin. Hemoglobin carries oxygen from the lungs to the other tissues, but methemoglobin cannot carry oxygen. Poisoning occurs when the methemoglobin concentration in the blood stream is so high that the oxygen carrying capacity of the blood is reduced to a critical level.

Over the years nitrate contamination has acquired alarming proportions due to seepage of nitrates of fertilizers into the soil. Though several methods of monitoring nitrate concentration have been devised with some success, but there is a persistent need for devising easily deployable and in-situ techniques for monitoring nitrates in groundwater. Fiber optic techniques are capable of meeting these requirements, besides offering several other important advantages. Fiber optic nitrate detection sensors have thus become quite attractive and are currently being investigated to address the high costs associated with the existing nitrate concentration monitoring procedures.

Fiber optics based direct absorption spectroscopic techniques investigated by some groups have used single fiber elements for recording the signal reflected from specimen at different wavelengths. As the light coupling efficiency of the single fiber elements is relatively poor in comparison with that of fiber bundles and the signal available for processing is weak, this chapter presents a simple and alternate technique based on the color matching principle of fiber optic colorimetry to detect nitrate concentration. It employs a thin Y-shaped/ bifurcated fiber optic bundle which increases the quantity of light energy coupled from a whitelight source. The light reflected off the sample is made incident on a silicon positive-intrinsic-negative (PIN) photo-detector of the Fiber Optic Interrogator through a complementary filter. The output of the PIN photodetector is amplified and converted to digital using ADC and then a microcontroller displays it on the LCD panel. An RS232 interface has been implemented for PC connectivity. Series of such probes can be safely embedded in boreholes at pre-determined locations. The experimental set up for this technique was implemented and feasibility of in-situ nitrate

detection in groundwater was demonstrated. Measurement data was acquired for groundwater samples and results analysed.

8.1. Introduction

Nitrate concentration in excessive levels can have harmful biological consequences. The current drinking water standard and health advisory level is of 45 ppm nitrate based on the human health risks due to nitrate consumption [174]. Although there have been studies performed attempting to link nitrate consumption to various diseases, only methemoglobinemia, (also infant cyanosis or blue-baby syndrome) has been proven to result from ingestion of water containing high nitrate concentrations, above 10 ppm [174]. Cases of blue-baby syndrome usually occur in rural areas which rely on wells as their primary source of drinking water. Often these wells become contaminated when they are dug or bored and are located close to cultivated fields, feedlots, manure lagoons or septic tanks [175]. The most contaminated wells are usually those that were dug rather than drilled and have poor or damaged casings [176]. Until recent awareness of the dangers of nitrate contaminated groundwater prompted testing for nitrate concentrations, along with other contaminants, wells with dangerously high nitrate concentrations usually went unnoticed until health problems were brought to attention. A few isolated cases of methemoglobinemia, have served as the catalyst for what has grown into a broad awareness and concern for nitrate contamination.

Methemoglobinemia is the condition in the blood which causes infant cyanosis, or blue-baby syndrome. Methemoglobin is probably formed in the intestinal tract of an infant when bacteria converts the nitrate ion to nitrite ion [175]. One nitrite molecule then reacts with two molecules of hemoglobin to form methemoglobin. In acid mediums, such as the stomach, the reaction occurs quite rapidly [175]. This altered form of blood protein prevents the blood cells from absorbing oxygen which leads to slow suffocation of the infant which may lead to death [175]. Because of the oxygen deprivation, the infant will often take on a blue or purple tinge in the lips and extremities, hence the name, blue baby syndrome [176]. Other signs of infant methemoglobinemia are gastrointestinal disturbances, such as vomiting and diarrhea, when severely cyanotic and irritable when mildly cyanotic, and chocolate-brown colored blood [175].

Treatment of infant cyanosis is simple once the condition has been recognized.

If the patient is mildly affected, then he/she must simply refrain from drinking from the contaminated well for a few days and the body will replenish the hemoglobin by itself in

a few days [176]. However, if the patient is severely cyanotic, methylene blue must be administered intravenously in a dosage of 1-2 mg/kg of body weight for a ten-minute period and improvement should be prompt [176].

Methemoglobinemia most often affects infants of less than six months in age. Several factors make infants more susceptible to nitrate compounds than adults. The primary reason is that infants possess much less oxidizable hemoglobin than adults, so a greater percentage of their hemoglobin is converted to methemoglobin which greatly decreases the blood's ability to carry oxygen. Other possible reasons are that nitrite ions may be more strongly bound by infantile hemoglobin due to immaturity of certain enzymes, and that the kidneys of infants have inferior excretory power which may favor retention of nitrite for longer periods of time [175].

Steps can be taken to prevent the child from becoming a victim of methemoglobinemia. Residents of rural areas should have their wells tested, especially if pregnant women or infants are consumers of the well water. If the well is contaminated, other water source alternatives like safe wells, bottled water, a new, deeper well, or a water purification system which is capable of removing the nitrates [176] should be used. Cyanotic babies usually contract methemoglobinemia from the water used to prepare their formulas, formulas which use diluted whole milk are less risky than those prepared from powdered or evaporated milk which require large amounts of water in preparation [177]. Breast feeding or the use of bottled water in formula preparation offer the safest solution especially if the groundwater quality is not known [176].

Since 1945, there have been over 2000 cases of infant methemoglobinemia reported in Europe and North America with 7 to 8 percent of the afflicted infants dying. However, problems can be severe as shown in a specific 1950 report, there were 144 cases of infant methemoglobinemia with 14 deaths in a 30 day period in Minnesota [176]. This of course was an isolated case. However, it shows that nitrate concentrations in well water can increase to deadly levels rapidly and the issue of nitrate contamination should not be ignored.

Nitrate represents a potential risk because of nitrosation reactions which, with appropriate substrates present, form N-nitroso compounds which are strongly carcinogenic in animals [177]. In other areas of the world such as Columbia, Chile, Japan, Denmark, Hungary, and Italy, similar studies have suggested a correlation, although there still exists no concrete evidence to support this theory [177].

Over the years, several methods of monitoring nitrates have been devised with some success. At present, there are only a few methods of determining in-situ nitrate concentration using optical fibers. Therefore, a persistent need exists for developing in-situ and cost-effective techniques for this purpose. Optical fiber based techniques are capable of in-situ measurements besides offering several other attractive features such as small size, flexibility & geometric versatility, light weight, inherent immunity to EMI/ RFI, low-loss, large bandwidth, increased sensitivity, resistance to corrosive and hazardous environments, non-intrusive, distributed sensing and compatibility to optical fiber data telemetry systems. A distributed and on-line optical fiber sensing system for nitrate detection will help reduce the costs associated with conventional systems.

Fiber optics systems based on direct absorption spectroscopic techniques investigated by some research groups have relied on using single fiber elements for recording the light signal reflected off from the specimen at different wavelengths [178]. This chapter reports a simple and alternate technique based on wavelength matching principle of colorimetry for detection of nitrates induced color changes in reagent. In contrast to single fiber elements, the present technique employs a thin Y-shaped optical fiber lightguide/ bundle which increases the quantity of light energy coupled from a white light source resulting in ease of optical signal processing. The technique actually involves detection of the blue color formed when reagent comes in contact with nitrates. For applications where accuracy requirement is not very critical, fiber optic sensing techniques based on multimode optical fibers/ bundles and components offer the advantages of simple construction, enhanced coupled optical power, ease of alignment & implementation and cost-effectiveness.

8.2. Principle

The principle of colorimetry is well-established but owing to the use of fiber optics, this technique has now become quite versatile and useful. In fact, the utilization of optical fiber technology for wavelength sensing represents a major advance in visible/ near IR photometry. It is now possible to perform in-situ/ on-line non-contact wavelength measurements of samples [179].

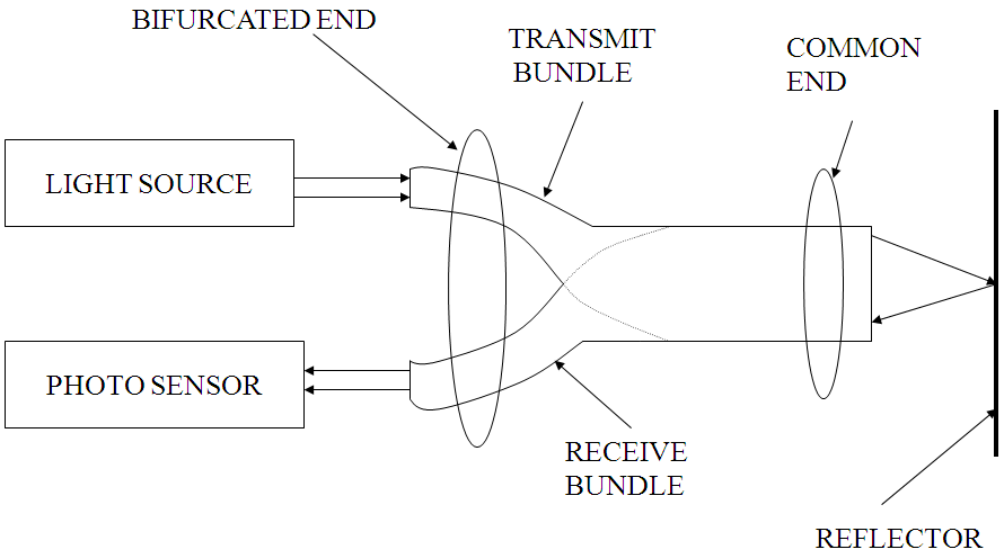

Figure 8.1a Block Diagram of Setup

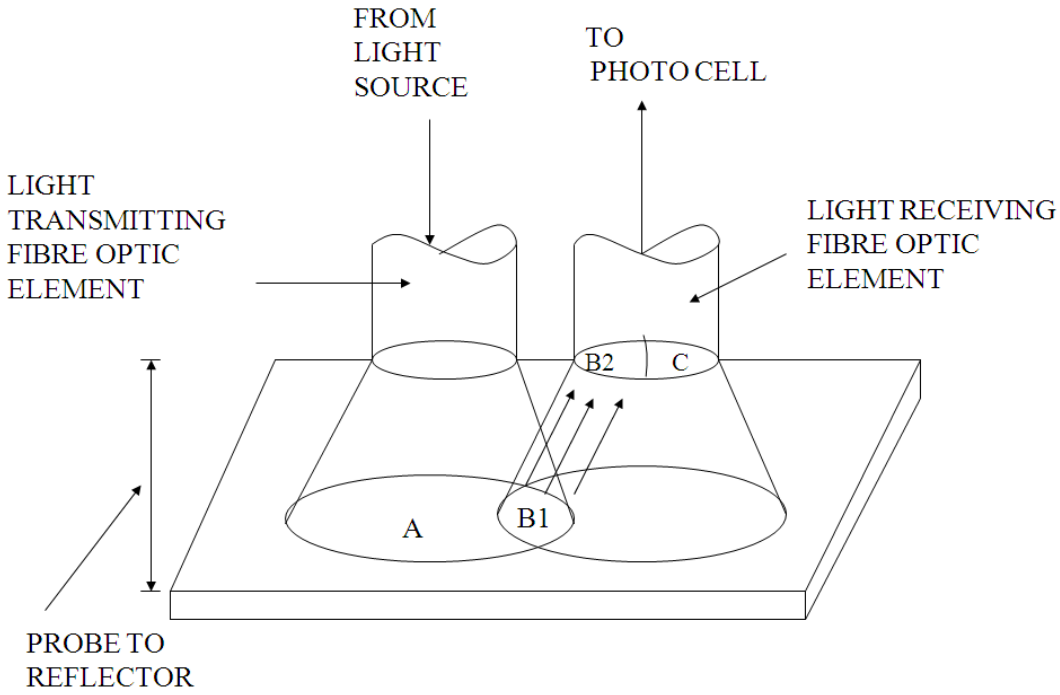

Figure 8.1b: Geometry of light source and pickup

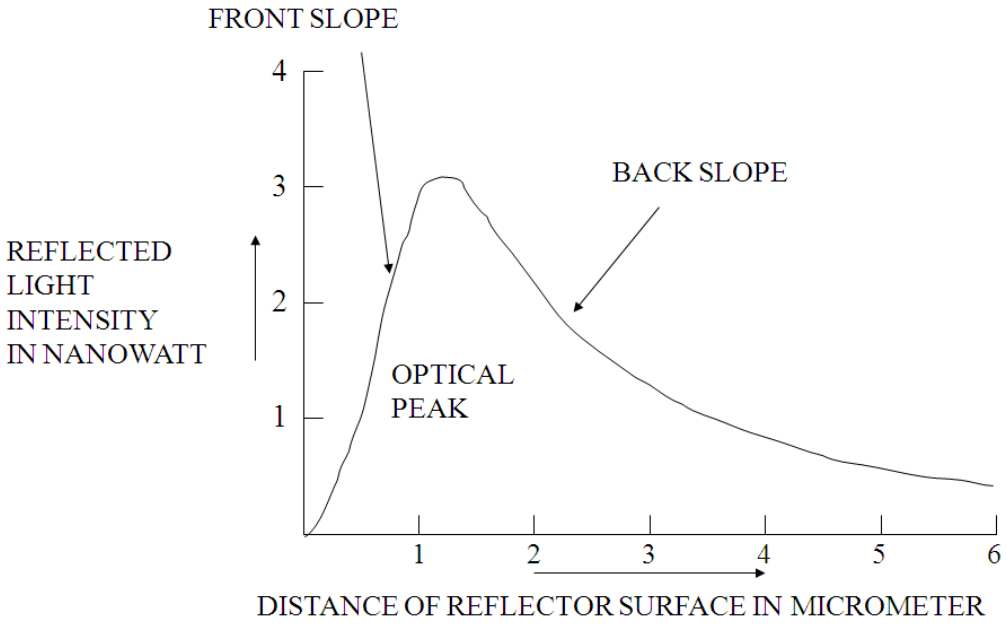

Figure 8.1c: Variation of reflected intensity with distance from sample

Through one arm of the optical fiber Y-guide, white light coupled from the source is made incident on the sample to be monitored for color changes and the reflected signal is carried by another arm of the Y-guide to a photo-detector. A complementary color filter is used before the photo-detector because color of the light absorbed is complimentary to the color of the corroded specimen and it is the intensity of the complimentary color that varies with color concentration of the sample. The accuracy of color measurement using this technique depends on the proper selection of the complimentary filter. The reflected light signal consequently varies in proportion to the color of the sample and, thus it is possible to assess the nitrate contamination.

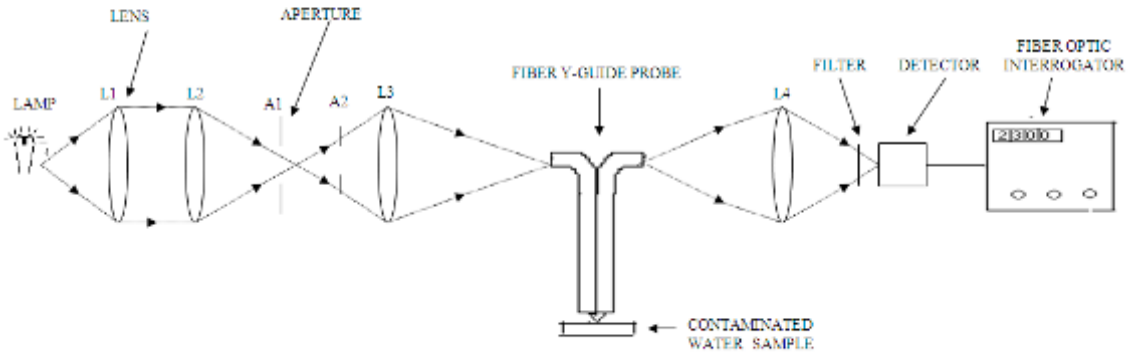

Figure 8.2: Experimental arrangement for fiber optic colorimetry

The technique is based on the principle of light being reflected off the specimen and then received back through a receive branch of a bifurcated fiber optic bundle (Y-guide) on to a photodiode. Keeping the displacement between the common end of the bundle and the target specimen as fixed and equal to that for the peak sensitivity value, the quantity of light reflected by the specimen gives a direct measure of nitrate contamination and it is displayed in the form of an electrical signal.

In the bifurcated fiber bundle developed and employed, one group of fibers transmits light from a stable source to a target reflector surface. The other group receives the light reflected from the target and transports it back to a photo-detector which converts it to an electrical signal proportional to the intensity of the reflected light as depicted in Figure 8.1, while Figure 8.2 depicts the action of an adjacent pair of fiber optic light transmitters and receivers as used to detect the position and or quality/condition of a reflective surface relative to the ends of the optical fibers.

Evidently, as the reflecting surface moves away from the set of optical fibers, the area A illuminated by the transmitting fiber optic element becomes larger and larger. The illuminated area of interface, B1, which is providing light to the surface of the receiving element as B2 also grows increasingly larger. There is a rapid and linear growth in the signal output as more of surface, C, is illuminated e.g. as the probe to target displacement

increases, increasing amounts of light are captured by the receiving fibers. This portion of the response curve is referred to as the `front slope' region. The point at which the entire surface, C, becomes covered with light is referred to as the "optical peak" point of the response curve as shown in Figure 8.1c.

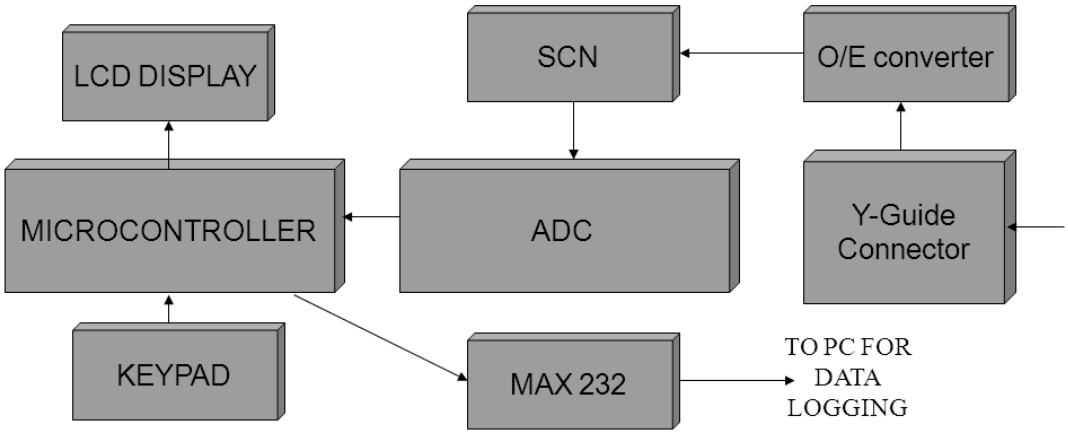

Figure 8.3: Block Diagram fo FBG Interrogator

This is a well-known experimental response curve of Y-guide type of reflective sensors which are quite popular amongst the intensity modulated fiber optic sensors. As the surface moves further away, the size of area B2 becomes larger than area C, reducing the detected light intensity. The light intensity-monitoring photosensitive detector output then begins to decrease, resulting in the back slope characteristic where the signal decreases proportional to the square of the displacement between the probe and the target surface because a continued increase in displacement will cause the diverging field of reflected light to exceed the field of view of the receiving /detector fibers producing a reversal in the output vs displacement signal relationship. This also becomes clear from the geometry of the arrangement used that as the target is moved away from the probe, area of the illuminated spot on the target increases in direct proportion to square of displacement while interception of the reflected light by the fiber probe will correspondingly decrease in proportion to square of displacement. Actually, these displacement dependent measurements of light coupling are based on the interaction between the field of

illumination of the transmitting /source fibers and the field of view of the receiving fibers [181-184].

The extremely rapid signal rise in the front slope region of the response curve permits high sensitivity measurements while the back slope region is used for measurements at greater displacements, where sensitivity, linearity, and accuracy requirements are less demanding. The "optical peak" region is used for optical inspection and comparison of surface conditions since at this position the output signal is more sensitive to light intensity variations than changes in displacement. The distribution of fibers at the common (distal) end of the bundle is a major factor determining displacement range and slope sensitivity of the probe. For example, the greater displacement sensitivity is obtained with a staggered/random fiber array [82-84]. Fiber Optic Colorimetry technique has been earlier also used for various applications like detection of corrosion of civil structures, etc. [185-186].

8.3. Experimental Details

The experimental arrangement realized in the laboratory for detection of nitrates in water is schematically depicted in Figure 8.2.

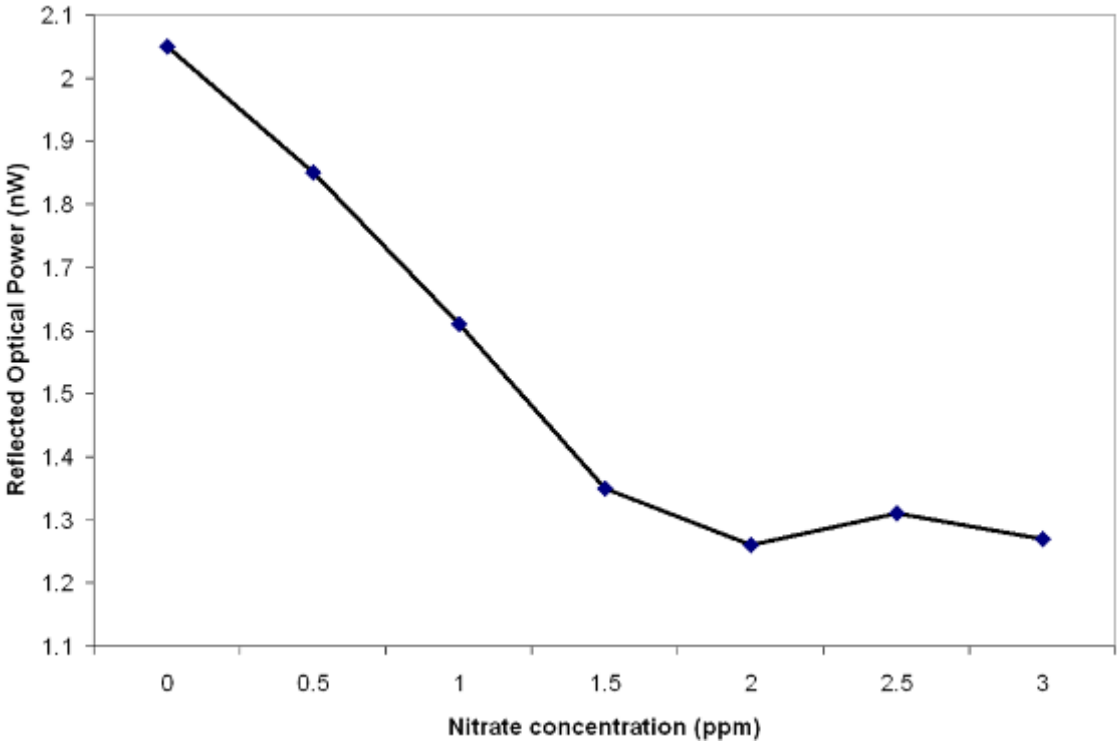

Figure 8.4: Trace of FBG Interrogator for different nitrate concentrations

The set up employs an indigenously built thin Y-shaped fiber optic bundle with half portion (a semi-circle) of its common end made from the source fibers and the other half from the detector fibers. The length of the fiber lightguide used is about 0.5 meter with both the source and detector arms being 15cm long. The diameter of the common end of the lightguide is 5mm while the source arm and detector arm end faces have a diameter of about 1.8 mm. This lightguide was developed indigenously using optical glass fibers of 60/120 microns size. Light from a 50 Watt quartz halogen lamp driven by a 12V (DC) stabilized power supply, was coupled to the source arm of the bundle using suitable optics. The water specimens were prepared in the laboratory by adding varying concentration of nitrate salts in water. The specimen is located very close to the common end of the Y-guide at a displacement of 5mm which corresponds to the peak sensitivity of the response of the lightguide and the reflected light picked up by the other arm of the bundle is made to pass through a complementary filter (Yellow) before it is incident on a photo-detector. The complimentary filter used in the present investigations is a commercially available interference filter with a typical bandwidth of 15nm. The light reflected off the sample is made incident on a silicon positive-intrinsic-negative (PIN) photo-detector of the Fiber Optic Interrogator through a complementary filter. The block diagram of Fiber Optic Interrogator is shown in Figure 8.5.

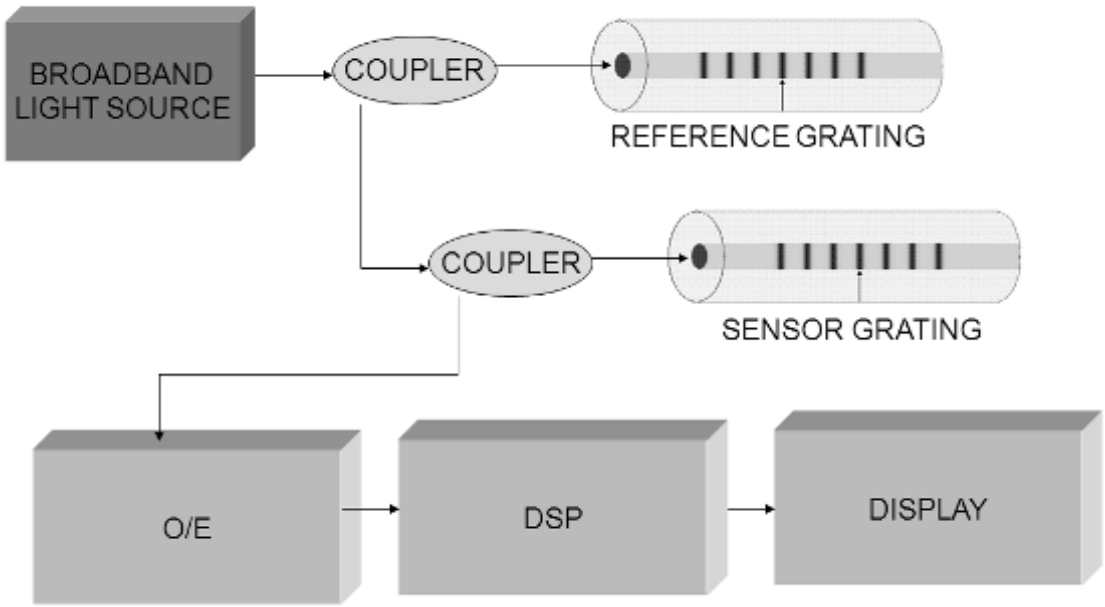

Figure 8.5: Block Diagram of FBG Interrogator

The output of the PIN photodetector is amplified and converted to digital using ADC and then a microcontroller displays it on the LCD panel. An RS232 interface has been implemented for PC connectivity. The programming of the microcontroller has been implemented in native MCS51 keeping the code compact and modular. Nitrate concentration measurement of water samples was thus carried out by adding the reagent in different samples and taking the readings.

8.4. Results

Data was recorded for a fixed displacement between the fiber end and water sample mixed with nitrate detection reagent both for pure water and contaminated water and the results have been found to be reproducible. A typical variation between concentration of nitrates in water solution and the reflected optical power is shown in Figure 8.4
It clearly indicates that at low concentrations, there is a linear increase in absorption (e.g. a decrease in reflected optical power) of the complementary color with the increase of concentration of nitrates which, however, tries to saturate at relatively higher concentration.
Different concentrations of nitrate ions in water samples were realized using titrations and then by mixing same quantity of reagent and concentrated sulphuric acid different reading were taken keeping the distance of the fiber end from the water sample constant.

8.5. Conclusion

This simple technique based on the principle of the colorimetry employing fiber optic bundle enables in-situ monitoring of the nitrate contamination in water. Such colorimetric fiber optic probes can be embedded into the boreholes dug in the ground at pre-determined sites for conveniently monitoring the contamination level. The technique can be easily calibrated using standard nitrate concentration water specimens. However, due to non-availability of standard specimens, such a calibration could not be undertaken. This technique is very useful to study the underground nitrate water contamination and further investigations are planned to be pursued in this direction in future. The technique can also be used for remote/ in-situ monitoring of boilers and other critical structures located in harsh environments such as in chemical industry, nuclear reactor buildings, mines etc.

Chapter 9

Conclusion Recommendation and Future Scope

9.1 Conclusion

Thus this thesis presents the Investigations on Fiber Bragg Gratings for Fiber Optic Communication Systems. The simulation of Fiber Bragg Gratings has been carried out and the results presented have been validated using theoretical and experimental work. The complex grating has been analysed using coupled mode theory applied to periodic structures. With this approach the deeper physical insight has been explored into the characteristics of gratings. To analyze the wave propagation in FBG, the Maxwell equations have been solved with appropriate boundary conditions. To solve them the weak guidance which allows the decomposition of modes into orthogonal set of transversely polarized modes has been considered. The solutions provide the basic field distributions of the bound and radiation modes of the waveguide. These modes propagate without coupling in the absence of any perturbation. If the waveguide has a phase and/or amplitude perturbation that is periodic with a perturbation phase/amplitude-constant close to the sum or difference then only that propagating modes will couple. The technique applied for solving this problem is coupled-mode theory. This method assumes that the mode fields of the unperturbed waveguide remain unchanged in the presence of weak perturbation. This approach provides a set of first-order differential equations for the change in the amplitude of the fields along the fiber, which have analytical solutions for uniform sinusoidal periodic perturbations. The generalized matrix approach has been used for nonlinear gratings. The matrix method has been modified to avoid the problem of varying refractive index modulation for Fiber Bragg Gratings. The transfer matrix method provides high accuracy for modeling in frequency domain and to analyze the practically realizable gratings. A marginal change in the model of FBG has been proposed to account for the loss in accuracy due to non-uniform refractive index modulation in the FBG.

The wavelength shift in Fiber Bragg Gratings on simulated external perturbation using a wideband source has also been observed. Three FBGs with different resonance wavelengths of 1549.576, 1548.426 and 1545.826 nm respectively were spliced together and connected to the interrogator in this order to demonstrate three different sensing elements. The three Bragg wavelengths were observed on the monitor under conditions of

zero loading. The first grating FBG1 was bonded to a metallic cantilever (39.5cm x 4.2cm) at a location of 12cm from the fixed end using araldite epoxy. It acted as a pressure sensor with different weights applied on the cantilever tip and the results obtained for different loading were quite linear. The second grating FBG2 was used as a strain sensor and it was held tight between two fiber holders and stretched longitudinally using a motorized linear precision stage with a pitch of 0.5 mm i.e. one complete rotation of the motor screw resulted in 0.5 mm movement of the linear stage which was the change in length of the fiber. A 30 cm length of the fiber with a grating element located in the middle position was stretched by the movement of the stage. Thus, for each rotation value of the screw the change in length is known and resulting strain was calculated. A maximum strain of ~2333 με was produced using this technique. The effect of the pulling strain on the Bragg wavelength was quite linear. The third grating FBG3, which demonstrated the effect of temperature on Bragg wavelength, was immersed in a glycerol bath kept in a second bigger bath containing water. The grating was heated indirectly to avoid rapid temperature rise. The temperature of the glycerol bath varied from 15^{o}C to 70^{o}C and was measured using thermometer immersed in the glycerol bath and the corresponding Bragg wavelength shift was recorded which showed a good linearity. The wavelength shift in FBGs on application of external perturbation, realized by splicing three Fiber Bragg Grating elements, was demonstrated for simultaneous measurement of strain and temperature. The three sensors exhibited a good linear performance as expected. The experiment has been performed in a controlled temperature laboratory environment but in actual applications, suitable compensation technique will have to be employed for variation in environmental temperature to obtain the realistic mechanical strain data. One approach is to use athermal coating on the FBG that can be embedded as strain sensor, or alternatively, two FBGs can be used; one bonded with the structure while the other is unbonded so that there is no strain effect. Thus the first grating senses both strain and temperature and the second one is just a temperature sensor. For the second FBG sensor, strain results from the direct pull, and its sensitivity has been estimated to be approximately 0.39 pm/με. The third grating which is used as temperature sensor has exhibited a sensitivity of 11.1 pm / ^{0}C. The first grating bonded to a cantilever has exhibited a response of 4.8 pm/gm. In this case bending the cantilever with pressure applied at its free end produces strain in the grating. Apart from being lightweight, low cost, immune to EMI/RFI, chemically inert; this device offers other advantages as well. For example, a good linear response is obtained in all the three cases and the sensed

parameter namely strain and temperature are wavelength encoded, and hence they are independent of fluctuations in the light source, connector or fiber losses etc. Another point that is crucial for structural health monitoring and sensing in hazardous environment is the feasibility of remote sensing. It is because the commercial fibers have very low loss in the operating wavelength range used in the present investigations and they are able to transmit sensed information to distant monitoring locations. Besides, the narrow bandwidth of FBG allows multiplexing of many sensing elements, which work independently without interfering each other. Thus, this study offers an efficient and inexpensive technique for structural health monitoring such as civil and aerospace structures and other applications involving hazardous environmental conditions such as oil and gas exploration wells and monitoring of load of power transmission lines in snow covered areas and hot zones.

Since the coefficient of thermal expansion of FBG made of silica is quite small, investigations were made to enhance temperature sensitivity of FBG sensors. For this purpose, a suitable metallic encapsulating fixture was designed and fabricated & its performance investigated. The fixture has a central hole of appropriate diameter along its length and an FBG was kept inside the hole with its ends bonded to the metal cap. The transducer was dipped in a hot water bath and the effect of heating on the Bragg wavelength was monitored and an improvement of sensitivity from 11 pm/ ^{o}C to 20pm/ ^{o}C was realized in the temperature range of 25 to 65 ^{o}C used. Further, the design of the fixture is being modified to realize a still higher multiplier effect of longitudinal expansion of the FBG. This study is important for realizing fire safety sensors for aircrafts, railways, industrial and building complexes and also as tunable components for sensors and communication applications.

A Fiber Bragg Grating Interrogator for Sensor/Communication systems has been designed. The challenge in this design is that since the wavelength shift to be measured is in picometers the electronics required to process it should be obviously very high speed by virtue of sampling theorem. Although many techniques have been reported to provide fast and reliably interconnecting MIN architectures but still it is yet not possible to take processing in the domain of THz. When developing fiber grating sensor heads, optical spectrum analyzers are indispensable in monitoring grating reflection or transmission spectra. However, optical spectrum analyzers are not appropriate for real sensor systems, not only because of their high prices but also because their slow scanning speed limits dynamic sensing. Precise wavelength measurement using FBG sensors has been a

challenging problem since the early stage of FBG sensing work. A Fabry Perot based Fiber Bragg Grating Interrogator has been designed. The Fabry–Perot filter (FPF) consists of two partially reflecting surfaces with a spatial separation. When a light is incident on this cavity, due to multiple reflections inside the cavity and interference of the multiply reflected lights, the transmittance of light through this cavity has a periodic characteristic with the variation of optical frequency or the spacing between the two reflecting surfaces. One of the most successful techniques for wavelength-change interrogators of FBG sensors is based on the use of the tunable bandpass filter. The most commonly used technique employs a fiber-pigtailed Fabry–Perot tunable filter as a narrow bandpass filter. The filter is sometimes referred to as a fiber Fabry–Perot interferometer. If the phase difference is a multiple of 2π radians, then the transmittance becomes maximum due to the constructive interference. The phase difference is inversely proportional to the wavelength, the small change in the phase difference is proportional to the small wavelength change shows that the phase difference is proportional to the cavity length. In this chapter the Fabry-Perot Tunable Filter has been designed for FBG Interrogator. The peak detection system for the same has also been developed.

A new technique for mitigating the errors due to effect of microbending in the fiber lead from Fiber Bragg Grating Sensor to the interrogator has also been incorporated in the design of FBG interrogator. The use of an edge filter is an inexpensive way of measuring Bragg wavelength shift but the accuracy is impaired by microbend losses that occur in the fiber connecting the Fiber Bragg Grating Interrogator to the Fiber Bragg Grating. If a portion of fiber is deformed, the fiber would exhibit excess light loss. Such perturbation of fiber axis results in redistribution of guided power between modes of the fiber and also coupling of the fiber from one mode/mode group to another. In ray description due to sharp bends in the fiber, there will be some light rays falling at the core cladding interface at an angle less than the critical angle, thus preventing their total internal reflection. These rays will thus be lost from the guiding structure. As the fiber is bent more and more sharply, so more and more number of rays will thus be lost and at a certain bend radius defined by the fiber geometrical characteristics, the bend loss becomes very steeply dependant on bend. The errors induced due to intensity fluctuations because of microbending are reduced by employing corrections based on the intensity modulation in the reference fiber. The Fiber Optic Receiver converts the light intensity from the optical fiber coming from the Fiber Bragg Grating Sensor fixed at the SMA connector into an

electrical signal. The broadband light from the source is initially filtered in the FBG sensor, which reflects a narrowband light to the second FBG filter. The portion now reflected by this filter corresponds to the convolution between both FBG reflectivity, and it is directed to the photodetector. So, the variation of the sensor Bragg wavelength is measured through the intensity of the light that reaches the photodetector. This signal is then amplified and given to filter circuit which conditions the signal to be input to the Analog to digital converter (ADC). The ADC converts the analog signal into digital which is given to the microcontroller to be analyzed. The microcontroller then uses a look up table or extended finite state machine to introduce corrections in the readings induced due to microbending losses. The embedded system can be further enhanced by Monotonic Partial Order Reduction as a Symbolic Partial Order Reduction Technique to enhance speed. The microbend loss magnitude is determined using the reference fiber input. The multiplexer in the ADC has eight input lines, so four such sensors can be interrogated with the same circuit.

The software has been implemented in native MCS51 assembly language keeping it compact and modular. Separate routines have implemented to initialize the system, handshake with the ADC for multiplexing and acquire and display the results after suitable correction due to microbend compensation from a lookup table. The experimental results demonstrate increased precision in the strain measurements using this technique.

The importance of this work cannot be overemphasized since Fiber Bragg Gratings have emerged as important components in a variety of applications. Their unique filtering properties and versatility as in-fiber devices is illustrated by their use in wavelength-stabilized lasers, fiber lasers, remotely pump amplifiers, Raman amplifiers, phase conjugators, wavelength converters, passive optical networks, wavelength division multiplexers (WDM's) demultiplexers, add/drop multiplexers, dispersion compensators, and gain equalizers. They are also stimulating growth in fiber optic applications outside of telecommunications, such as nonlinear frequency conversion, spectroscopy, and remote sensing.

Two new sensors based on FBGs have been developed and characterized in this work. One application is in the field of landslide monitoring and the other is for ground water nitrate detection.

A system of monitoring landslide activity using an indigenously developed Fiber Optic Interrogator has been presented. This system can prevent damage to life and property by

issuing a warning if the landslide is impeding in an area. The unique feature of this system is that it is economical, easy to install and monitor. In this system a Fiber Optic Sensor Cable with anchors is lowered in a borehole where landslide activity has to be monitored. When there is relative slippage of soil due to landslide activity this sensor cable is perturbed. This perturbation causes modulation of light signal which can easily be detected by a Fiber Optic Interrogator installed at a remote site. The design details of this system along with the results of the field trials performed by installing this system in an active landslide test site have been presented.

The experiments were performed at an active landslide site. Fiber Optic Interrogation System was installed along with the conventional instrumentation at landslide prone locations. The idea was to fix the thresholds by comparing the data obtained from the Fiber Optic Interrogator with that obtained from conventional instrumentation like tiltmeter, inclinometer etc. When the Fiber was subjected to perturbation the system enunciated an alarm and the data collected showed a corresponding change in the level of light intensity measured. Advantages of such a system over the traditional methods include: easy installation; less time consuming data collection; disposable cable; no need to clean debris from the inclinometer hole before taking measurements; EMI/EMC immunity and no effect of moisture ingress in cable and ability of remote monitoring at multiple locations using dataloggers and modern communication facilities.

Thus with the investigations carried out in the field of FBGs for communication and sensor networks in this thesis work the model of FBG has been improved by incorporating changes due to non-unifrom refractive index modulation in FBG. Moreover with the study of wavelength change on external perturbation of FBG an interrogation system has also been developed which not only is compact, rugged and low cost since one FBG interrogates the other, but the errors due to microbending in the fiber from FBG to the interrogation unit have been mitigated. This will help the growth in the field of Fiber Optic communications and Fiber Optic Sensor Systems

9.2 Recommendation

From the work carried out in the thesis work a marginal change in the model for FBG has been recommended. By incorporating this change the traces of output spectrum of FBG can be estimated more accurately as compared to the response of the actual experimental data of fabricated FBG.

It is also recommended to employ the microbend loss error mitigating system to Fiber Bragg Grating Interrogator to improve its accuracy. Generally all the other interrogator schemes use either wavelength sweeping to identify the wavelength reflected from FBG or Filter sweeping to select the reflected wavelength from the FBG, but the technique presented here uses one FBG to interrogate the other FBG. The only problem with this arrangement is that the losses induced in the connecting fiber can induce errors in the reading. This problem has been circumvented in the technique presented in the present work and can be successfully utilized to make low cost Fiber Bragg Grating Interrogation Systems.

Interrogators can be designed using this technique. FBG sensors are passive and require no electrical power. Because of this, they are totally immune to interference from electrostatic or radio frequency sources. Furthermore, they are intrinsically safe and can be used to instrument the most hazardous explosive environments. Optical fiber is a very efficient signal carrier. Because of this, the electrical interrogation unit can be sited many tens on Kms away from the sensing location, whereas conventional electrical strain gauge systems require regular amplification to avoid signal to noise degradation. For monitoring large, remote structures such as sea-bed pipelines or a long rail tunnels, this is a unique and invaluable benefit. Since the microbend compensation can be implemented using this technique it is not possible for the value of a remote sensor to be corrupted while being transmitted along a long fiber.

The two Fiber Bragg Grating Sensing Systems presented in this thesis work i.e. the Landslide monitoring System and Underground Nitrate detection System both require typically that the monitoring site and sensor location are quite far away, making the system more prone to errors due to signal degradation in the connecting fibers. The microbending compensation technique presented in this thesis work to mitigate the signal degradation can be used to such other applications also.

9.3 Future Scope

In this work investigations have been carried out in the field of Fiber Bragg Gratings as Sensor and Communication elements. Further work can be carried out in other components such as Long Period Gratings and Fabry Perot Devices.

Even in the field of Fiber Bragg Gratings more sensor applications can be investigated and theoretical/experimental work can be carried out to further improve the Fiber Bragg Grating Interrogator.

The Fiber Bragg Grating Interrogator has been developed in a modular design and it can be easily extended with suitable modifications to interrogate other devices such as Long Period Gratings and Fabry Perot Devices

The technique that has been used to circumvent the errors due to microbending losses can also be extended to nullify the effects of temperature in strain sensing applications. For this another grating can be used in the FBG interrogator which is not perturbed by the strain measurement and then from the wavelength shift in this grating the effect of temperature change can be compensated.

Optical fibers have revolutionized telecommunication. The market for optical fiber continues to grow. Major trunk routes and metropolitan areas have already seen a large deployment of fiber. The next stage in the field of communication is the mass delivery of integrated services, such as home banking, shopping, Internet services, and entertainment using video-on-demand. Although the bandwidth available on single mode fiber should meet the ever-increasing demand for information capacity, architectures for future networks need to exploit technologies which have the potential of driving down cost to make services economically viable. Fiber Bragg Grating Technology enables the avoidance of costly signal conversions from optical domain to electrical and back. So further research in perfecting the model of Fiber Bragg Grating by taking into account other manufacturing process factors such as backlash errors in Fiber Pulling Devices in Fiber Bragg Grating Inscribing Equipment can improve the simulation results of Fiber Bragg Grating further to closely match with the experimental data in characterizing the Fiber Bragg Grating Elements

References:

1. Chien-Hung Yeh and Sien Chi, “Utilizations of Fiber Bragg Gratings and Fabry–Perot lasers for fast wavelength switching technique”, Optics Communications, vol. 256, Issues 1-3, pp.73-77, 1 December 2005.

2. Charlotte Marra, Ampalavanapillai (Thas) Nirmalathas, Dalma Novak, Christina Lim, Laurence Reekie, James A. Besley, Conan Weeks, and Neil Baker, "Wavelength-Interleaved OADMs Incorporating Optimized Multiple Phase-Shifted FBGs for Fiber-Radio Systems," J. Lightwave Technol. 21, 32- (2003)

3. Harpreet Singh, "Implementation of Optical and Optoelectronics Circuits", Applied Optics, vol. 8, no. 1, pp. 178-181, January 1989.

4. Xiufeng Yang, Chunliu Zhao, Jun Hong Ng, Jing Zhang, Xinyong Dong, Kok Hian Ng, Xin Guo, Xiaoqun Zhou and Chao Lu, “Simultaneous dispersion slope compensation for WDM channels using a Fabry–Perot Etalon formed by double FBGs”, Optics Communications, vol. 231, Issues 1-6, pp.227-231, 15 Feb. 2004.

5. B. Dabarsyah, S. Y. Set, C. S. Goh, S. K. Khijwania, and K. Kikuchi, “An Adjustable Dispersion Compensator with Wavelength Tunability Using Thermally Chirped Fiber Bragg Grating”, IEEE Photon. Technol. Lett., vol. 15, pp. 416-418, March 2003.

6. C. Caucheteur, F. Lhommé, K. Chah, M. Blondel and P. Mégret, “Simultaneous strain and temperature sensor based on the numerical reconstruction of polarization maintaining Fiber Bragg Gratings”, Optics and Lasers in Engineering, vol. 44, Issue 5, pp. 411-422, May 2006.

7. C. Caucheteur, F. Lhommé, K. Chah, M. Blondel and P. Mégret, “Simultaneous strain and temperature sensor based on the numerical reconstruction of polarization maintaining Fiber Bragg Gratings”, Optics and Lasers in Engineering, vol. 44, Issue 5, pp. 411-422, May 2006.

8. Hang-yin Ling, Kin-tak Lau, Li Cheng and Wei Jin, “Viability of using an embedded FBG sensor in a composite structure for dynamic strain measurement”, Measurement, vol. 39, Issue 4, pp. 328-334, May 2006.

9. Hiroshi Tsuda, “Ultrasound and damage detection in CFRP using Fiber Bragg Grating sensors”, Composites Science and Technology, vol.66, Issue 5, pp. 676-683, May 2006.

10. S. Baskar, P.N. Suganthan, N.Q. Ngo, A. Alphones and R.T. Zheng, “Design of triangular FBG filter for sensor applications using covariance matrix adapted evolution algorithm”, Optics Communications, vol. 260, Issue 2, pp. 716-722, 15 April 2006.

11. T.H.T. Chan, L. Yu, H.Y. Tam, Y.Q. Ni, S.Y. Liu, W.H. Chung and L.K. Cheng, “Fiber Bragg Grating sensors for structural health monitoring of Tsing Ma bridge: Background and experimental observation”, Engineering Structures, vol. 28, Issue 5, pp. 648-659, April 2006.

12. Fang Xie, Xianfeng Chen, Lin Zhang and Ming Song, “Realisation of an effective dual-parameter sensor employing a single Fiber Bragg Grating structure”, Optics and Lasers in Engineering, vol. 44, Issue 10, pp. 1088-1095, October 2006.

13. M. Ussorio, H. Wang, S.L. Ogin, A.M. Thorne, G.T. Reed, S.C. Tjin and R. Suresh, “Modifications to FBG sensor spectra due to matrix cracking in a GFRP composite, Construction and Building Materials”, vol. 20, Issues 1-2, pp.111-118, February-March 2006.

14. Koulaxouzidis, A.V.; Holmes, M.J.; Roberts, C.V.; Handerek, V.A., "A shear and vertical stress sensor for physiological measurements using Fiber Bragg Gratings," Engineering in Medicine and Biology Society, 2000. Proceedings of the 22nd Annual International Conference of the IEEE , vol.1, no., pp.55-58 vol.1, 2000

15. Andre, P.S.; Pinto, A.N.; Pinto, J.L.; Almeida, T.; Pousa, M., "Tunable transparent and cost effective optical add-drop multiplexer based on Fiber Bragg Grating for DWDM networks," Advanced Semiconductor Lasers and Applications/Ultraviolet and Blue Lasers and Their Applications/Ultralong Haul DWDM Transmission and Networking/WDM Components, 2001 Digest of the LEOS Summer Topical Meetings , vol., no., pp.2 pp.-, 2001

16. Andre, P.S.; Pinto, A.N.; Pinto, J.L.; Almeida, T.; Pousa, M., "Selective wavelength transparent optical add-drop multiplexer based on Fiber Bragg Gratings," Transparent Optical Networks, 2000 2nd International Conference on , vol., no., pp.15-18, 2000

17. Stoll, D.; Leisching, P.; Bock, H.; Richter, A., "Metropolitan DWDM: a dynamically configurable ring for the KomNet field trial in Berlin," Communications Magazine, IEEE , vol.39, no.2, pp.106-113, Feb 2001

18. Ramadas, M.R.; Varshney, R.K.; Thyagarajan, K.; Ghatak, A.K., "A matrix approach to study the propagation characteristics of a general nonlinear planar waveguide," Lightwave Technology, Journal of , vol.7, no.12, pp.1901-1905, Dec 1989.

19. Rajiv Srivastava, Rajat Kumar Singh, Y.N.Singh, "Optical Packet Switch Based on Tunable Fiber Bragg Grating," IEEE Tencon 2008, Hyderabad, pp.4,19-21 Nov.2008.

20. Ritwick Das and K Thyagarajan, Enhanced bandwidth optical parametric amplifier using Bragg reflection waveguide, Frontiers in Optics 2007/Laser Science XXIII conferences, San Jose, September, 2007.

21. Hang-yin Ling, Kin-tak Lau, Li Cheng and Wei Jin, “Viability of using an embedded FBG sensor in a composite structure for dynamic strain measurement”, Measurement, vol. 39, Issue, pp. 328-3344, May 2006.

22. Hiroshi Tsuda, “Ultrasound and damage detection in CFRP using Fiber Bragg Grating sensors”, Composites Science and Technology, vol. 66, Issue, pp. 676-683, 5 May 2006.

23. S. Baskar, P.N. Suganthan, N.Q. Ngo, A. Alphones and R.T. Zheng “Design of triangular FBG filter for sensor applications using covariance matrix adapted evolution algorithm”, Optics Communications, vol. 260, Issue 2, pp.716-722, 15 April 2006.

24. T.H.T. Chan, L. Yu, H.Y. Tam, Y.Q. Ni, S.Y. Liu, W.H. Chung and L.K. Cheng, ”Fiber Bragg Grating sensors for structural health monitoring of Tsing Ma

bridge: Background and experimental observation", Engineering Structures, vol.28, Issue 5,, pp. 648-659, April 2006.

25. A. Iadicicco, S. Campopiano, A. Cutolo, M. Giordano and A. Cusano, "Self temperature referenced refractive index sensor by non-uniform thinned Fiber Bragg Gratings", Sensors and Actuators B: Chemical, In Press, Corrected Proof, Available online 31 March 2006.

26. Fang Xie, Xianfeng Chen, Lin Zhang and Ming Song, "Realisation of an effective dual-parameter sensor employing a single Fiber Bragg Grating structure", Optics and Lasers in Engineering, vol. 44, Issue 10, pp.1088-1095, Oct.2006.

27. T.A. Dawood, R.A. Shenoi and M. Sahin, "A procedure to embed Fiber Bragg Grating strain sensors into GFRP sandwich structures, Composites" Part A: Applied Science and Manufacturing, In Press, Corrected Proof, Available online 20 March 2006.

28. M. Ussorio, H. Wang, S.L. Ogin, A.M. Thorne, G.T. Reed, S.C. Tjin and R. Suresh, "Modifications to FBG sensor spectra due to matrix cracking in a GFRP composite", Construction and Building Materials, vol. 20, Issues 1-2, pp.111-118, February-March 2006.

29. Yong Zhao, Qing-yao Meng and Kun Chen, "Novel current measurement method based on Fiber Bragg Grating sensor technology", Sensors and Actuators A: Physical, vol 126, Issue 1, pp. 112-116, 26 Jan. 2006.

30. Jean C. Cardozo da Silva, Ilda Abe, Roberta C. Chaves, José L. Fabris, João L. Pinto, Hypolito J. Kalinowski and Carmen L. Barbosa "Development of Bragg grating sensors at CEFET-PR", Optics and Lasers in Engineering, Vol. 39, Issues 5-6, pp.511-523, May-June 2003.

31. Andreas Othonosa, "Fiber Bragg Gratings", Rev. Sci. Instrum. 68, pp. 4309-4341, December 1997.

32. Kenneth O Hill and Gerald Meltz, "Fiber Bragg Grating Technology Fundamentals and Overview", Journal of Lightwave Technology, vol 15, no. 8, pp. 1263-1274, Aug.19997.

33. Kashyap, Raman, “Fiber Bragg Gratings”, Academic Press, March 1999.

34. Xinzhu Sang, Pak L. Chu, Chongxiu Yu and Robust Lai, “Growth dynamics of Bragg gratings in multimode optical Fiber”, Optics Communications, vol. 260, Issue 1, pp 131-135,1 April 2004 .

35. Nahar Singh, Subhash C. Jain and A. K. Aggarwal, “Fabrication Technology of optical Fiber Bragg Gratings”, Journal of the instrument society of India,vol l32 no.2, pp.148-156.

36. Nahar Singh, Subhash C. Jain and A. K. Aggarwal, “Fabrication of In-Fiber Bragg Gratings using phase mask technique”, National conference on Advances in contemporary physics and energy, pp.172-173, Feb8-9, 2002.

37. Oleg V. Ivanov, “Near-field effects in fabrication of Fiber Bragg Gratings using phase masks”, Optics Communications, Volume 229, Issues 1-6, pp. 167-172,2Jan.2004.

38. http://www.optiwave.com/

39. http://www.apollophoton.com/

40. http://www.pcgrate.com/

41. http://www.rsoft.com/

42. Xu, M.G.; Geiger, H.; Archambault, J.L.; Reekie, L.; Dakin, J.P., "Novel interrogating system for Fiber Bragg Grating sensors using an acousto-optic tunable filter," Electronics Letters , vol.29, no.17, pp.1510-1511, 19 Aug. 1993.

43. Foote, P.D., "Optical Fiber Bragg Grating sensors for aerospace smart structures ," Optical Fiber Gratings and Their Applications, IEEE Colloquium on , vol., no., pp.14/1-14/6, 30 Jan 1995.

44. H.J. Patrick; G.M. Williams; A.D. Kersey; J.R. Pedrazzani; A.M. Vengsarkar, "Hybrid Fiber Bragg Grating/long period fiber grating sensor for strain/temperature discrimination," Photonics Technology Letters, IEEE , vol.8, no.9, pp.1223-1225, Sept. 1996.

45. T.A. Berkoff; A.D. Kersey, "Fiber Bragg Grating array sensor system using a bandpass wavelength division multiplexer and interferometric detection," Photonics Technology Letters, IEEE , vol.8, no.11, pp.1522-1524, Nov. 1996.

46. Davis, M.A.; Bellemore, D.G.; Putnam, M.A.; Kersey, A.D., "Interrogation of 60 Fiber Bragg Grating sensors with microstrain resolution capability," Electronics Letters , vol.32, no.15, pp.1393-1394, 18 Jul. 1996.

47. L.A. Ferreira; J.L. Santos; F. Farahi, "Pseudoheterodyne demodulation technique for Fiber Bragg Grating sensors using two matched gratings," Photonics Technology Letters, IEEE , vol.9, no.4, pp.487-489, April 1997.

48. Ezbiri, A.; Munoz, A.; Kanellopoulos, S.E.; Handerek, V.A., "High resolution Fiber Bragg Grating sensor demodulation using a diffraction grating spectrometer and CCD detection," Optical Techniques for Smart Structures and Structural Mmonitoring (Digest No. 1997/033), IEEE Colloquium on , vol. no., pp.5/1-5/6, 17 Feb 1997.

49. Ferreira, L.A.; Diatzikis, E.V.; Santos, J.L.; Farahi, F., "Frequency-modulated multimode laser diode for Fiber Bragg Grating sensors," Lightwave Technology, Journal of , vol.16, no.9, pp.1620-1630, Sep 1998.

50. Gang-Chih Lin; Wang, L.; Yang, C.C.; Shih, M.C.; Chuang, T.J., "Thermal performance of metal-clad Fiber Bragg Grating sensors," Photonics Technology Letters, IEEE , vol.10, no.3, pp.406-408, Mar.1998.

51. Sung Chul Kang; Se Yoon Kim; Sang Bae Lee; Seo Won Kwon; Sang Sam Choi; Byoungho Lee, "Temperature-independent strain sensor system using a tilted Fiber Bragg Grating demodulator," Photonics Technology Letters, IEEE , vol.10, no.10, pp.1461-1463, Oct. 1998.

52. Cavaleiro, P.M.; Araujo, F.M.; Ribeiro, A.B.L., "Metal-coated Fiber Bragg Grating sensor for electric current metering," Electronics Letters , vol.34, no.11, pp.1133-1135, 28 May 1998.

53. Chan, C.C.; Win, W.; Demokan, M.S., "Enhancement of measurement accuracy in Fiber Bragg Grating sensors by using digital signal processing," Lasers and Electro-Optics, 1998. CLEO 98. Technical Digest. Summaries of papers presented at the Conference, vol., no., pp.311-312, 3-8 May 1998.

54. Sung Chul Kang; Se Yoon Kim; Sang Bae Lee; Seo Won Kwon; SangSam Choi; Byoungho Lee, "Temperature-independent demodulation technique for Fiber Bragg Grating strain sensors using a tilted Fiber Bragg Grating," Lasers and Electro-Optics, 1998. CLEO 98. Technical Digest. Summaries of papers presented at the Conference, vol., no., pp.329-330, 3-8 May 1998.

55. Jaehoon Jung; Hui Nam; Byoungho Lee, "Fiber Bragg Grating temperature sensor with controllable high sensitivity," Lasers and Electro-Optics Society Annual Meeting, 1998. LEOS '98. IEEE , vol.1, no., pp.405-406 vol.1, 1-4 Dec 1998.

56. Spammer, S.J.; Fuhr, P.L., "Concrete embedded optical Fiber Bragg Grating strain sensors," Industrial Electronics, 1998. Proceedings. ISIE '98. IEEE International Symposium , vol.1, no., pp.330-334 vol.1, 7-10 Jul 1998.

57. Sung Chul Kang; Sang Bae Lee; Sang Sam Choi; Byoungho Lee, "A novel method to measure dynamic strain using optical-path controlled Mach-Zehnder interferometer and Fiber Bragg Grating sensor ," Lasers and Electro-Optics Society Annual Meeting, 1998. LEOS '98. IEEE , vol.1, no., pp.401-402 vol.1, 1-4 Dec 1998.

58. Li, Shenping; Chan, K. T., "Optical fiber temperature sensor using a gain-switched Fabry–Perot semiconductor laser self-seeded from a linearly chirped Fiber Bragg Grating," Applied Physics Letters , vol.73, no.23, pp.3354-3356, Dec 1998.

59. Rochford, K.B.; Dyer, S.D., "Demultiplexing of interferometrically interrogated Fiber Bragg Grating sensors using Hilbert transform processing," Lightwave Technology, Journal of , vol.17, no.5, pp.831-836, May 1999.

60. Wei-Chong Du; Xiao-Ming Tao; Hwa-Yaw Tam, "Fiber Bragg Grating cavity sensor for simultaneous measurement of strain and temperature," Photonics Technology Letters, IEEE , vol.11, no.1, pp.105-107, Jan 1999.

61. Moreira, P.J.; Ferreira, L.A.; Santos, J.L.; Farahi, F., "Dynamic range enhancement in Fiber Bragg Grating sensors using a multimode laser diode," Photonics Technology Letters, IEEE , vol.11, no.6, pp.703-705, Jun 1999.

62. Chan, P.K.C.; Jin, W.; Gong, J.M.; Demokan, N.S., "Multiplexing of Fiber Bragg Grating sensors using a FMCW technique ," Photonics Technology Letters, IEEE , vol.11, no.11, pp.1470-1472, Nov 1999.

63. Youlong Yu; Hwayaw Tam; Zhiguo Liu; Wenghong Chung; Shuwei Geng, "Passive temperature compensation technique for Fiber Bragg Grating displacement sensor," Electronics Letters , vol.35, no.25, pp.2224-2226, 9 Dec 1999.

64. Koo, K.P.; Tveten, A.B.; Vohra, S.T., "Dense wavelength division multiplexing of Fiber Bragg Grating sensors using CDMA," Electronics Letters , vol.35, no.2, pp.165-167, 21 Jan 1999.

65. Koo, K.P.; Tveten, A.B.; Vohra, S.T., "DWDM of Fiber Bragg Grating sensors without sensor spectral dynamic range limitation using CDMA," Optical Fiber Communication Conference, 1999, and the International Conference on Integrated Optics and Optical Fiber Communication. OFC/IOOC '99. Technical Digest , vol.4, no., pp.168-170 vol.4, 1999.

66. Sung Chul Kang; Sang Bae Lee; Sang Sam Choi; Byoungho Lee, "A novel demodulation technique for the wavelength shift of Fiber Bragg Grating sensors using the I/Q signal processing scheme," Lasers and Electro-Optics, 1999. CLEO/Pacific Rim '99. The Pacific Rim Conference on , vol.2, no., pp.135-136 vol.2, 1999.

67. Chi Chiu Chan; Wei Jin; Ho, H.L.; Suleyman Demokan, M., "Performance analysis of a time-division-multiplexed Fiber Bragg Grating sensor array by use of

a tunable laser source," Selected Topics in Quantum Electronics, IEEE Journal of , vol.6, no.5, pp.741-749, Sep/Oct 2000.

68. Chan, P.K.C.; Wei Jin; Suleyman Demokan, M., "FMCW multiplexing of Fiber Bragg Grating sensors," Selected Topics in Quantum Electronics, IEEE Journal of , vol.6, no.5, pp.756-763, Sep/Oct 2000.

69. Jaehoon Jung; Yong Wook Lee; Byoungho Lee, "Novel interrogation system for dynamic strain measurement based on Fiber Bragg Grating sensor using long period grating pair and EDF," Lasers and Electro-Optics Society 2000 Annual Meeting. LEOS 2000. 13th Annual Meeting. IEEE , vol.2, no., pp.679-680 vol.2, 2000.

70. Sennhauser, U.; Frank, A.; Mauron, P.; Nellen, P.M., "Reliability of optical Fiber Bragg Grating sensors at elevated temperature," Reliability Physics Symposium, 2000. Proceedings. 38th Annual 2000 IEEE International , vol., no., pp.264-269, 2000

71. P. K. Bansal, R. C. Joshi, K. Singh, “On a Fault-Tolerant Multistage Interconnection Network”, Journal of Computers and Electrical Engg. Vol. 20, No. 4, pp. 335-345, 1994.

72. Seungwoo Kim; Sungchul Kim; Jaejoong Kwon; Byoungho Lee, "Novel Fiber Bragg Grating sensor demodulator using fiber birefringence," Lasers and Electro-Optics Society 2000 Annual Meeting. LEOS 2000. 13th Annual Meeting. IEEE , vol.2, no., pp.687-688 vol.2, 2000.

73. Youlong Yu; Luenfu Lui; Hwayaw Tam; Wenghong Chung, "Fiber-laser-based wavelength-division multiplexed Fiber Bragg Grating sensor system," Photonics Technology Letters, IEEE , vol.13, no.7, pp.702-704, Jul 2001.

74. Sungchul Kim; Seungwoo Kim; Jaejoon Kwon; Byoungho Lee, "Fiber Bragg Grating strain sensor demodulator using a chirped fiber grating," Photonics Technology Letters, IEEE , vol.13, no.8, pp.839-841, Aug 2001.

75. Seunghwan Chung; Jungho Kim; Bong-Ahn Yu; Byoungho Lee, "A Fiber Bragg Grating sensor demodulation technique using a polarization maintaining fiber loop

mirror," Photonics Technology Letters, IEEE , vol.13, no.12, pp.1343-1345, Dec 2001.

76. Ying Zhang; Dejun Feng; Zhiguo Liu; Zhuanyun Guo; Xiaoyi Dong; Chiang, K.S.; Chu, B.C.B., "High-sensitivity pressure sensor using a shielded polymer-coated Fiber Bragg Grating," Photonics Technology Letters, IEEE , vol.13, no.6, pp.618-619, Jun 2001.

77. Wait, P.C.; Hartog, A.H., "Spontaneous Brillouin-based distributed temperature sensor utilizing a Fiber Bragg Grating notch filter for the separation of the Brillouin signal," Photonics Technology Letters, IEEE , vol.13, no.5, pp.508-510, May 2001.

78. Boulet, C.; Webb, D.J.; Douay, M.; Niay, P., "Simultaneous interrogation of Fiber Bragg Grating sensors using an acoustooptic tunable filter," Photonics Technology Letters, IEEE , vol.13, no.11, pp.1215-1217, Nov 2001.

79. Chan, C.C.; Jin, W.; Ho, H.L.; Wang, D.N.; Wang, Y., "Improvement of measurement accuracy of Fiber Bragg Grating sensor systems by use of gas absorption lines as multi-wavelength references," Electronics Letters , vol.37, no.12, pp.742-743, 7 Jun 2001.

80. Cooper, D.J.F.; Smith, P.W.E., "A high-sensitivity, simple, low-cost method for the measurement of time-multiplexed Fiber Bragg Grating sensors," Lasers and Electro-Optics Society, 2001. LEOS 2001. The 14th Annual Meeting of the IEEE , vol.2, no., pp.867-868, vol.2, 2001.

81. da Silva, J.C.C.; Kalinowski, H.J., "Strain studies in electrical energy transmission cables using an optical Fiber Bragg Grating sensor," Microwave and Optoelectronics Conference, 2001. IMOC 2001.Proceedings of the 2001 SBMO/IEEE MTT-S International , vol.1, no., pp. 313-316 vol.1, 2001.

82. Barbosa, C.L.; Cazo, R.M.; Hattori, H.T.; Rabelo, R.C.; Lisboa, O., "Experimental study of a multimode Fiber Bragg Grating temperature sensor," Microwave and Optoelectronics Conference, 2001. IMOC 2001.Proceedings of the 2001 SBMO/IEEE MTT-S International , vol.1, no., pp. 317-319 vol.1, 2001.

83. Seunghwan Chung; Jungho Kim; Bong-Ahn Yu; Byoungho Lee, "A Fiber Bragg Grating sensor demodulation technique using a polarization maintaining fiber loop mirror," Lasers and Electro-Optics, 2001. CLEO/Pacific Rim 2001. The 4th Pacific Rim Conference on , vol.1, no., pp.I-502-I-503 vol.1, 2001.

84. Wade, S. A.; Forsyth, D. I.; Grattan, K. T. V.; Guofu, Q., "Fiber optic sensor for dual measurement of temperature and strain using a combined fluorescence lifetime decay and Fiber Bragg Grating technique," Review of Scientific Instruments , vol.72, no.8, pp.3186-3190, Aug 2001.

85. Arregui, F.J.; Matias, I.R.; Cooper, K.L.; Claus, R.O., "Simultaneous measurement of humidity and temperature by combining a reflective intensity-based optical fiber sensor and a Fiber Bragg Grating," Sensors Journal, IEEE , vol.2, no.5, pp. 482-487, Oct 2002.

86. Gong, J.M.; MacAlpine, J.M.K.; Chan, C.C.; Jin, W.; Zhang, M.; Liao, Y.B., "A novel wavelength detection technique for Fiber Bragg Grating sensors," Photonics Technology Letters, IEEE , vol.14, no.5, pp.678-680, May 2002.

87. Frazao, O.; Romero, R.; Rego, G.; Marques, P.V.S.; Salgado, H.M.; Santos, J.L., "Sampled Fiber Bragg Grating sensors for simultaneous strain and temperature measurement," Electronics Letters , vol.38, no.14, pp.693-695, 4 Jul 2002.

88. Murphy, D.F.; Flavin, D.A.; McBride, R.; Jones, J.D.C., "Spatially scanned interferometric interrogation of Fiber Bragg Grating sensors based on Hilbert transform processing," Optical Fiber Sensors Conference Technical Digest, 2002. OFS 2002, 15th , vol., no., pp. 379-382 vol.1, 2002.

89. Teunissen, J.; Merte, R.; Peier, D., "Stability of Fiber Bragg Grating sensors for integration into high-voltage transformers for online monitoring," Optical Fiber Sensors Conference Technical Digest, 2002. OFS 2002, 15th , vol., no., pp. 541-544 vol.1, 2002.

90. Fernandez, A.F.; Brichard, B.; Borgermans, P.; Berghmans, F.; Decreton, M.; Megret, P.; Blondel, M.; Delchambre, A., "Fiber Bragg Grating temperature

sensors for harsh nuclear environments," Optical Fiber Sensors Conference Technical Digest, 2002. OFS 2002, 15th , vol., no., pp. 63-66 vol.1, 2002.

91. Betz, D.; Staudigel, L.; Trutzel, M.N., "Test of a Fiber Bragg Grating sensor network for commercial aircraft structures," Optical Fiber Sensors Conference Technical Digest, 2002. OFS 2002, 15th , vol., no., pp. 55-58 vol.1, 2002.

92. Hua Lu; Hussain, R.; Ming Zhou; Xijia Gu, "Fiber Bragg Grating Sensors for Failure Detection of Flip Chip Ball Grid Array in Four-Point Bend Tests," Sensors Journal, IEEE , vol.9, no.4, pp.457-463, April 2009.

93. Ping Lu; Liqiu Men; Qiying Chen, "Polymer-Coated Fiber Bragg Grating Sensors for Simultaneous Monitoring of Soluble Analytes and Temperature," Sensors Journal, IEEE , vol.9, no.4, pp.340-345, April 2009.

94. Peng-Chun Peng; Kuan-Yan Huang, "Fiber Bragg Grating Sensor System With Two-Level Ring Architecture," Sensors Journal, IEEE , vol.9, no.4, pp.309-313, April 2009.

95. Song, D.; Wei, Z.; Zou, J.; Yang, S.; Du, E.; Cui, H.-L., "Pressure Sensor Based on Fiber Bragg Grating and Carbon Fiber Ribbon-Wound Composite Cylindrical Shell," Sensors Journal, IEEE , vol.9, no.7, pp.828-831, July 2009.

96. Yinping Miao; Bo Liu; Hao Zhang; Yuan Li; Haibin Zhou; Hua Sun; Weihua Zhang; Qida Zhao, "Relative Humidity Sensor Based on Tilted Fiber Bragg Grating With Polyvinyl Alcohol Coating," Photonics Technology Letters, IEEE , vol.21, no.7, pp.441-443, April 2009.

97. Muller, M.S.; Hoffmann, L.; Sandmair, A.; Koch, A.W., "Full Strain Tensor Treatment of Fiber Bragg Grating Sensors," Quantum Electronics, IEEE Journal , vol.45, no.5, pp.547-553, May 2009.

98. Seongmin Ju; Watekar, P.R.; Won-Taek Han, "Highly sensitive temperature sensor using Fiber Bragg Grating on Pb/Ge-codoped fiber," Optical Fiber Communication - 2009. OFC 2009. Conference on , vol., no., pp.1-3, 22-26, Mar. 2009.

99. Han, Young-Geun, "Directional bending sensor with temperature insensitivity using a sampled chirped Fiber Bragg Grating," Journal of Applied Physics , vol.105, no.6, pp.063103-063103-4, Mar. 2009.

100. Ambrosino, C.; Campopiano, S.; Cutolo, A.; Cusano, A., "Sensitivity Tuning in Terfenol-D Based Fiber Bragg Grating Magnetic Sensors," Sensors Journal, IEEE , vol.8, no.9, pp.1519-1520, Sept. 2008.

101. Grobnic, D.; Mihailov, S.J.; Smelser, C.W.; Walker, R.B., "Multiparameter Sensor Based on Single High-Order Fiber Bragg Grating Made With IR-Femtosecond Radiation in Single-Mode Fibers," Sensors Journal, IEEE , vol.8, no.7, pp.1223-1228, July 2008.

102. Bo Dong; Qida Zhao; Lihui Liu; Guiling Huang; Long Jin; Jin Zhou; Tongqing Liao, "Tunable Chirped Fiber Bragg Grating Filter Based on Special Strain Function Modulation and Its Application in Fiber Sensor," Lightwave Technology, Journal of , vol.26, no.14, pp.2286-2290, 15 July 2008.

103. Fu, H.Y.; Liu, H.L.; Chung, W.H.; Tam, H.Y., "A Novel Fiber Bragg Grating Sensor Configuration for Long-Distance Quasi-Distributed Measurement," Sensors Journal, IEEE , vol.8, no.9, pp.1598-1602, Sept. 2008.

104. Suleiman, M.; Seat, H.C.; Bosch, T., "Interrogation of Fiber Bragg Grating Dynamic Strain Sensors by Self-Mixing Interferometry," Sensors Journal, IEEE , vol.8, no.7, pp.1317-1323, July 2008.

105. Caucheteur, C.; Debliquy, M.; Lahem, D.; Megret, P., "Catalytic Fiber Bragg Grating Sensor for Hydrogen Leak Detection in Air," Photonics Technology Letters, IEEE , vol.20, no.2, pp.96-98, 15 Jan. 2008.

106. Qizhen Sun; Deming Liu; Li Xia; Jian Wang; Hairong Liu; Shum, P., "Experimental Demonstration of Multipoint Temperature Warning Sensor Using a Multichannel Matched Fiber Bragg Grating," Photonics Technology Letters, IEEE , vol.20, no.11, pp.933-935,1 June 2008.

107. Yong Zhao; Hua-wei Zhao; Xin-yuan Zhang; Qing-yao Meng; Bo Yuan, "A Novel Double-Arched-Beam-Based Fiber Bragg Grating Sensor for Displacement

Measurement," Photonics Technology Letters, IEEE , vol.20, no.15, pp.1296-1298, 1 Aug. 2008.

108. Wei, Z.; Song, D.; Zhao, Q.; Cui, H.-L., "High Pressure Sensor Based on Fiber Bragg Grating and Carbon Fiber Laminated Composite," Sensors Journal, IEEE , vol.8, no.10, pp.1615-1619, Oct. 2008.

109. Fu, H.Y.; Liu, H.L.; Dong, X.; Tam, H.Y.; Wai, P.K.A.; Lu, C., "High-speed Fiber Bragg Grating sensor interrogation using dispersion compensation fiber," Electronics Letters , vol.44, no.10, pp.618-619, 8 May 2008.

110. Tosi, D.; Olivero, M.; Perrone, G., "Self-mixing based interrogation techniques for high-reflectivity Fiber Bragg Grating sensors," Electronics Letters , vol.44, no.6, pp.405-406, 13 Mar. 2008.

111. Yong-Lae Park; Seok Chang Ryu; Black, R.J.; Moslehi, B.; Cutkosky, M.R., "Fingertip force control with embedded Fiber Bragg Grating sensors," Robotics and Automation, 2008. ICRA 2008. IEEE International Conference on , vol., no., pp.3431-3436, 19-23 May 2008.

112. Wei Wu; Xin Liu, "The Application of Improved Genetic Algorithm in Fiber Bragg Grating (FBG) Sensor Network," Genetic and Evolutionary Computing, 2008. WGEC '08. Second International Conference on , vol., no., pp.3-6, 25-26 Sept. 2008.

113. Haibin Zhou; Bo Liu; Yange Liu, "Fiber Bragg Grating Wireless Sensors Network," Wireless Communications, Networking and Mobile Computing, 2008. WiCOM '08. 4th International Conference on , vol., no., pp.1-3, 12-14 Oct. 2008.

114. Myonghwan Kim; June-Ho Lee; Ja-Yoon Koo; Minho Song, "A study on internal temperature monitoring system for power transformer using pptical Fiber Bragg Grating sensors," Electrical Insulating Materials, 2008. (ISEIM 2008). International Symposium on, vol., no., pp.163-166, 7-11 Sept. 2008.

115. Kunzler, W.; Zixu Zhu; Selfridge, R.; Schultz, S.; Wirthlin, M., "Integrating Fiber Bragg Grating sensors with sensor networks," AUTOTESTCON, 2008 IEEE, vol., no., pp.354-359, 8-11 Sept. 2008.

116. Hwa-yaw Tam, "Applications of Fiber Bragg Grating sensors in railways," Opto-Electronics and Communications Conference, 2008 and the 2008 Australian Conference on Optical Fiber Technology. OECC/ACOFT 2008. Joint conference of the , vol., no., pp.1-4, 7-10 July 2008.

117. Wild, G.; Hinckley, S., "An Intensiometric Detection System for Fiber Bragg Grating sensors," Opto-Electronics and Communications Conference, 2008 and the 2008 Australian Conference on Optical Fiber Technology. OECC/ACOFT 2008. Joint conference of the , vol., no., pp.1-2, 7-10 July 2008.

118. Foo Siang Fook, V.; Kng Poh Leong; Hao Jian Zhong, E.; Jayachandran, M.; Aung Aung Phyo Wai; Biswas, J.; Lin Wei Si; Yap, P., "Non-intrusive respiratory monitoring system using Fiber Bragg Grating sensor," e-health Networking, Applications and Services, 2008. HealthCom 2008. 10th International Conference on , vol., no., pp.160-164, 7-9 July 2008.

119. Canning, J.; Bandyopadhyay, S.; Stevenson, M.; Cook, K., "Fiber Bragg Grating sensor for high temperature application," Opto-Electronics and Communications Conference, 2008 and the 2008 Australian Conference on Optical Fiber Technology. OECC/ACOFT 2008. Joint conference of the , vol., no., pp.1-2, 7-10 July 2008,

120. Franke, R.; Hoffmann, F.; Bertram, T., "Observation of link deformations of a robotic manipulator with Fiber Bragg Grating sensors," Advanced Intelligent Mechatronics, 2008. AIM 2008. IEEE/ASME International Conference on , vol., no., pp.90-95, 2-5 July 2008

121. Arkwright, J.W.; Doe, S.N.; Blenman, N.G.; Underhill, I.D.; Maunder, S.A.; Lim, B.; Szczesniak, M.M.; Dinning, P.G.; Cook, I.J., "The use of wavelength division multiplexed Fiber Bragg Grating sensors for distributed sensing of pressure in the gastrointestinal tract," PhotonicsGlobal@Singapore, 2008. IPGC 2008. IEEE, vol., no., pp.1-4, 8-11 Dec. 2008.

122. Xinyong Dong; Tam, H.Y.; Shum, P., "Intensity-Modulated Fiber Bragg Grating Sensor System Employing Fiber Dispersion," PhotonicsGlobal@Singapore, 2008. IPGC 2008. IEEE, vol., no., pp.1-4, 8-11 Dec. 2008.

123. Mondal, S.K.; Mitra, A.; Tiwari, U.; Pant, J.; Jain, S.C.; Mishra, V.; Poddar, G.C.; Singh, N.; Kapur, P., "Embedded dual Fiber Bragg Grating sensor for temperature-load (strain) discrimination," Recent Advances in Microwave Theory and Applications, 2008. MICROWAVE 2008. International Conference on , vol., no., pp.400-403, 21-24 Nov. 2008.

124. Qizhen Sun; Doming Liu; Jian Wang; Hairong Liu; Li Xia; Shum, P., "Multi-Point Temperature Warning Sensor Using a Multi-channel Matched Fiber Bragg Grating," Optical Fiber communication/National Fiber Optic Engineers Conference, 2008. OFC/NFOEC 2008. Conference on , vol., no., pp.1-3, 24-28 Feb. 2008.

125. Xinlong Chang; Xiangyong He; Jianghua Hu; Jinjun Li, "Experimental Research on Embedded Fiber Bragg Grating Sensors Network for Solid Rocket Motors Health Monitor," Intelligent Networks and Intelligent Systems, 2008. ICINIS '08. First International Conference, vol., no., pp.170-173, 1-3 Nov. 2008.

126. Ke Wen; Rong Wang; Min Wang; Jianhua Li; Jingyuan Wang, "A new temperature sensor based on Fiber Bragg Grating in photonic crystal fibers," Communication Systems, 2008. ICCS 2008. 11th IEEE Singapore International Conference on , vol., no., pp.1218-1221, 19-21 Nov. 2008.

127. Du Yanliang; Li Jianzhi; Liu Chenxi, "A Novel Fiber Bragg Grating Temperature Compensated Strain Sensor," Intelligent Networks and Intelligent Systems, 2008. ICINIS '08. First International Conference, vol., no., pp.569-572, 1-3 Nov. 2008.

128. Hongyan Fu; Kaiming Zhou; Saffari, P.; Chengbo Mou; Lin Zhang; Sailing He; Bennion, I., "Microchannelled chirped Fiber Bragg Grating based refractive index sensor formed by femto-second laser processing and hf-etching," Optical Communication, 2008. ECOC 2008. 34th European Conference on , vol., no., pp.1-2, 21-25 Sept. 2008.

129. Men, Liqiu; Lu, Ping; Chen, Qiying, "A multiplexed Fiber Bragg Grating sensor for simultaneous salinity and temperature measurement," Journal of Applied Physics , vol.103, no.5, pp.053107-053107-7, Mar 2008.

130. Espejo, R.J.; Dyer, S.D., "Transverse-Stress Fiber Bragg Grating Sensor With High Spatial Resolution and Temperature Stability," Lightwave Technology, Journal of , vol.25, no.7, pp.1777-1785, July 2007.

131. Saini, S.S.; Stanford, C.; Lee, S.M.; Park, J.; DeShong, P.; Bentley, W.E.; Dagenais, M., "Monolayer Detection of Biochemical Agents Using Etched-Core Fiber Bragg Grating Sensors," Photonics Technology Letters, IEEE , vol.19, no.18, pp.1341-1343, 15 Sept. 2007.

132. Shengchun Liu; Youlong Yu; Jintao Zhang; Xiangfei Chen, "Real-Time Monitoring Sensor System for Fiber Bragg Grating Array," Photonics Technology Letters, IEEE , vol.19, no.19, pp.1493-1495, 1 Oct. 2007.

133. Saitoh, T.; Nakamura, K.; Takahashi, Y.; Iida, H.; Iki, Y.; Miyagi, K., "Ultra-Long-Distance Fiber Bragg Grating Sensor System," Photonics Technology Letters, IEEE , vol.19, no.20, pp.1616-1618, 15.Oct.2007.

134. Binfeng Yun; Na Chen; Yiping Cui, "Highly Sensitive Liquid-Level Sensor Based on Etched Fiber Bragg Grating," Photonics Technology Letters, IEEE , vol.19, no.21, pp.1747-1749, 1.Nov. 2007.

135. Ambrosino, C.; Capoluongo, P.; Campopiano, S.; Cutolo, A.; Giordano, M.; Davino, D.; Visone, C.; Cusano, A., "Fiber Bragg Grating and Magnetic Shape Memory Alloy: Novel High-Sensitivity Magnetic Sensor," Sensors Journal, IEEE , vol.7, no.2, pp.228-229, Feb. 2007.

136. Michael Buric; Kevin P. Chen; Matrika Bhattarai; Philip R. Swinehart; Mokhtar Maklad, "Active Fiber Bragg Grating Hydrogen Sensors for All-Temperature Operation," Photonics Technology Letters, IEEE , vol.19, no.5, pp.255-257, 1 March 2007.

137. Huang, C.; Jing, W.; Liu, K.; Zhang, Y.; Peng, G.-D., "Demodulation of Fiber Bragg Grating Sensor Using Cross-Correlation Algorithm," Photonics Technology Letters, IEEE , vol.19, no.9, pp.707-709, 1 May 2007.

138. Yiping Wang; Na Chen; Binfeng Yun; Yiping Cui, "Use of Fiber Bragg Grating Sensors for Determination of a Simply Supported Rectangular Plane Plate

Deformation," Photonics Technology Letters, IEEE , vol.19, no.16, pp.1242-1244, 15.Aug.2007.

139. Bowei Zhang; Mojtaba Kahrizi, "High-Temperature Resistance Fiber Bragg Grating Temperature Sensor Fabrication," Sensors Journal, IEEE , vol.7, no.4, pp.586-591, April 2007.

140. Guo, T.; Yang, J.; Zhao, Q.D.; Huang, G.L.; Xue, L.F.; Zhang, H.; Dong, X.Y., "Temperature-immune and intensity-referenced pressure sensor based on strain-induced quadratic-chirped Fiber Bragg Grating," Electronics Letters , vol.43, no.2, pp.90-92, 18 Jan.2007.

141. A.K. Ghatak and K. Thyagarajan, Introduction to Fiber Optics, Cambridge University Press, Cambridge, UK, 1989.

142. S C Jain, Nahar Singh, J K Chhabra and A K Aggarwal, "Experimental Feasibility Study of Fiber Optic Extrinsic Fabry-Perot Interferometric Sensor for Civil Structures and Other Applications", Journal of Scientific & Industrial Research, vol 60, pp.779-785, Oct. 2001.

143. Udd Eric, Fiber Optic Sensors – An Introduction for Engineers and Scientists John Wiley & Sons, Inc., NY, 1991.

144. Grattan K T V & Meggitt B T, "Optical Fiber Sensor Technology Chapman & Hall", London 1995.

145. Fuhr P L, Huston D R, Kajenski P J & Ambrose T P, Performance and health monitoring of Stafford Medical Building using embedded sensors, Smart Mater. & Struct, 1 (1) 63-68, 1992.

146. Mendez A & Morse T F, "Overview of optical fiber sensors embedded in concrete", Proc SPIE, Fiber Optic Smart Structures and Skins V , (1798), pp 205-216, 1992.

147. Habel Wolfgang R & Polster Helmut., "The influence of cementitious building materials on polymeric surfaces of embedded optical fibers for sensors", J Lightwave Technol., 13 (7), pp 1324-1330, 1995.

148. Dasgupta Abhijit & Sirkis James S, “Importance of coatings to optical fiber sensors embedded in “smart” structures”, Am Inst Aeronaut Astronaut J, 30, pp1337-1343, 1992.

149. Udd Eric, Fiber Optic Smart Structures (John Wiley & Sons Inc., NY) 1995.

150. Martelluci Sergio, Chester Arthur N & Mignani Anna Grazia, “Optical Sensors and Microsystems” Kluwer Academic/Plenum Publishers, NY, 2000.

151. A. Fernandez Fernandez, B. Brichard, P. Borgermans, F. Berghmans, M. Decr´eton, P. M´egret, M. Blondel and A. Delchambre, “Fiber Bragg Grating temperature sensor for harsh nuclear environments”, Proceeding in 15th International Conference on Optical Fiber Sensors, pp. 63-66, 2002.

152. G. Rego, A. Fernandez Fernandez, J.-L. Santos, H. Salgado, F. Berghmans, and A. Gusarov, “Optical fiber sensors for nuclear environments”, Proc. Applied Physics 2003, 2003.

153. A. Gusarov, A. Fernandez Fernandez, F. Berghmans, O. Deparis, Y. Defosse, W. Mégret, M. Decréton, and M. Blondel, “Temperature monitoring with Fiber Bragg Grating sensors for MGy dose level gamma radiation environments”, OPTORAD98, Europhysique symposium, France, 1998.

154. A. Gusarov, A. Fernandez Fernandez, F. Berghmans, O. Deparis, Y. Defosse, W. Mégret, M. Decréton, and M. Blondel, “Temperature monitoring with Fiber Bragg Grating sensors for MGy dose level gamma radiation environments”, OPTORAD98, Europhysique symposium, France, 1998.

155. R. Kashyap, “Fiber Bragg Gratings”, Academic Press 458, 1999.

156. John Dakin & Brian Culshaw, “Optical Fiber Sensors,Components and Subsystems”, Volume III, Artech House Boston London, pp. 45-49, 1997

157. Gerd Keiser, Optical Fiber Communications, pp. 92-93.

158. Nahar Singh, Subhash C. Jain and A. K. Aggarwal, “Fabrication Technology of optical Fiber Bragg Gratings”, Journal of the instrument society of India,vol .32 No.2, pp. 148-156.

159. Nahar Singh, Subhash C. Jain and A. K. Aggarwal, “Fabrication of In-Fiber Bragg Gratings using phase mask technique”, National conference on Advances in contemporary physics and energy, pp. 172-173., Feb 8-9,2002.

160. A. D. Kersey, M. A. Davis, H. J. Patrick, M. LeBlanc, K. P. Koo, C. G. Askins, M. A. Putnam, and E. J. Friebele, “Fiber grating sensors,” J. Lightwave Technol., vol. 15, pp. 1442–1463, Aug. 1997.

161. Y.-J. Rao, “In-Fiber Bragg Grating sensors,” Meas. Sci. Technol., vol. 8, no. 4, pp. 335–375, 1997.

162. A. A. Chtcherbakov and P. L. Swart, “Multiplexed Bragg grating sensor with chirped fiber optic grating interrogator,” in Tech. Dig. 16th Int.Conf. Optical Fiber Sensors (OFS-16), K. Hotate and H. Nagai, Eds., Nara, Japan, pp. 552–555, Oct. 13–17, 2003

163. Chtcherbakov, A.A.; Swart, P.L, “Chirped fiber-optic Bragg grating interrogator in a multiplexed Bragg grating sensor configuration” Lightwave Technology, Journal of Volume 22, Issue 6, pp.1543 – 1547, June 2004.

164. Chtcherbakov, A.A.; Swart, P.L.;”Optical Chirped fiber optic Bragg grating interrogator for a Bragg grating strain sensor”, Fiber Sensors Conference Technical Digest, 2002. OFS 2002, vol.115th, pp.227 – 230, 6-10 May 2002.

165. Sano, Y.; Yoshino, T “Fast optical wavelength interrogator employing arrayed waveguide grating for distributed Fiber Bragg Grating sensors”, Lightwave Technology, Journal of, vol. 21, Issue 1, pp.132 – 139, Jan 2003.

166. A.C.; Veiga, C.; Encinas, L.S.;Unambiguous “Signal Processing and Measuring Range Extension for Fiber Bragg Gratings Sensors Using Artificial Neural Networks - A Temperature Case Zimmermann”, , Sensors Journal, IEEE, vol. 8, Issue 7, pp.1229 – 1235, July 2008.

167. Gaozhi Xiao; Mrad, N.; Fang Wu; Zhiyi Zhang; Fengguo Sun;, “Miniaturized Optical Fiber Sensor Interrogation System Employing Echelle Diffractive Gratings Demultiplexer for Potential Aerospace Applications”, Sensors Journal, IEEE, vol. 8, Issue 7, pp.1202 – 1207, July 2008.

168. Fu, H.Y.; Liu, H.L.; Dong, X.; Tam, H.Y.; Wai, P.K.A.; Lu, C.;,"High-speed Fiber Bragg Grating sensor interrogation using dispersion compensation fiber", Electronics Letters, vol. 44, Issue 10, pp.618 – 619, 8 May 2008.

169. Samrat S. Batth, M. ¨Umit Uyar, Yu Wang and Mariusz A. Fecko, "Multiple Fault Models in Timed FSMs", In proceedings IEEE 23rd Instrumentation and Measurement Technology Conference (IMTC), Sorrento, Italy, 2006.

170. V. Kahlon, C. Wang and A. Gupta, "Monotonic Partial Order Reduction: An Optimal Symbolic Partial Order Reduction Technique" 21st International Conference on Computer Aided Verification (CAV), Grenoble, France. June 2009.

171. Dunnicliff, J. and Green G.E., "Geotechnical Instrumentation for Monitoring Field Performance", A Wiley Interscience Publication, 1988.

172. Willaim F. Kane, Timothy J. Beck, "Development of Time Domain Reflectometry System to Monitor Landslide Activity", Proceedings, 45th Highway Geology Symposium, Portland, OR, pp.163-173, August 17-19,1994.

173. N. S. Aulakh, J.K. Chhabra, Nahar Singh, Subhash Jain, "Optical Fiber Sensing System using Microbend Resolution Enhancer for Early Warning and Detection of Landslides", Experimental Techniques, pp.37-42, May - June 2004.

174. Kross, B.C., G.R Hallberg, D.R. Bruner, K. Cherryholmes, and J.K. Johnson "The Nitrate Contamination of Private Well Water in Iowa". Am J Public Health, pp 270-272, February 1993.

175. Comly H. "Cyanosis in infants caused by nitrates in well water". JAMA 129, pp 112-116, 1995.

176. Johnson CJ, Bonrud P. "Methemoglobinemia: is it coming back to haunt us?", Health Environ Digest 1(12), pp 3-4, 1988.

177. Lukens JN. "The legacy of well-water methemoglobinemia". JAMA 257:2793-2795, May 1987.

178. Forman, D., Al-Dabbagh, S., and Doll, R., "Nitrates, nitrites and gastric cancer in Great Britain", Nature, v. 313, pp. 620-625, February 1995.

179. Peter L. Fuhr, “Fiber optic corrosion sensing for bridges and roadway surfaces”, SPIE(USA), vol.2446, pp. 2-8, March 1995.

180. Nahar Singh, “Development and experimental investigations of a fiber optic color sensing probe”, J SCI IND RES, vol. 58, pp. 359-363, May 1999.

181. Bishnu P.Pal “Fundamentals of Fiber Optics in Telecommunication and Sensor Systems” Intensity Modulated Fiber Optic Sensors, (Ed.), Wiley Eastern Limited, New Delhi, 1992.

182. Leo Hoogenboom et.al, “Theoretical and experimental analysis of a Fiber optic proximity probe”, Proc. SPIE Fiber Optic and Laser Sensors II, vol. 478, pp. 46-57. 1984.

183. Charles M Davis, “Fiber Optic Sensor : an overview”, Optical Engg. 24(2), pp.347-351, 1985.

184. Mignani, A.G.; Mencaglia, A.A., “Direct and chemically-mediated absorption spectroscopy using optical fiber instrumentation”, Sensors Journal, IEEE Volume 2, Issue 1, pp.52 - 57 , Feb. 2002 .

185. Kumar Dattamajumdar, A.; Blount, P.L.; Myers, J.A.; Proctor, A.H.; Goldman, B.H.; Reid, B.J.; Martin, R.W.; “A low-cost fiber-optic instrument to colorimetrically detect patients with Barrett's esophagus for early detection of esophageal adenocarcinoma”, Biomedical Engineering, IEEE Transactions on vol.48, Issue 6, pp.695 – 705, June 2001.

186. N. Singh, S.C. Jain, N.S. Aulakh, J.K. Chhabra, M.L. Singh, A.K. Aggarwal, R.P. Bajpai, “Fiber Optic Colorimetry Technique For In-Situ Measurement Of Corrosion In Civil Structures”, Experimental Techniques 28 (1), pp 23–26, February 2004

LIST OF PUBLICATIONS

1. N. S. Aulakh, R. S. Kaler, "Fiber Optic Interrogator based Landslide Monitoring", Photonics Spectra, pp 64-66, August 2008

2. N. S. Aulakh, R. S. Kaler, "Fiber optic interrogator for in-situ nitrate detection in groundwater based on colorimetry technique", Optica Applicata, Vol. XXXVIII, No. 4, 2008, pp 575-579, December 2008

3. N. S. Aulakh, R. S. Kaler, "Fiber Bragg Grating Interrogator using Edge Filtering Technique with Microbend Loss Error Mitigation", in press Optik, International Journal for Light and Electron Optics, Elseveir.

4. N. S. Aulakh, R. S. Kaler, "Simulation of Fiber Bragg Grating", communicated Optik, International Journal for Light and Electron Optics, Elseveir.

5. N. S. Aulakh, R. S. Kaler, "Fiber Optic Interrogator with 3G Cellular interface for remote monitoring", National Seminar on 3G Networking Optimisation and Emerging Communication Technologies, Chandigarh, August 24^{th}-25^{th}, 2007

6. N. S. Aulakh, R. S. Kaler, "Fiber Bragg Grating Based Liquid Level Gage"- Technical Digest, XXXIII Optical Society of India Symposium 2007 on Optics and Optoelectronics, 18^{th} – 20^{th} December 2007.

7. N. S. Aulakh, R. S. Kaler, "Fiber Optic Strain Sensor for Aircraft Using FBG Interrogator" Proceedings of National Seminar on Recent Advances in Aerospace Technologies Maintenance and Optimization, November 14^{th} - 15^{th} 2008

8. N. S. Aulakh, R. S. Kaler, "Fiber Bragg Grating Interrogator with microbend attenuation compensated Edge Filtering Technique" - presented at Photonics 2008, IIT Delhi. December 15-17, 2008

9. N. S. Aulakh, R. S. Kaler, "Microbend Attenuation Compensated FBG Interrogator" - 2nd National Conference on Wireless and Optical Communication (Woc-2008)" , Punjab Engineering College, Chandigarh, December 18-19, 2008

10. N. S. Aulakh, R. S. Kaler, "Landslide Monitoring Using Fiber Optic Interrogator With Bluetooth Based Early Warning On Cellular Phone" – presented at "40^{th} IETE Mid Term Symposium on Information & Communication Technologies for Disaster Management (ICTDM-2009)" organized at CSIO on April 17-18, 2009

11. N. S. Aulakh, R. S. Kaler, "Fiber Optic Interrogator for In-Situ Nitrate Detection in Groundwater based on Colorimetry Technique" – "International Conference on Optics and Photonics", Central Scientific Instruments Organisation, Chandigarh on October 30- November 1, 2009